



A Study
of
Cryptate Complexes
and
Pendant Arm Ligand
Complexes

by
Philip Clarke B.Sc.(Hons.) (Adelaide)

A Thesis Presented for
the Degree of Doctor of Philosophy.

The Department of Physical and Inorganic Chemistry,
The University of Adelaide.

March, 1992.

"What we see is not reality in itself, but reality
exposed to our method of questioning."

-Werner Heisenburg

"Knowledge comes, but wisdom lingers."

-Alfred, Lord Tennyson

Contents :

	PAGE No.
Contents:	iii
Abstract:	vii
Acknowledgements:	viii
Statement:	viii
Abbreviations:	ix
CHAPTER 1: Cryptands and Cryptates - Structural Aspects	1
1.1 Introduction to Cryptate Chemistry	1
1.1.1 Structural Aspects of Cryptates	3
1.2 Crystal Structures of Some Alkali Metal Ion Cryptates	7
1.2.1 The Crystal Structure of [Na.C22C5]ClO ₄	7
1.2.2 The Crystal Structure of [K.C22C5]ClO ₄	11
1.2.3 The Crystal Structure of [Cs.C22C5]ClO ₄	16
1.2.4 The Crystal Structure of [H ₃ O.C22C5]ClO ₄	20
1.2.5 Summary of Crystal Structure Data.....	23
Bibliography :	27
CHAPTER 2: Cryptate Equilibria	29
2.1 Introduction	29
2.2 Equilibria in Aqueous Solution.....	32
2.2.1 Protonation of C22C ₅ in Aqueous Solution.....	32
2.2.2 Complexation of Selected Monovalent Metal Ions by C22C ₅ in Aqueous Solution.....	35
2.3 Equilibria in Aqueous and Non-Aqueous Solution	37
2.3.1 Complexation of Monovalent Metal Ions by C22C ₅ in Aqueous and Non-Aqueous Solution.....	37
2.4 Sodium(I) Ion Complexation by Diaza-Crown Ether C21 and Cryptands C21C ₅ and C211 in Non-Aqueous Solution.....	44
2.5 Experimental Methods.....	46
2.5.1 Analysis of pH-Metric Titration Data in Aqueous Solution.....	46
2.5.2 Analysis of Potentiometric Titration Data in Aqueous and Non-Aqueous Solution.....	48
Bibliography :	58
CHAPTER 3: Dynamics of Cryptate Complexation	61
3.1 Introduction	61
3.2 Exchange Kinetics for [M.C22C ₅] ⁺ Systems in Selected Solvents	64
3.2.1 Exchange Kinetics of Na ⁺ on [Na.C22C ₅] ⁺ in Methanol.....	65
3.2.2 A Qualitative Study of [Li.C22C ₅] ⁺ and [Na.C22C ₅] ⁺ Metal Ion Exchange Kinetics in a Range of Solvents	68
3.2.3 Dynamic Aspects of Cryptate Exchange for Related Systems...	70

3.3	Exchange Kinetics for [Na.C211] ⁺ , [Na.C21C ₅] ⁺ and [Na.C21] ⁺ in N,N-Dimethylformamide, N,N-Diethylformamide and N,N-Dimethylacetamide.....	73
3.3.1	Exchange Kinetics of Na ⁺ on [Na.C211] ⁺ in N,N-Diethylformamide and N,N-Dimethylacetamide	73
3.3.2	Exchange Kinetics for Related Systems Containing [Na.C211] ⁺ , [Na.C21C ₅] ⁺ and [Na.C21] ⁺	77
3.4	General Conclusions.....	81
	Bibliography :	83
CHAPTER 4: Pendant Arm Ligand Complexes.....		86
4.1	Introduction	86
4.2	The Structures of Selected Divalent Metal Ion Complexes of 1,4,8,11-Tetrakis(2-hydroxyethyl)-1,4,8,11-tetraazacyclotetradecane	88
4.2.1	Assignment of Structures in Solution.....	88
4.2.2	Assignment of Structures in the Solid-State	93
4.3	Ligand Exchange Processes of [M(THEC)] ²⁺ in <i>d</i> ₄ -Methanol..	96
4.3.1	Intermolecular Ligand Exchange of [1,4,8,11-Tetrakis(2-hydroxyethyl)-1,4,8,11-tetraazacyclotetradecane]cadmium(II), [Cd(THEC)] ²⁺ , and its Mercury(II) and Lead(II) Analogues. A Natural Abundance ¹³ C NMR Study.....	96
4.3.2	Intermolecular Metal Ion Exchange of [1,4,8,11-Tetrakis(2-hydroxyethyl)-1,4,8,11-tetraazacyclotetradecane]cadmium(II), [Cd(THEC)] ²⁺ . A ¹¹³ Cd NMR Study.....	97
4.3.3	Intramolecular Ligand Exchange of [1,4,8,11-Tetrakis(2-hydroxyethyl)-1,4,8,11-tetraazacyclotetradecane]cadmium(II), [Cd(THEC)] ²⁺ , and its Mercury(II) and Lead(II) Analogues. A Natural Abundance ¹³ C NMR Study.....	99
4.4	¹³ C Enriched [M(THEC*)] ²⁺ Spectra and Intramolecular Exchange Processes in <i>d</i> ₄ -Methanol.....	104
4.4.1	Intramolecular Ligand Exchange of [1,4,8,11-Tetrakis(2-hydroxyethyl)-1,4,8,11-tetraazacyclotetradecane]cadmium(II), [Cd(THEC*)] ²⁺ , in <i>d</i> ₄ -Methanol. A ¹³ C-Enriched NMR Study.....	104
4.4.2	Intramolecular Ligand Exchange of [1,4,8,11-Tetrakis(2-hydroxyethyl)-1,4,8,11-tetraazacyclotetradecane]mercury(II), [Hg(THEC*)] ²⁺ , and its Lead(II) Analogue in <i>d</i> ₄ -Methanol. A ¹³ C-Enriched NMR Study	105
4.4.3	[M(THEC*)] ²⁺ , Intramolecular Exchange Processes.....	110
4.5	Additional Studies of 1,4,8,11-Tetrakis(2-hydroxyethyl)-1,4,8,11-tetraazacyclotetradecane, THEC.....	113
4.5.1	[1,4,8,11-Tetrakis(2-hydroxyethyl)-1,4,8,11-tetraazacyclotetradecane]zinc(II), [Zn(THEC)] ²⁺ , in <i>d</i> ₄ -Methanol. A Natural Abundance ¹³ C NMR Study.....	113

4.5.2	[1,4,8,11-Tetrakis(2-hydroxyethyl)-1,4,8,11-tetraazacyclo- tetradecane]nickel(II), [Ni(THEC)] ²⁺ , in <i>d</i> ₄ -Methanol. A Natural Abundance ¹³ C NMR Investigation.....	114
4.5.3	1,4,8,11-Tetrakis(2-hydroxyethyl)-1,4,8,11-tetraazacyclo- tetradecane, THEC*, and [Ba(THEC*)] ²⁺ in <i>d</i> ₄ -Methanol. A Variable Temperature ¹³ C-Enriched NMR Study.....	115
4.5.4	Permutations of Coupling and Chemical Shift Differences of ¹³ C-Enriched Hydroxyethyl Arms of [M.THEC*] ²⁺	116
4.6	General Conclusions.....	119
Bibliography :		120
CHAPTER 5: Experimental.		123
5.1	Cryptands and Cryptates.....	123
5.1.1	Origin and Purification of Chemicals.....	123
5.1.2	Origin and Purification of Solvents.....	124
5.1.3	Synthesis and Purification of Cryptand.....	124
5.1.4	Crystal Preparation	126
5.1.5	X-Ray Structure Determination.....	126
5.1.6	Solution Studies, Potentiometric Titrations.....	128
5.1.7	Solution Studies, pH-metric Titrations in Aqueous Solution... ..	129
5.1.8	Solution Studies, Multinuclear Variable Temperature Nuclear Magnetic Resonance Spectroscopy.....	131
5.2	1,4,8,11-Tetrakis(2-hydroxyethyl)-1,4,8,11-tetraaza- cyclotetradecane, (THEC)	132
5.2.1	Origin and Purification of Chemicals.....	132
5.2.2	Nuclear Magnetic Resonance Spectroscopy.....	133
Bibliography :		135
CHAPTER 6: Analysis of the NMR Spectra for Chemical Systems Undergoing Site Exchange		137
6.1	Two-Site Lineshape Analysis.....	137
6.1.1	Simplified Kinetic Analysis for Systems in Slow Exchange....	142
6.1.2	Simplified Kinetic Analysis for Systems at Intermediate Rates of Exchange	143
6.1.3	Simplified Kinetic Analysis for Systems in Fast Exchange	145
6.2	Lineshape Analysis for Two-Site Exchange Between Coupled Sites.....	147
6.3	Calculation of Kinetic Parameters	152
6.3.1	NMR Data Handling.....	152
6.3.2	Calculation of Kinetic Data from the Results of Lineshape Analysis.....	153
Bibliography :		155

Publications : 157

Appendices:

A.i	FORTRAN-77 - Stability Constant Program STAB	Ai
A.ii	FORTRAN-77 - Titration Curve Program VISP.....	Avii
A.iii	FORTRAN-77 - Lineshape Program LINSHP.....	Axvi
A.iv	The Equivalence of Continuous Wave and Fourier Transform NMR for Chemical Exchange Phenomena.....	Axxviii
A.v	The Gutmann Donor Number, D_N , as a Measure of Solvent Strength	Axxx

Abstract:

The first part of this work entails the study of the complexation of various monovalent metal ions by the diaza-crown ether C21 and the cryptands, C211 and C22C₅ to form cryptates in various solvents. These results are discussed in conjunction with other studies on similar cryptands, C21C₅, C22C₂, C22C₈ and C221.

The stability constants of these complexes were measured in the various solvents by potentiometric titration, using either a sodium ion selective glass electrode, a silver wire electrode, or a pH-electrode.

The results are discussed in terms of the effects of the various metal ion - cryptand bonding interactions, the solvent interactions, and the influences of the different size and shapes of the various cryptands.

The kinetics of decomplexation of the cryptates were measured using ⁷Li and ²³Na variable temperature NMR. Subsequently, two-site lineshape analysis was used to derive the kinetic parameters of these systems. The mechanistic processes for the complexation and decomplexation of the cryptates are discussed in terms of the metal ion and cryptand cavity size, the effect of solvent, and the solid state structures obtained from single-crystal X-ray crystallography.

The second part of this work was to investigate the kinetics for the interaction of the pendant arm ligand 1,4,8,11-tetrakis(2-hydroxyethyl)-1,4,8,11-tetraazacyclotetradecane (THEC) with the divalent metal ions Cd²⁺, Hg²⁺ and Pb²⁺.

The mechanism of intramolecular exchange for [M(THEC)]²⁺ in *d*₄-methanol solution was investigated using ¹³C natural abundance and ¹³C selectively enriched, variable temperature NMR. As a result of this investigation, it is proposed that the mechanism for the intramolecular exchange is a novel transannular oscillation of the metal ion through the ligand.

Additional studies on intermolecular exchange for the [M(THEC)]²⁺ systems using NMR techniques, and theoretical aspects of the NMR spectral variations exhibited by strongly coupled ABA'B' systems undergoing site exchange are also discussed.

Acknowledgements :


I hereby wish to extend my most sincere gratitude and thanks to my supervisors Stephen Lincoln and John Coates for their inestimable help and encouragement throughout this project. I would also like to thank my many co-workers especially Ashley Stephens, Jeremy Lucas and Sue Brown, and all the other people in this department, for their invaluable aid and support, especially I would like to acknowledge my wife, Sue for the help and assistance she provided in proof-reading this thesis. Finally I would like to thank my parents for their patience and support for the last 26 years.

I wish to dedicate this thesis to my dearest of friends, Penny, Richard and of course, my wife Sue.

Statement :

To the best of my knowledge and belief, this thesis contains no material which has been submitted for any other degree or diploma in any University, nor any material previously published or written by another author except where due reference is made in the text.

I consent to making this thesis available for copying or loan.

Signed 

Philip Clarke

Abbreviations :

The following abbreviations have been used in this study:

C21	4,7,13-trioxa-1,10-diazacyclopentadecane
C22	4,7,13,16-tetraoxa-1,10-diazacyclooctadecane
C21C ₅	4,7,13-trioxa-1,10-diazabicyclo[8.5.5]eicosane
C22C ₂	4,7,13,16-tetraoxa-1,10-diazabicyclo[8.8.2]eicosane
C211	4,7,13,18-tetraoxa-1,10-diazabicyclo[8.5.5]eicosane
C22C ₅	4,7,13,16-tetraoxa-1,10-diazabicyclo[8.8.5]tricosane
C221	4,7,13,16,21-pentaoxa-1,10-diazabicyclo[8.8.5]tricosane
C22C ₈	4,7,13,16-tetraoxa-1,10-diazabicyclo[8.8.8]octacosane
C222	4,7,13,16,21,24-hexaoxa-1,10-diazabicyclo[8.8.8]octacosane
cyclam	1,4,8,11-tetraazacyclotetradecane
THEC	1,4,8,11-tetrakis(2-hydroxyethyl)-1,4,8,11-tetraazacyclotetradecane (tetrahydroxyethylcyclam)
THEC*	99 atom % ¹³ C enriched (in the hydroxyethyl arms) THEC
THEC-H	mono-deprotonated THEC
TMC	1,4,8,11-tetramethyl-1,4,8,11-tetraazacyclotetradecane (tetramethylcyclam)
DMF	N,N-dimethylformamide
DEF	N,N-diethylformamide
DMA	N,N-dimethylacetamide
propylene carbonate	1,2-propanediol cyclic carbonate
TEAP	tetraethylammonium perchlorate
TEAOH	tetraethylammonium hydroxide
TBAP	tetrabutylammonium perchlorate
TEACl	tetraethylammonium chloride
TEABr	tetraethylammonium bromide
<i>d_n</i> -	n-deuterated
<i>D_N</i>	Gutmann donor number
ΔG_d^\ddagger	free energy of activation (kJ mol ⁻¹)
ΔH_d^\ddagger	enthalpy of activation (kJ mol ⁻¹)
ΔS_d^\ddagger	entropy of activation (J K ⁻¹ mol ⁻¹)

Å	ångström (10^{-10} meters)
r	radius
pH	$-\log_{10}[\text{H}^+]$
pOH	$-\log_{10}[\text{OH}^-]$
[X]	concentration of species X (mol dm^{-3})
expt.	experimental
calc.	calculated
obs.	observed
R	universal gas constant ($8.314 \text{ J K}^{-1} \text{ mol}^{-1}$)
T	temperature (in degrees Kelvin)
mV	millivolts (10^{-3} volts)
ISE	ion -selective electrode
EMF	electromotive force (volts)
E	observed potential (volts)
E_0	standard electrode potential (volts)
NMR	nuclear magnetic resonance (spectroscopy)
DNMR	dynamic nuclear magnetic resonance (spectroscopy)
CPMAS	cross polarization, magic angle spinning
FID	free induction decay
FT	Fourier transform
cw	continuous wave
rf	radio frequency
Hz	hertz (s^{-1})
MHz	megahertz (10^6 s^{-1})
ppm	parts per million
δ	chemical shift (in ppm)
ω	resonant frequency (in rad. s^{-1})
ν	resonant frequency (in s^{-1})
$W_{1/2}$	the full width at half maximum resonance signal height. (s^{-1})
T_1	longitudinal relaxation time (s)
T_2	transverse relaxation time (s)
od	outer diameter (millimeters)
deg.	degree ($180/\pi$ radians)
J	internuclear coupling constant (s^{-1})
D	chemical shift difference in the absence of coupling (s^{-1} or ppm)



Chapter 1 : Cryptands and Cryptates - Structural Aspects

1.1 : Introduction to Cryptate Chemistry

Nobel Laureate C.J. Pedersen, in 1967, was first to discover the interesting complexation properties of macrocyclic crown ethers with alkali metal ions.^{1,2} When reacting catechol (which was a minor impurity in the reactants Pedersen used in his research into multidentate ligands for vanadyl groups) with *bis*(2-chloroethyl)ether in the presence of sodium hydroxide in the solvent 1-butanol, a white fibrous crystalline product formed (Figure 1.1). This crown ether product, dibenzo-18-crown-6, had a low solubility in methanol, but an increased solubility when in the presence of soluble Na⁺ salts.

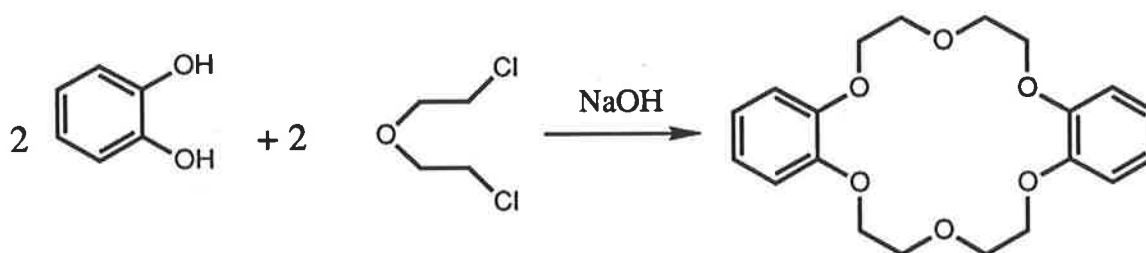


Figure 1.1 Formation of the crown ether, 2,3,11,12-dibenzo-1,4,7,10,13,16-hexaoxacyclooctadeca-2,11-diene (IUPAC), or dibenzo-18-crown-6.

The original and commonly used name, dibenzo-18-crown-6, denotes the eighteen membered ring, the 6 oxygen donor atoms in the ring, and the two benzo substituents. This was the first of the family of compounds known as *crown ethers*,^{2,3} so named because of its similarity to a crown in shape when viewed from the side.

A subsequent discovery in this field of research was by another Nobel Laureate, J.-M. Lehn,⁴ who in 1969 published the results of an idea to extend the two dimensional crown ethers into three dimensional crypt molecules using nitrogen-bridgeheads. The first published results in this area were of the synthesis of *cryptand* C222, and its reaction with the alkali metal ion potassium (K⁺) to form a *cryptate*, as shown in Figure 1.2.^{5,6}

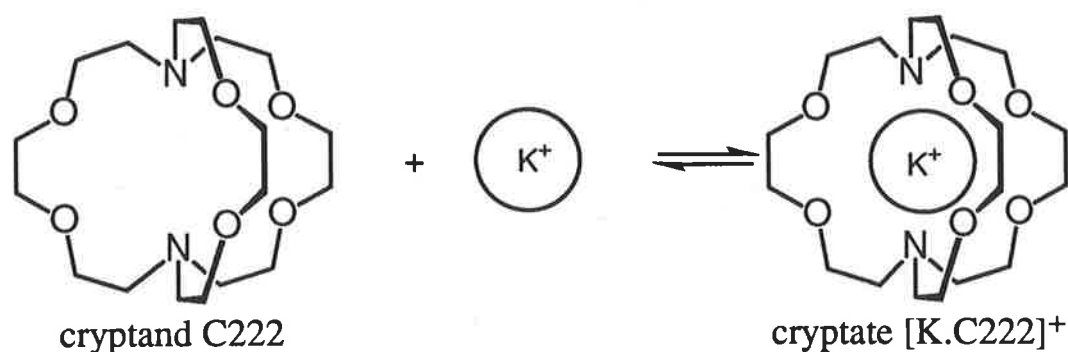


Figure 1.2 The cryptand 4,7,13,16,21,24-hexaoxa-1,10-diazabicyclo[8.8.8]-hexacosane (C222) and its potassium ion cryptate [K.C222]⁺.

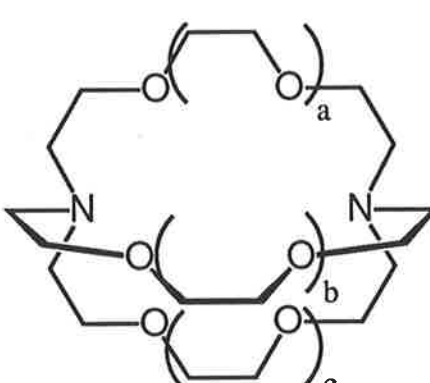
This initial work by Lehn *et al* was stimulated by the publication of the alkali metal ion complexation selectivity exhibited by naturally occurring macrocyclic complexes, nonactin, monactin, enniatin and valinomycin.⁷⁻⁹

Cryptate chemistry is part of a wider area of molecular recognition chemistry, which Lehn called *supramolecular chemistry*,^{10,11} to denote that the points of interest are the specific chemical interactions between two entities which do not include the formation of covalent bonds. The applications stemming from supramolecular chemistry have since become wide and diverse fields in both basic and applied research. Indeed the third Nobel Laureate⁴ D.J.Cram has said of supramolecular chemistry,¹² “by the turn of the century at least 40% of chemists will be directly employing molecular recognition systems”.

The cryptands are substrate specific receptor molecules, the study of which has been generated through the current interest in molecular recognition chemistry. The selective complexation of metal ions by cryptands and the stability of the cryptates formed, depends upon a number of factors. These include, the relative sizes of the cryptate cavity and the metal ion, the structural flexibility and the number and type of donor atoms of the cryptand, the bond strength, bond lability, type of interaction and solvation energy of the metal ion.^{10,11,13-19}

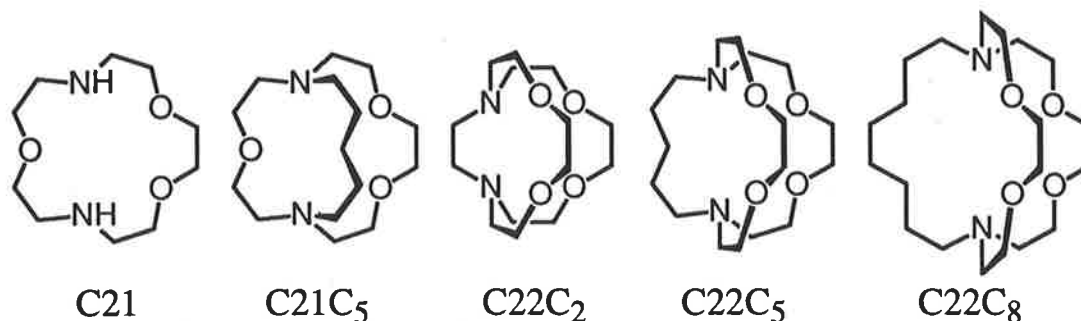
1.1.1: Structural Aspects of Cryptates

This study explores a number of specific thermodynamic and kinetic interactions of the alkali metal ions in a variety of solvents, with the cryptand C211, the aliphatic third bridge cryptand C22C₅, and the diaza-crown ether C21, which is similar to the cryptands with the exception that the third nitrogen to nitrogen bridge is absent, as may be seen in Figures 1.3 and 1.4. The structure of some aliphatic bridge cryptands discussed in this study are shown in Figure 1.4. The results are discussed and compared with those characterising other cryptands and diaza-crown ethers from the literature.

<u>Cryptands</u>	a	b	c	cryptand	donor atoms
	0	0	0	C111	5 (2N, 3O)
	1	0	0	C211	6 (2N, 4O)
	1	1	0	C221	7 (2N, 5O)
	1	1	1	C222	8 (2N, 6O)
	2	1	1	C322	9 (2N, 7O)
	2	2	1	C332	10 (2N, 8O)
	2	2	2	C333	11 (2N, 9O)
	1	0	C ₅	C21C ₅	5 (2N, 3O)
	1	1	C ₂	C22C ₂	6 (2N, 4O)
	1	1	C ₅	C22C ₅	6 (2N, 4O)
	1	1	C ₈	C22C ₈	6 (2N, 4O)

Where C_x denotes an aliphatic bridge CH_x units long.

Figure 1.3 Cryptand bridge size, and abbreviated nomenclature. Lengthening the bridges of the cryptands from C111 to C333 leads to a large but gradual change in radius of the cavity from about 0.5 to 2.4 Å.¹⁴



where:

C21 is 4,7,13-trioxa-1,10-diazacyclopentadecane;

C21C₅ is 4,7,13-trioxa-1,10-diazabicyclo[8.5.5]eicosane;

C22C₂ is 4,7,13,16-tetraoxa-1,10-diazabicyclo[8.8.2]eicosane;

C22C₅ is 4,7,13,16-tetraoxa-1,10-diazabicyclo[8.8.5]tricosane;

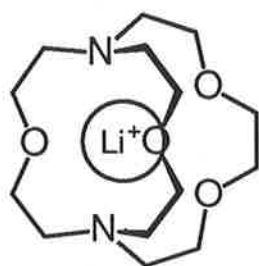
C22C₈ is 4,7,13,16-tetraoxa-1,10-diazabicyclo[8.8.8]hexacosane.

Figure 1.4 Diaza-crown ether C21 and selected aliphatic bridge cryptand structures and IUPAC nomenclatures.

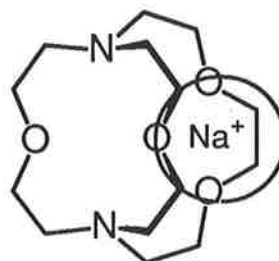
A knowledge of the structure of the cryptates formed through complexation of metal ions by cryptands is important in the interpretation of their thermodynamic and kinetic properties. Although the solid state structure of the cryptate cannot be assumed to unequivocally represent the cryptate structures in solution owing to solvation and conformational changes upon dissolution, such solid state structures appear to at least indicate the major structural characteristics of the cryptate in solution. A strong correlation exists between the cation size, cryptand cavity size, cryptate structure, and thermodynamic stability for complexation of the alkali metal ions with cryptands.¹⁴

Cryptates may exist in two extreme forms - *inclusive* or *exclusive*. In *inclusive* cryptates, the metal ion is encapsulated by the cryptand and has minimal interaction with the anion in the solid state or with the solvent in solution. For example, the cryptand C221 with a cavity radius of about 1.10 Å,¹⁴ accommodates the Na⁺ ion with a radius of 1.02 Å,²⁰ in the centre of the cryptand cavity to form *inclusive* [Na.221]⁺. However, in *exclusive* cryptates, the metal ion is located on an outside face of the cryptand, as delineated by two of the three nitrogen to nitrogen bridges (as a polyoxadiazacycloalkane ring as in Figure 1.5). In these cryptates, the anion(s) or solvent molecule may interact directly with the metal ion. The K⁺ (r = 1.38 Å) is too large to be

accommodated entirely within the cryptand C221, and thus forms an *exclusive* cryptate, $[\text{K.C221}]^+$.²¹ These size correlations, as illustrated in Table 1.1, are reflected in the variation of the stability of $[\text{M.C221}]^+$ with M^+ in the sequence $\text{Li}^+ < \text{Na}^+ > \text{K}^+$ for a range of solvents. These correlations of metal ion size with the stability of the cryptates are consistent with the Li^+ ion (radius = 0.76 Å) easily entering the C221 cavity to form an *inclusive* cryptate, but being too small to establish optimal bond distances, and the *inclusive* structure and optimal bonding distances of $[\text{Na.C221}]^+$ conferring a greater stability on this cryptate than that characterising the *exclusive* cryptate, $[\text{K.C221}]^+$.



cryptate $[\text{Li.C211}]^+$
(*inclusive*)



cryptate $[\text{Na.C211}]^+$
(*exclusive*)

Figure 1.5 An example of *inclusive*²² and *exclusive*²³ cryptates as determined by single crystal X-ray crystallography.

Table 1.1 Ionic Radii of the Alkali, Tl⁺, and Ag⁺ Metal Ions and Approximate Cavity Radii of Selected Cryptands.

Cation	Ionic Radius Å ^a	Cryptand	Cavity Radius Å ^b	Number of Coordinating Sites
Li ⁺	0.76	C111	0.5	5
Na ⁺	1.02	C211, C21C ₅	0.8	6, 5
K ⁺	1.38	C221, C22C ₅	1.1	7, 6
Rb ⁺	1.52	C222, C22C ₈	1.4	8, 6
Cs ⁺	1.67	C322	1.8	9
Ag ⁺	1.00	C332	2.1	10
Tl ⁺	1.50	C333	2.4	11
		C21 ^{c,d}	~1.1	5
		C22 ^d	~1.5	6

^a The values used in this study are based on those derived by Shannon²⁰ for six coordinate metal ions. The larger alkali metal ions, K⁺, Rb⁺ and Cs⁺, usually have a coordination number larger than six, and hence an ionic radii larger than that for six coordinate ions. Therefore it is assumed these values are the minimum appropriate ionic radius of the metal ions;

^b The cavity radii are based on the values derived by Lehn *et al*²⁴ and the values for the alkyl bridged cryptands are based on an isostructural cryptand;

^c C21 and C22 are not cryptands, but are closely related monocyclic diaza-crown ethers, and are considerably more flexible;

^d The value of ~1.1 Å for the radius of the C21 ring cavity was estimated from that for the isostructural crown ether, 1,4,7,10,13-pentaoxacyclopentadecane (15-crown-5), with allowances made for the binding site radii differences between oxygen and nitrogen donor atoms.¹⁴

1.2 : Crystal Structures of Some Alkali Metal Ion Cryptates

In this study a number of cryptate structures have been determined in the solid state by single crystal X-ray crystallography. These structures are the C22C₅ cryptates of the alkali metal ions Na⁺, K⁺, Cs⁺ and the hydronium ion H₃O⁺ (in all cases perchlorate anions are the counter ions). These structures are now discussed in detail.

1.2.1 : The Crystal Structure of [Na.C22C₅]ClO₄

The crystal structure determination of [Na.C22C₅]ClO₄ (Figure 1.6) indicates that the cryptate cation exists in the *exclusive* form in the solid state. Bond distances, bond angles and fractional atomic coordinates appear in Tables 1.2 and 1.3. The Na⁺ cation forms close interactions with the four ether oxygen atoms (O(4)...Na = 2.394(4), O(7)...Na = 2.453(4), O(13)...Na = 2.417(4), O(16)...Na = 2.481(3) Å) and lies slightly below the mean plane formed by cryptand oxygens O(4), O(7), O(13) and O(16) (atom labelling as in Figure 1.6). The endocyclic cryptand nitrogens do not interact significantly with Na⁺ as indicated by the bond distances, Na...N(1) = 3.003(5) Å, and Na...N(10) = 3.025(5) Å, and the nitrogens are 1.060(3) and 2.203(3) Å below the mean plane of the cryptand oxygens, respectively. The fifth coordination site about Na⁺ is an oxygen atom, O(21) from the ClO₄⁻ anion at a distance of 2.437(4) Å. To a reasonable approximation, the Na⁺ ion may be considered to be in a square-pyramidal environment. The remaining interatomic distances and angles of [Na.C22C₅]ClO₄ are as expected, and do not warrant further discussion.

The structure of *exclusive* [Na.C22C₅]⁺ contrasts with that of *inclusive* [Na.C221]⁺, where Na⁺ occupies the centre of the cryptand cavity and is within bonding distance for all five cryptand oxygens (O(4)...Na = 2.491(2), O(7)...Na = 2.499(2), O(13)...Na = 2.451, O(16)...Na = 2.519 and O(21)...Na = 2.446(2) Å) as well as within bonding distance to both the nitrogens (N(1)...Na = 2.703(3) and N(10)...Na = 2.591(2) and Å).¹⁶ This is the major structural consequence of replacing the donor oxygen of the third bridge in [Na.C221]⁺ with a methylene moiety to produce [Na.C22C₅]⁺. This demonstrates that although the nitrogen lone pairs in the [Na.C22C₅]⁺ cryptate are in the *endo-endo* configuration (where they are directed toward the centre of the cryptand cavity), the overall effect is that the electrostatic attraction of the lone pairs is insufficient to attract the Na⁺ into the cryptand cavity to form an

inclusive cryptate. In contrast, both $[\text{Li}.\text{C211}]^+$ and $[\text{Li}.\text{C21C}_5]^+$ (Li^+ $r = 0.76$ Å, cavity radius of C211 and C21C₅ are 0.8 Å) exist in the *inclusive* form in the solid state, despite the absence of an oxygen in the C₅ bridge of C21C₅.²⁵ The cryptand C21C₅ is less flexible than the larger C22C₅ so it is possible that the *inclusive* $[\text{Li}.\text{C21C}_5]^+$ formation is a consequence of the fortuitous appropriate disposition of the five donor atoms, which is not the case for C22C₅ where the C₅ bridge apparently prevents the attainment of a conformation similar to that of C22 in $[\text{K}.\text{C22}]^+$, where all six donor atoms are within bonding distance²⁶ ($\text{K}\dots\text{O} = 2.836(3)$, $2.825(3)$ and $\text{K}\dots\text{N} = 2.856(3)$ Å) and the SCN^- anion interacts significantly less with the metal ion ($\text{K}\dots\text{anion} = 3.33(1)$ Å). There is no $[\text{Na}.\text{C22}]^+$ structure available for comparison.

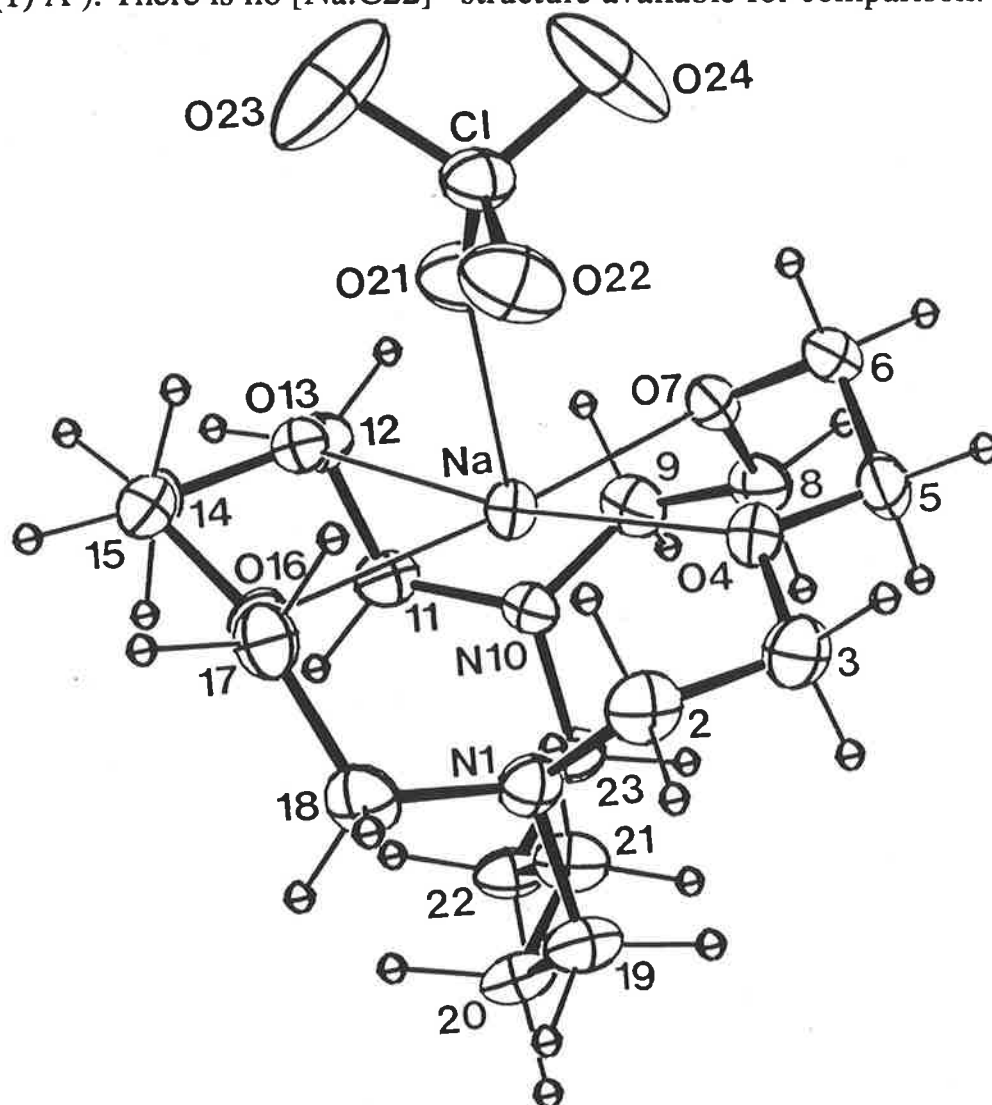


Figure 1.6 ORTEP²⁷ plot of the structure of $[\text{Na}.\text{C22C}_5]\text{ClO}_4$ showing atomic numbering. Atom centres are represented by 25% probability ellipsoids.

Table 1.2 Bond Distances (Å) and Bond Angles (deg.) for [Na.C22C₅](ClO₄)

O(4)	----	Na	2.394(4)	O(7)	----	Na	2.453(4)
O(13)	----	Na	2.417(4)	O(16)	----	Na	2.481(3)
O(21)	----	Na	2.437(4)	N(1)	----	C(2)	1.463(7)
N(1)	----	C(18)	1.467(6)	N(1)	----	C(19)	1.476(6)
C(2)	----	C(3)	1.508(7)	C(3)	----	O(4)	1.428(6)
O(4)	----	C(5)	1.418(6)	C(5)	----	C(6)	1.496(7)
C(6)	----	O(7)	1.432(6)	O(7)	----	C(8)	1.429(6)
C(8)	----	C(9)	1.498(8)	C(9)	----	N(10)	1.470(6)
N(10)	----	C(11)	1.468(6)	N(10)	----	C(23)	1.478(6)
C(11)	----	C(12)	1.531(7)	C(12)	----	O(13)	1.426(6)
O(13)	----	C(14)	1.419(6)	C(14)	----	C(15)	1.484(7)
C(15)	----	O(16)	1.423(5)	O(16)	----	C(17)	1.426(6)
C(17)	----	C(18)	1.501(7)	C(19)	----	C(20)	1.515(7)
C(20)	----	C(21)	1.496(7)	C(21)	----	C(22)	1.507(7)
C(22)	----	C(23)	1.507(7)	Cl	----	O(21)	1.424(4)
Cl	----	O(22)	1.417(4)	Cl	----	O(23)	1.386(5)
Cl	----	O(24)	1.393(5)				
O(4)	- Na	- O(7)	70.8(1)	O(4)	- Na	- O(13)	168.9(1)
O(4)	- Na	- O(16)	121.2(1)	O(7)	- Na	- O(13)	99.2(1)
O(7)	- Na	- O(16)	167.7(1)	O(13)	- Na	- O(16)	69.1(1)
O(4)	- Na	- O(21)	85.5(1)	O(7)	- Na	- O(21)	98.1(1)
O(13)	- Na	- O(21)	91.4(1)	O(16)	- Na	- O(21)	86.4(1)
C(2)	- N(1)	- C(18)	111.4(4)	C(2)	- N(1)	- C(19)	112.8(4)
C(18)	- N(1)	- C(19)	109.8(4)	N(1)	- C(2)	- C(3)	112.7(4)
C(2)	- C(3)	- O(4)	109.2(4)	C(3)	- O(4)	- C(5)	112.3(4)
O(4)	- C(5)	- C(6)	107.7(4)	C(5)	- C(6)	- O(7)	111.9(4)
C(6)	- O(7)	- C(8)	114.0(4)	O(7)	- C(8)	- C(9)	107.9(4)
C(8)	- C(9)	- N(10)	110.9(4)	C(9)	- N(10)	- C(11)	111.1(4)
C(9)	- N(10)	- C(23)	110.1(4)	C(11)	- N(10)	- C(23)	109.7(4)
N(10)	- C(11)	- C(12)	112.4(4)	C(11)	- C(12)	- O(13)	111.8(4)
C(12)	- O(13)	- C(14)	113.8(4)	O(13)	- C(14)	- C(15)	108.1(4)
C(14)	- C(15)	- O(16)	108.2(4)	C(15)	- O(16)	- C(17)	114.1(4)
O(16)	- C(17)	- C(18)	106.4(4)	N(1)	- C(18)	- C(17)	112.2(4)
N(1)	- C(19)	- C(20)	111.5(4)	C(19)	- C(20)	- C(21)	111.3(5)
C(20)	- C(21)	- C(22)	117.6(5)	C(21)	- C(22)	- C(23)	109.9(4)
N(10)	- C(23)	- C(22)	113.0(4)	O(21)	- Cl	- O(22)	110.5(2)
O(21)	- Cl	- O(23)	108.3(3)	O(21)	- Cl	- O(24)	109.2(3)
O(22)	- Cl	- O(23)	113.3(3)	O(22)	- Cl	- O(24)	108.4(3)
O(23)	- Cl	- O(24)	107.1(4)				

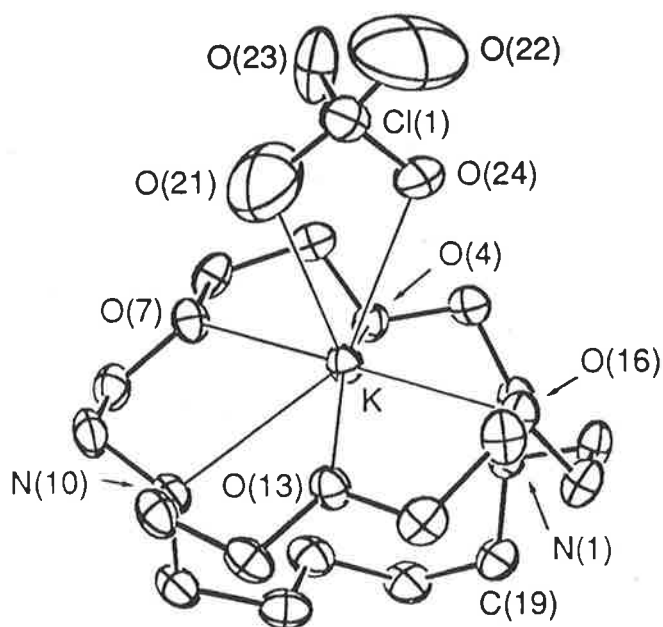
Table 1.3 Fractional Atomic Coordinates ($\times 10^4$) for $[\text{Na.C}_{22}\text{C}_5](\text{ClO}_4)$

Atom	x	y	z
Na	2951 (1)	1557 (1)	4033 (1)
N(1)	4095 (2)	0240 (2)	3364 (2)
C(2)	4065 (4)	0569 (3)	2590 (3)
C(3)	3181 (4)	0622 (4)	2283 (3)
O(4)	2704 (2)	1200 (2)	2734 (2)
C(5)	1854 (3)	1256 (3)	2497 (3)
C(6)	1451 (4)	1966 (3)	2926 (3)
O(7)	1469 (2)	1824 (2)	3726 (2)
C(8)	0832 (3)	1258 (3)	3992 (3)
C(9)	0875 (3)	1239 (3)	4840 (3)
N(10)	1651 (2)	0821 (2)	5067 (2)
C(11)	1914 (3)	1143 (3)	5841 (3)
C(12)	2260 (3)	2048 (3)	5799 (3)
O(13)	2975 (2)	2103 (2)	5312 (2)
C(14)	3754 (3)	1997 (3)	5693 (3)
C(15)	4436 (3)	2034 (3)	5120 (3)
O(16)	4346 (2)	1325 (2)	4628 (2)
C(17)	4965 (3)	1284 (3)	4045 (3)
C(18)	4913 (3)	0407 (3)	3719 (3)
C(19)	3901 (4)	-0674 (3)	3407 (3)
C(20)	3550 (4)	-0913 (3)	4176 (3)
C(21)	2731 (4)	-0467 (3)	4325 (3)
C(22)	2335 (3)	-0598 (3)	5093 (3)
C(23)	1524 (3)	-0105 (3)	5138 (3)
Cl	3955 (1)	3364 (1)	2978 (1)
O(21)	3535 (3)	2874 (2)	3540 (2)
O(22)	4454 (3)	2837 (3)	2510 (2)
O(23)	4413 (4)	3993 (4)	3339 (4)
O(24)	3358 (4)	3767 (4)	2526 (3)

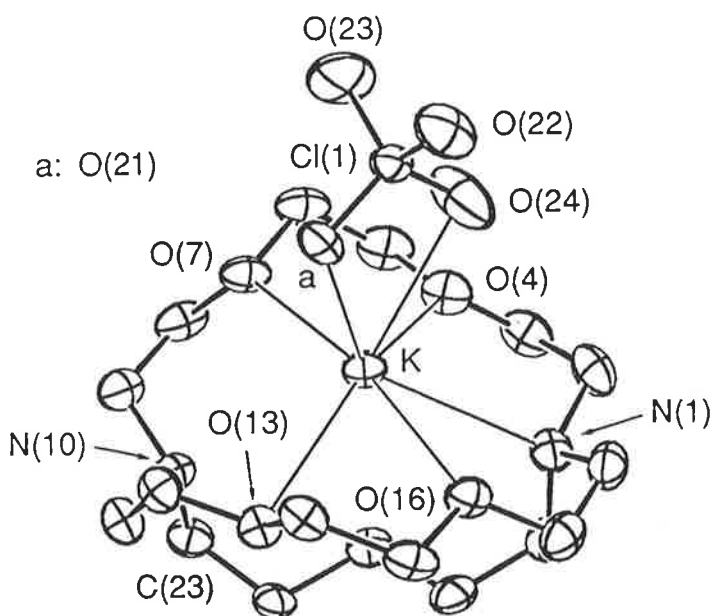
1.2.2 : The Crystal Structure of [K.C22C5]ClO₄

The crystal structure determination of [K.C22C₅]ClO₄ (Figure 1.7) shows that it is comprised of two independent species, labelled molecule a and b. Bond distances, bond angles and fractional atomic coordinates are shown in Tables 1.4 - 1.6. In molecule a of [K.C22C₅]ClO₄, (atomic numbering as labelled in Figure 1.7) K⁺ lies 0.369(1) Å above the mean plane of the four cryptand oxygens with which it has close interactions O(4a)...K = 2.844(4), O(7a)...K = 2.718(3), O(13a)...K = 2.689(4), O(16a)...K = 2.701(3) Å. However, the cryptand oxygens O(4a) and O(13a) are, respectively, 0.257(3) and 0.239(3) Å below the mean plane and O(7a) and O(16a) are, respectively, 0.257(4) and 0.252(4) Å above. As may be seen in the data above, the positions of the cryptand oxygens deviate significantly from a mean plane for molecule a in contrast to the almost coplanar cryptand oxygens of [Na.C22C₅]ClO₄. More distant interactions exist between K and the two cryptand nitrogens (K...N(1a) = 3.132(4), K...N(10a) = 2.939(4) Å) where N(1a) and N(10a) are, respectively, 1.581(4) and 1.180(4) Å below the mean plane of the cryptand oxygens. Two closer interactions occur between K and two oxygen atoms of the perchlorate anion (K...O(21a) = 2.900(5), K...O(24a) = 2.794 Å). Therefore K⁺ may be described as six-coordinate only if the six oxygen interactions are considered, and eight-coordinate if the two nitrogens are included.

Molecule b has a similar structure to molecule a as seen in Tables 1.4 - 1.6 and Figure 1.7. Deviations from the mean plane of the cryptand oxygens, O(4), O(7), O(13) and O(16) are -0.295(4), 0.286(4), -0.234(3) and 0.255(4) Å respectively. The K cation lies 0.441(1) Å above this plane.



Molecule a



Molecule b

Figure 1.7 ORTEP²⁷ plots of the structures of the two molecules a and b, in the asymmetric unit of $[K.C22C_5]ClO_4$ showing atomic numbering. Atom centres are drawn at 25% probability ellipsoids.

Table 1.4 Bond Distances (Å) and Bond Angles (deg.) for [K.C22C5](ClO₄)

O(4a)	---	K(1)	2.844(4)	O(4b)	---	K(2)	2.736(3)				
O(7a)	---	K(1)	2.718(3)	O(7b)	---	K(2)	2.739(4)				
O(13a)	---	K(1)	2.689(4)	O(13b)	---	K(2)	2.822(4)				
O(16a)	---	K(1)	2.701(3)	O(16b)	---	K(2)	2.710(4)				
N(1a)	---	K(1)	3.132(4)	N(4b)	---	K(2)	2.971(4)				
N(10a)	---	K(1)	2.939(4)	N(7b)	---	K(2)	3.256(4)				
O(21a)	---	K(1)	2.900(5)	O(21b)	---	K(2)	2.890(4)				
O(24a)	---	K(1)	2.794(5)	O(24b)	---	K(2)	2.883(4)				
C(2a)	---	N(1a)	1.470(7)	C(18a)	---	N(1a)	1.474(6)				
C(19a)	---	N(1a)	1.470(7)	C(3a)	---	C(2a)	1.491(7)				
O(4a)	---	C(3a)	1.413(5)	C(5a)	---	O(4a)	1.419(6)				
C(6a)	---	C(5a)	1.487(7)	O(7a)	---	C(6a)	1.411(7)				
C(8a)	---	O(7a)	1.430(7)	C(9a)	---	C(8a)	1.486(8)				
N(10a)	---	C(9a)	1.480(6)	C(11a)	---	N(10a)	1.467(7)				
C(23a)	---	N(10a)	1.493(7)	C(12a)	---	C(11a)	1.498(7)				
O(13a)	---	C(12a)	1.424(6)	C(14a)	---	O(13a)	1.421(6)				
C(15a)	---	C(14a)	1.517(8)	O(16a)	---	C(15a)	1.416(6)				
C(17a)	---	O(16a)	1.408(6)	C(18a)	---	C(17a)	1.522(8)				
C(20a)	---	C(19a)	1.529(8)	C(21a)	---	C(20a)	1.524(7)				
C(22a)	---	C(21a)	1.491(9)	C(23a)	---	C(22a)	1.557(7)				
C(2b)	---	N(1b)	1.480(7)	C(18b)	---	N(1b)	1.469(7)				
C(19b)	---	N(1b)	1.491(7)	C(3b)	---	C(2b)	1.491(9)				
O(4b)	---	C(3b)	1.409(7)	C(5b)	---	O(4b)	1.409(7)				
C(6b)	---	C(5b)	1.511(8)	O(7b)	---	C(6b)	1.412(7)				
C(8b)	---	O(7b)	1.413(7)	C(9b)	---	C(8b)	1.508(8)				
N(10b)	---	C(9b)	1.455(8)	C(11b)	---	N(10b)	1.481(6)				
C(23b)	---	N(10b)	1.477(6)	C(12b)	---	C(11b)	1.508(7)				
O(13b)	---	C(12b)	1.407(7)	C(14b)	---	O(13b)	1.425(6)				
C(15b)	---	C(14b)	1.502(8)	O(16b)	---	C(15b)	1.413(6)				
C(17b)	---	O(16b)	1.404(7)	C(18b)	---	C(17b)	1.483(7)				
C(20b)	---	C(19b)	1.532(8)	C(21b)	---	C(20b)	1.512(9)				
C(22b)	---	C(21b)	1.535(8)	C(23b)	---	C(22b)	1.497(9)				
O(21a)	---	Cl(1a)	1.374(9)	O(22a)	---	Cl(1a)	1.248(10)				
O(23a)	---	Cl(1a)	1.404(8)	O(23')	---	Cl(1a)	1.477(8)				
O(24a)	---	Cl(1a)	1.432(7)	O(24')	---	Cl(1a)	1.437(10)				
O(23')	---	O(22a)	1.826(12)	O(24')	---	O(24a)	1.516(14)				
O(21b)	---	Cl(1b)	1.425(4)	O(22b)	---	Cl(1b)	1.411(5)				
O(23b)	---	Cl(1b)	1.399(6)	O(24b)	---	Cl(1b)	1.373(4)				
O(13a)	-	K(1)	-	O(7a)	122.7(1)	O(16a)	-	K(1)	-	O(7a)	171.7(1)
O(16a)	-	K(1)	-	O(13a)	62.6(1)	O(7b)	-	K(2)	-	O(4b)	63.0(1)
O(16b)	-	K(2)	-	O(4b)	121.6(1)	O(16b)	-	K(2)	-	O(7b)	169.8(1)
C(18a)	-	N(1a)	-	C(2a)	108.4(4)	C(19a)	-	N(1a)	-	C(2a)	112.5(4)
C(19a)	-	N(1a)	-	C(18a)	109.9(4)	C(3a)	-	C(2a)	-	N(1a)	113.0(4)
O(4a)	-	C(3a)	-	C(2a)	106.9(4)	C(5a)	-	O(4a)	-	C(3a)	115.5(4)
C(6a)	-	C(5a)	-	O(4a)	106.4(4)	O(7a)	-	C(6a)	-	C(5a)	108.9(4)
C(6a)	-	O(7a)	-	K(1)	117.1(2)	C(8a)	-	O(7a)	-	K(1)	118.9(3)
C(8a)	-	O(7a)	-	C(6a)	113.3(4)	C(9a)	-	C(8a)	-	O(7a)	109.4(4)
N(10a)	-	C(9a)	-	C(8a)	115.0(4)	C(11a)	-	N(10a)	-	C(9a)	110.9(4)
C(23a)	-	N(10a)	-	C(9a)	111.4(4)	C(23a)	-	N(10a)	-	C(11a)	110.8(4)
C(12a)	-	C(11a)	-	N(10a)	115.0(4)	O(13a)	-	C(12a)	-	C(11a)	106.9(4)
C(12a)	-	O(13a)	-	K(1)	122.6(3)	C(14a)	-	O(13a)	-	K(1)	119.4(3)
C(14a)	-	O(13a)	-	C(12a)	112.0(4)	C(15a)	-	C(14a)	-	O(13a)	107.8(4)
O(16a)	-	C(15a)	-	C(14a)	112.3(5)	C(15a)	-	O(16a)	-	K(1)	109.8(2)
C(17a)	-	O(16a)	-	K(1)	119.6(3)	C(17a)	-	O(16a)	-	C(15a)	113.8(4)
C(18a)	-	C(17a)	-	O(16a)	107.7(4)	C(17a)	-	C(18a)	-	N(1a)	114.2(4)
C(20a)	-	C(19a)	-	N(1a)	115.1(4)	C(21a)	-	C(20a)	-	C(19a)	117.1(5)
C(22a)	-	C(21a)	-	C(20a)	114.3(5)	C(23a)	-	C(22a)	-	C(21a)	112.7(5)
C(22a)	-	C(23a)	-	N(10a)	112.6(4)	C(18b)	-	N(1b)	-	C(2b)	109.6(4)
C(19b)	-	N(1b)	-	C(2b)	111.5(4)	C(19b)	-	N(1b)	-	C(18b)	111.4(5)
C(3b)	-	C(2b)	-	N(1b)	113.0(5)	O(4b)	-	C(3b)	-	C(2b)	109.2(4)
C(3b)	-	O(4b)	-	K(2)	121.1(3)	C(5b)	-	O(4b)	-	K(2)	117.0(3)

Table 1.4 Continued

C(5b) - O(4b) - C(3b)	114.8(4)	C(6b) - C(5b) - O(4b)	108.9(4)
O(7b) - C(6b) - C(5b)	113.3(5)	C(6b) - O(7b) - K(2)	107.2(3)
C(8b) - O(7b) - K(2)	123.1(3)	C(8b) - O(7b) - C(6b)	113.5(4)
C(9b) - C(8b) - O(7b)	108.6(4)	N(10b) - C(9b) - C(8b)	113.6(5)
C(11b) - N(10b) - C(9b)	110.7(4)	C(23b) - N(10b) - C(9b)	110.9(4)
C(23b) - N(10b) - C(11b)	110.5(4)	C(12b) - C(11b) - N(10b)	112.8(4)
O(13b) - C(12b) - C(11b)	107.5(4)	C(14b) - O(13b) - C(12b)	114.0(3)
C(15b) - C(14b) - O(13b)	107.3(4)	O(16b) - C(15b) - C(14b)	107.7(4)
C(15b) - O(16b) - K(2)	117.4(3)	C(17b) - O(16b) - K(2)	122.3(3)
C(17b) - O(16b) - C(15b)	114.7(4)	C(18b) - C(17b) - O(16b)	108.8(5)
C(17b) - C(18b) - N(1b)	115.4(5)	C(20b) - C(19b) - N(1b)	113.3(4)
C(21b) - C(20b) - C(19b)	113.5(5)	C(22b) - C(21b) - C(20b)	112.7(5)
C(23b) - C(22b) - C(21b)	111.6(5)	C(22b) - C(23b) - N(10b)	111.9(4)
O(22a) - Cl(1a) - O(21a)	168.8(5)	O(23a) - Cl(1a) - O(21a)	88.5(5)
O(23a) - Cl(1a) - O(22a)	91.0(6)	O(23') - Cl(1a) - O(21a)	85.8(5)
O(23') - Cl(1a) - O(22a)	83.7(6)	O(23') - Cl(1a) - O(23a)	106.2(5)
O(24a) - Cl(1a) - O(21a)	95.6(5)	O(24a) - Cl(1a) - O(22a)	95.6(5)
O(24a) - Cl(1a) - O(23a)	96.1(5)	O(24a) - Cl(1a) - O(23')	157.6(5)
O(24') - Cl(1a) - O(21a)	87.3(5)	O(24') - Cl(1a) - O(22a)	97.1(6)
O(24') - Cl(1a) - O(23a)	158.9(5)	O(24') - Cl(1a) - O(23')	94.0(5)
O(24') - Cl(1a) - O(24a)	63.8(5)	O(23') - O(22a) - Cl(1a)	53.5(5)
O(22a) - O(23') - Cl(1a)	42.8(3)	O(24') - O(24a) - Cl(1a)	58.3(4)
O(24a) - O(24') - Cl(1a)	57.9(5)	O(22b) - Cl(1b) - O(21b)	111.0(3)
O(23b) - Cl(1b) - O(21b)	111.6(3)	O(23b) - Cl(1b) - O(22b)	105.0(3)
O(24b) - Cl(1b) - O(21b)	108.6(3)	O(24b) - Cl(1b) - O(22b)	108.0(3)
O(24b) - Cl(1b) - O(23b)	112.5(4)		

Table 1.5 Fractional Atomic Coordinates ($\times 10^4$) for $[\text{K}.\text{C}_{22}\text{C}_5](\text{ClO}_4)$

Atom	x	y	z
K(1)	2613(1)	1738(1)	656(1)
K(2)	-2143(1)	3358(1)	7020(1)
N(1a)	1807(3)	165(3)	-1576(3)
C(2a)	2257(4)	-602(3)	-1325(4)
C(3a)	2723(4)	-479(3)	-61(4)
O(4a)	3585(3)	250(2)	176(3)
C(5a)	4199(4)	413(3)	1310(4)
C(6a)	5057(4)	1192(3)	1364(5)
O(7a)	4665(2)	1980(2)	1296(3)
C(8a)	5314(4)	2652(4)	876(5)
C(9a)	4855(4)	3464(3)	865(5)
N(10a)	3878(3)	3302(3)	36(3)
C(11a)	3330(4)	4029(3)	338(5)
C(12a)	2247(4)	3836(3)	-290(5)
O(13a)	1714(3)	3068(2)	72(3)
C(14a)	656(4)	2857(4)	-411(5)
C(15a)	158(4)	2054(3)	59(5)
O(16a)	590(2)	1284(2)	-210(3)
C(17a)	230(4)	774(4)	-1365(5)
C(18a)	719(4)	-51(3)	-1503(5)
C(19a)	1921(4)	357(4)	-2737(4)
C(20a)	3020(5)	667(4)	-2891(5)
C(21a)	3673(4)	1502(4)	-2013(5)
C(22a)	3303(4)	2361(4)	-2045(5)
C(23a)	4036(4)	3210(4)	-1205(5)
N(1b)	-4052(3)	3517(3)	5553(4)
C(2b)	-4824(4)	2742(4)	5699(5)
C(3b)	-4540(4)	1843(4)	5380(5)
O(4b)	-3659(3)	1826(3)	6168(3)
C(5b)	-3367(5)	980(3)	6034(5)
C(6b)	-2423(5)	1062(4)	6937(5)
O(7b)	-1580(3)	1710(2)	6814(3)

Table 1.5 Continued

C(8b)	-1066 (5)	1379 (4)	5926 (5)
C(9b)	-164 (4)	2117 (4)	5906 (5)
N(10b)	-445 (3)	2887 (3)	5464 (3)
C(11b)	394 (4)	3709 (4)	5863 (5)
C(12b)	267 (4)	4329 (4)	6955 (5)
O(13b)	-575 (3)	4712 (2)	6647 (3)
C(14b)	-691 (4)	5429 (3)	7540 (4)
C(15b)	-1613 (4)	5761 (3)	7075 (5)
O(16b)	-2475 (3)	5048 (2)	6952 (3)
C(17b)	-3379 (4)	5187 (4)	6333 (5)
C(18b)	-4204 (4)	4374 (4)	6226 (5)
C(19b)	-4083 (4)	3549 (4)	4289 (5)
C(20b)	-3024 (4)	3776 (4)	3976 (5)
C(21b)	-2473 (4)	2999 (4)	3944 (4)
C(22b)	-1384 (4)	3263 (4)	3720 (4)
C(23b)	-725 (4)	2665 (4)	4169 (4)
C(11a)	2265 (1)	1703 (1)	-6396 (2)
O(21a)	2991 (6)	2259 (7)	3200 (6)
O(22a)	1663 (7)	1311 (7)	4154 (7)
O(23a)	3026 (5)	1266 (5)	4021 (7)
O(23') ^a	2323 (7)	2510 (5)	4533 (7)
O(24a)	1894 (6)	1063 (6)	2508 (6)
O(24') ^a	1514 (7)	1937 (6)	2784 (8)
C(11b)	-2214 (1)	3493 (1)	-46 (1)
O(21b)	-1370 (3)	3929 (3)	-481 (4)
O(22b)	-2434 (3)	4090 (3)	897 (4)
O(23b)	-2004 (4)	2749 (3)	417 (5)
O(24b)	-3054 (3)	3253 (5)	-932 (4)

^a Atom has site occupancy factor = 0.562(1); see Experimental

Table 1.6 Geometric Parameters (deg) for K⁺ in [K.C22C₅](ClO₄)

Molecule a			
K...O(4)	2.844 (4)	K...O(7)	2.718 (3)
K...O(13)	2.689 (4)	K...O(16)	2.701 (3)
K...N(1)	3.132 (4)	K...N(10)	2.939 (4)
K...O(21)	2.900 (5)	K...O(24)	2.794 (5)
O(4)...K...O(7)	59.5 (1)	O(4)...K...O(13)	154.0 (1)
O(4)...K...O(16)	112.8 (1)	O(4)...K...N(10)	106.3 (1)
O(4)...K...O(21)	104.5 (1)	O(4)...K...O(24)	90.7 (1)
O(7)...K...O(13)	122.7 (1)	O(7)...K...O(16)	171.7 (1)
O(7)...K...N(10)	63.0 (1)	O(7)...K...O(21)	75.7 (1)
O(7)...K...O(24)	102.7 (1)	O(13)...K...O(16)	62.6 (1)
O(13)...K...N(10)	62.0 (1)	O(13)...K...O(21)	100.8 (1)
O(13)...K...O(24)	112.4 (1)	O(16)...K...N(10)	119.4 (1)
O(16)...K...O(21)	110.5 (1)	O(16)...K...O(24)	79.7 (1)
N(10)...K...O(21)	101.8 (1)	N(10)...K...O(24)	144.3 (1)
O(21)...K...O(24)	42.8 (1)		
Molecule b			
K...O(4)	2.7376 (3)	K...O(7)	2.739 (4)
K...O(13)	2.822 (4)	K...O(16)	2.710 (4)
K...N(1)	2.971 (4)	K...N(10)	3.256 (4)
K...O(21)	2.890 (4)	K...O(24)	2.883 (4)
O(4)...K...O(7)	63.0 (1)	O(4)...K...O(13)	150.2 (1)
O(4)...K...O(16)	121.6 (1)	O(4)...K...N(1)	61.3 (1)
O(4)...K...O(21)	119.9 (1)	O(4)...K...O(24)	79.6 (1)
O(7)...K...O(13)	110.7 (1)	O(7)...K...O(16)	169.8 (1)
O(7)...K...N(1)	120.0 (1)	O(7)...K...O(21)	95.0 (1)
O(7)...K...O(24)	96.9 (1)	O(13)...K...O(16)	60.5 (1)
O(13)...K...N(1)	106.4 (1)	O(13)...K...O(21)	89.0 (1)
O(13)...K...O(24)	129.9 (1)	O(16)...K...N(1)	61.6 (1)
O(16)...K...O(21)	90.0 (1)	O(16)...K...O(24)	93.1 (1)
N(1)...K...O(21)	131.4 (1)	N(1)...K...O(24)	93.7 (1)
O(21)...K...O(24)	46.3 (1)		

1.2.3 : The Crystal Structure of [Cs.C₂₂C₅]ClO₄

The crystal structure determination of [Cs.C₂₂C₅]ClO₄ (Figure 1.8) shows two anions and two cryptates per unit cell in the structures, which are identical. Bond distances, bond angles and fractional atomic coordinates are shown in Tables 1.7 - 1.9. The Cs⁺ ion lies 1.2996 Å above the mean plane of the four cryptand oxygens, with which it has close interactions O(4)...Cs = 3.069(4), O(7)...Cs = 3.012(5), O(13)...Cs = 3.275(4) and O(16)...Cs = 3.023(5) Å. The four cryptand oxygens, O(4), O(7), O(13), O(16), deviate significantly from the mean plane, where O(4) and O(13) are, respectively, 0.263(5) and 0.257(4) Å below the mean plane and O(7) and O(16) are, respectively, 0.319(5) and 0.318(4) Å above the mean plane. More distant interactions exist between Cs and the two cryptand nitrogens (Cs...N(1) = 3.395(5), and Cs...N(10) = 3.703(5) Å), where N(1) and N(10) are, respectively, 0.988(6) and 1.242(5) Å below the mean plane of the cryptand oxygens. Interactions also occur between Cs⁺ and two perchlorate anions (Cs...O(22) = 3.348(8), Cs...O(23) = 3.407, Cs...O(23') = 3.447(5) Å, where the primed atom is related by a crystallographic centre of inversion). Thus Cs⁺ may be described as seven-coordinate if the seven oxygen interactions are included, and nine-coordinate if the two nitrogens interactions are also considered. As may be seen from Figure 1.8, O(23) of the perchlorate anion bridges the two Cs⁺ ions, leading to a loosely associated donor in the crystalline state. The remaining interatomic distances and angles are as anticipated and do not merit further discussion.

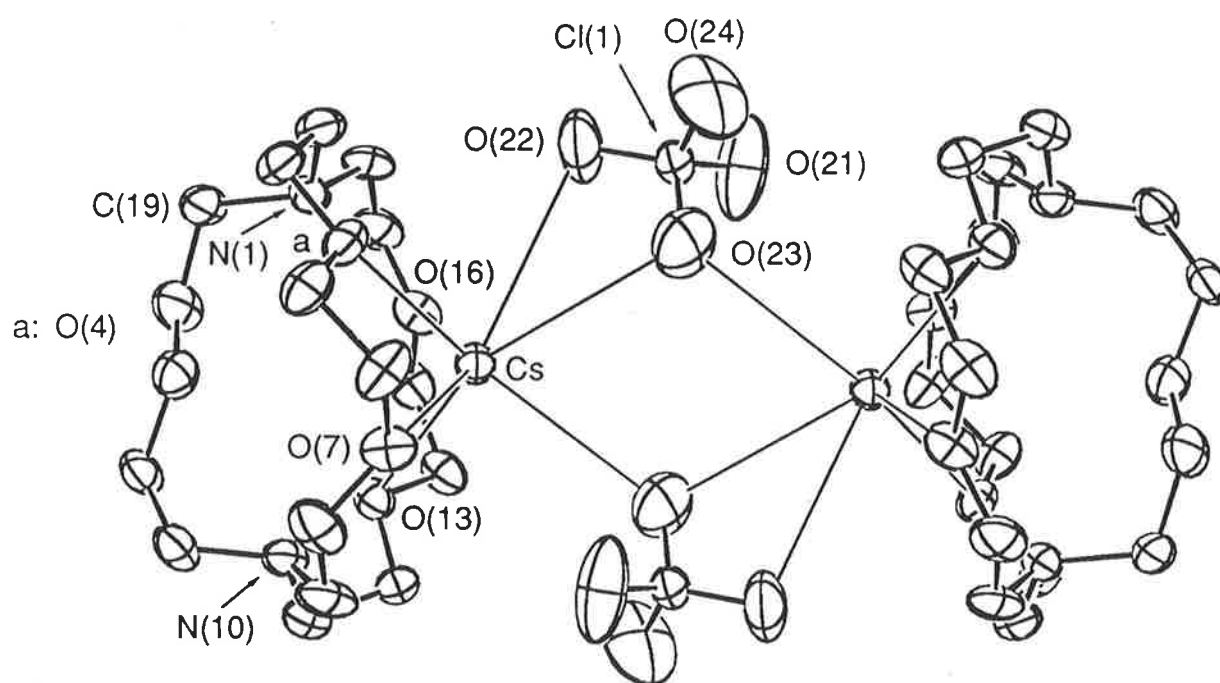


Figure 1.8 ORTEP²⁷ plot of the structure of [Cs.C₂₂C₅]ClO₄ showing atomic numbering and the two identical cryptates of the unit cell which are related by a centre of inversion. Atom centres are represented by 25% probability ellipsoids.

Table 1.7 Bond Distances (Å) and Bond Angles (deg.) for [Cs.C22C₅](ClO₄)

N(1)	---	Cs	3.390 (5)	O(4)	---	Cs	3.069 (4)				
O(7)	---	Cs	3.012 (5)	O(13)	---	Cs	3.275 (4)				
O(16)	---	Cs	3.023 (5)	O(22)	---	Cs	3.348 (8)				
C(2)	---	N(1)	1.444 (8)	C(18)	---	N(1)	1.458 (9)				
C(19)	---	N(1)	1.481 (8)	C(3)	---	C(2)	1.503 (10)				
O(4)	---	C(3)	1.424 (7)	C(5)	---	O(4)	1.414 (8)				
C(6)	---	C(5)	1.468 (10)	O(7)	---	C(6)	1.450 (9)				
C(8)	---	O(7)	1.363 (9)	C(9)	---	C(8)	1.496 (11)				
N(10)	---	C(9)	1.471 (9)	C(11)	---	N(10)	1.440 (9)				
C(23)	---	N(10)	1.476 (9)	C(12)	---	C(11)	1.508 (10)				
O(13)	---	C(12)	1.416 (8)	C(14)	---	O(13)	1.397 (8)				
C(15)	---	C(14)	1.486 (11)	O(16)	---	C(15)	1.412 (8)				
C(17)	---	O(16)	1.385 (9)	C(18)	---	C(17)	1.494 (10)				
C(20)	---	C(19)	1.482 (10)	C(21)	---	C(20)	1.467 (11)				
C(22)	---	C(21)	1.522 (11)	C(23)	---	C(22)	1.528 (10)				
O(21)	---	Cl(1)	1.349 (8)	O(22)	---	Cl(1)	1.373 (6)				
O(23)	---	Cl(1)	1.402 (8)	O(24)	---	Cl(1)	1.332 (8)				
O(4)	-	Cs	-	N(1)	54.7 (1)	O(7)	-	Cs	-	N(1)	103.2 (1)
O(7)	-	Cs	-	O(4)	56.4 (1)	O(13)	-	Cs	-	N(1)	87.4 (1)
O(13)	-	Cs	-	O(4)	120.9 (1)	O(13)	-	Cs	-	O(7)	101.3 (1)
O(16)	-	Cs	-	N(1)	54.0 (1)	O(16)	-	Cs	-	O(4)	108.6 (1)
O(16)	-	Cs	-	O(7)	141.2 (1)	O(16)	-	Cs	-	O(13)	52.6 (1)
O(22)	-	Cs	-	N(1)	69.3 (1)	O(22)	-	Cs	-	O(4)	76.4 (2)
O(22)	-	Cs	-	O(7)	120.7 (2)	O(22)	-	Cs	-	O(13)	135.1 (2)
O(22)	-	Cs	-	O(16)	83.2 (2)	C(2)	-	N(1)	-	Cs	98.1 (3)
C(18)	-	N(1)	-	Cs	94.4 (4)	C(18)	-	N(1)	-	C(2)	109.9 (5)
C(19)	-	N(1)	-	Cs	128.5 (4)	C(19)	-	N(1)	-	C(2)	112.3 (6)
C(19)	-	N(1)	-	C(18)	111.4 (6)	C(3)	-	C(2)	-	N(1)	115.6 (6)
O(4)	-	C(3)	-	C(2)	109.3 (5)	C(3)	-	O(4)	-	Cs	124.0 (4)
C(5)	-	O(4)	-	Cs	118.7 (4)	C(5)	-	O(4)	-	C(3)	112.4 (5)
C(6)	-	C(5)	-	O(4)	109.8 (6)	O(7)	-	C(6)	-	C(5)	113.4 (6)
C(6)	-	O(7)	-	Cs	108.5 (4)	C(8)	-	O(7)	-	Cs	129.6 (4)
C(8)	-	O(7)	-	C(6)	115.5 (6)	C(9)	-	C(8)	-	O(7)	112.4 (6)
N(10)	-	C(9)	-	C(8)	115.5 (6)	C(11)	-	N(10)	-	C(9)	112.8 (5)
C(23)	-	N(10)	-	C(9)	110.6 (6)	C(23)	-	N(10)	-	C(11)	109.1 (6)
C(12)	-	C(11)	-	N(10)	114.2 (6)	O(13)	-	C(12)	-	C(11)	107.7 (5)
C(12)	-	O(13)	-	Cs	96.4 (3)	C(14)	-	O(13)	-	Cs	92.0 (4)
C(14)	-	O(13)	-	C(12)	113.0 (6)	C(15)	-	C(14)	-	O(13)	108.3 (6)
O(16)	-	C(15)	-	C(14)	109.4 (6)	C(15)	-	O(16)	-	Cs	119.3 (4)
C(17)	-	O(16)	-	Cs	124.7 (4)	C(17)	-	O(16)	-	C(15)	114.6 (6)
C(18)	-	C(17)	-	O(16)	110.6 (6)	C(17)	-	C(18)	-	N(1)	116.4 (6)
C(20)	-	C(19)	-	N(1)	115.7 (6)	C(21)	-	C(20)	-	C(19)	115.9 (7)
C(22)	-	C(21)	-	C(20)	114.5 (7)	C(23)	-	C(22)	-	C(21)	111.5 (6)
C(22)	-	C(23)	-	N(10)	111.2 (6)	O(22)	-	Cl(1)	-	O(21)	116.8 (5)
O(23)	-	Cl(1)	-	O(21)	111.4 (7)	O(23)	-	Cl(1)	-	O(22)	112.3 (5)
O(24)	-	Cl(1)	-	O(21)	105.2 (8)	O(24)	-	Cl(1)	-	O(22)	111.0 (7)
O(24)	-	Cl(1)	-	O(23)	98.2 (8)	Cl(1)	-	O(22)	-	Cs	102.8 (4)

Table 1.8 Fractional Atomic Coordinates ($\times 10^5$ for Cs, $\times 10^4$ others) for $[\text{Cs.C}_{22}\text{C}_5](\text{ClO}_4)$

Atom	x	y	z
Cs	65181 (2)	36404 (4)	50451 (2)
N(1)	7478 (4)	684 (6)	5968 (3)
C(2)	7716 (5)	1200 (7)	6818 (4)
C(3)	8415 (5)	2307 (8)	6977 (4)
O(4)	8086 (3)	3556 (4)	6544 (3)
C(5)	8730 (5)	4615 (8)	6615 (5)
C(6)	8341 (5)	5894 (8)	6191 (5)
O(7)	8004 (3)	5711 (5)	5297 (3)
C(8)	8582 (6)	5984 (9)	4803 (6)
C(9)	8221 (6)	5627 (8)	3903 (5)
N(10)	8130 (3)	4121 (6)	3711 (3)
C(11)	7642 (5)	3846 (7)	2872 (5)
C(12)	6688 (5)	3524 (7)	2816 (4)
O(13)	6640 (3)	2243 (5)	3242 (3)
C(14)	5789 (4)	1719 (9)	3120 (5)
C(15)	5816 (5)	385 (9)	3596 (5)
O(16)	6063 (3)	669 (5)	4464 (3)
C(17)	6252 (6)	-510 (9)	4967 (5)
C(18)	6663 (5)	-104 (8)	5847 (5)
C(19)	8183 (6)	-161 (8)	5738 (5)
C(20)	8385 (5)	169 (9)	4914 (6)
C(21)	8743 (6)	1571 (8)	4832 (6)
C(22)	8940 (5)	1875 (8)	3977 (5)
C(23)	8997 (5)	3451 (8)	3826 (5)
Cl(1)	5051 (1)	3754 (2)	6684 (1)
O(21)	4195 (5)	3458 (8)	6411 (9)
O(22)	5632 (5)	2688 (7)	6650 (6)
O(23)	5278 (6)	4999 (9)	6327 (7)
O(24)	5128 (7)	4213 (17)	7467 (5)

Table 1.9 Geometric Parameters (deg) for Cs^+ in $[\text{Cs.C}_{22}\text{C}_5](\text{ClO}_4)$

Cs...O(4)	3.069 (4)	Cs...O(7)	3.012 (5)
Cs...O(13)	3.275 (4)	Cs...O(16)	3.023 (5)
Cs...N(1)	3.395 (5)	Cs...N(10)	3.703 (5)
Cs...O(22)	3.348 (8)	Cs...O(23)	3.407 (5)
Cs...O(23) ^a	3.447 (5)		
O(4)...Cs...O(7)	56.5 (1)	O(4)...Cs...O(13)	120.9 (1)
O(4)...Cs...O(16)	108.6 (1)	O(4)...Cs...O(22)	76.4 (1)
O(4)...Cs...O(23)	89.1 (1)	O(4)...Cs...O(23) ^a	158.0 (1)
O(7)...Cs...O(13)	101.3 (1)	O(7)...Cs...O(16)	141.2 (1)
O(7)...Cs...O(22)	120.7 (1)	O(7)...Cs...O(23)	101.2 (1)
O(7)...Cs...O(23) ^a	109.9 (1)	O(13)...Cs...O(16)	52.6 (1)
O(13)...Cs...O(22)	135.2 (1)	O(13)...Cs...O(23)	149.3 (1)
O(13)...Cs...O(23) ^a	76.5 (1)	O(16)...Cs...O(22)	83.2 (1)
O(16)...Cs...O(23)	115.0 (1)	O(16)...Cs...O(23) ^a	92.6 (1)
O(22)...Cs...O(23)	39.9 (1)	O(22)...Cs...O(23) ^a	101.1 (1)
O(23)...Cs...O(23) ^a	76.3 (1)		

^a primed atom related by centre of inversion

1.2.4 : The Crystal Structure of $[\text{H}_3\text{O}.\text{C}_{22}\text{H}_{28}\text{N}_2]\text{ClO}_4$

The crystal structure determination of $[\text{H}_3\text{O}.\text{C}_{22}\text{H}_{28}\text{N}_2]\text{ClO}_4$ (Figure 1.9) shows that the ClO_4^- anion does not interact with the cryptate with any appreciable significance. Bond distances, bond angles and fractional atomic coordinates are shown in Tables 1.10 - 1.12. The four cryptand oxygen atoms, O(4), O(7), O(13) and O(16), are coplanar to within $\pm 0.019(4)$ Å and the H_3O^+ oxygen O(1) atom lies $0.666(3)$ Å above the plane. The four cryptand oxygens and the two endocyclic nitrogens interact significantly with the H_3O^+ ion where the distances are $\text{O}(1)\dots\text{O}(4) = 2.862(5)$, $\text{O}(1)\dots\text{O}(7) = 3.016(5)$, $\text{O}(1)\dots\text{O}(13) = 3.028(5)$, $\text{O}(1)\dots\text{O}(16) = 2.869(5)$, $\text{O}(1)\dots\text{N}(1) = 3.180(5)$ and $\text{O}(1)\dots\text{N}(10) = 2.853(5)$ Å. The location of three residual electron density peaks in the vicinity of the O(1) atom is consistent with the presence of three protons, and confirms the assignment of the cation as H_3O^+ . As may be seen from the ORTEP plot in Figure 1.9, the H_3O^+ ion is six coordinate and the C_5 bridge is reasonably distant from the O(1) centre.

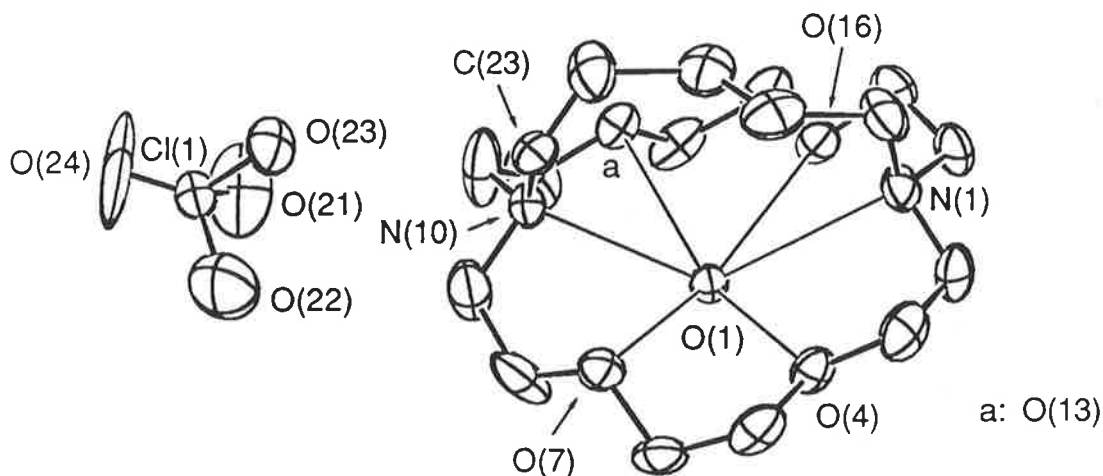


Figure 1.9 ORTEP²⁷ plot of the structure of $[\text{H}_3\text{O}.\text{C}_{22}\text{H}_{28}\text{N}_2]\text{ClO}_4$ showing the atomic numbering, with atoms drawn at 25% probability ellipsoids.

Table 1.10 Bond Distances (Å), Bond Angles (deg.) for [H₃O.C₂₂C₅]ClO₄

O(1)	---	O(4)	2.862(5)	O(1)	---	O(7)	3.016(5)				
O(1)	---	O(13)	3.028(5)	O(1)	---	O(16)	2.869(5)				
O(1)	---	N(1)	3.180(5)	O(1)	---	N(10)	2.853(5)				
Hw(1)	---	O(1)	1.090(3)	Hw(2)	---	O(1)	1.178(3)				
Hw(3)	---	O(1)	0.663(3)	C(2)	---	N(1)	1.458(7)				
C(18)	---	N(1)	1.460(7)	C(19)	---	N(1)	1.446(7)				
C(3)	---	C(2)	1.486(8)	O(4)	---	C(3)	1.427(7)				
C(5)	---	O(4)	1.413(6)	C(6)	---	C(5)	1.458(8)				
O(7)	---	C(6)	1.414(6)	C(8)	---	O(7)	1.419(7)				
C(9)	---	C(8)	1.414(9)	N(10)	---	C(9)	1.467(7)				
C(11)	---	N(10)	1.438(7)	C(23)	---	N(10)	1.586(9)				
C(23')	---	N(10)	1.566(14)	C(12)	---	C(11)	1.416(10)				
O(13)	---	C(12)	1.419(7)	C(14)	---	O(13)	1.396(7)				
C(15)	---	C(14)	1.489(9)	O(16)	---	C(15)	1.425(6)				
C(17)	---	O(16)	1.417(7)	C(18)	---	C(17)	1.495(8)				
C(20)	---	C(19)	1.569(9)	C(21)	---	C(20)	1.453(8)				
C(22)	---	C(21)	1.602(9)	C(23)	---	C(22)	1.339(9)				
C(23')	---	C(22)	1.342(13)	C(23')	---	C(23)	1.247(13)				
O(21)	---	Cl(1)	1.383(6)	O(22)	---	Cl(1)	1.383(7)				
O(23)	---	Cl(1)	1.413(7)	O(23')	---	Cl(1)	1.318(11)				
O(24)	---	Cl(1)	1.133(9)	O(24')	---	Cl(1)	1.440(8)				
O(23')	---	O(23)	1.180(17)	O(24)	---	O(23')	1.350(16)				
O(24')	---	O(24)	0.967(15)								
Hw(2)	-	O(1)	-	Hw(1)	118.9(3)	Hw(3)	-	O(1)	-	Hw(1)	86.2(3)
Hw(3)	-	O(1)	-	Hw(2)	91.7(3)	C(18)	-	N(1)	-	C(2)	107.9(5)
C(19)	-	N(1)	-	C(2)	112.6(5)	C(19)	-	N(1)	-	C(18)	113.0(5)
C(3)	-	C(2)	-	N(1)	115.1(5)	O(4)	-	C(3)	-	C(2)	109.2(4)
C(5)	-	O(4)	-	C(3)	112.7(4)	C(6)	-	C(5)	-	O(4)	108.9(4)
O(7)	-	C(6)	-	C(5)	108.8(5)	C(8)	-	O(7)	-	C(6)	114.1(5)
C(9)	-	C(8)	-	O(7)	112.2(6)	N(10)	-	C(9)	-	C(8)	117.8(5)
C(11)	-	N(10)	-	C(9)	108.8(5)	C(23)	-	N(10)	-	C(9)	96.8(5)
C(23)	-	N(10)	-	C(11)	126.1(6)	C(23')	-	N(10)	-	C(9)	133.9(6)
C(23')	-	N(10)	-	C(11)	83.7(6)	C(23')	-	N(10)	-	C(23)	46.6(5)
C(12)	-	C(11)	-	N(10)	116.8(6)	O(13)	-	C(12)	-	C(11)	110.3(6)
C(14)	-	O(13)	-	C(12)	114.9(5)	C(15)	-	C(14)	-	O(13)	107.2(5)
O(16)	-	C(15)	-	C(14)	108.6(5)	C(17)	-	O(16)	-	C(15)	113.3(5)
C(18)	-	C(17)	-	O(16)	109.3(5)	C(17)	-	C(18)	-	N(1)	113.0(5)
C(20)	-	C(19)	-	N(1)	113.9(5)	C(21)	-	C(20)	-	C(19)	111.1(6)
C(22)	-	C(21)	-	C(20)	112.1(6)	C(23)	-	C(22)	-	C(21)	123.2(7)
C(23')	-	C(22)	-	C(21)	112.2(7)	C(23')	-	C(22)	-	C(23)	55.5(6)
C(22)	-	C(23)	-	N(10)	116.8(6)	C(23')	-	C(23)	-	N(10)	65.8(7)
C(23')	-	C(23)	-	C(22)	62.4(7)	C(22)	-	C(23')	-	N(10)	118.0(8)
C(23)	-	C(23')	-	N(10)	67.5(7)	C(23)	-	C(23')	-	C(22)	62.2(6)
O(22)	-	Cl(1)	-	O(21)	104.0(6)	O(23)	-	Cl(1)	-	O(21)	99.1(4)
O(23)	-	Cl(1)	-	O(22)	91.8(5)	O(23')	-	Cl(1)	-	O(21)	115.4(6)
O(23')	-	Cl(1)	-	O(22)	128.0(7)	O(23')	-	Cl(1)	-	O(23)	51.1(7)
O(24)	-	Cl(1)	-	O(21)	124.3(7)	O(24)	-	Cl(1)	-	O(22)	116.8(8)
O(24)	-	Cl(1)	-	O(23)	114.9(7)	O(24)	-	Cl(1)	-	O(23')	66.4(9)
O(24')	-	Cl(1)	-	O(21)	99.2(5)	O(24')	-	Cl(1)	-	O(22)	97.6(5)
O(24')	-	Cl(1)	-	O(23)	156.7(6)	O(24')	-	Cl(1)	-	O(23')	107.6(9)
O(24')	-	Cl(1)	-	O(24)	42.1(7)	O(23')	-	O(23)	-	Cl(1)	60.3(7)
O(23)	-	O(23')	-	Cl(1)	68.7(8)	O(24)	-	O(23')	-	Cl(1)	50.2(6)
O(24)	-	O(23')	-	O(23)	116.3(11)	O(23')	-	O(24)	-	Cl(1)	63.4(8)
O(24')	-	O(24)	-	Cl(1)	86.2(11)	O(24')	-	O(24)	-	O(23')	147.3(13)
O(24)	-	O(24')	-	Cl(1)	51.7(7)	N(1)	-	O(1)	-	N(10)	115.5(2)
O(4)	-	O(1)	-	O(7)	57.2(2)	O(4)	-	O(1)	-	O(13)	154.3(2)
O(4)	-	O(1)	-	O(16)	113.1(2)	O(4)	-	O(1)	-	N(1)	57.9(2)
O(4)	-	O(1)	-	N(10)	109.8(2)	O(7)	-	O(1)	-	O(13)	118.7(2)
O(7)	-	O(1)	-	O(16)	152.9(2)	O(7)	-	O(1)	-	N(1)	103.4(2)
O(7)	-	O(1)	-	N(10)	59.3(2)	O(13)	-	O(1)	-	O(16)	57.5(2)
O(13)	-	O(1)	-	N(1)	103.5(2)	O(13)	-	O(1)	-	N(10)	59.5(2)
O(16)	-	O(1)	-	N(1)	56.9(2)	O(16)	-	O(1)	-	N(10)	109.6(2)

Table 1.11 Fractional Atomic Coordinates ($\times 10^4$) for $[\text{H}_3\text{O}.\text{C}_{22}\text{H}_5](\text{ClO}_4)$

Atom	x	y	z
O(1)	6605 (2)	2533 (3)	3233 (2)
N(1)	8458 (3)	2205 (4)	4783 (3)
C(2)	8949 (4)	1211 (6)	4412 (5)
C(3)	8402 (4)	47 (6)	4266 (5)
O(4)	7553 (3)	230 (3)	3597 (3)
C(5)	6998 (4)	-844 (5)	3408 (5)
C(6)	6093 (5)	-541 (5)	2809 (4)
O(7)	5530 (3)	168 (3)	3297 (3)
C(8)	4752 (5)	784 (6)	2743 (5)
C(9)	4253 (4)	1551 (6)	3254 (6)
N(10)	4808 (3)	2487 (4)	3827 (3)
C(11)	4349 (5)	3650 (6)	3620 (7)
C(12)	4843 (5)	4516 (6)	3178 (6)
O(13)	5711 (3)	4874 (3)	3755 (3)
C(14)	6328 (5)	5570 (5)	3337 (5)
C(15)	7251 (5)	5692 (5)	3998 (5)
O(16)	7736 (3)	4547 (3)	4065 (3)
C(17)	8480 (5)	4453 (6)	4840 (5)
C(18)	9037 (4)	3307 (6)	4780 (5)
C(19)	8254 (4)	1922 (6)	5668 (4)
C(20)	7179 (5)	1563 (6)	5653 (4)
C(21)	6561 (5)	2632 (6)	5534 (4)
C(22)	5453 (5)	2285 (6)	5487 (5)
C(23)	4905 (6)	1771 (8)	4758 (5)
C(23') ^a	4866 (9)	2902 (10)	4834 (9)
Cl(1)	1591 (1)	2374 (1)	3460 (1)
O(21)	1947 (5)	3385 (7)	3081 (6)
O(22)	1883 (5)	1400 (7)	2992 (6)
O(23)	2353 (6)	2185 (7)	4204 (5)
O(23') ^b	1584 (11)	2452 (9)	4335 (7)
O(24)	846 (6)	2315 (12)	3627 (8)
O(24') ^b	609 (6)	2423 (7)	2984 (8)

^a Atom has site occupancy factor = 0.634(1); see Experimental

^b Atom has site occupancy factor = 0.548(1).

Table 1.12 Geometric Parameters (\AA , deg.) for H_3O^+ in $[\text{H}_3\text{O}.\text{C}_{22}\text{H}_5](\text{ClO}_4)$

O(1) ... O(4)	2.862 (5)	O(1) ... O(7)	3.016 (5)
O(1) ... O(13)	3.028 (5)	O(1) ... O(16)	2.869 (5)
O(1) ... N(1)	3.180 (5)	O(1) ... N(10)	2.853 (5)
O(4) ... O(1) ... O(7)	57.2 (2)	O(4) ... O(1) ... O(13)	154.3 (2)
O(4) ... O(1) ... O(16)	113.1 (2)	O(4) ... O(1) ... N(1)	57.9 (2)
O(4) ... O(1) ... N(10)	109.8 (2)	O(7) ... O(1) ... O(13)	118.7 (2)
O(7) ... O(1) ... O(16)	152.9 (2)	O(7) ... O(1) ... N(1)	103.4 (2)
O(7) ... O(1) ... N(10)	59.3 (2)	O(13) ... O(1) ... O(16)	57.5 (2)
O(13) ... O(1) ... N(1)	103.5 (2)	O(13) ... O(1) ... N(10)	59.5 (2)
O(16) ... O(1) ... N(1)	56.9 (2)	O(16) ... O(1) ... N(10)	109.6 (2)
N(1) ... O(1) ... N(10)	115.5 (2)		

1.2.5 Summary of Crystal Structure Data

From the crystallographic data it is apparent that there is a general trend in the structure of $[M.C22C_5]ClO_4$, where M^+ moves further out of the plane delineated by the cryptand oxygens as the metal ion radius increases, and the cryptand oxygens deviate from coplanarity with increasing radius of M^+ (Figure 1.10 shows a space filling representation, and Table 1.13). By comparison, the four cryptand oxygens in the structure of $[H_3O.C22C_5]ClO_4$ are coplanar to within $\pm 0.019(4)$ Å. In all four $[M.C22C_5]ClO_4$ species the cryptand is in the *endo-endo* conformation, (for a more detailed description on conformation see Chapter 2, Figure 2.1) where the lone pairs of electrons of the nitrogens are directed toward the centre of the cavity.

Table 1.13 Distances (Å) of M, O(4), O(7), O(13) and O (16) from the Mean Plane of the Cryptand Oxygens in $[M.C22C_5]ClO_4$

M	Distance (Å) from the mean plane of O(4), O(7), O(13) and O(16)			
	O(4)	O(7)	O(13)	O(16)
Na	0.077(3)	-0.088(3)	0.089(3)	-0.078(3)
K (molecule a)	-0.257(3)	0.275(4)	-0.239(3)	0.252(4)
K (molecule b)	-0.295(4)	0.286(4)	-0.234(3)	0.255(4)
Cs	-0.263(5)	-0.319(3)	-0.257(4)	0.318(4)
H ₃ O	0.017(4)	-0.017(4)	0.017(4)	-0.019(4)

	M	N(1)	N(10)
Na	-0.011(2)	-1.060(3)	-2.203(3)
K (molecule a)	0.369(1)	-1.581(4)	-1.180(4)
K (molecule b)	0.441(1)	-1.110(4)	-1.472(4)
Cs	1.296(3)	-0.988(6)	-1.242(5)
H ₃ O	0.666(3)	-1.254(4)	-0.642(5)

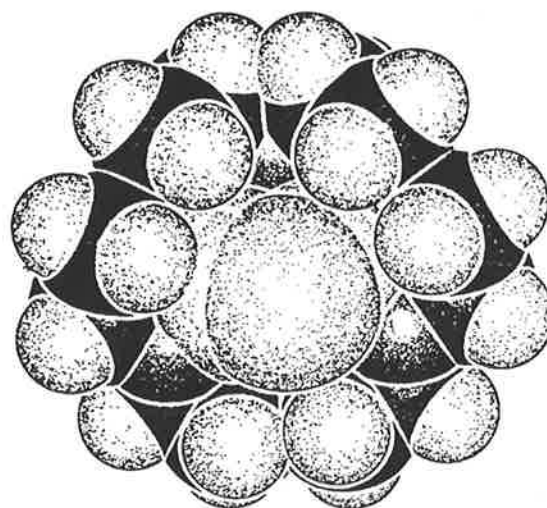
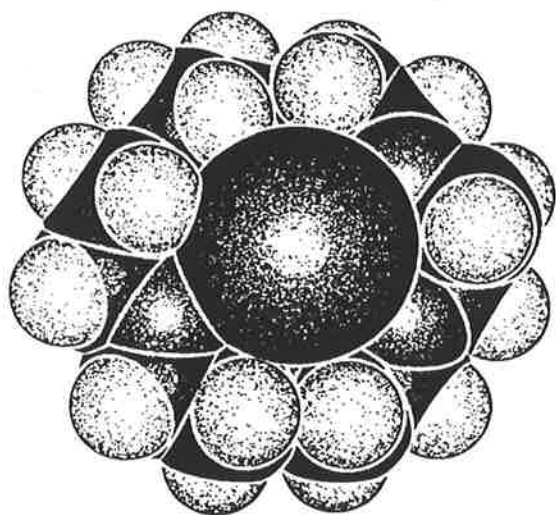
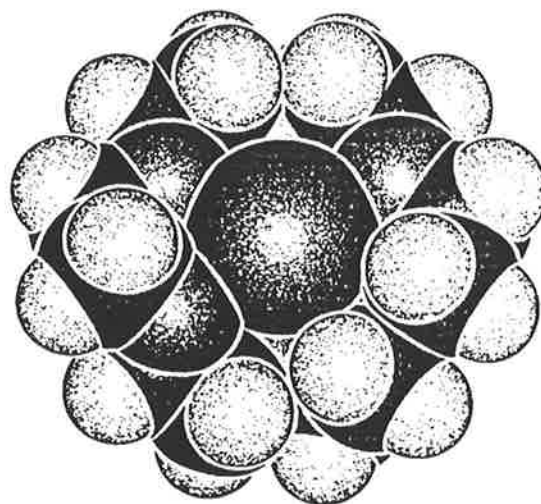
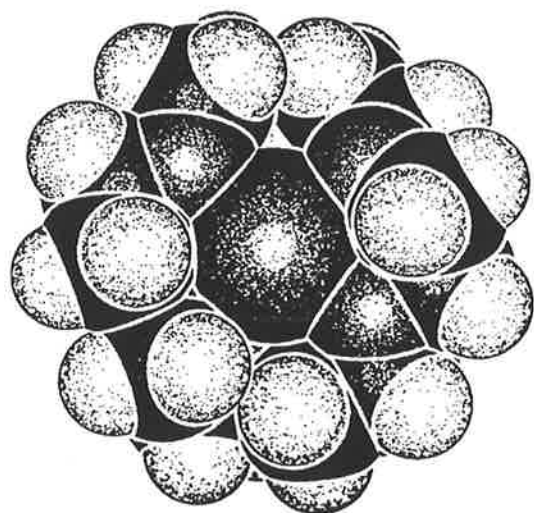


Figure 1.10 SCHAKAL²⁸ plots of the cryptate structures $[\text{Na.C22C}_5]^+$, $[\text{K.C22C}_5]^+$ and $[\text{Cs.C22C}_5]^+$, showing the progression of the metal ion away from the eighteen membered ring face of the cryptand C22C_5 . The structure of $[\text{H}_3\text{O.C22C}_5]^+$ is included for comparison only. In all cases the anion has been omitted from view.

In the diaza-crown ether complex structure, [K.C22]SCN, K⁺ is in the plane defined by the four oxygens of the diaza-crown ether, C22 (K...O distances = 2.830(3) Å), and the macrocyclic nitrogens (K...N distances = 2.856(3) Å), respectively 0.64 Å above and below this plane.²⁶ The interaction with the anion SCN⁻ is characterised by K...N and K...S distances of 3.33(1) Å, which, if included in bonding, the K⁺ is eight-coordinate. The comparison with [K.C22C₅]ClO₄ indicates that the -(CH₂)₅- joining the cryptand nitrogens prevents the 4,7,13,16-tetraoxa-1,10-diazacyclooctadecane (C22-) ring of the C22C₅ from assuming a conformation which can accommodate K⁺ in the plane of the four oxygens. As the Na⁺ is almost coplanar with the cryptand oxygens in [Na.C22C₅]ClO₄, it appears that the conformational constraints restrict the effective radius of the hole in C22C₅ delineated by these oxygens to between 1.02 Å, the Na⁺ radius and 1.38 Å, the K⁺ radius (this compares with the C22 radius ~ 1.5 Å).

The space filling sodium cryptate structures, derived from single crystal X-ray crystallography, for the series [Na.C21C₅]⁺,²³ [Na.C211]⁺,²³ [Na.C22C₅]⁺ and [Na.C221]⁺,¹⁶ clearly show (Figure 1.11) the increasing degree of inclusion of the Na⁺ ion into the cryptate cavity. In the solid state structures of [Na.C21C₅]⁺ and [Na.C211]⁺, the Na⁺ ions are 0.37, and 0.14 Å above the planes defined by the three oxygen atoms of the 1,10-diaza-4,7,13-trioxacyclopentadecane rings. This indicates that the extra oxygen of C211 results in a greater attraction of C211 for the Na⁺ ion by comparison with C21C₅. In the solid state structure of [Na.C22C₅]⁺, the Na⁺ ion is 0.011 Å below the plane defined by the four oxygens of the 1,10-diaza-4,7,13,16-tetraoxacyclooctadecane ring of C22C₅. The solid state structure of [Na.C221]⁺ shows it to be *inclusive*, with the Na⁺ ion positioned well inside the cryptand cavity, where the Na⁺ ion is a similar distance from the planes defined by the 1,10-diaza-4,7,13,16-tetraoxacyclooctadecane ring and both 1,10-diaza-4,7,13-trioxacyclopentadecane rings.

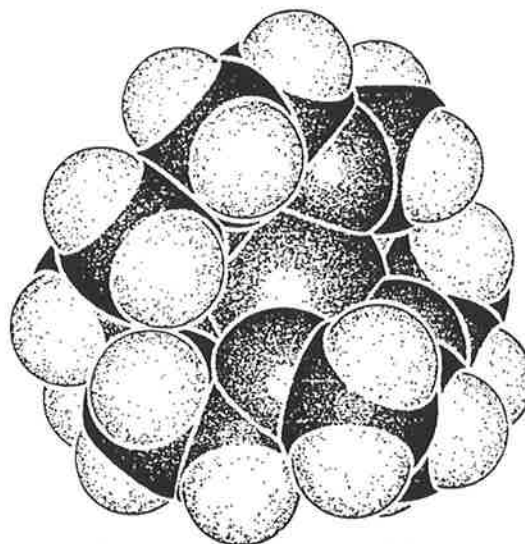
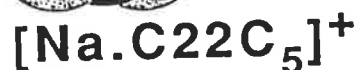
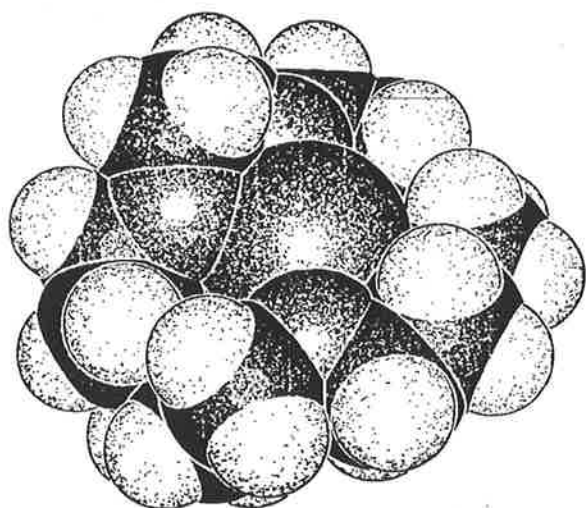
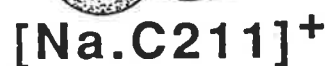
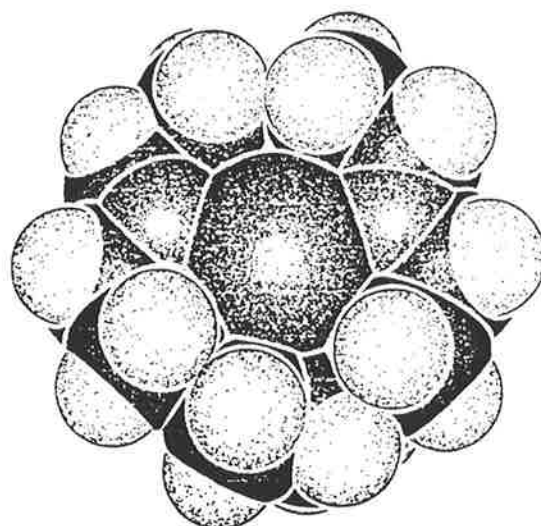
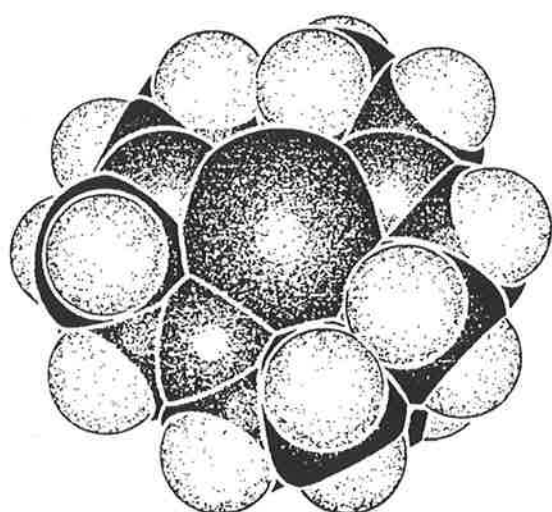


Figure 1.11 SCHAKAL²⁸ plots of selected sodium cryptate structures, show the increasing progression of the Na⁺ ion into the cryptand cavity, in the series $[\text{Na.C21C}_5]^+ \leq [\text{Na.C211}]^+ \leq [\text{Na.C22C}_5]^+ \leq [\text{Na.C221}]^+$. The crystal structures from which these plots were derived, $[\text{Na.C21C}_5]^+$ and $[\text{Na.C211}]^+$ are from reference 23, $[\text{Na.C221}]^+$ is from reference 16 and $[\text{Na.C22C}_5]^+$ is from this study. In all cases the anion has been omitted from view.

- 1 Pedersen C.J., *Angew. Chem., Int. Ed. Engl.*, **1988**, 27, 1021 - 1027.
- 2 Pedersen C.J., *J. Am. Chem. Soc.*, **1967**, 89, 7017 - 7036.
- 3 Pedersen C.J., *J. Am. Chem. Soc.*, **1967**, 89, 2495 - 2496.
- 4 Donald J. Cram, Jean-Marie Lehn and Charles J. Pedersen have received the 1987 Nobel prize in chemistry "for their development and use of molecules with structure-specific interactions of high selectivity". This award pays homage to the scientists that have introduced a completely novel view of chemistry, starting a real revolution in the way the chemists look at molecular interactions" from,
Dietrich B., Sauvage J.-P., *New J. Chem.*, **1988**, 12, 725 - 728.
- 5 Dietrich B., Lehn J.-M., Sauvage J.-P., *Tetrahedr. Lett.*, **1969**, 2885 - 2888.
- 6 Dietrich B., Lehn J.-M., Sauvage J.-P., *Tetrahedr. Lett.*, **1969**, 2889 - 2892.
- 7 Pioda L.A.R., Wachter H.A., Dohner R.E., Simon W., *Helv. Chim. Acta* **1967**, 50, 1373 - 1376.
- 8 Mueller P., Rudin D.O., *Biochem. Biophys. Res. Comm.*, **1967**, 26, 398 - 404, Although the structural hypotheses put forward were later found to be erroneous, they were of great conceptual importance, reference 4.
- 9 Kilbourn B.T., Dunitz J.D., Pioda L.A.R., Simon W., *J. Mol. Biol.*, **1967**, 30, 559 - 563.
- 10 Lehn J.-M., *Pure Appl. Chem.*, **1979**, 51, 979 - 997.
- 11 Lehn J.-M., *Acc. Chem. Res.*, **1978**, 11, 49 - 57.
- 12 Lewin R. *Science* , **1987**, 238, 611 - 612.
- 13 Cox B. G., Garcia-Rosa J., Schneider H., *J. Am. Chem. Soc.*, **1981**, 103, 1384-1389.
- 14 Lehn J.-M., *Struct. Bonding (Berlin)*, **1973**, 16, 1 - 69.
- 15 Lehn J.-M., Sauvage J.-P., *J. Am. Chem. Soc.*, **1975**, 97, 6700 - 6707.
- 16 Mathieu F., Metz B., Moras D., Weiss R., *J. Am. Chem. Soc.*, **1978**, 100, 4412 - 4416.
- 17 Clarke P., Lincoln S.F., Tiekink E.R.T., *Inorg. Chem.*, **1991**, 30, 2747 - 2751.
- 18 Abou-Hamdan A., Lincoln S.F., *Inorg. Chem.*, **1991**, 30, 462 - 466.
- 19 Lincoln S.F., Brereton I.M., Spotswood T.M., *J. Am. Chem. Soc.*, **1986**, 108, 8134 - 8138.
- 20 Shannon R.D., *Acta Cryst., Sect.A: Cryst. Phys. Diffr., Theor. Gen. Crystallog.*, **1976**, A32, 751 - 767.
- 21 Tsukube H., *J.Coord.Chem.* **1987**, 16, 101 - 129.

-
- 22 Moras D., Weiss R., *Acta Cryst., Sect. B*, **1973**, B29, 400.
- 23 Lincoln S.F., Horn E., Snow M.R., Hambley T.W., Brereton I.M., Spotswood T.M., *J. Chem. Soc., Dalton Trans.*, **1986**, 1075 - 1080.
- 24 Lehn J.-M., Sauvage J.-P., *J. Chem. Soc., Chem. Commun.*, **1971**, 440.
- 25 Abou-Hamdan A., Hounslow A.M., Lincoln S.F., Hambley T.W., *J. Chem. Soc., Dalton Trans.*, **1987**, 489 - 492.
- 26 Moras D., Metz B., Herceg M., Weiss R., *Bull. Soc. Chim. Fr.*, **1972**, 551 - 555.
- 27 Johnson C.K., "ORTEP, Thermal Ellipsoid Plotting Program", Report ORNL-3794 Oak Ridge National Laboratory, Oak Ridge, Tennessee, **1971**.
Sheldrick G.M., "SHELX 86, Program for the Automatic Solution of Crystal Structure", University of Göttingen, Germany, **1986**.
- 28 Keller E., The FORTRAN-77 (compiled) program SCHAKAL, Institut für Anorganische Chemie der Universität Freiburg, Germany.

Chapter 2 : Cryptate Equilibria

2.1 : Introduction

In aqueous and polar non-aqueous solutions of metal ions and cryptands, an equilibrium exists between the solvated metal ion, M^+ , the cryptand, L , and the cryptate, $[M.L]^+$, as defined by the equation:



where the concentration stability constant, K_s , is defined:

$$K_s = \frac{[M.L^+]}{[M^+][L]} \quad 2.2$$

The selective complexation of the metal ion by the cryptand and the stability of the cryptates formed, are dependent on the relative sizes of the cryptand cavity and the metal ion, the structural flexibility and the number and type of donor atoms of the cryptand, and the solvation energy of the metal ion.¹⁻⁸

The main aim in this chapter is to explore a number of aspects of the interactions between these factors for systems based on the eighteen membered 4,7,13,16-tetraoxa-1,10-diazacyclooctadecane, or C22- ring. The major systems studied herein are the cryptates formed between the cryptand C22C₅ and a range of monovalent metal ions in several solvents. These systems are compared with similar systems based on the C22- ring.

Previous studies of the cryptand C221 show that it accommodates the alkali metal ion, Na^+ ($r = 1.02 \text{ \AA}$), entirely within the intramolecular cryptand cavity (cavity radius $r = 1.1 \text{ \AA}$ ⁹), to form an *inclusive* cryptate $[Na.C221]^+$.¹¹ In contrast, K^+ ($r = 1.38 \text{ \AA}$ ¹⁰) is too large to be accommodated entirely within the cryptand cavity, and forms an *exclusive* cryptate, $[K.C221]^+$, in which K^+ resides on the face of defined by the eighteen membered, 4,7,13,16-tetraoxa-1,10-diazacyclooctadecane ring (C22- ring).¹¹

In solution, the variation of stability constants of the alkali metal ion C221 cryptates, $[M.C221]^+$, with M^+ in the sequence $Li^+ < Na^+ > K^+$ in a range of solvents. This observed variation is also consistent with Li^+ ($r = 0.76 \text{ \AA}$)

forming an *inclusive* structure, but being too small to establish optimal bonding distances, and Na⁺ forming an *inclusive* structure where the optimal bonding distances of [Na.C221]⁺ confer a greater stability on this cryptate than that of the *exclusive* [K.C221]⁺.^{2,4} This dependence of selectivity on the relative sizes of the cryptand cavity and the metal ion, is reflected in the stability constants of the alkali metal ion cryptates of C211, C221, C22C₈, C222 and C322, as exemplified in the solvent methanol (Table 2.1), where the cryptand that has an intramolecular cavity radius that approximately matches that for an alkali metal ion radius forms the cryptate with highest stability.

Table 2.1 Variation of Stability Constant, K_s , with Cavity Radius and Metal Ion Radius in Methanol Solution

Cryptand (donor atoms)	Cavity Radius Å ^a	log (K_s / dm ³ mol ⁻¹)				
		Li ⁺ 0.76 Å	Na ⁺ 1.02 Å	K ⁺ 1.38 Å	Rb ⁺ 1.52 Å	Cs ⁺ 1.67 Å
C211 (6)	0.8	> 7.5, 8.04 ^b	6.1 6.7 ^c	2.3	1.9	—
C221 (7)	1.1	> 6.0, 5.38 ^b	> 8.0 9.65 ^b	> 8.0, 8.54	> 6.0, 6.74	5.0
C22C ₅ (6)	1.1	2.3 ^d	5.41 ^d	5.8 ^d	5.7 ^d	4.8 ^d
C22C ₈ (6)	1.4	2.2, < 2.0 ^e	3.5	5.2, 4.35 ^e	3.4	2.7
C222 (8)	1.4	2.65	7.98 ^b	10.41	8.98 ^b	4.4
C22 (6)	~1.5 ^g	1.07 ^f	1.0	2.0	1.2	—
C322 (9)	1.8	2.3	5.0	7.6	7.9	~8.0

All results are from reference 1 except: ^a Reference 10, the cationic radii are based on those derived for the six coordinate metal ions; ^b Reference 4; ^c Reference 13 ^d This study; ^e Reference 2; ^f Reference 12 (95:5 methanol to water); ^g References 14,15, the value of ~1.5 Å for the radius of the C22 ring cavity was estimated from that for the isostructural crown ether, 1,4,7,10,13,16-hexaoxacyclooctadecane (18-crown-6), with allowances made for the binding site radii differences between oxygen and nitrogen donor atoms.

The monocyclic diaza-crown ether C22 shows a maximum selectivity in methanol, for the K^+ ion (Table 2.1). This is consistent with K^+ positioned in the cavity formed by the plane of the four ether oxygens of the eighteen membered ring of C22, which has a radius of approximately 1.5 Å.^{14,15} The lower stability and small variation of the C22 complexes in comparison with the C221 cryptates, may be attributable to the presence of the extra oxygen donor atom in C221 and the decreased flexibility of its corresponding eighteen membered C22- ring. The lower stability generally observed for alkali metal ion $[M.C21]^+$ complexes^{1,16-18} in comparison with $[M.C211]^+$ cryptates^{1,2,5,19} in a range of solvents may be attributed to the same origin.

The cryptand C22C₅ has a similar structure and cavity size to C221, where all the donor atoms are on the C22- ring, and are the same number and type as those in the diaza-crown ether C22. Thus, it is of interest to study the solution equilibria of the alkali metal ion $[M.C22C_5]^+$ cryptates, and to distinguish between the origins of the stability differences observed for $[M.C221]^+$, $[M.C22]^+$ and the other aliphatic bridged cryptates $[M.C22C_2]^+$ ^{8,20} and $[M.C22C_8]^+$.^{1,21}

In the next section, the apparent stability constants of $[M.C22C_5]^+$ have been determined in aqueous solution, by competitive acid-base potentiometric (pH-metric) titration. In order to derive these results it was necessary to measure the protonation constants K_1 and K_2 for C22C₅ in water. In addition, it is of interest to compare the K_1 and K_2 values with those for other cryptands and diaza-crown ethers that may be found in the literature.

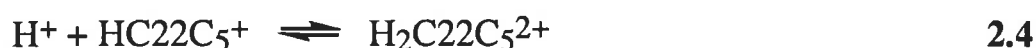
2.2 : Equilibria in Aqueous Solution

2.2.1 : Protonation of C22C₅ in Aqueous Solution

In water, the cryptand C22C₅ is a dibasic species for which both protonation constants have been determined at 298.2 K and ionic strength $I = 0.10$ (using 0.100 mol dm⁻³ TEAP as the supporting electrolyte). The experimental details are discussed in section 2.5. The protonation constants K_1 and K_2 , of the cryptand C22C₅ and related cryptands given in Table 2.2 below, are defined:



$$K_1 = \frac{[\text{HC22C}_5^+]}{[\text{H}^+][\text{C22C}_5]}$$



$$K_2 = \frac{[\text{H}_2\text{C22C}_5^{2+}]}{[\text{H}^+][\text{HC22C}_5^+]}$$

In the solid state structures of the mono-protonated $[\text{H}_3\text{O}.\text{C22C}_5]\text{ClO}_4$ and metal ion cryptates in general, the predominant conformation is *endo - endo* (Figure 2.1), where the lone pairs of electrons of the two nitrogens are directed to the centre of the cryptand cavity, and it is anticipated that this is the dominant conformer in solution. The other possible conformers: *exo - exo* and *endo - exo* are shown in Figure 2.1.

Table 2.2 Protonation Constants for C22C₅ and Related Ligands at 298.2 K in Aqueous Solution

Ligand	log K_1	log K_2
C21 ^a	8.76	8.04
C211 ^b	11.32	8.14
C21C ₅ ^c	11.6	7.73
C22 ^a	9.08	7.94
C22C ₂ ^d	10.92	3.42
C22C ₅ ^e	11.25 ± 0.04	8.16 ± 0.03
C221 ^a	11.02	7.74
C22C ₈ ^d	11.1	8.41

^a Reference 22, ^b Reference 23, ^c Reference 24, ^d Reference 21, ^e This study, (all solutions 0.100 mol dm⁻³ TEAP supporting electrolyte).

The similarity in the values of K_1 for the cryptands in Table 2.2, is consistent with the structure of the cryptand and the number of oxygen donor atoms present having little influence on the basicity of the tertiary amine nitrogens. A similar observation applies to the basicity of the diaza-crown ethers.

The extra electronic repulsion caused by addition of a second positive charge results in the trend $K_2 > K_1$ for the cryptands and diaza-crown ethers. The destabilising effect of the close proximity of the proton charges is reflected in very low K_2 for C22C2, where the nitrogens are constrained to be in close proximity by the short -N-(CH₂)₂-N- linkage (as seen in the comparison of cryptands in Figure 2.2).

The K_1 of the diaza-crown ethers, C21 and C22 are substantially less than the K_1 values for the cryptands in Table 2.2. This is consistent with the nitrogens in the diaza-crown ethers being less able to compete for a proton with water, by comparison with the cryptands. As the relatively small K_1 values for C21 and C22 are also observed for a number of other diaza-crown ethers,²⁵ this suggests that the cryptand nitrogens sites in the mono-protonated form have only a small solvent interaction (consistent with the [H₃O.C22C₅]⁺ existing in the *endo - endo* conformation).

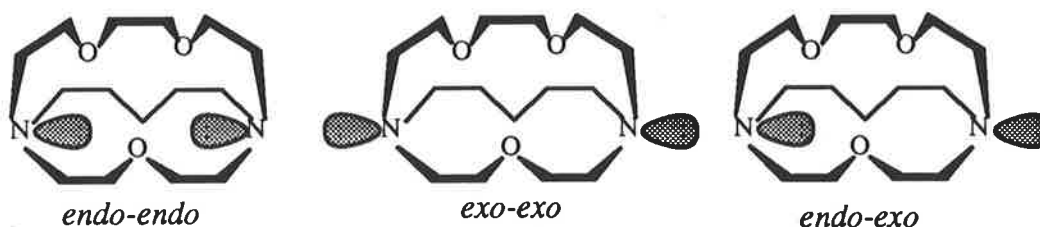


Figure 2.1 The cryptand C21C₅ is used to demonstrate that cryptands can assume any of three conformations according to the configuration of the two nitrogen bridgeheads. The *endo - endo* form is the most probable conformer for a cryptate as the lone pairs of electrons of both the nitrogen atoms are directed toward the electrophilic substrate inside of the intramolecular cavity.

A comparison of the protonation constants,⁵⁰ $\log K_1$ in aqueous solution of tertiary substituted amines, $(\text{CH}_3)_3\text{N}$, $(\text{CH}_3\text{CH}_2)_3\text{N}$ and $(\text{CH}_3\text{CH}_2\text{CH}_2)_3\text{N}$ (9.77, 10.70, 10.65, respectively) with the secondary substituted amines $(\text{CH}_3)_2\text{NH}$, $(\text{CH}_3\text{CH}_2)_2\text{NH}$ and $(\text{CH}_3\text{CH}_2\text{CH}_2)_2\text{NH}$ (10.75, 11.0, 11.00, respectively) depict a decrease in $\log K_1$ of between 0.3 and 1.0 log units. This is in contrast to the observed magnitude of increased basicity of the cryptands tertiary nitrogen donor atoms when compared with the secondary nitrogen donor atoms of the diaza-crown ethers, where, for the cryptands in Table 2.2, $\log K_1 \approx 10.9 - 11.3$ compare with the diaza-crown ethers, $\log K_1 \approx 8.8 - 9.1$.

In the case of the doubly protonated species, the close proximity of the two protons inside the cavity in the *endo - endo* conformation may result in one or both of the nitrogens directing their lone pair out into the solvent, where the conformation *endo - exo* or *exo - exo* would be adopted for the cryptands C211, C21C₅, C22C₅, C22C₈ and C221. The increased interaction of these cryptand nitrogens with the solvent is consistent with the similarity of the K_2 values of these cryptand to those of the more flexible C21 and C22.

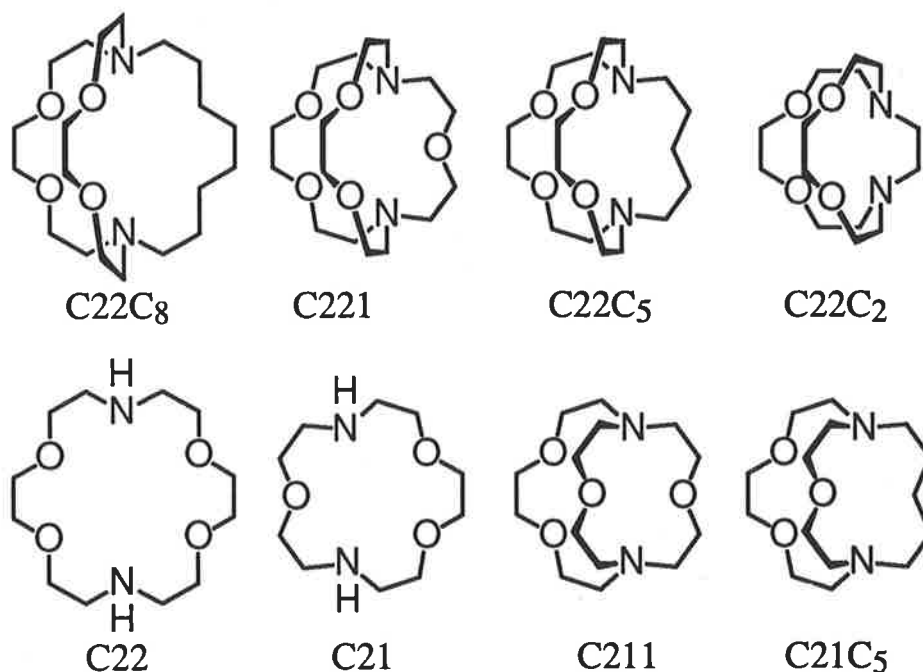
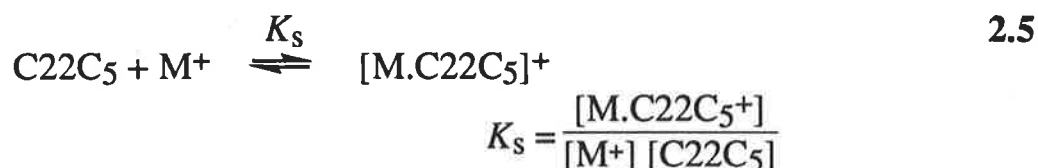


Figure 2.2 C22C₈, C221, C22C₅ and C22C₂, may be viewed as modifications of C22, where the two amine hydrogens have been replaced by a $-(\text{CH}_2)_8-$, $-(\text{CH}_2)_2-\text{O}-(\text{CH}_2)_2-$, $-(\text{CH}_2)_5-$ and $-(\text{CH}_2)_2-$ bridge, respectively. Similarly, C211 and C21C₅ may be viewed as modification of C21, where the two amine hydrogens have been replaced by a $-(\text{CH}_2)_2-\text{O}-(\text{CH}_2)_2-$ and $-(\text{CH}_2)_5-$ bridge, respectively.

2.2.2 : Complexation of Selected Monovalent Metal Ions by C22C5 in Aqueous Solution

The apparent stability constants, K_s , for the metal ion cryptates, $[M.C22C5]^+$ ($M = Li^+, Na^+, K^+, Rb^+, Cs^+, Tl^+$ and Ag^+) have been determined in aqueous solution (Table 2.3). The complexation of the metal ion M^+ by the cryptand C22C5 and apparent stability constants may be defined:



where $M^+ = Li^+, Na^+, K^+, Rb^+, Cs^+, Tl^+$ and Ag^+ .

Table 2.3 Apparent Stability Constants for the Complexation of the Cryptand C22C5 with Tl^+ , Ag^+ and the Alkali Metal Ions, Li^+ , Na^+ , K^+ , Rb^+ and Cs^+ , in Aqueous Solution at 298.2 K

Metal ion	Ionic radius ^a (Å)	log ($K_s / dm^3 mol^{-1}$)
Li ⁺	0.76	2.08 ± 0.10
Na ⁺	1.02	2.58 ± 0.04
K ⁺	1.38	3.41 ± 0.11
Rb ⁺	1.52	3.28 ± 0.07
Cs ⁺	1.67	3.31 ± 0.11
Tl ⁺	1.50	4.10 ± 0.02
Ag ⁺	1.00	9.31 ± 0.05

All solution 0.100 mol dm⁻³ in TEAP supporting electrolyte. This study except, ^a Reference 10, the values are based on those derived by Shannon for six coordinate metal ions.

The magnitude of K_s varies substantially with the nature of the metal ion. The high stability shown by $[Ag.C22C5]^+$ in aqueous solution may be attributed to the increased bonding interaction of the soft acid Ag^+ ion with the nitrogen donor atoms²⁶ of the cryptand. In addition, the stability constant for the $[Tl.C22C5]^+$ is consistent with the cryptand nitrogens competing more effectively for the intermediate soft/hard acid Tl^+ ion, than for the hard acid alkali metal ions.

For the alkali metal ion $[M.C22C_5]^+$ cryptates, the variation of stability is $Li^+ < Na^+ < K^+ \geq Rb^+ \geq Cs^+$. The dependence of selectivity on the relative sizes of the cryptand cavity and the size of the metal ion, has been demonstrated for various alkali metal ion cryptate systems²⁷ (Table 2.1). The cryptand C22C₅ has a cavity radius of 1.1 Å (see Table 2.1) and the closest matching alkali metal ion is Na⁺ ($r = 1.02$ Å), but the most stable alkali metal ion cryptate formed is $[K.C22C_5]^+$. However, in the solid state Na⁺ does not occupy the centre of the C22C₅ cavity in $[Na.C22C_5]ClO_4$. Instead, $[Na.C22C_5]^+$ has an *exclusive* structure where the Na⁺ is positioned 0.011(2) Å below the common plane of the four cryptand oxygens, and the nitrogens shows minimal interactions with the metal ion. It is a reasonable assumption that the solid state structure $[Na.C22C_5]ClO_4$ is, to a large extent, retained in solution, with the interactions between M⁺ and ClO₄⁻ being replaced by M⁺ and solvent interactions. Thus, no extra stability is conferred on *exclusive* $[Na.C22C_5]^+$, and its stability relative to *exclusive* $[K.C22C_5]^+$ is mainly a consequence of the balance of the competition between the interaction of the C22C₅ oxygens and the water with the two metal ions, with the result that the less strongly solvated K⁺ forms the more stable cryptate.

These observations are consistent with the replacement of the fifth oxygen donor atom of C221 by a methylene, $-(CH_2)-$, moiety in C22C₅ resulting in an overall decrease in the electrostatic interactions between Na⁺ and C22C₅, by comparison with $[Na.C221]^+$ and $[K.C221]^+$.

2.3 : Equilibria in Aqueous and Non-Aqueous Solution

In addition to the study of the cryptate stabilities in water, it is of interest to examine the effects of other solvents on cryptate equilibria. The stability constants for the cryptates of $C22C_5$ have been determined for a selection of non-aqueous solvents, by potentiometric titration (the method is discussed in detail in section 2.5). In addition, some stability constants have been derived by potentiometric titration in aqueous solution, and are compared with the stability constant values derived by pH-metric titration (Table 2.4).

2.3.1 : Complexation of Monovalent Metal Ions by $C22C_5$ in Aqueous and Non-Aqueous Solution

The apparent stability constants, K_s , of $[M.C22C_5]^+$, where $M^+ = Ag^+, Tl^+, Li^+, Na^+, K^+, Rb^+$ and Cs^+ , have been determined in methanol, DMF and water (Table 2.4). The variation of stability for the alkali metal ion cryptates is $Li^+ < Na^+ < K^+ \geq Rb^+ \geq Cs^+$. The stability constants of $[M.C22C_5]^+$ have been determined in acetonitrile for Li^+, Na^+ and Ag^+ , and in the solvents, acetone, dimethyl sulfoxide and pyridine for Na^+ . In addition, the stability constants of $[M.C22C_5]^+$ have been determined⁵² in propylene carbonate for Li^+, Na^+, Tl^+ , and Ag^+ , and are included for comparison.

The high stability constant of $[Ag.C22C_5]^+$ in the oxygen donor solvents, methanol, DMF and water, is consistent with observations made on the aqueous system discussed in the previous section, where there is increased bonding interaction of the nitrogen donor atoms²⁶ of the cryptand, with the soft acid Ag^+ . However, in the nitrogen donor solvent, acetonitrile, the stabilities of the alkali metal ion cryptates approach those of $[Ag.C22C_5]^+$, (Table 2.5) and is consistent with the ability of the nitrogen donor solvent to compete more effectively for Ag^+ than for the alkali metal ions.³⁴ These trends are also observed for the cryptates $[M.C221]^+$, $[M.C22C_2]^+$ and the diaza-crown ether complexes $[M.C22]^+$ (Table 2.5). In comparing the stability of the Tl^+ and Rb^+ cryptates and diaza-crown ether complexes, (Table 2.5) the trend in stabilities is $Tl^+ > Rb^+$. This observation may be attributed to a stronger electrostatic interaction of the cryptand donor nitrogen atoms with Tl^+ due to its partial soft acid nature.²⁸ (The ionic radius of Rb^+ , $r = 1.52 \text{ \AA}$, most closely resembles that of Tl^+ , $r = 1.50 \text{ \AA}$, thus minimising any effect attributed to difference in cation size.)

The stability of a cryptate in solution generally decreases with the increasing electron pair donating power of the solvent, as measured by the Gutmann donor number,²⁹ D_N , and is consistent with increasingly strong metal ion solvation causing a decrease in cryptate stability.^{5,51} If the value used for water is, $D_N = 33.0$,^{30,31} then with the exception of pyridine, this trend may be seen in Tables 2.4 and 2.5 (A discussion of the Gutmann donor number appears in Appendix v).

In comparing the stability constants for $[\text{Na.C22C}_5]^+$ in pyridine ($\log K_s = 6.41$) with those for $[\text{Na.C22C}_5]^+$ in other solvents (Table 2.4), it appears to be much higher than would be predicted from the donor number of pyridine. The larger than predicted stability constant for $[\text{Na.C22C}_5]^+$ in pyridine may be due to the incorporation of the nitrogen donor atom into the aromatic ring structure causing a degree of steric hindrance for the coordinating electron pair, lowering its ability to compete with the cryptand for the metal ion. Alternatively, it has been suggested³² that the aromatic ring nitrogen of pyridine is a soft base and does not solvate the alkali metal ions to the extent predicted by the donor number. A similar variation of stability constants has been observed for $[\text{Na.C21C}_5]^+$ ³³ and $[\text{Na.C22C}_2]^+$ ⁸ in pyridine and other solvents.

Table 2.4 Stability Constants for the Complexation of the Metal Ions Ag⁺, Tl⁺, Li⁺, Na⁺, K⁺, Rb⁺ and Cs⁺ by the Cryptand C22C₅ in Selected Solvents at 298.2 K

solvent	D_N	$\log(K_s / \text{dm}^3 \text{ mol}^{-1})$ (298.2 K)						
		Li ⁺	Na ⁺	K ⁺	Rb ⁺	Cs ⁺	Tl ⁺	Ag ⁺
acetonitrile	14.1	6.07 ± 0.04	7.55 ± 0.13 ^c	—	—	—	—	8.27 ± 0.02 ^a
propylene carbonate	15.1	5.36 ^d	5.25 ^{c,d}	—	—	—	7.78 ^d	14.51 ^d
water	18.0	2.08 ± 0.10 ^e	2.58 ± 0.04 ^e	3.41 ± 0.11 ^e	3.28 ± 0.07 ^e	3.31 ± 0.11 ^e	4.10 ± 0.02 ^e	9.31 ± 0.05 ^e
	(33.0) ^f	2.2 ± 0.2	≤2 ^{b,g}	3.5 ± 0.2 ^h		3.4 ± 0.3 ^h	3.9 ± 0.2 ^h	9.22 ± 0.12 ^a
acetone	17.0	—	6.09 ± 0.14 ^b	—	—	—	—	—
methanol	19.0	2.30 ± 0.21	5.41 ± 0.06 ^b	5.8 ± 0.3 ^h	5.7 ± 0.2 ^h	4.8 ± 0.2 ^h	6.48 ± 0.14	11.13 ± 0.12 ^a
	(23.5) ^f							
dimethyl-formamide	26.6	2.21 ± 0.18	3.66 ± 0.06 ^b	3.85 ± 0.14	3.82 ± 0.13	2.90 ± 0.13	5.05 ± 0.15	9.40 ± 0.13 ^a
dimethyl sulfoxide	29.8	—	3.15 ± 0.05 ^b	—	—	—	—	—
pyridine	33.1	—	6.41 ± 0.02 ^b	—	—	—	—	—

All solutions are $0.0500 \text{ mol dm}^{-3}$ TEAP, supporting electrolyte, except where stated otherwise.

^a Determined directly using an Ag^+ ISE; ^b Determined directly using a Na^+ ISE. All other stability constants determined competitively using an Ag^+ ISE; ^c Measurements in this solvent resulted in the solvated Na^+ being below the reliable detection limit for the Na^+ ISE in this solvent. All stability constants above are derived from this study, except ^d reference 52; ^e Determined competitively by pH-metric methods ($0.100 \text{ mol dm}^{-3}$ TEAP as supporting electrolyte); ^f It has been suggested that $D_{\text{N}} = 33$ and 23.5 are more appropriate in water and methanol solutions, references 30,31 than $D_{\text{N}} = 18.0$ and 19.0 , respectively, originally proposed by Gutmann, reference 29; ^g The relatively small change in mV over the course of the titration(s) (*ca.* 10 mV) led to poor resolution of the value for the K_{S} of $[\text{Na}.\text{C}_{22}\text{C}_5]^+$ in water.; ^h The relatively large errors attained are due to the low solubility of the perchlorate salts of K^+ , Rb^+ , Cs^+ , and Tl^+ , which in these solvents, are only partially soluble at 0.01 mol dm^{-3} and therefore the titrations were carried out at $1/5^{\text{th}}$ of normal experimental concentrations (approximately $2 \times 10^{-3} \text{ mol dm}^{-3}$).

Table 2.5 Apparent Stability Constants of [M.C221]⁺, [M.C22C₅]⁺, [M.C22C₂]⁺ and [M.C22]⁺ in Four Solvents at 298.2 K

Species ^a	log ($K_s / \text{dm}^3 \text{mol}^{-1}$)			
	methanol ($D_N = 19.0^b$ or 23.5^c)	DMF (26.6^b)	water (18.0^b or 33.0^c)	acetonitrile (14.1^b)
[Li.C221] ⁺ ^d	5.38	3.58	2.50	10.33
[Na.C221] ⁺ ^d	8.65	7.93	5.4	>11.3
[K.C221] ⁺ ^d	8.54	6.66	3.95	9.5
[Rb.C221] ⁺ ^d	6.74	5.35	2.55	7.27
[Cs.C221] ⁺ ^d	4.33	3.61	<2.0	5.15
[Tl.C221] ⁺ ^e	10.75	8.61	6.8	11.92
[Ag.C221] ⁺ ^e	14.64	12.41	10.6	11.24
[Li.C22C ₅] ⁺ ^f	2.30 ± 0.21	2.21 ± 0.18	2.08 ± 0.10	6.07 ± 0.04
[Na.C22C ₅] ⁺ ^f	5.41 ± 0.06	3.66 ± 0.06	2.58 ± 0.04	7.55 ± 0.13
[K.C22C ₅] ⁺ ^f	5.8 ± 0.3	3.85 ± 0.14	3.41 ± 0.11	—
[Rb.C22C ₅] ⁺ ^f	5.7 ± 0.2	3.82 ± 0.13	3.28 ± 0.07	—
[Cs.C22C ₅] ⁺ ^f	4.8 ± 0.2	2.90 ± 0.13	3.31 ± 0.11	—
[Tl.C22C ₅] ⁺ ^f	6.48 ± 0.14	5.05 ± 0.15	4.10 ± 0.02	—
[Ag.C22C ₅] ⁺ ^f	11.13 ± 0.12	9.40 ± 0.13	9.31 ± 0.05	8.27 ± 0.02
[Li.C22C ₂] ⁺ ^g	4.0	3.5	<2	7.8
[Na.C22C ₂] ⁺ ^h	6.6	6.1	3.2	9.4
[K.C22C ₂] ⁺ ^h	—	3.2	<2	7.2
[Cs.C22C ₂] ⁺ ^h	—	2.7	<2	5.0
[Tl.C22C ₂] ⁺ ^h	7.8	6.7	—	10.4
[Ag.C22C ₂] ⁺ ^h	10.2	9.4	6.0	9.4
[Li.C22] ⁺	1.07 ⁱ	~0.0 ⁱ	—	4.39 ⁱ
[Na.C22] ⁺	1.0 ^j	—	—	4.49 ^k , 4.30 ^l
[K.C22] ⁺	2.04 ^m	—	—	4.35 ^k , 4.32 ^l
[Rb.C22] ⁺	1.2 ^j	—	—	3.37 ^l
[Cs.C22] ⁺	—	0.61 ⁱ	—	2.25 ^k , 2.48 ^l
[Tl.C22] ⁺	3.54 ⁿ	3.41 ⁿ , 3.22 ⁱ	1.1 ^o	6.82 ⁿ
[Ag.C22] ⁺	9.99 ⁿ	9.91 ⁿ	8.08 ^l	7.94 ⁿ

^a Reference 10, the six-coordinate ionic radii are Li⁺, 0.76; Na⁺, 1.02; K⁺, 1.38; Rb⁺, 1.52; Cs⁺, 1.67; Tl⁺, 1.50; Ag⁺, 1.00; ^b Reference 29 and ^c References 30,31; ^d Reference 5 and references therein; ^e Reference 34; ^f This study, errors represent one standard deviation; ^g Reference 7; ^h Reference 8; ⁱ Reference 16; ^j Reference 1; ^k Reference 17; ^l Reference 18; ^m Reference 35; ⁿ Reference 36; ^o Reference 12.

The stability constants of $[M.C22C_5]^+$, where $M^+ = Li^+, Na^+, K^+, Rb^+, Cs^+, Tl^+$ and Ag^+ , are now compared with results from the literature for $[M.C221]^+$, $[M.C22C_2]^+$ and $[M.C22]^+$ in methanol, DMF, water and acetonitrile (Table 2.5). The diaza-crown ether C22, and the cryptands C221, C22C₅, and C22C₂, all have the eighteen membered, C22- ring as a common structural feature (Figure 2.2).

The variation in stability of the alkali metal ion cryptates, in all four solvents (Table 2.5) $[M.C221]^+$, is $Li^+ < Na^+ > K^+ > Cs^+$ which contrasts with $[M.C22C_5]^+$ where the observed variation is $Li^+ < Na^+ < K^+ \geq Rb^+ \geq Cs^+$. As was observed previously in aqueous solution, the variation in stability constant is smaller with $[K.C22C_5]^+ \geq [Rb.C22C_5]^+ \geq [Cs.C22C_5]^+$ than it is with $[K.C22C_5]^+ > [Na.C22C_5]^+ > [Li.C22C_5]^+$. This is consistent with a greater solvation energy experienced by smaller ions (solvation energy decreases from Li^+ to Cs^+) decreasing the cryptate stability for the oxygen donor solvents, methanol, water and DMF, and could explain the shift in selectivity from Na^+ in C221, to K^+ in C22C₅.

In the solid state structures, $[Na.C221]SCN$ forms an *inclusive* cryptate¹¹ consistent with Na^+ ($r = 1.02 \text{ \AA}$) and the cryptand ($r = 1.1 \text{ \AA}$) donor sites achieving optimum bonding interaction. There is minimal interaction between Na^+ and SCN^- . In contrast, $[Na.C22C_5]ClO_4$ forms an *exclusive* cryptate with C22C₅, where Na^+ is $0.011(2) \text{ \AA}$ below the common plane delineated by the four cryptand oxygens of the C22- ring, and does interact with the anion. In comparison, for K^+ (which forms the most stable cryptate with C22C₅ in solution) there are two independent *exclusive* $[K.C22C_5]ClO_4$ species in the solid state, where K^+ is either $0.369(1)$ or $0.441(1) \text{ \AA}$ above the analogous plane. In the solid state structures $[M.C22C_5]^+$, ($M^+ = Na^+, K^+$ and Cs^+) the bulk of the electrostatic interactions of the metal ion are with the four cryptand oxygen atoms (there are only distant interactions between the metal ion and the cryptand nitrogens) and the anion (ClO_4^-).

These observations in solution and solid state, are indicative of the weaker electrostatic interaction between C22C₅ and the metal ions, compared to C221 with these ions, and illustrates the effect of the replacement of the fifth oxygen donor atom of C221 by a methylene $-(CH_2)-$ moiety in C22C₅.

The variation in stability of the alkali metal ion cryptates $[M.C22C_2]^+$ is $Li^+ < Na^+ > K^+ > Cs^+$ (the same trend is observed for $[M.C221]^+$). The topology of $C22C_2$ in the solid state has been described³⁷ as a hinged double tablet, where both $-N-(CH_2)_2-O-(CH_2)_2-O-(CH_2)_2-N-$ arms are hinged by the $-N-(CH_2)_2-N-$ arm. The planes of the tablets, as delineated by the two oxygens of each arm and the two nitrogens, bisect at an angle of 88.4° , this compares with 70.9 , 89.6 and 100° for the solid state structures $[Li.C22C_2]^+$, $[Na.C22C_2]^+$ and $[K.C22C_2]^+$ respectively. Thus, a correlation may be made between the maximum of stability in solution and the $[M.C22C_2]^+$ structure, in which the bisecting angle that most closely matches that of the free ligand (88.4°) experiences the least strain.⁸

The diaza-crown ether, $C22$, has a greater degree of flexibility by comparison with the $C22-$ rings of $C221$, $C22C_5$ and $C22C_2$, where the additional nitrogen to nitrogen bridge replaces the amine protons of $C22$ (Figure 2.2). The $[M.C22C_5]^+$ and $[M.C22C_2]^+$ cryptates are more stable than $[M.C22]^+$, which has the same number and type of donor atoms. This is consistent with the exclusion of the solvent from approaching one side of the metal ion in $[M.C22C_5]^+$ and $[M.C22C_2]^+$, which combined with the relative inflexibility of the corresponding cryptand, increases their stability by comparison with $[M.C22]^+$ whose structure and greater flexibility of $C22$ exposes the metal ion to a greater contact with the solvent.

2.4: Sodium(I) Ion Complexation by Diaza-Crown Ether C21 and Cryptands C21C5 and C211 in Non-Aqueous Solution

The cryptands C211 and C21C₅ and the diaza-crown ether C21 have the same fifteen membered 4,7,13-trioxa-1,10-diazacyclopentadecane, or C21- ring as a common structural feature. However, in the case of C211 and C21C₅ there are additional nitrogen to nitrogen linkages, $-(\text{CH}_2)_2\text{-O-}(\text{CH}_2)_2\text{-}$ and $-(\text{CH}_2)_5\text{-}$ respectively, while C21 has no such linkage. These differences facilitate an examination of the effect of a systematic variation of ligand structure on the equilibria of the Na⁺ ion complexes they form. This section of the study is carried out in three solvents - N,N-dimethylformamide (DMF), N,N-diethylformamide (DEF) and N,N-dimethylacetamide (DMA). These solvents are similar in their electron donating abilities as expressed by their Gutmann donor numbers²⁹ (26.6, 30.9 and 27.8 respectively), but have significantly different molecular shapes and sizes. They have been shown to produce marked variations in the solvent lability and stoichiometries for solvated cobalt(II) and nickel(II) ions.³⁸ Thus, it is of interest to examine the effects of these solvents on the complexation of Na⁺ by the three ligands, C21, C211 and C21C₅.^{5,6,39,40}

The stability constants of [Na.C211]⁺ in DEF and DMA have been determined, and are compared with literature data, for [Na.C211]⁺ in DMF,⁵ and [Na.C21]⁺ and [Na.C21C₅]⁺ in the three solvents DMF, DMA and DEF^{6,40} (Table 2.6).

The Na⁺ ion ($r = 1.02 \text{ \AA}$) is too large (C211 and C21C₅, $r = 0.8 \text{ \AA}$, see Table 1.1, Chapter 1) to fit in the cavities of either C211 or C21C₅, and from X-ray crystallographic studies⁴¹ both [Na.C211]⁺ and [Na.C21C₅]⁺ form *exclusive* cryptates, where the cation is bound to the fifteen membered ring containing three ether oxygens and two amine nitrogens (the Na⁺ ion is also bound to the anion for both cryptate structures). There are no published X-ray crystallographic studies of any [Na.C21]X structures. However, it has been shown for the K⁺ analogue, [K.C21]SCN, that K⁺ is sited directly above the C21 (bound to the fifteen membered ring containing three ether oxygens and two amine nitrogens) which exhibits a puckered planar conformation⁴² (the K⁺ ion is also bound to the SCN⁻ anion).

Table 2.6 Apparent Stability Constants of [Na.C21]⁺, [Na.C21C₅]⁺ and [Na.C211]⁺ in Three Related Solvents, N,N-Dimethylformamide (DMF), N,N-Dimethylacetamide (DMA), and N,N-Diethylformamide (DEF)

Solvent	D_N^a	$\log (K_s / \text{dm}^3 \text{ mol}^{-1})$ at 298.2 K		
		[Na.C21] ⁺	[Na.C21C ₅] ⁺	[Na.C211] ⁺
DMF	26.6	2.10	2.87 ^b	5.20 ^c
DMA	27.8	2.88	2.05	4.74
DEF	30.9	3.19	2.52	5.10

This study in collaboration, reference 40 except ^a Reference 29; ^b Reference 6; ^c Reference 5. All errors are ± 0.1 log units, all solution $0.0500 \text{ mol dm}^{-3}$ in TEAP as background electrolyte

The stability constants characterising [Na.C211]⁺ are greater than those for [Na.C21C₅]⁺ and [Na.C21]⁺ by two orders of magnitude or more for each of the three solvents. The greater stability of the [Na.C211]⁺ may be attributed to an additional (fourth) coordinating oxygen of the C211 ligand compared to the C21C₅ and C21 ligands,⁴³ even though the metal ion interaction with the fourth oxygen is weak by comparison to the other oxygens in the solid state crystal structure.⁴¹

The similarity of the stability constants for the [Na.C21C₅]⁺ and [Na.C21]⁺ complexes in the three solvents DMF, DMA and DEF (Table 2.6) infers that the -(CH₂)₅- bridge in C21C₅ makes a negligible contribution to the stabilization of the cryptate. This is in contrast to the effect found in aqueous solution for the protonation equilibria, where the K_1 values for the diaza-crown ethers C21 and C22 are two to three orders of magnitude less than the comparable aliphatic bridged cryptands, C21C₅ and C22C₅, respectively.

A comparison of the stability constant values in each each of the three solvents does not show any specific trend with the solvent donor power (D_N) which may be attributed to the small variation in donor number (Table 2.6). The stability constants of [Na.C211]⁺ and [Na.C21C₅]⁺ cryptates do decrease marginally in order of increasing solvent size, DMF < DEF < DMA,³⁸ where the increased steric bulk of the solvent marginally destabilises the complexed metal ion - solvent interaction.

2.5 : Experimental Methods

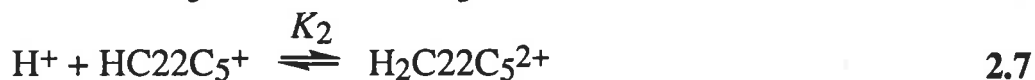
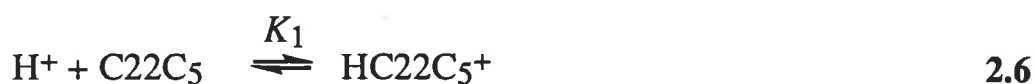
In this section, the methods used to derive the apparent protonation and stability constants are discussed. In addition, typical experimental results are presented to illustrate the discussion.

2.5.1 : Analysis of pH-Metric Titration Data in Aqueous Solution

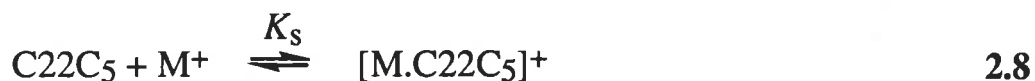
The apparent protonation constants K_1 and K_2 of C22C₅ given in Table 2.2 were the mean values found by duplicate titrations of a solution (10.00 cm³) containing 1.00×10^{-3} mol dm⁻³ C22C₅ and 4.204×10^{-3} mol dm⁻³ HClO₄ with 0.100 mol dm⁻³ TEAP as background electrolyte, with 0.1222 mol dm⁻³ TEAOH (base). The calibration values used for this experiment were, $pK_w = 13.709$ and $E_0 = 496.775$ mV (Figure 2.3).

The apparent stability constants, K_s , of [M.C22C₅]⁺, where M⁺ = Li⁺, Na⁺, K⁺, Rb⁺, Cs⁺, Tl⁺ and Ag⁺, given in Table 2.3 were the mean values found by titrating similar solutions containing MClO₄. For each metal ion at least two titrations were performed, in which the metal ion to cryptand concentration ratio was varied.

The protonation constants, K_1 and K_2 , were determined from the experimental titration data (for example Figure 2.3), using the program MINIQUAD,⁴⁴⁻⁴⁶ for the following reactions:



The stability constants, K_s , were determined for the experimental titration data (for example Figure 2.4), using MINIQUAD, and incorporating the values K_1 and K_2 as determined above, for the following reaction:



where M⁺ = Li⁺, Na⁺, K⁺, Rb⁺, Cs⁺, Tl⁺ and Ag⁺.

There was no evidence of the formation of any 2:1 or 1:2 metal ion to cryptand species, nor other possible species such as [M.HC22C₅]²⁺ or [M(OH).C22C₅].

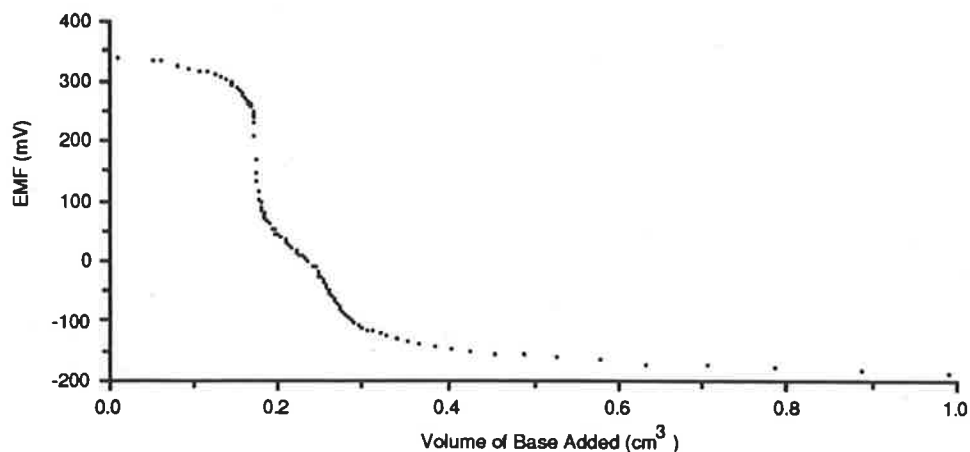


Figure 2.3 A typical titration curve used for calculation of the protonation constants of the cryptand C22C5. A solution of 10.0 cm³ containing 1.000 × 10⁻³ mol dm⁻³ C22C5 and 4.204 × 10⁻³ mol dm⁻³ HClO₄ with 0.100 mol dm⁻³ TEAP as background electrolyte, was titrated with 0.1222 mol dm⁻³ TEAOH (base). The calibration values used for this titration were, pK_w = 13.709 and E₀ = 496.775 mV.

Using 60 points,⁴⁷ with 7 iterations of the program MINIQUAD⁴⁴⁻⁴⁶ with a R factor⁴⁸ = 0.00248, the results calculated for this titration were:
 $\log \beta_a (\log K_1) = 11.260 \pm 0.013$; $\log \beta_b (\log K_1 + \log K_2) = 19.418 \pm 0.023$.

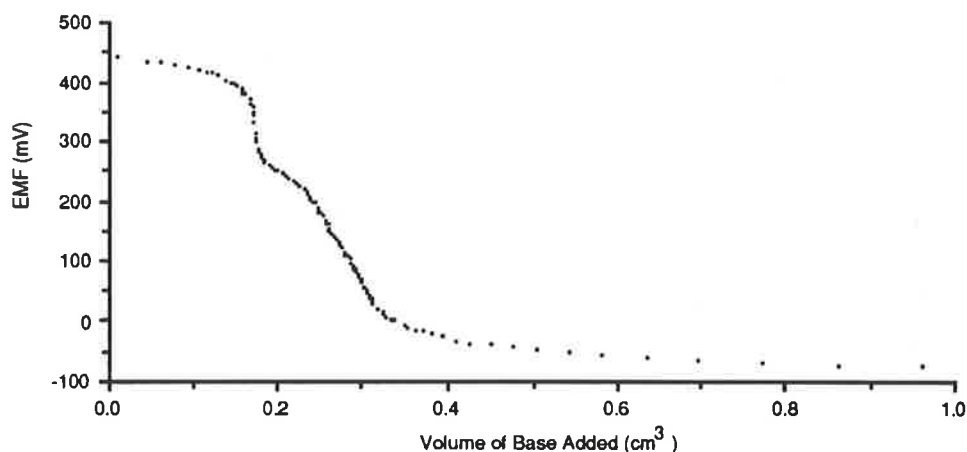


Figure 2.4 A typical titration curve used for calculation of the apparent stability constant of [Ag.C22C5]⁺. A solution of 10.05 cm³ containing 9.95 × 10⁻⁴ mol dm⁻³ C22C5 and 4.089 × 10⁻³ mol dm⁻³ HClO₄ with 0.100 mol dm⁻³ TEAP as background electrolyte, was titrated with 0.1222 mol dm⁻³ TEAOH (base). The calibration values used for this experiment were, pK_w = 13.775 and E₀ = 599.432 mV and the protonation constants for C22C5, $\log \beta_a (\log K_1) = 11.25$; $\log \beta_b (\log K_1 + \log K_2) = 19.41$.

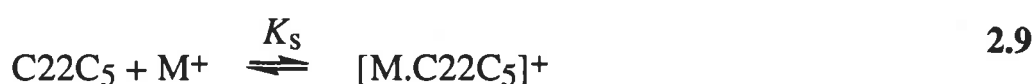
Using 26 points, with 12 iterations of the program MINIQUAD and a metal to ligand ratio of 1:2, with an R factor = 0.00283, the results were:
 $\log K_s [\text{Ag.C22C5}]^+ = 9.31 \pm 0.05$.

Errors represent one standard deviation of experimental to calculated data, as generated by the program MINIQUAD.

2.5.2 : Analysis of Potentiometric Titration Data in Aqueous and Non-Aqueous Solution

There are two basic methods of potentiometric titration applied in this study, aside from the pH-metric studies discussed in the previous section.

One method is the direct titration of cryptand into a solution containing $MClO_4$, where an ion selective electrode (ISE) is used to measure the solvated metal ion concentration. This was used, for $[Na.C22C5]^+$ and $[Ag.C22C5]^+$, in a variety of solvents to measure the stability constants, K_s , as defined below:



$$K_s = \frac{[M.C22C5^+]}{[M^+][C22C5]}$$

where $M^+ = Na^+$ or Ag^+

The other method used in this study is the measurement of the equilibrium constant of $[Ag.C22C5]^+$ in the presence of a competing metal ion, M^+ :



$$K_{sE} = \frac{[Ag.C22C5^+][M^+]}{[M.C22C5^+][Ag^+]}$$

where $M^+ = Li^+, Na^+, K^+, Rb^+, Cs^+$ or Tl^+

Thus if the $[Ag.C22C5]^+$ stability constant, $K_s(Ag)$, is known in the absence of the competing metal ion, then the cryptate, $[M.C22C5]^+$, stability constant, $K_s(M)$, may be found from the equilibrium constant:

$$K_s(M) = \frac{K_s(Ag)}{K_{sE}} = \frac{[M.C22C5^+]}{[C22C5][M^+]} \quad 2.11$$

It has been reported in the literature² that in systems where $K_s > 10^6 \text{ dm}^3 \text{ mol}^{-1}$ in methanol the Na^+ concentration may be below the limit of detectability for the Na^+ ISE (depending upon the total reactant concentrations, and the solvent used). Under these conditions the electrode behaviour

may no longer be described as pseudo Nernstian (experimental section 5.1.6 in Chapter 5). Consequently, the competitive titration method was used to determine the stability constant for the cryptate $[\text{Na.C22C}_5]^+$ in acetonitrile.

The stability constants derived for aqueous systems by potentiometric titration are within experimental error for $[\text{M.C22C}_5]^+$, where $\text{M}^+ = \text{Li}^+, \text{K}^+, \text{Rb}^+, \text{Cs}^+, \text{Tl}^+$ and Ag^+ . In the case of the $[\text{Na.C22C}_5]^+$ stability constant value determined by potentiometric titrations, the EMF varied over only *ca.* 10 mV in the course of a titration, (this compares with *ca.* 30 mV for the next lowest stability determined by this method, for $[\text{Na.C22C}_5]^+$ in dimethyl sulfoxide) and may indicate a resolvable lower limit of about $\log K_s \geq 2.5$ in the solvent water.

The determination of the stability constant by direct titration was achieved using the linear solution method, shown below, as discussed by Rossotti and Rossotti,⁴⁹ and used in the FORTRAN-77 program STAB (Appendix i). The results found by this method were then confirmed, by a second method of analysis, using the FORTRAN-77 program VISP (Appendix ii), which determines the stability constant, K_s , for a calculated titration curve that best fits the experimental data.

It is now appropriate to discuss the mathematical detail for the derivation of stability constant values by these two methods for both direct and competitive titration methods.

In the direct titration experiment, the value K_s (as defined in Equation 2.9) may be derived from known or measurable experimental quantities:

$$K_s = \frac{[\text{M}_{\text{tot}}^+] - [\text{M}^+]}{[\text{M}^+] [\text{L}]} \quad 2.12$$

where $[\text{M.L}^+] = [\text{M}_{\text{tot}}^+] - [\text{M}^+]$

Equation 2.12 may be rearranged into the form expressed by Rossotti⁴⁹ and Rossotti:

$$\frac{1 - \alpha_1}{\alpha_1} = K_s [L] \quad 2.13$$

where α_1 = the mole fraction of solvated metal ion $\frac{[M^+]}{[M_{\text{tot}}^+]}$, and
 [L] is the free ligand concentration.

The values of $\frac{1 - \alpha_1}{\alpha_1}$ and [L] were calculated for each point in the titration:

$$[L] = [L_{\text{tot}}^+] - [M.L^+] \quad 2.14$$

in terms of experimentally determined variables:

$$[L] = [L_{\text{tot}}^+] - [M_{\text{tot}}^+] + [M^+] \quad 2.14a$$

A plot of [L] versus $\frac{1 - \alpha_1}{\alpha_1}$ (Equation 2.13) yields a straight line of slope = K_s .

Under experimental conditions where the ligand is titrated into a solution containing $MClO_4$, the free ligand concentration, [L], is very small before the equivalence point. Consequently, any experimental errors in the parameters used to derive [L] (Equation 2.14a) are vastly magnified, and so these data points are not used in determining the stability constant by this method.

Sample potentiometric titration data and the parameters calculated from the STAB program are shown in Table 2.7. The titration curve is shown in Figure 2.5, and the straight line plot of [L] versus $\frac{1 - \alpha_1}{\alpha_1}$ in Figure 2.6.

Table 2.7 Experimental and Calculated Results for the Stability Constant Determination of $[\text{Na.C22C}_5]^+$ in Dimethyl Sulfoxide, $\log K_s = 3.15 \pm 0.05$

Titre (cm^3)	EMF (expt) mV	EMF (calc) mV	$[\text{Na}^+]$ (expt) mol dm^{-3}	$[\text{Na}^+]_{\text{(total)}}$ mol dm^{-3}	$[\text{C22C}_5]$ mol dm^{-3}	$(1-\alpha_1)$ α_1
2.600	-279.20	-278.5	0.0005133934	0.001158407	0.00082410	1.26
2.700	-279.80	-279.2	0.0005004514	0.001153304	0.00086605	1.30
2.800	-280.50	-279.8	0.0004857642	0.001148246	0.00090576	1.36
2.900	-281.60	-280.5	0.0004635503	0.001143231	0.00093748	1.47
3.120	-283.20	-282.0	0.0004330398	0.001132353	0.00102397	1.61
3.200	-284.00	-282.5	0.0004185461	0.001128448	0.00105148	1.70
3.300	-284.60	-283.1	0.0004079951	0.001123605	0.00109302	1.75
3.400	-285.30	-283.7	0.0003960213	0.001118803	0.00113269	1.83
3.500	-286.20	-284.3	0.0003811413	0.001114043	0.00116901	1.92
3.600	-286.80	-284.9	0.0003715332	0.001109322	0.00121018	1.99
3.700	-287.60	-285.5	0.0003590981	0.001104641	0.00124809	2.08
3.800	-288.30	-286.1	0.0003485593	0.001100000	0.00128747	2.16
3.900	-289.00	-286.6	0.0003383298	0.001095397	0.00132674	2.24
4.000	-289.60	-287.2	0.0003298009	0.001090833	0.00136730	2.31
4.100	-290.20	-287.7	0.0003214871	0.001086307	0.00140767	2.38
4.200	-290.80	-288.2	0.0003133828	0.001081818	0.00144785	2.45
4.300	-291.50	-288.8	0.0003041857	0.001077366	0.00148653	2.54
4.400	-292.00	-289.3	0.0002977820	0.001072951	0.00152762	2.60
4.500	-292.60	-289.9	0.0002902753	0.001068571	0.00156721	2.68
4.600	-293.20	-290.3	0.0002829578	0.001064228	0.00160662	2.76
4.700	-293.90	-290.8	0.0002746536	0.001059919	0.00164465	2.86
4.800	-294.40	-291.3	0.0002688716	0.001055645	0.00168484	2.93
4.900	-295.00	-291.7	0.0002620937	0.001051406	0.00172366	3.01
5.000	-295.50	-292.2	0.0002565761	0.001047200	0.00176338	3.08

A solution of 20.00 cm^3 of $1.309 \times 10^{-3} \text{ mol dm}^{-3}$ NaClO_4 in dimethyl sulfoxide, was titrated with $0.01277 \text{ mol dm}^{-3}$ C22C_5 in DMSO (all solutions in a background electrolyte of $0.0500 \text{ mol dm}^{-3}$ TEAP). The data points are those falling in the most accurate region of the titration curve as described by Rossotti and Rossotti.⁴⁹

Values for solvated Na^+ were derived from calibration over the concentration range of $5 \times 10^{-6} \text{ mol dm}^{-3}$ to $5 \times 10^{-3} \text{ mol dm}^{-3}$ $[\text{Na}^+]$. For dimethyl sulfoxide, it was found that $C = 23.50 \text{ mV}$, and $E_0 = -101.2 \text{ mV}$ and $[\text{Na}^+]_{\text{total}} = 1.31 \times 10^{-3} \text{ mol dm}^{-3}$, in which $[\text{Na}^+]$ was calculated for each titration point using the mass balance equation, i.e. $[\text{Na}^+]_{\text{total}} = 20.00 / (20.00 + x) \times [\text{Na}^+]_{\text{initial}}$. Similarly, $[\text{C22C}_5]_{\text{total}} = x / (20.00 + x) \times [\text{C22C}_5]_{\text{initial}}$, where x is the volume in cm^3 of added titrant, and 20.00 is the initial volume in cm^3 of the measured solution. Subsequently, K_s was determined from the slope of a plot of $(1-\alpha_1)/\alpha_1$ against $[\text{C22C}_5]$.

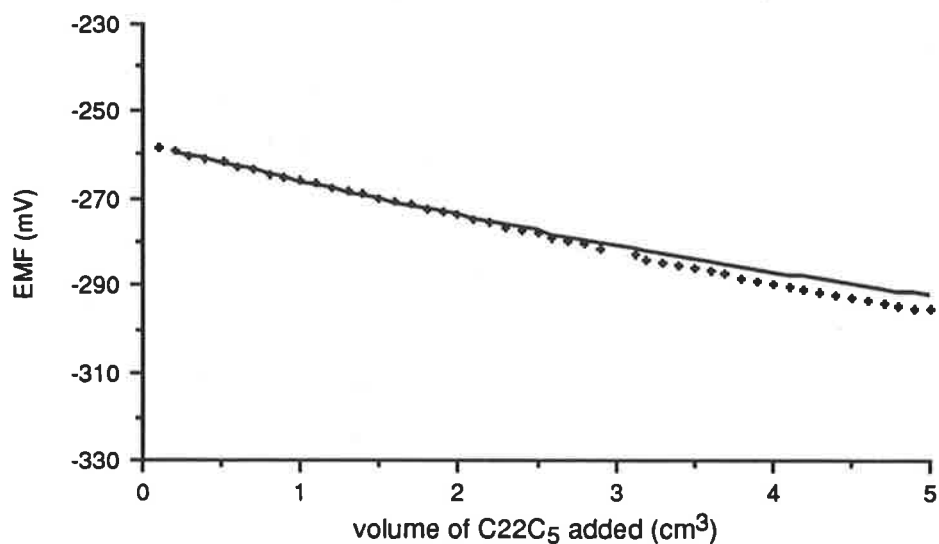


Figure 2.5 Plot of titration volume (cm^3) against $\text{EMF}_{(\text{expt})}$ and $\text{EMF}_{(\text{calc})}$ (both in mV) for the titration of C22C_5 with NaClO_4 in dimethyl sulfoxide, with a stability constant $\log K_s = 3.15 \pm 0.05$.

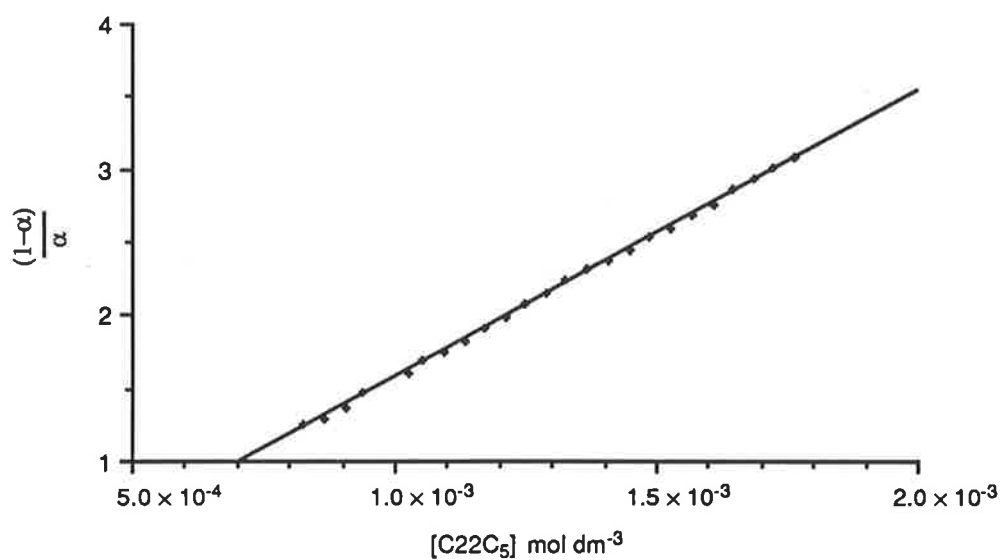


Figure 2.6 Plot of $[L]$ versus $\frac{1 - \alpha_1}{\alpha_1}$ for the cryptate $[\text{Na.C22C}_5]^+$ in dimethyl sulfoxide, showing the line of best fit.

In the competitive titration experiment, the value K_s for the competing metal ion cryptate (as defined in the Equations 2.10 and 2.11) may be derived in an analogous manner to that of the direct titration experiment, from known or measurable experimental quantities:

$$K_s = \frac{[Ag_{tot}^+] - [Ag^+]}{[Ag^+]} \times \frac{[M^+]}{[M.L^+]} \quad 2.15$$

Dividing through by $[Ag_{tot}^+]$, and substituting $\alpha_1 = \frac{[Ag^+]}{[Ag_{tot}^+]}$:

$$[M.L^+] K_s = \frac{1 - \alpha_1}{\alpha_1} [M^+] \quad 2.16$$

where

$$[M.L^+] = [L_{tot}^+] - [Ag.L^+] - [L] \quad 2.17$$

$$= [L_{tot}^+] - [Ag_{tot}^+] + [Ag^+] - [L] \quad 2.17a$$

Experimentally $[M_{tot}^+] > [L_{tot}^+]$, and so for a stability constant $> 10^2$, the total amount free $[L]$ is negligible, and Equation 2.17a becomes:

$$[M.L^+] = [L_{tot}^+] - [Ag_{tot}^+] + [Ag^+] \quad \text{and} \quad 2.17b$$

$$[M^+] = [M_{tot}^+] - [M.L^+]$$

The value derived for K_s may then be calculated from linear regression of Equation 2.13 for the direct titration experiment, or Equation 2.16 for the competitive titration experiment. For both the direct and competitive titration models, K_s was found by simple linear regression analysis of the results from the program STAB (Appendix i). It is apparent that for the data points on the titration curve after the equivalence point, the function describes a straight line, where the slope is the stability constant K_s . The quoted errors are one standard deviation of the slope based on the experimental scatter of the points.

Sample potentiometric titration data and the parameters calculated from the STAB program for a competitive titration, are shown in Table 2.8. The titration curve is shown in Figure 2.7, and the straight line plot of $[M.L^+]$ versus $\frac{1 - \alpha_1}{\alpha_1} \times [M^+]$ in Figure 2.8.

Table 2.8 Experimental and Calculated Results for the Stability Constant Determination of [Cs.C22C5]⁺ in N,N-Dimethylformamide (DMF)log $K_{SE} = 6.51 \pm 0.03$, $K_S(\text{Cs}^+) = 2.90 \pm 0.13$

Titre (cm ³)	EMF (expt) mV	EMF (calc) mV	[Ag ⁺] × 10 ⁷ mol dm ⁻³	[Cs ⁺] × 10 ³ mol dm ⁻³	[Cs.C22C5] ⁺ × 10 ³ mol dm ⁻³	[Cs ⁺] × (1-α ₁) α ₁
1.96	-318.2	-309.0	0.6061	4.551	0.015	67.82
2.00	-334.0	-330.4	0.3389	4.617	0.034	122.8
2.04	-345.2	-342.0	0.2245	4.683	0.052	187.8
2.08	-351.7	-350.0	0.1767	4.749	0.071	241.4
2.12	-356.5	-355.9	0.1481	4.814	0.089	291.5
2.16	-361.1	-360.7	0.1250	4.879	0.108	349.2
2.20	-364.9	-364.7	0.1087	4.944	0.126	406.3
2.24	-368.5	-368.0	0.0952	5.009	0.144	469.0
2.28	-371.1	-371.0	0.0866	5.073	0.162	521.8
2.32	-373.5	-373.5	0.0792	5.137	0.181	576.1
2.36	-375.9	-375.8	0.0725	5.201	0.199	636.0
2.40	-377.9	-377.9	0.0674	5.265	0.217	691.7
2.44	-379.9	-379.8	0.0633	5.328	0.235	743.9
2.50	-382.2	-382.3	0.0575	5.423	0.262	830.9
2.56	-384.4	-384.6	0.0531	5.517	0.288	914.2
2.64	-387.2	-387.2	0.0479	5.642	0.324	1032
2.70	-388.8	-389.0	0.0451	5.735	0.350	1110
2.80	-391.4	-391.6	0.0410	5.890	0.394	1249
2.90	-393.7	-393.8	0.0377	6.042	0.437	1389
3.00	-395.8	-395.8	0.0349	6.194	0.480	1531
3.10	-397.6	-397.6	0.0327	6.344	0.522	1668
3.20	-399.1	-399.2	0.0309	6.493	0.564	1797
3.30	-400.6	-400.6	0.0292	6.640	0.606	1933
3.40	-402.0	-401.9	0.0278	6.787	0.647	2071
3.60	-404.3	-404.3	0.0255	7.075	0.729	2331
3.80	-406.4	-406.3	0.0236	7.359	0.809	2597
4.00	-408.2	-408.0	0.0221	7.639	0.888	2856
4.20	-409.9	-409.5	0.0208	7.913	0.966	3124
4.60	-412.8	-412.2	0.0187	8.449	1.118	3650
5.00	-415.0	-414.3	0.0172	8.968	1.264	4134

A solution of 20.00 cm³ of 9.92×10⁻⁴ mol dm⁻³ AgClO₄ in DMF, was titrated with a solution containing 0.01029 mol dm⁻³ C22C₅ and 0.05116 mol dm⁻³ CsClO₄ in DMF (all solutions in a background electrolyte of 0.0500 mol dm⁻³ TEAP). The data points are those falling in the most accurate region of the titration curve as described by Rossotti and Rossotti.⁴⁹ Values for the solvated Ag⁺ were derived from calibration over the concentration range of 2×10⁻⁹ to 5×10⁻³ mol dm⁻³ [Ag⁺]. For DMF, it was found that $C = 27.18$ mV, and $E_0 = 133.5$ mV, and $[\text{Ag}^+]_{\text{total}} = 9.92 \times 10^{-4}$ mol dm⁻³, in which [Ag⁺] was calculated for each titration point using the mass balance equation, that is $[\text{Ag}^+]_{\text{total}} = 20.00 / (20.00 + x) \times [\text{Ag}^+]_{\text{initial}}$. Similarly, $[\text{Cs.C22C}_5^+]_{\text{total}} = x / (20.00 + x) \times [\text{Cs.C22C}_5^+]_{\text{initial}}$, where x is the volume in cm³ of added titrant, and 20.00 is the initial volume in cm³ of the measured solution, and [C22C₅] was assumed to be zero. Subsequently, K_S was determined from the slope of the plot of $[\text{Cs}^+] \times (1 - \alpha_1) / \alpha_1$ against [Cs.C22C₅⁺].

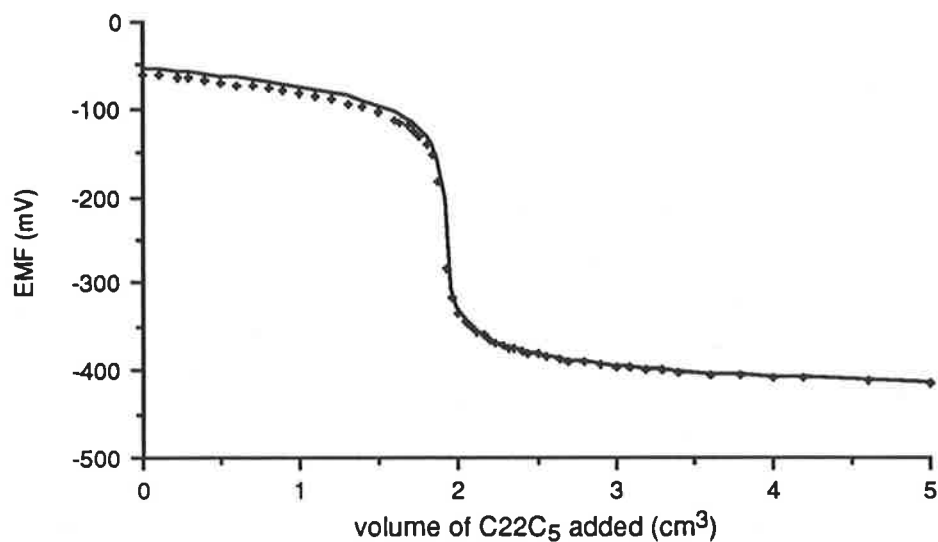


Figure 2.7 Plot of titration volume (cm^3) against $\text{EMF}_{(\text{expt})}$ and $\text{EMF}_{(\text{calc})}$ (mV) for the titration of $[\text{Cs.C22C5}]^+$ with Ag^+ in DMF, with an equilibrium stability constant $\log K_{\text{sE}} \left(\frac{[\text{Ag.C22C5}]^+}{[\text{Cs.C22C5}]^+} \right) = 6.51 \pm 0.03$; and $\log K_{\text{s[M]}} = (9.40 \pm 0.13 - 6.51 \pm 0.03) = 2.89 \pm 0.13$.

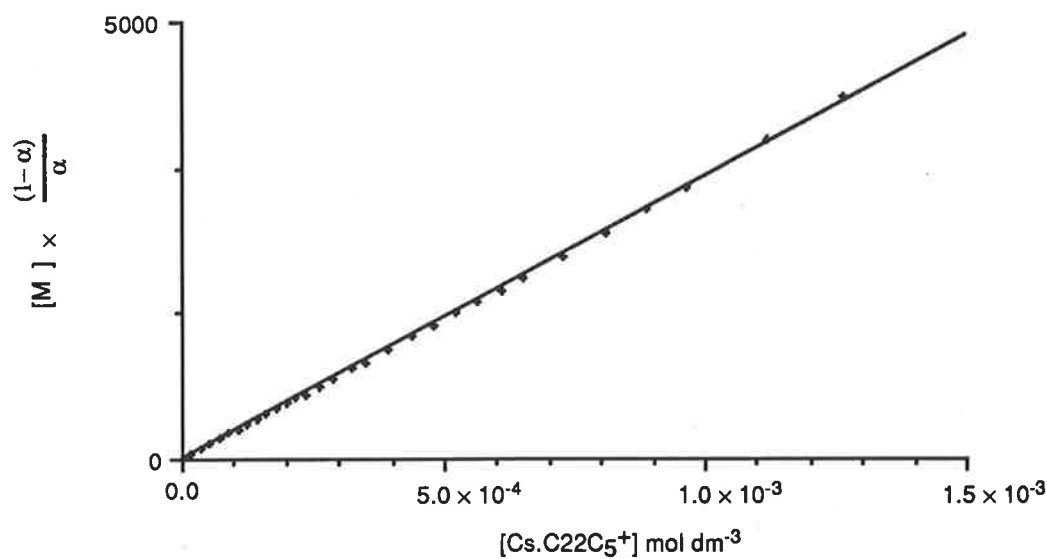


Figure 2.8 Plot of $[\text{Cs.C22C5}^+]$ versus $\frac{1-\alpha_1}{\alpha_1} [\text{Cs}^+]$ for the cryptate $[\text{Cs.C22C5}]^+$ in DMF.

The program VISP (Appendix ii) calculates a titration curve for volume of titrant added versus EMF, from known experimental parameters, initial concentrations of the various species, volumes of the solutions, and calibrated electrode response. The model used in the program VISP, to describe the titration curve function is described below:

For simplicity, if the following definitions are used:

$$T = [Ag_{tot}^+];$$

$$L = [L_{tot}^+] \text{ (or for the competitive case = } [L.X_{tot}^+] \text{)};$$

$$X = [M_{tot}^+] \text{ (competitive only); and}$$

F = solvated $[Ag^+]$ in solution, as directly measured from the EMF of the calibrated cell,

then Equation 2.9 becomes:

$$K_s = \frac{T - F}{F \times (L - T + F)} \quad 2.18$$

and Equation 2.11 becomes:

$$K_{sE} = \frac{(T - F) \times (X - L + T - F)}{F \times (L - T + F)} \quad 2.19$$

Then, rearranging Equation 2.18 for the direct titrations case:

$$K_s F^2 + (K_s L - K_s T + 1) F - T = 0 \quad 2.20$$

and solving for F:

$$F = \frac{(K_s T - K_s L - 1) + \sqrt{K_s^2(L - T)^2 + 2 K_s(L + T) + 1}}{2K_s} \quad 2.21$$

Each term in Equation 2.21 must be positive to be physically meaningful.

Similarly, for the competitive titration case, rearranging Equation 2.19:

$$(K_s - 1)F^2 + (K_s L - K_s T + 2T + X - L) F + (L - X - T)T = 0 \quad 2.22$$

solving for F:

$$F = \frac{(K_S - 2)T + (1 - K_S)L - X + \sqrt{\text{Surd}}}{2(K_S - 1)} \quad 2.23$$

where the Surd = $K_S^2(L - T)^2 + K_S(X\{2T + L\} + 2L\{T - L\}) + (L - X)^2$

The value of K_S may be derived by this method by minimising the sum of residuals for calculated and experimental data, in EMF by systematic variation of K_S . The results may be presented graphically for visual comparison as in Figures 2.5 and 2.7.

- 1 Lehn J.-M., *Struct. Bonding (Berlin)*, **1973**, 16, 1 - 69.
- 2 Lehn J.-M., Sauvage J.-P., *J. Am. Chem. Soc.*, **1975**, 97, 6700 - 6707.
- 3 Lehn J.-M., *Pure Appl. Chem.*, **1979**, 51, 979 - 997.
- 4 Cox B.G., Schneider H., Stroka J.J., *J. Am. Chem. Soc.*, **1978**, 100, 4746 - 4749.
- 5 Cox B.G., Garcia-Rosas J., Schneider H., *J. Am. Chem. Soc.*, **1981**, 103, 1384 - 1389.
- 6 Lincoln S.F., Brereton I.M., Spotswood T.M. *J. Am. Chem. Soc.*, **1986**, 108, 8134 - 8138.
- 7 Abou-Hamdan A., Lincoln S.F., *Inorg. Chem.*, **1991**, 30, 462 - 466.
- 8 Lincoln S.F., Stephens A.K.W., *Inorg. Chem.*, **1991**, 30, 3529 - 3534.
- 9 Lehn J.-M., Sauvage J.-P., *J. Chem. Soc., Chem. Commun.*, **1971**, 440.
- 10 Shannon R.D., *Acta Cryst., Sect. A: Cryst. Phys. Diffr., Theor. Gen. Crystallog.*, **1976**, A32, 751 - 767.
- 11 Mathieu F., Metz B., Moras D., Weiss R., *J. Am. Chem. Soc.*, **1978**, 100, 4412 - 4416.
- 12 Anderegg G., *Helv. Chim. Acta*, **1981**, 64, 1790 - 1795, *Ibid*, **1975**, 58, 1218 - 1225.
- 13 Lejaille M.-F., Livertoux M.-H., Guidon C., Bessiere J., *Bull. Soc. Chim. Fr.*, **1978**, 19, 1373 - 1377.
- 14 Dalley N.K., in "Synthetic Multidentate Macrocyclic Compounds", Izzat R.M., Christensen J.J., Eds., **1978**, Academic Press (New York).
- 15 Pedersen C.J., Frensdorff H.K., *Angew. Chem., Int. Ed. Engl.*, **1972**, 11, 16 - 22.
- 16 Shamsipur M., Popov A.I., *Inorg. Chim. Acta*, **1980**, 43, 243 - 247.
- 17 Boss R.D., Popov A.I., *Inorg. Chem.*, **1986**, 25, 1747 - 1750.
- 18 Kulstadt S., Malmsten L.A., *J. Inorg. Nucl. Chem.*, **1980**, 42, 573 - 578.
- 19 Izzat R.M., Bradshaw J.S., Nielsen S.A., Lamb J.D., Christensen J.J., *Chem. Rev.*, **1985**, 85, 271 - 339.
- 20 Lincoln S.F., Abou-Hamdan A., *Inorg. Chem.*, **1990**, 29, 3584 - 3589.
- 21 Lincoln S.F., Stephens A.K.W., **1992**, Unpublished Results.
- 22 Arnaud-Neu F., Spiess B., Schwing-Weill M., *Helv. Chim. Acta*, **1977**, 60, 2633 - 2643.
- 23 Arnaud-Neu F., Spiess B., Schwing-Weill M., *J. Chem. Res., Synop*, **1982**, 10 - 11.

-
- 24 Duckworth P.A., Lincoln S.F., Lucas J., *Inorg. Chim. Acta*, **1991**, 188, 55 - 59.
- 25 Luboch E., Cygan A., Biernat J.F., *Inorg. Chim. Acta*, **1983**, 68, 201 - 204.
- 26 Pearson R.G., *Coord. Chem. Rev.*, **1990**, 100, 403 - 425.
- 27 Lehn J.-M., *Acc. Chem. Res.*, **1978**, 11, 49 - 57.
- 28 Gutknecht J., Schneider H., Stroka J., *Inorg. Chem.*, **1978**, 17, 3326 - 3329.
- 29 Gutmann V., "Coordination Chemistry in Non-Aqueous Solvents", **1968**, Springer (New York).
- 30 Erlich R.H., Roach E., Popov A.I., *J. Am. Chem. Soc.*, **1970**, 92, 4989 - 4990.
- 31 DeWitte W.J., Popov A.I., *J. Soln. Chem.*, **1976**, 5, 231 - 240.
- 32 Popov A.I., *Pure Appl. Chem.*, **1979**, 51, 101 - 110.
- 33 Lincoln S.F., Steel B.J., Brereton I.M., Spotswood T.M., *Polyhedron*, **1986**, 5, 1597 - 1600.
- 34 Cox B. G., Schneider I., Schneider H., *J. Chem. Soc., Faraday Trans. 1*, **1989**, 85, 187 - 198.
- 35 Frensdorff H.K., *J. Am. Chem. Soc.*, **1971**, 93, 600 - 606.
- 36 Cox B.G., Firman P., Horst H., Schneider H., *Polyhedron*, **1983**, 2, 343 - 347.
- 37 Alfheim T., Dale J., Groth P., Krautwurst K.D., *J. Chem. Soc., Chem. Commun.*, **1984**, 1502 - 1504.
- 38 Lincoln S.F., Hounslow A.M., Boffa A.N., *Inorg. Chem.*, **1986**, 25, 1038 - 1042.
- 39 Lincoln S.F., Brereton I.M., Spotswood T.M., *J. Chem. Soc., Faraday Trans. 1*, **1985**, 81, 1623 - 1630.
- 40 This study in collaboration
Clarke P., Abou-Hamdan A., Hounslow A.M., Lincoln S.F., *Inorg. Chim. Acta*, **1988**, 154, 83 - 87.
- 41 Lincoln S.F., Horn E., Snow M.R., Hambley T.W., Brereton I.M., Spotswood T.M., *J. Chem. Soc., Dalton Trans.*, **1986**, 1075 - 1080.
- 42 Abou-Hamdan A., Lincoln S.F., Snow M.R., Tiekink E.R.T., *Aust. J. Chem.*, **1988**, 41, 1363 - 1367.
- 43 Abou-Hamdan A., Hounslow A.M., Lincoln S.F., Hambley T.W., *J. Chem. Soc., Dalton Trans.*, **1987**, 489 - 492.
- 44 Sabatini A., Vacca A., Gans P., *Talanta*, **1974**, 21, 53 - 77.

-
- 45 Gans P., Sabatini A., Vacca A., *Inorg. Chim. Acta*, **1976**, 18, 237 - 239.
- 46 Micheloni M., Sabatini A., Vacca A., *Inorg. Chim. Acta*, **1977**, 25, 41 - 48.
- 47 Some points from the titration were not used to calculate the derived values. The points discarded were either at high pH where precipitation of MOH species occurred, or at high and low pH where there were no appreciable amounts of the relevant species formed.
- 48 As defined by the program MINQUAD, where a lower "R Factor" implies a better fit to the complexation model. Values for $R < 0.004$ were taken to mean that the titration data fitted the protonation and complexation model.
- 49 Rossotti F.J.C., Rossotti H., "The Determination of Stability Constants" Chapter 5, **1961**, McGraw-Hill (New York).
- 50 Morrison R.T., Boyd R.N., "Organic Chemistry", Fourth Ed., **1983**, Chapter 23, Allyn and Bacon (New York).
- 51 Cox B.G., Schneider H., *Pure Appl. Chem.*, **1990**, 62, 2259 - 2268.
- 52 Dhillon R.S., Lincoln S.F., **1991**, unpublished observations.

Chapter 3 : Cryptate Complexation Dynamics

3.1 : Introduction

The formation and decomplexation rates of alkali metal cryptates have been subject to a number of kinetic and mechanistic studies.¹⁻²⁷ Cryptate lability is influenced by a number of factors. These include the relative sizes of the cryptand cavity and the metal ion, the structural flexibility and the number and type of donor atoms of the cryptand, and the nature and solvation energy of the metal ion. For example, the structural changes resulting from the replacement of an oxygen donor atom of a cryptand with a methylene moiety, $-(CH_2)-$, results in a substantial increase in the lability of the resulting cryptate,^{1,12,17,21,43} and an improved ability of the cryptand to catalyse alkali metal ion transport through lipid membranes.^{40,49,52}

Cryptate formation in solution involves a combination of conformational, coordination and solvational changes in the metal ion and cryptand, where each step contributes to the overall rate. This may be described by a simplified reaction scheme^{1,19,53} where the formation of the cryptate occurs in a sequence of steps.¹⁹ The first step is the formation of an encounter complex between the cryptand and solvated alkali metal ion, occurring at a diffusion controlled rate. The next step involves metal ion - cryptand bond formation, partial metal ion desolvation and conformational rearrangements of the cryptand. Subsequent steps involve further metal ion - cryptand bond formation and progressive desolvation of the metal ion (it is assumed that solvent interactions of the neutral cryptand and the diffuse anion, are negligible compared with those of the compact metal ion).

Two different exchange mechanisms may be operative for the overall exchange process (as also described for exchange of alkali metal ions between solvated and complexed states with crown ethers^{29,30,32}). The two exchange mechanisms may be described as:

- (1) The first order monomolecular mechanism, where the rate determining step is the decomplexation of the metal ion;
- (2) The second order bimolecular mechanism, where the rate determining step is a displacement of the metal ion in the cryptate by another metal ion.

A monomolecular exchange mechanism of decomplexation (Equation 3.1) of the metal ion from the cryptate in solution may be described by the overall reaction:



where:

k_f is the rate constant of cryptate formation;

k_d is the rate constant of decomplexation; and

$\frac{k_f}{k_d} = K_s$, the stability constant.

For this process, the rate of exchange is independent of the concentration of solvated metal ion, M^+ :

$$\text{exchange rate} = k_d [\text{M.Cryptand}^+] \quad 3.2$$

The observed species lifetimes are:

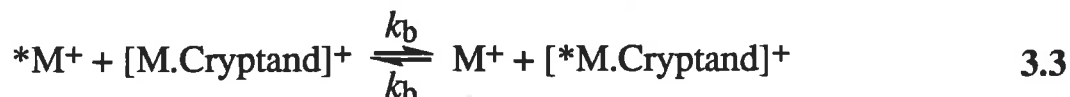
$$\tau_c = \frac{1}{k_d} = \frac{\tau_s \chi_c}{\chi_s} \quad 3.2a$$

where χ_c and χ_s are the mole fractions of the metal ion M^+ in the complexed and solvated environments respectively;

τ_c is the mean lifetime of the cryptate; and

τ_s is the mean lifetime of the solvated metal ion, M^+ .

For a bimolecular mechanism of exchange, the decomplexation and solvation of the complexed metal ion coincides with the complexation and desolvation of another metal ion, and may be described as:



where k_b is the rate constant for the bimolecular interchange

In contrast to the monomolecular exchange, the rate of bimolecular exchange is dependant on the concentration of solvated metal ion, M^+ , where the rate law and the observed species lifetimes may be described as:

$$\text{exchange rate} = k_b [\text{M.Cryptand}^+] [\text{M}^+] \quad 3.4$$

$$\text{where, } \tau_c = \frac{1}{k_b [\text{M}^+]} = \frac{\chi_s}{\tau_s \chi_c}$$

If the two mechanisms are in operation simultaneously,¹³ then the overall observed rate of exchange, k_{obs} , may be described as below:

$$\begin{aligned} \text{exchange rate} &= k_{\text{obs}} [\text{M.Cryptand}^+] \\ &= (k_{\text{d}} + k_{\text{b}}[\text{M}^+]) [\text{M.Cryptand}^+] \end{aligned} \quad 3.5$$

where the observed lifetime, τ_{c} , is given by :

$$\tau_{\text{c}} = \frac{1}{k_{\text{obs}}} = \frac{1}{(k_{\text{d}} + k_{\text{b}}[\text{M}^+])} \quad 3.5a$$

The standard state activation parameters, k_{d} , $\Delta G_{\text{d}}^{\ddagger}$, $\Delta H_{\text{d}}^{\ddagger}$ and $\Delta S_{\text{d}}^{\ddagger}$ are derived from the temperature variation of the observed lifetime of the cryptate τ_{c} through Equation 3.6 (The method of calculating these parameters is discussed in Chapter 6, section 6.3.2).

$$k_{\text{d}} = \frac{1}{\tau_{\text{c}}} = \frac{k_{\text{B}}T}{h} e^{\left(\frac{-\Delta G_{\text{d}}^{\ddagger}}{RT}\right)} = \frac{k_{\text{B}}T}{h} e^{\left(\frac{-\Delta H_{\text{d}}^{\ddagger}}{RT} + \frac{\Delta S_{\text{d}}^{\ddagger}}{R}\right)} \quad 3.6$$

where τ_{c} is the mean lifetime of the cryptate;

k_{d} is the decomplexation rate constant;

k_{B} is Boltzmann's constant;

h is Planck's constant;

$\Delta G_{\text{d}}^{\ddagger}$ the free energy of activation; and

$\Delta H_{\text{d}}^{\ddagger}$ and $\Delta S_{\text{d}}^{\ddagger}$ are the enthalpy and entropy of activation respectively, for the decomplexation reaction.

Rearranging Equation 3.6:

$$\ln(T \tau_{\text{c}}) = \frac{-\Delta H_{\text{d}}^{\ddagger}}{R} \left(\frac{1}{T}\right) + \left[\ln\left(\frac{k_{\text{B}}}{h}\right) - \frac{\Delta S_{\text{d}}^{\ddagger}}{R} \right] \quad 3.6a$$

From the rearranged equation it may be seen that a plot of $\log(T \tau_{\text{c}})$ against $1/T$ will yield a straight line. Similar equations may be applied for a bimolecular mechanism from the temperature variation of k_{b} .

3.2 : Exchange Kinetics for [M.C22C5]⁺ Systems in Selected Solvents

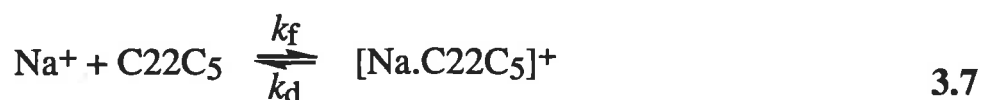
The rates of metal ion exchange of Li⁺ on [Li.C22C5]⁺ and Na⁺ on [Na.C22C5]⁺, have been investigated in a range of solvents. The available results are compared with kinetic data from the literature for similar systems based on the eighteen membered 4,7,13,16-tetraoxa-1,10-diaza (C22-) ring.

The mean lifetimes of the metal ion in solvated and complexed environments (specifically, Na⁺ and [Na.C22C5]⁺ in methanol) were determined by the complete lineshape analysis of the ²³Na variable temperature NMR spectra of solutions containing both species in equilibrium. The activation parameters were subsequently determined from the temperature variation of the lifetimes (Equation 3.6). Other rates of exchange of Li⁺ and Na⁺ on [M.C22C5]⁺ systems in a number of solvents were estimated by simplified analysis of their ⁷Li and ²³Na NMR spectra. The theory of the NMR techniques used for the study of the rate processes are discussed in Chapter 6 and may be compared to similar methods used for other cryptate systems.^{3,4,11-13,24}

The ⁷Li nucleus has a natural isotopic abundance of 92.6 %, an intrinsic NMR sensitivity 29.4 % of the ¹H nucleus, and a quadrupolar charge distribution, with a spin of 3/2.³¹ Similarly, the ²³Na nucleus has a natural isotopic abundance of 100 %, an intrinsic NMR sensitivity 9.3 % of the ¹H nucleus, 580 % of the ¹³C nucleus and a quadrupolar charge distribution, with a spin of 3/2. These alkali metal ion nuclei are very sensitive to the immediate environment and show a large range of chemical shifts in a range of solvents, the useful range of chemical shifts are ~10 ppm for ⁷Li and ~ 40 ppm for ²³Na.³³

3.2.1 : Exchange Kinetics of Na⁺ on [Na.C22C5]⁺ in Methanol

The temperature dependent coalescence of the ²³Na resonances arising from solvated Na⁺ and [Na.C22C5]⁺ in methanol (Figure 3.1) yields the kinetic parameters of [Na.C22C5]⁺ decomplexation for the reaction below.



These parameters are derived from the temperature variation of the mean lifetime of [Na.C22C5]⁺, τ_c , through Equation 3.6, where the τ_c values are derived through complete lineshape analysis³⁴ of the coalescing ²³Na resonances observed for solutions i - iii (Table 3.1) as exemplified by solution ii, Figure 3.1. The τ_c values derived for each of the solutions studied are covariant with temperature (Figure 3.2). Thus the mean lifetime of [Na.C22C5]⁺ ($\tau_c = 1/k_d$) is independent of solvated metal ion concentration, [Na⁺], over the range of concentration studied, and is consistent with the operation of a monomolecular mechanism for decomplexation of Na⁺ from the cryptand (Equations 3.2). The formation rate constant, k_f (298.2 K) = $1.05 \times 10^7 \text{ dm}^3 \text{ mol}^{-1} \text{ s}^{-1}$ is derived through the relationship below, and is within the range usually observed for cryptates :

$$\frac{k_f}{k_d} = K_s \quad 3.8$$

Table 3.1 Activation Parameters and Solution Compositions, for the Exchange of Na⁺ on [Na.C22C5]⁺ in Methanol

Solution	Na ⁺ mol dm ⁻³	[Na.C22C5] ⁺ mol dm ⁻³	$k_d(325.0 \text{ K})$ s ⁻¹ ^a	$k_d(298.2 \text{ K})$ s ⁻¹	ΔH_d^\ddagger kJ mol ⁻¹	ΔS_d^\ddagger J K ⁻¹ mol ⁻¹
i	0.0341	0.0159	271 ± 9	42.3 ± 5.0	53.2 ± 3.1	-28.5 ± 4.7
ii	0.0257	0.0243	286 ± 3	40.2 ± 1.7	56.2 ± 1.2	-19.3 ± 4.2
iii	0.0095	0.0405	289 ± 3	37.9 ± 1.1	58.4 ± 0.7	-4.7 ± 2.3
(i - iii)			281 ± 3	41.0 ± 1.7	55.1 ± 1.1	-29.2 ± 3.8

^a The rate parameter k_d is derived at 325.0 K which is the temperature in the midst of the coalescence region where the most reliable kinetic data are obtained.

All errors represent one standard deviation from the regression analysis of the experimental lifetimes, τ_c , to Equation 3.6.

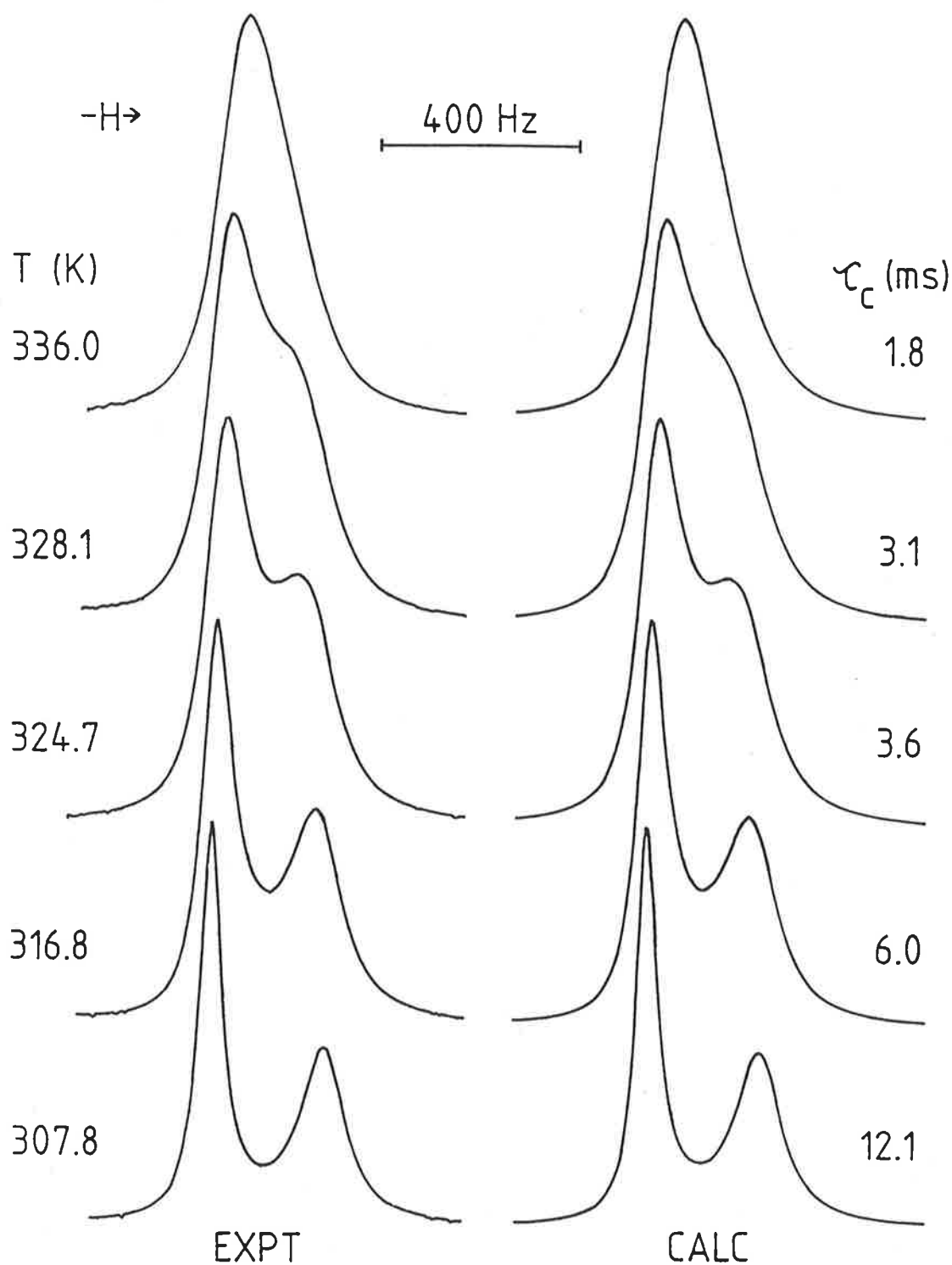


Figure 3.1 Typical exchange modified 79.39 MHz ^{23}Na NMR spectra of a methanol solution of NaClO_4 ($0.0500 \text{ mol dm}^{-3}$) and C_{22}C_5 ($0.0243 \text{ mol dm}^{-3}$). Experimental temperatures and spectra appear at the left of the figure. Best fit calculated lineshapes and corresponding τ_c values appear to the right. The resonance of $[\text{Na} \cdot \text{C}_{22}\text{C}_5]^+$ appears upfield from that of solvated Na^+ .

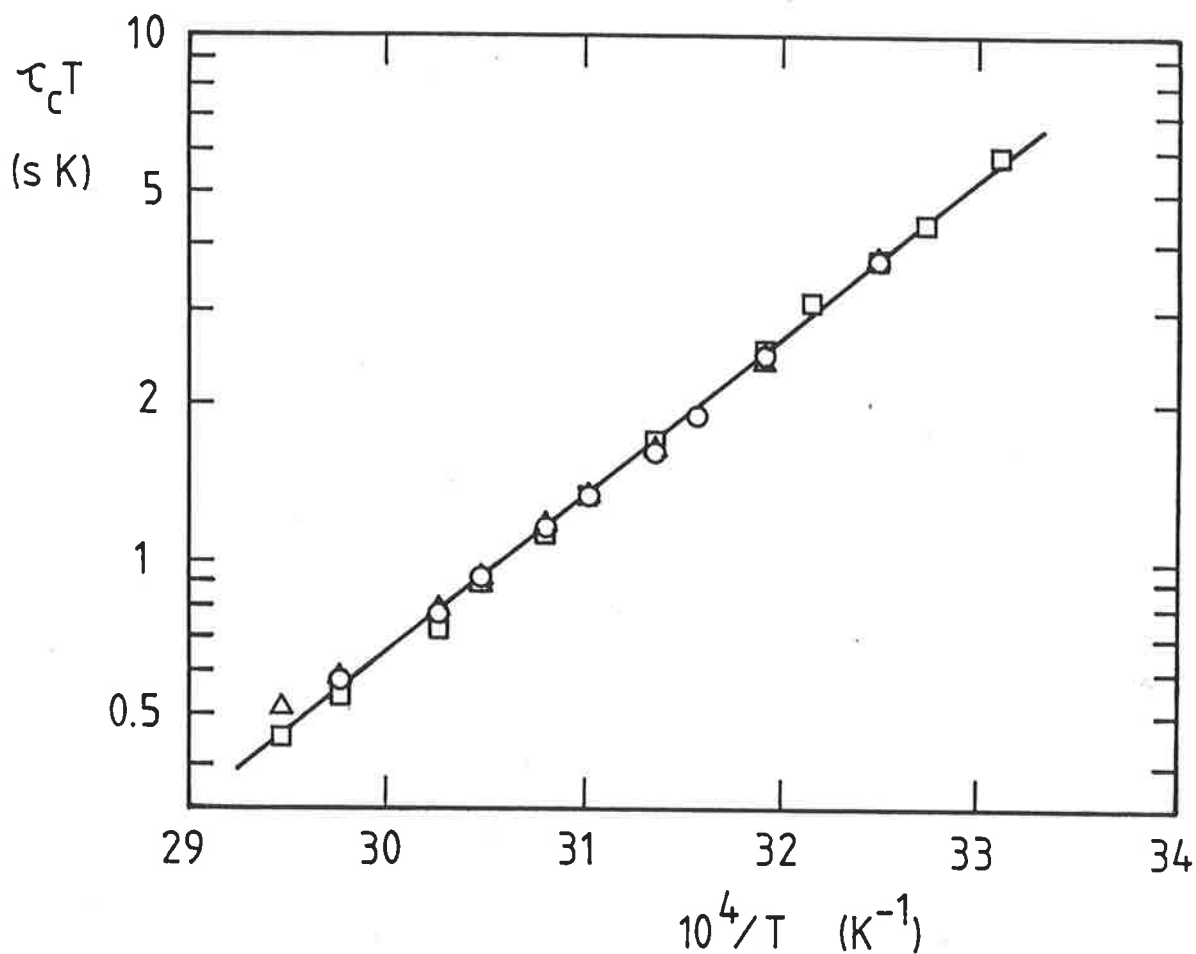


Figure 3.2 The temperature variation of $T\tau_c$ for Na^+ exchange on $[\text{Na.C22C}_5]^+$ in methanol. Results for solutions i, ii and iii are represented by triangles, circles and squares respectively. The solid curve represents the best fit of the combination of all three solutions to Equation 3.6.

3.2.2 : A Qualitative Study of $[\text{Li.C22C}_5]^+$ and $[\text{Na.C22C}_5]^+$, Metal Ion Exchange Kinetics in a Range of Solvents

A quantitative study of the lability of $[\text{Li.C22C}_5]^+$ in acetone and water and of $[\text{Na.C22C}_5]^+$ in acetonitrile, acetone and water, was prevented by the insufficient cryptate solubility for reliable ^7Li or ^{23}Na studies. The exchange between $[\text{Li.C22C}_5]^+$ and solvated Li^+ in dimethyl sulfoxide, *N,N*-dimethylformamide and methanol solution are in the fast exchange limit at temperatures approaching the solvent freezing point, as characterised by a single ^7Li resonance where for approximately 1:1 solutions, $W_{1/2} = 1.2$ Hz at 300 K in dimethyl sulfoxide, 2.0 Hz at 235 K in *N,N*-dimethylformamide, and 3.0 Hz at 200 K, methanol, respectively, and were not studied any further.

A single exchange broadened ^{23}Na NMR signal is observed in dimethyl sulfoxide and propylene carbonate solutions containing $[\text{Na.C22C}_5]^+$ and solvated Na^+ at temperatures just above the solvent freezing point, indicating exchange between the two sites to be in the region of fast exchange of the NMR timescale. Approximate upper limits for the apparent decomplexation rate constants, k_d ($1/\tau_c$), (Table 3.2) are calculated using the fast exchange approximation (Chapter 6, section 6.1.3) at 300 K for dimethyl sulfoxide and at 280 K for propylene carbonate.

For $[\text{Na.C22C}_5]^+$ and Na^+ in *N,N*-dimethylformamide, a broad resonance was observed at 220 K, which partially resolved into two broad coalescing resonances ($[\text{Na.C22C}_5]^+$ upfield) in the temperature range 240 - 280 K. This broadening probably arises from a combination of viscosity and exchange broadening dominating at lower and higher temperatures, respectively. As the resolution of this coalescence was insufficient for the quantitative derivation of exchange rate constants, they were estimated (Table 3.2) using the square top approximation method³⁵ (discussed further in Chapter 6, section 6.1.2).

For the systems subjected to the simplified kinetic analysis in the fast and intermediate exchange, the chemical shifts and linewidths in the absence of exchange were determined from solutions containing the complexed metal ion and the solvated metal ion, alone, at the same temperature and total metal ion concentration as that of the exchanging solution (Table 3.2).

Spectra of $[M.C22C_5]^+$, where $M^+ = Li^+$ or Na^+ , exchange systems in pyridine, show two well resolved resonances. In each system, there was no broadening of these resonances up to the highest temperature studied, 360 K. These observations are consistent with the exchange between the solvated metal ion and the complexed metal ion environments being in the very slow exchange region of the NMR timescale. The upper limit for the apparent rate of exchange (Table 3.2) was estimated using the slow exchange approximation (discussed in Chapter 6, section 6.1.1).

Table 3.2 Kinetic and Equilibrium Parameters for Li^+ and Na^+ Exchange on $[Li.C22C_5]^+$ and $[Na.C22C_5]^+$ in a Range of Solvents at 298.2 K

Solvent	D_N^a	k_d	$\log K_s$	k_d	$\log K_s$
		(s^{-1})	($K \text{ dm}^3 \text{ mol}^{-1}$)	(s^{-1})	($K \text{ dm}^3 \text{ mol}^{-1}$)
		$[Li.C22C_5]^+$		$[Na.C22C_5]^+$	
propylene carbonate	15.1	356 ^b	5.35 ^b	≥ 265 ^c	5.95 ^b
methanol	19.0 (23.5) ^d	fast ^e	2.3 ± 0.2	41.0 ± 1.7 ^f	5.41 \pm 0.06
N,N-dimethyl formamide	26.6	fast ^e	2.21 ± 0.18	≈ 500 ^g	3.66 \pm 0.06
dimethyl sulfoxide	29.8	fast ^e	—	≥ 3000 ^c	3.15 \pm 0.05
pyridine	33.1	≤ 30 ^h	—	≤ 500 ^h	6.41 \pm 0.02

Results of this study unless stated otherwise. ^a Reference 36; ^b Reference 51; ^c Estimated by fast exchange approximation (Chapter 6, section 6.1.3) using ^{23}Na NMR, where the parameters derived for these systems (in the complexed and solvated Na^+ environments), χ_c , χ_s , chemical shift difference ($\nu_c - \nu_s$) in Hz, widths at half peak height $W_{1/2c}$, $W_{1/2s}$ and $W_{1/2obs}$ in Hz are: 0.33, 0.67, 530, 265, 60, 310 for Na^+ and $[Na.C22C_5]^+$ in dimethyl sulfoxide at 300 K and 0.34, 0.66, 186, 760, 92, 560 for Na^+ and $[Na.C22C_5]^+$ in propylene carbonate at 280 K; ^d References 37, 38; ^e In the fast exchange limit on the NMR timescale; ^f Determined by complete lineshape analysis (discussed in Chapter 6); ^g Estimated from the square top approximation (Chapter 6, section 6.1.2) for Na^+ in N,N-dimethylformamide at intermediate rates of exchange, where $(\nu_c - \nu_s) = 241$ Hz; ^h Estimated from the slow exchange approximation (Chapter 6, section 6.1.1) for the ^7Li resonance of $[Li.C22C_5]^+$ in pyridine at 330 K, $W_{1/2c} = 18$ Hz, and for the ^{23}Na resonance of $[Na.C22C_5]^+$ in pyridine at 360 K, $W_{1/2c} = 350$ Hz.

3.2.3 : Dynamic Aspects of Related Cryptate Systems

Additional insight into the kinetic and mechanistic factors influencing cryptate exchange processes for C22C₅ systems may be gained by systematic comparison of the cryptand structure and solvent properties. Consequently, the kinetic data available for Na⁺ metal ion exchange on [Na.C22C₅]⁺ (Table 3.2) in methanol, N,N-Dimethylformamide and dimethyl sulfoxide are compared with related systems based on the eighteen membered 4,7,13,16-tetraoxa-1,10-diaza (C22-) ring (specifically, C221^{7,13} and C22C₂^{22,23}) in the same solvents (Table 3.3).

Table 3.3 Kinetic and Equilibrium Parameters of [Na.C221]⁺ and [Na.C22C₂]⁺ in Methanol, N,N-Dimethylformamide and Dimethyl Sulfoxide at 298.2 K

Solvent	D_N^a	k_d	$\log K_s$
		(s ⁻¹)	(K / dm ³ mol ⁻¹)
[Na.C221]⁺			
methanol	19.0 (23.5) ^b	0.02 ^c	9.65 ^d
N,N-dimethyl formamide	26.6	0.25 ^e	7.93 ^d
dimethyl sulfoxide	29.8	0.75 ^f	6.98 ^d
[Na.C22C₂]⁺ g			
methanol	19.0 (23.5) ^b	slow	6.6
N,N-dimethyl formamide	26.6	12.3	6.1
dimethyl sulfoxide	29.8	11.1	5.6

^a Reference 36; ^b References 37,38; ^c References 7,19; ^d Reference 27; ^e Reference 7; ^f Reference 10; ^g References 22, 23.

The rates of Na^+ exchange on the cryptate $[\text{Na.C22C}_5]^+$ (Table 3.2) varies with the nature of the solvent in the sequence methanol < N,N-dimethylformamide < dimethyl sulfoxide. This is consistent with the general observation in a wide range of solvents, that cryptate lability increases with increasing solvent electron donor power, D_N , which suggests that the transition state for the rate determining step is more similar to the solvated metal ion and free cryptand than to the cryptate.^{4,8,10,13,21} On the basis of the $D_N = 33.0$ for pyridine, the upper limits for k_d of Li^+ and Na^+ on $[\text{M.C22C}_5]^+$ are much lower than expected with comparison to other solvents. Similar trends have been found for other cryptate systems in pyridine, where the anomalous solvation nature of pyridine may be attributed to a relatively weak solvent interaction of the hard-acid alkali metal cations with the soft-base nitrogen donor atoms of pyridine.^{4,16,33,50}

The kinetic data for the systems containing $[\text{Na.C22C}_5]^+$ may be compared with those available for $[\text{Na.C221}]^+$ and $[\text{Na.C22C}_2]^+$ (Table 3.3), where a monomolecular mechanism of decomplexation operates for $[\text{Na.C22C}_5]^+$ in N,N-dimethylformamide and all systems in the solvents listed in Table 3.3.^{7,10,23,27} Although the mechanism of cryptate decomplexation appears to be predominantly monomolecular in solvents of higher D_N ,^{19,23} this is not invariably the case.¹³ The solvent influence on the mechanism may be observed for $[\text{Li.C221}]^+$, where the predominant exchange mechanism is monomolecular (Equation 3.1) in methanol and pyridine, $D_N = 23.5$ and 33.1 respectively, and bimolecular (Equation 3.3) in propylene carbonate and acetonitrile, $D_N = 15.1$ and 14.1 , respectively.¹³ (In the bimolecular mechanism, the complexing and decomplexing Li^+ ions are simultaneously coordinated to the cryptand in the transition state.)

The lower stability and increased lability of $[\text{Na.C22C}_5]^+$ by comparison with $[\text{Na.C221}]^+$, suggests that the equilibrium solution structure of $[\text{Na.C22C}_5]^+$ bears a closer resemblance to the transition state. This is consistent with the decomplexation process involving a progressive increase in metal ion solvation with the extent of reaction. Similarly, in the solid state, Na^+ , resides within the cryptate cavity in $[\text{Na.C221}]^+$, in an *inclusive* cryptate, and has minimal interactions with the anion, whereas, for $[\text{Na.C22C}_5]^+$, the Na^+ resides on the face delineated by the four oxygens, and has strong anion interactions.

It is generally observed that for the Li^+ cryptates the formation rates are lower than for the corresponding Na^+ cryptates.^{8,10,21} These lower formation rates may be attributed to a stronger solvation of Li^+ , compared with solvation of Na^+ , resulting in an increased contribution of desolvation to activation energy for cryptate formation. Similarly, a greater electrostatic interaction of Li^+ with the cryptand (compared with Na^+ and the cryptand) results in an increase in the activation energy required for cryptate decomplexation. Although there is only minimal kinetic data available for $[\text{Li}.\text{C22C}_5]^+$, a comparison of the kinetic data for $[\text{Li}.\text{C22C}_5]^+$ and $[\text{Na}.\text{C22C}_5]^+$ (Table 3.2) are consistent with the above trends.

3.3 : Exchange Kinetics for [Na.C211]⁺, [Na.C21C₅]⁺ and [Na.C21]⁺ in N,N-Dimethylformamide, N,N-Diethylformamide and N,N-Dimethylacetamide

The intramolecular cavities of cryptands C211 and C21C₅ ($r = 0.8 \text{ \AA}^{40}$) are too small to accommodate the alkali metal ion, Na⁺ ($r = 1.02 \text{ \AA}^{41}$). Previous X-ray crystallographic studies show that in the solid state, both [Na.C211]SCN and [Na.C21C₅]SCN⁴² exist as *exclusive* cryptates, where in each case Na⁺ is bound to a C21- ring containing three ether oxygens and two amine nitrogens (Na⁺ is also bound to SCN⁻ in both cryptate structures). There are no published X-ray crystallographic studies of any [Na.C21]X structures. However, it has been shown that for [K.C21]SCN, the cation, K⁺, is sited directly above the C21 (bound to the fifteen membered ring containing three ether oxygens and two amine nitrogens) which exhibits a puckered planar conformation⁴³ (K⁺ is also bound to the SCN⁻ anion). In solution, the cryptates [Na.C211]⁺ and [Na.C21C₅]⁺ are expected to retain the *exclusive* structures observed in the solid state. It is assumed that the electrostatic anion-cryptate interactions in the solid state are replaced by solvent-cryptate interactions in solution. The lability of these systems are investigated in three solvents of similar type, N,N-dimethylformamide (DMF), N,N-diethylformamide (DEF) and N,N-dimethylacetamide (DMA). These solvents have similar electron pair donor strength, as measured by the Gutmann donor numbers (D_N) of 26.6, 30.9 and 27.8 for DMF, DEF and DMA respectively, but different molecular shapes and sizes.

3.3.1 : Exchange Kinetics of Na⁺ on [Na.C211]⁺ in N,N-Diethylformamide and N,N-Dimethylacetamide

In DEF and DMA solution, the Na⁺ exchange between solvated Na⁺ and [Na.C211]⁺ states is sufficiently slow that separate ²³Na resonances are observed (Figure 3.3). As the rate of exchange of Na⁺ between the two environments increases with temperature, the two resonances broaden and coalesce to a single resonance at high temperature (360 K). The lifetimes of Na⁺ in the cryptate, τ_c , and solvated, τ_s , environments were determined by complete line-shape analysis over the temperature range 320 to 360 K. The site lifetime, τ_c , in both DEF and DMA, are derived for three solutions of different Na⁺ to [Na.C211⁺] ratios and constant total Na⁺ concentration. The semi-logarithm plots of $T\tau_c$ against $1/T$ (Figure 3.4) for these systems, show that τ_c is concentration independent over the concentration ranges in both solvents (Table 3.4).

These results are consistent with the predominant decomplexation mechanism being a monomolecular decomplexation of $[\text{Na.C211}]^+$, where the solvated cation, Na^+ , does not participate in the rate determining step. This is observed for $[\text{Na.C211}]^+$ in a range of solvents including DMF.¹² The activation parameters of the decomplexation process of $[\text{Na.C211}]^+$ in DEF and DMA were calculated for each system using a best fit model of the temperature variation of τ_c with Equation 3.6. These parameters have been calculated for each of the six solutions and for both sets of three solutions in the same solvent (Table 3.4).

Table 3.4 Kinetic Parameters for $[\text{Na.C211}]^+$ Decomplexation in N,N-Diethylformamide (DEF) and N,N-Dimethylacetamide (DMA)

Solution	Na^+ mol dm^{-3}	$[\text{Na.C211}^+]$ mol dm^{-3}	k_d (350.0 K) s^{-1} ^a	ΔH_d^\ddagger kJ mol^{-1}	ΔS_d^\ddagger $\text{J K}^{-1} \text{mol}^{-1}$
DEF					
iv	0.068	0.037	1150 ± 40	65.0 ± 2.8	-1.8 ± 7.9
v	0.051	0.040	1220 ± 40	69.8 ± 2.8	12.3 ± 7.8
vi	0.024	0.069	1190 ± 40	66.7 ± 3.1	3.1 ± 8.5
(iv - vi)			1180 ± 30	67.1 ± 1.9	4.4 ± 5.0
DMA					
vii	0.067	0.039	2510 ± 70	64.2 ± 2.0	2.2 ± 5.9
viii	0.059	0.052	2580 ± 70	67.2 ± 1.9	11.1 ± 5.4
ix	0.033	0.068	2590 ± 90	62.1 ± 2.6	-3.5 ± 7.2
(iv - ix)			2550 ± 55	64.8 ± 1.5	4.3 ± 4.4

The quoted errors represent two standard deviations for the regression fit of each set of data to Equation 3.6. ^a The decomplexation rate constant, k_d , was derived at 350.0 K which is the temperature in the midst of the coalescence region where the most reliable kinetic data are obtained.

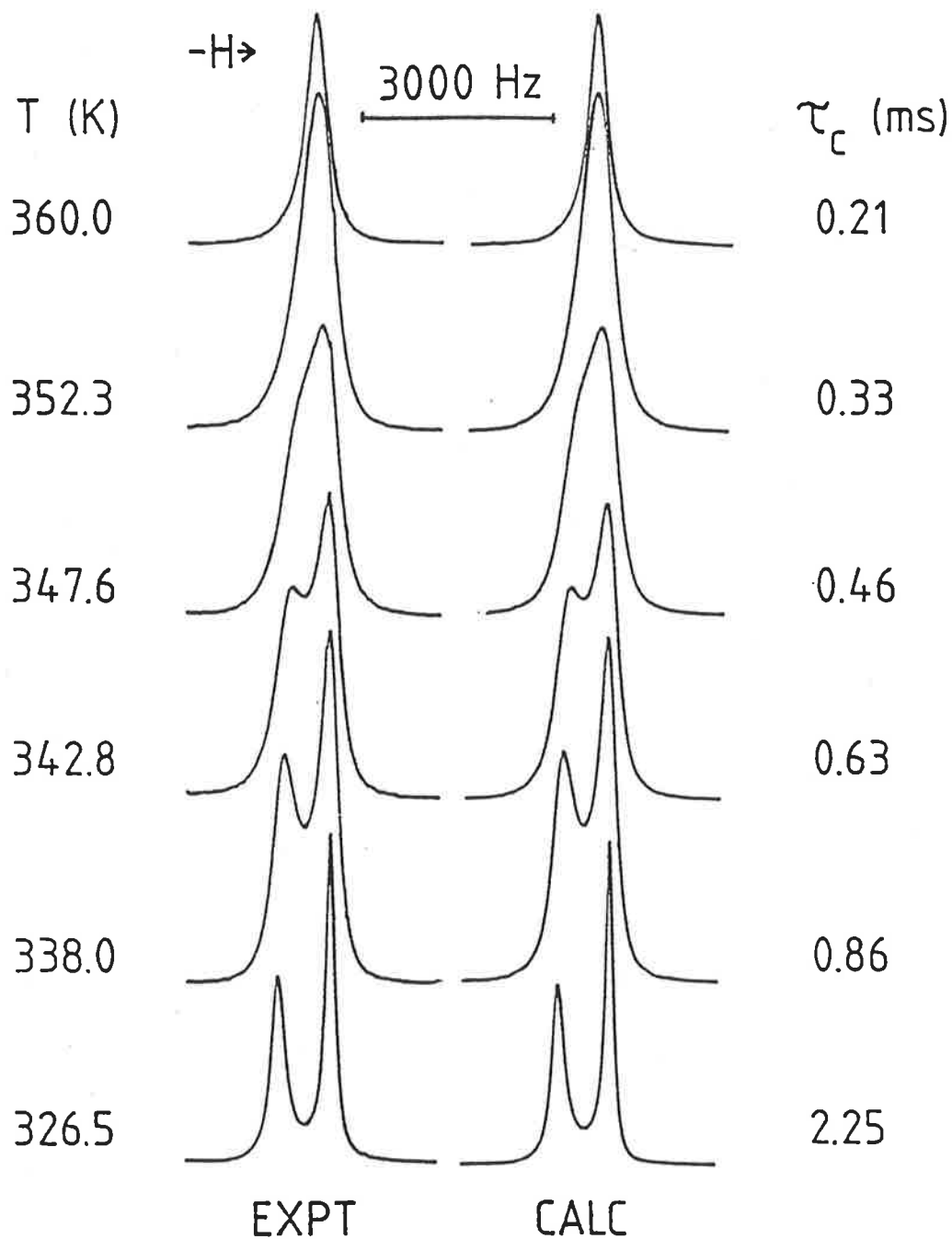


Figure 3.3 Typical exchange modified 79.39 MHz ^{23}Na NMR spectra of a N,N-dimethylacetamide solution of NaClO_4 ($0.111 \text{ mol dm}^{-3}$) and C211 ($0.052 \text{ mol dm}^{-3}$). Experimental temperatures and spectra appear at the left of the figure. Best fit calculated lineshapes and corresponding τ_c values appear to the right. The resonance of $[\text{Na.C211}]^+$ appears downfield from that of solvated Na^+ .

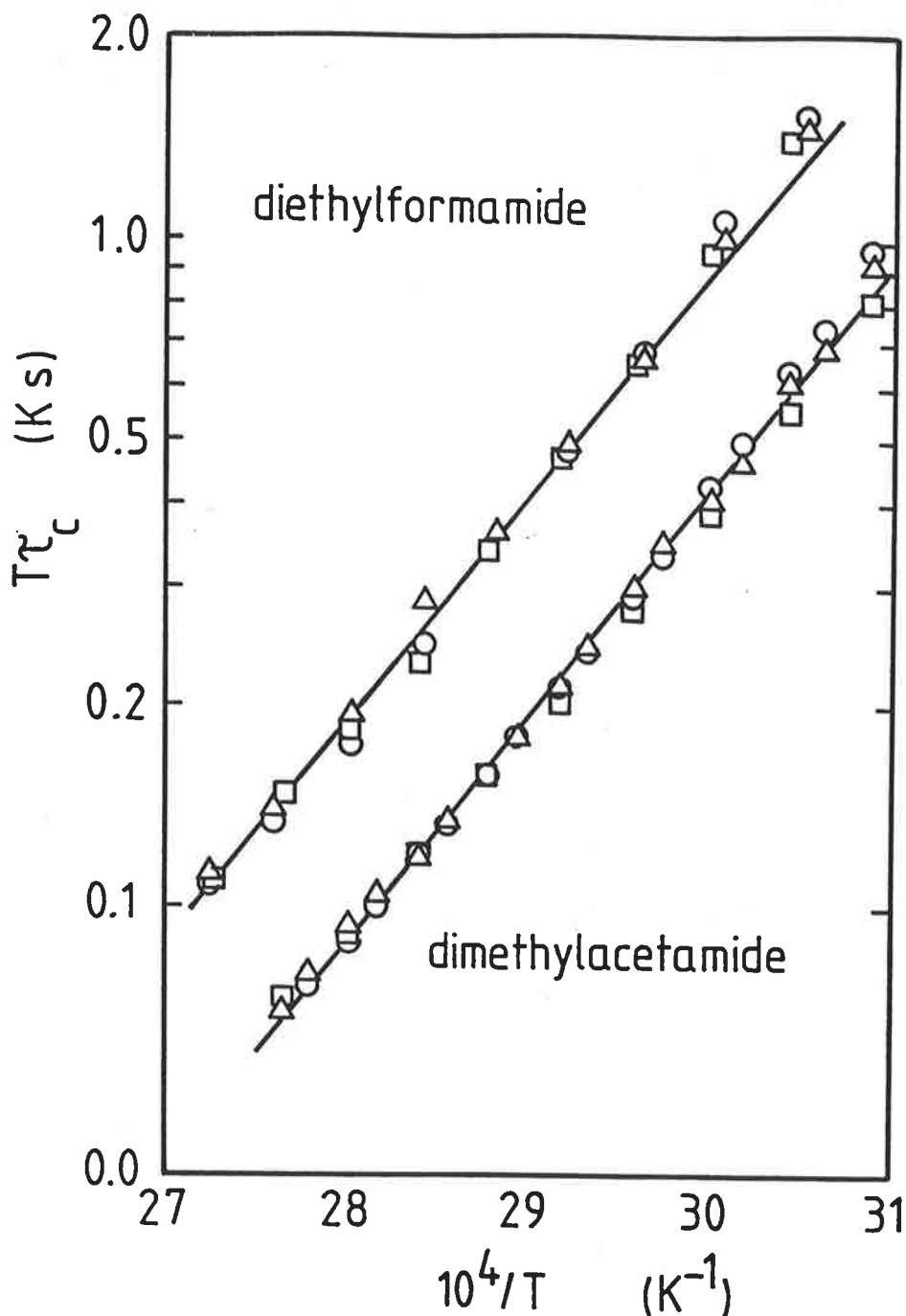


Figure 3.4 The temperature variation of $T\tau_c$ for Na^+ exchange on $[\text{Na.C211}]^+$. The upper set is derived from N,N-diethylformamide solutions (iv, v and vi) whose data points are represented by triangles, circles and squares respectively. The lower data set is derived from N,N-dimethylacetamide solutions (vii, viii and ix) whose data points are represented by triangles, circles and squares respectively. The solid curves represent the simultaneous best fit of the data derived from each set of three solutions to Equation 3.6.

3.3.2 : Exchange Kinetics for Related Systems Containing [Na.C211]⁺, [Na.C21C5]⁺ and [Na.C21]⁺

The ²³Na spectra of solutions containing Na⁺ and [Na.C21]⁺ (~ 0.1 mol dm⁻³ total [Na⁺]) in DMF, DEF and DMA, show only a single narrow resonance at temperatures approaching the solvent freezing points. Thus, the exchange process is at the fast exchange limit of the ²³Na NMR timescale. The exchange process observed for [Na.C21C5]⁺ in DEF and DMA is also in fast exchange limit of the ²³Na NMR timescale.⁴⁴ In contrast, the exchange process for [Na.C21C5]⁺ in DMF is slower than in DEF and DMA and the rate of exchange falls within the NMR timescale.¹² All these systems are substantially more labile than for systems of [Li.C21C5]⁺ in the same solvents (Table 3.5).

The kinetic data for Na⁺ exchange of systems containing [Na.C21C5]⁺ and [Na.C211]⁺, in an extended range of solvents show a corresponding increase in the rate of decomplexation with increasing D_N .¹² The decomplexation rate constant, k_d , increases over several orders of magnitude, whereas the effect on formation rate constant, k_f , is much smaller. Thus, the substantial variations in K_S are principally a consequence of variation of k_d , and are consistent with a substantial solvent interaction in the transition state of the rate determining step of the exchange process. However, in the three solvents, DMF, DMA and DEF, which have similar electron donor power, the differences in molecular size result in only minor variations in k_d and K_S for [Na.C211]⁺ (Table 3.5).

The greater variation of k_d with D_N with solvent by comparison with that of k_f indicates that for the decomplexation process the transition state more closely resembles the products (solvated metal ion and cryptand) than the reactant (cryptate and solvent). Thus, as D_N varies, the difference between G^\ddagger and G_{product} varies much less than the difference between G^\ddagger and G_{reactant} . This may be illustrated through a simple model in which $G^\ddagger - G_{\text{product}}$ (ΔG_f^\ddagger) may be considered invariant with D_N and $\Delta G_d^\ddagger = \Delta G_d^\ddagger_{\text{rearr.}} - \Delta G_s^\ddagger$, where the right hand terms respectively, are the free energy change characterising the geometric rearrangement and the solvation change in forming the transition state (Figure 3.5).

Table 3.5 Kinetic and Equilibrium Data for the Sodium(I) and Lithium(I) Cryptates, [M.C211]⁺, [M.C21C₅]⁺ and [M.C21]⁺ Systems in DMF, DEF and DMA

System	10 ⁻⁶ <i>k_f</i> (298.2 K) dm ³ mol ⁻¹ s ⁻¹	<i>k_d</i> (298.2 K) s ⁻¹	ΔH_d^\ddagger kJ mol ⁻¹	ΔS_d^\ddagger J K ⁻¹ mol ⁻¹	log <i>K_s</i> (298.2 K) dm ³ mol ⁻¹
DMF					
[Na.C211] ⁺ ^a	1.92	12.1	83.5	55.8	5.20 ^c
[Na.C21C ₅] ⁺ ^b	21.4	28800	40.0	-25.3	2.87 ^b
[Na.C21] ⁺ ^d	fast	fast			2.10 ^d
DEF					
[Na.C211] ⁺ ^e	2.29	18.2	67.1	4.4	5.10
[Na.C21C ₅] ⁺ ^d	fast	fast			2.52 ^d
[Na.C21] ⁺ ^d	fast	fast			3.19 ^d
DMA					
[Na.C211] ⁺ ^e	2.49	45.2	64.8	4.3	4.74
[Na.C21C ₅] ⁺ ^d	fast	fast			2.05 ^d
[Na.C21] ⁺ ^e	fast	fast			2.88 ^d
DMF					
[Li.C211] ⁺ ^f	0.127	0.0130	64.4	-64.8	6.99
[Li.C21C ₅] ⁺ ^g	0.0073	116	38.4	-76.5	1.80
DEF					
[Li.C21C ₅] ⁺ ^g	0.0149	210	27.8	-108	1.72
DMA					
[Li.C21C ₅] ⁺ ^g	0.0124	237	49.0	-35.0	1.85

^a Reference 11; ^b Reference 12; ^c Reference 45; ^d Reference 44; ^e This Study; ^f Reference 4; ^g Reference 21.

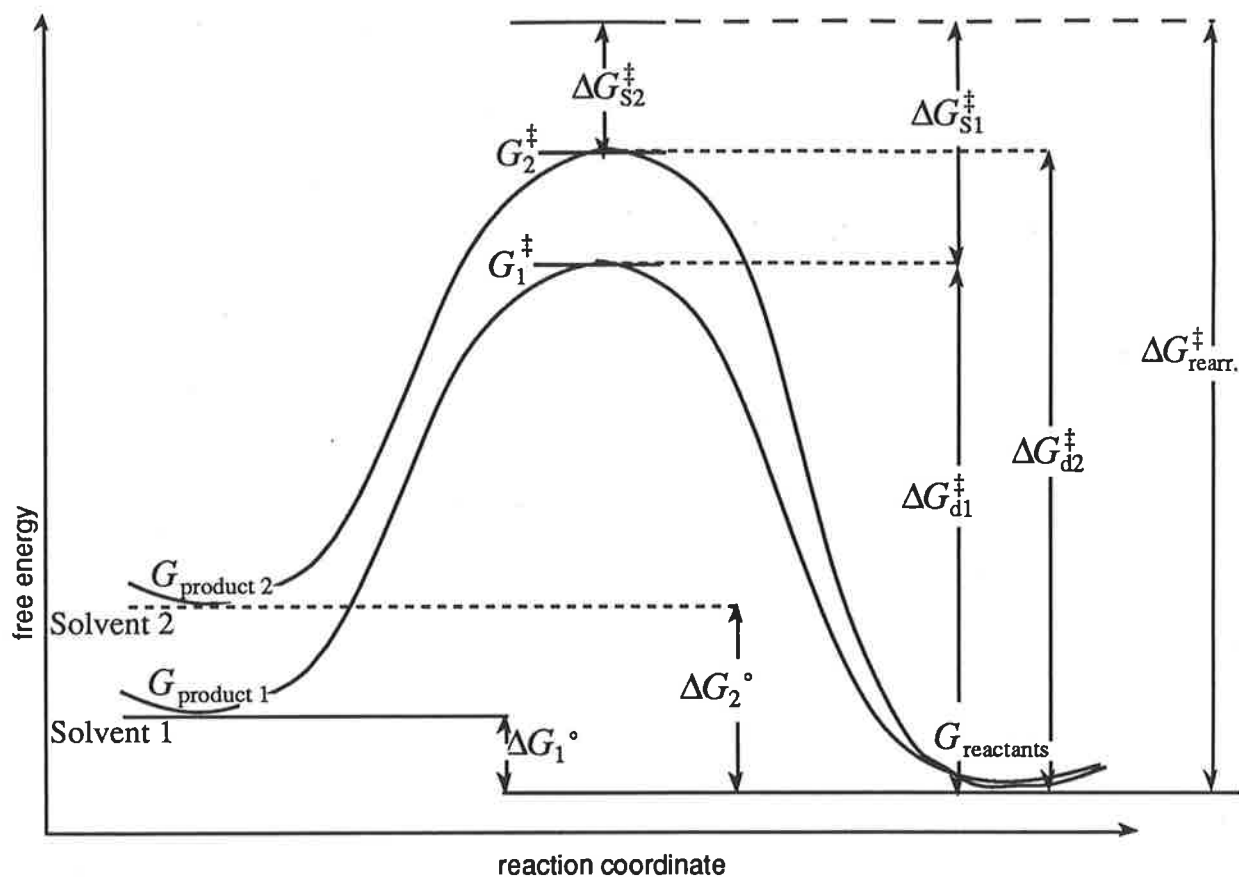


Figure 3.5 A simplified representation of cryptate complexation and decomplexation in two solvents where $G_{\text{reactant}1}$ and $G_{\text{reactant}2}$ are normalised to the same value, highlighting the variation in k_d with the nature of the solvent. Under these conditions $\Delta G_{f1}^\ddagger = \Delta G_{f2}^\ddagger$ and $\Delta G_{s1}^\ddagger > \Delta G_{s2}^\ddagger$ therefore $\Delta G_{d1}^\ddagger < \Delta G_{d2}^\ddagger$ and $\Delta G_1^\circ < \Delta G_2^\circ$ where $D_{N1} > D_{N2}$.

In DMF, k_d for $[\text{Na.C21C}_5]^+$ is ~ 2000 times greater than k_d for $[\text{Na.C211}]^+$. In addition, there is a small increase in k_d observed for $[\text{Na.C211}]^+$ in changing solvents from DMF to DEF and DMA. A similar trend may be observed for $[\text{Na.C21C}_5]^+$, more specifically, in DMF, the exchange is within the NMR timescale, whereas in DEF and DMA the exchange process is much faster. Thus, it is reasonable to conclude that the variation observed in K_s for $[\text{Na.C21C}_5]^+$ in these solvents is mostly as a consequence of variations in k_d rather than in k_f .

The large variations in magnitude of k_d , and small variations of k_f , over a wide range of solvents observed for the Na^+ cryptate exchange systems are also observed for $[\text{Li.C211}]^+$ and $[\text{Li.C21C}_5]^+$ exchange systems²¹ (Table 3.5). There is an increase of k_d in the sequence, $[\text{Li.C211}]^+ < [\text{Na.C211}]^+ < [\text{Li.C21C}_5]^+ < [\text{Na.C21C}_5]^+$. This indicates a greater electrostatic interaction of C211 with Li^+ and Na^+ compared to C21C₅ with Li^+ and Na^+ , where the degree of electrostatic interaction is an important factor in determining the rate of decomplexation. In addition, the greater K_s observed for $[\text{Na.C21C}_5]^+$ over $[\text{Li.C21C}_5]^+$ in DMF is attributed to the 200 fold greater k_d and a 3000 fold greater k_f observed for $[\text{Na.C21C}_5]^+$. The lower k_f for $[\text{Li.C21C}_5]^+$ is consistent with the smaller Li^+ forming stronger electrostatic interactions with the solvent, thus increasing the activation energy required to sequentially desolvate the Li^+ in the formation reaction. Similarly, the lower k_d is consistent with an increased activation energy required for Li^+ to dissociate from the cryptand compared with Na^+ and the same cryptand.

The small variation observed in the decomplexation rates, k_d , of $[\text{Na.C211}]^+$ and $[\text{Li.C21C}_5]^+$ in DMF, DEF and DMA, is in contrast with the variation of several orders of magnitude in the rate constant of the solvent exchange process observed with increasing solvent size for $[\text{Co}(\text{DMF})_6]^+$, $[\text{Co}(\text{DEF})_6]^+$ and $[\text{Co}(\text{DMA})_6]^+$ and for the comparable Ni^{2+} systems.⁴⁶ The increase in lability for the solvent exchange processes is attributed to the increased steric crowding of the solvent in a dissociatively activated mechanism of solvent exchange. In contrast, the variations in size and steric interactions of DMF, DEF and DMA have only a minimal effect on k_d for the alkali metal ion cryptates exchange processes discussed in this study.

3.4 : General Conclusions

In these first three chapters of this study, the solid state cryptate structures, and the stability and lability data for the cryptates formed between the cryptand C22C₅ and a range of monovalent metal ions in several solvents have been compared with similar systems based on the 4,7,13,16-tetraoxa-1,10-diaza (C22-) ring, C221, C22C₈, C22C₂ and C22. In addition, the stability and lability data of [Na.C211]⁺ in DEF and DMA have been compared with similar systems based on the 4,7,13,16-tetraoxa-1,10-diaza (C21-) ring, C211 and C21, in DMF, DEF and DMA. The variation in the molecular size of the three solvents of similar electron donating strength, DMF, DEF and DMA, appears to have little effect on the stability and lability of the Na⁺ cryptates formed.

The replacement of an oxygen donor atom by a methylene moiety, where the basic molecular shape is retained, were investigated in detail. A comparison of the structural, stability and lability data for alkali metal ion exchange of the cryptates, [M.C221]⁺ with [M.C22C₅]⁺ and [M.C211]⁺ with [M.C21C₅]⁺, illustrated the effect of such molecular variation upon the cryptate complexation characteristics. In the solid state, it was observed that the cryptate structures change from *inclusive* [Na.C221]⁺ to *exclusive* [Na.C22C₅]⁺. Similarly in solution, a substantial decrease in the stability and increase in the lability occurs for [M.C22C₅]⁺ compared with [M.C221]⁺. This generally observed decrease in stability and increase in lability of the alkali metal ion cryptates, [M.C22C₅]⁺, and the change in the solid state from *inclusive* [Na.C221]⁺ to *exclusive* [Na.C22C₅]⁺ suggest a lower electrostatic attraction between the cryptand, C22C₅, and the alkali metal ions by comparison with C221 and these ions. Corresponding observations of the complexation data of [Na.C21]⁺, [Na.C211]⁺ and [Na.C21C₅]⁺ are consistent with a decreased electrostatic attraction between Na⁺ and the aliphatic substituted cryptand, C21C₅, by comparison with C211.

The cryptands discussed in this study may be viewed as modifications of either diaza-crown ether C21 or C22, in which the amine hydrogens of the diaza-crown ether has been replaced by a third nitrogen to nitrogen bridge. There is a significantly decreased flexibility for the bicyclic cryptates compared with the monocyclic diaza-crown ethers. This phenomena is consistent with a comparison of the difference between the solid state structures of [K.C22]⁺ and [K.C22C₅]⁺, where the C22- ring in C22C₅ is geometrically constrained by the nitrogen to nitrogen -(CH₂)₅- linkage. In the solid state structure of [K.C22]⁺, the cation, K⁺, is coordinated to all six donor atoms, and resides within the plane

delineated by the four oxygens, with one nitrogen above and the other below this plane. This contrasts with the solid state structure of $[\text{K.C22C}_5]^+$, where K^+ does not form significant interactions with either nitrogen atom, and is positioned $0.369(1) \text{ \AA}$ above the mean plane of the four oxygens, with both nitrogen atoms below this plane. Similarly in solution, there is a general decrease in stability, and increase in lability of $[\text{M.C22}]^+$ compared with $[\text{M.C22C}_5]^+$. These observations indicate a greater interaction of the solvent (or anion) with the diaza-crown ether complexes by comparison with the cryptates, and was attributed to a number of possible influences. The lone pair electrons of the nitrogens of a diaza-crown ether complex in an *endo - endo* configuration (where the bulk of the electron density is directed toward the cation) are less constrained than in a cryptate. As a consequence, the nitrogens of the diaza-crown ether complex are more likely to be in an *endo - exo* or *exo - exo* configuration, resulting in an increased influence of the solvent. The larger cation surface exposed to bulk solvent interactions of the diaza-crown ether complexes combined with the greater flexibility of the diaza-crown ethers, suggesting that the metal is more accessible to solvent by comparison with the corresponding cryptate.

The high stability, high selectivity and slow rates of decomplexation of the C221 and C211 cryptates contrast with the lower stability, selectivity, and increased rates of exchange of the aliphatic bridged C22C₅ and C21C₅ cryptates. The ability to form stable alkali metal ion complexes of high metal ion specificity and rapid rates of exchange are also characteristic of a number of biologically active macrocyclic ligands,⁴⁷ and are optimal characteristics for a cation phase transfer catalyst.² These observations are consistent with the efficiency of a given cryptand in transporting alkali metal ions through non-polar membranes. In studies involving membrane transport system studies^{48,52} assessing cryptands as phase transfer catalysts, the highly stable cryptates, $[\text{M.C211}]^+$, $[\text{M.C221}]^+$ and $[\text{M.C222}]^+$, where $\text{M}^+ = \text{Li}^+, \text{Na}^+ \text{ or } \text{K}^+$, result in only a very inefficient transfer of alkali metal ions through a lipid membrane. In contrast, experiments with aliphatic bridged cryptates, $[\text{M.C21C}_5]^+$, $[\text{M.C22C}_5]^+$ and $[\text{M.C22C}_8]^+$, demonstrate much improved metal ion transport rates through lipid membranes. The improved alkali metal ion transport properties of the aliphatic bridged cryptands, C21C₅, C22C₅ and C22C₈ by comparison with C211, C221 and C222, may be attributed to their decreased extraction ability (lower K_s) and faster cryptate decomplexation rates (increased k_d), resulting in a lower concentration of the metal ion within the carrier medium⁴⁹ (lipid membrane). Thus, any possible metal ion saturation effects are minimised and the concentration of the free cryptand available for back diffusion is increased.

- 1 Lehn J.-M., Sauvage J.-P., Dietrich B., *J. Am. Chem. Soc.*, **1970**, 92, 2916 - 2918.
- 2 Lehn J.-M., *Struct. Bonding*, **1973**, 16, 1 - 69.
- 3 Ceraso J.M., Dye J.L., *J. Am. Chem. Soc.*, **1973**, 95, 4432 - 4434.
- 4 Cahen Y.M., Dye J.L., Popov A.I., *J. Phys. Chem.*, **1975**, 79, 1292 - 1295.
- 5 Cahen Y.M., Popov A.I., *J. Solution Chem.*, **1975**, 4, 599 - 608.
- 6 Cox B.G., Schneider H., *J. Am. Chem. Soc.*, **1977**, 99, 2809 - 2811.
- 7 Cox B.G., Schneider H., Stroka J., *J. Am. Chem. Soc.*, **1978**, 100, 4746 - 4749.
- 8 Cox B.G., Schneider I., Schneider H., *Ber. Bunsenges., Phys. Chem.*, **1980**, 84, 470 - 474.
- 9 Liesegang G.W., *J. Am. Chem. Soc.*, **1981**, 103, 953 - 955.
- 10 Cox B.G., Garcia-Rosas J., Schneider H., *J. Am. Chem. Soc.*, **1981**, 103, 1054 - 1059.
- 11 Lincoln S.F., Brereton I.M., Spotswood T.M., *J. Chem. Soc., Faraday Trans. 1*, **1985**, 81, 1623 - 1630.
- 12 Lincoln S.F., Brereton I.M., Spotswood T.M., *J. Am. Chem. Soc.*, **1986**, 108, 8134 - 8138.
- 13 Shamsipur M., Popov A.I., *J. Phys. Chem.*, **1986**, 90, 5997 - 5999.
- 14 Cox B.G., Stroka J., Schneider H., *Inorg. Chim. Acta*, **1987**, 128, 207 - 213.
- 15 Ishihara K., Miura H., Funahashi S., Tanaka M., *Inorg. Chem.*, **1988**, 27, 1706 - 1710.
- 16 Mei E., Popov A.I., Dye J.L., *J. Phys. Chem.*, **1977**, 81, 1677 - 1681.
- 17 Lincoln S.F., Steel B.J., Brereton I.M., Spotswood T.M., *Polyhedron*, **1986**, 5, 1597 - 1600.
- 18 Rodriguez L.J., Eyring E.M., Petrucci S., *J. Phys. Chem.*, **1989**, 93, 5087 - 5095.
- 19 Cox B.G., Schneider H., *Pure Appl. Chem.*, **1990**, 62, 2259 - 2268.
- 20 Pietraszkiewicz M., *J. Incl. Phenom.*, **1988**, 6, 625 - 628.
- 21 Lincoln S.F., Abou-Hamdan A., *Inorg. Chem.*, **1990**, 29, 3584 - 3589.
- 22 Abou-Hamdan A., Lincoln S.F., *Inorg. Chem.*, **1991**, 30, 462 - 466.
- 23 Lincoln S.F., Stephens A.K.W., *Inorg. Chem.*, **1991**, 30, 3529 - 3534.
- 24 Ceraso J.M., Smith P.W., Landers J.S., Dye J.L., *J. Phys. Chem.*, **1977**, 81, 760 - 766.

-
- 25 Cox B.G., Knop D., Schneider H., *J. Phys. Chem.*, **1980**, 84, 320 - 323.
 - 26 Cox B.G., Firman P., Schneider I., Schneider H., *Inorg. Chim. Acta*, **1986**, 49, 153 - 158.
 - 27 Cox B.G., Garcia-Rosas J., Schneider H., *J. Phys. Chem.*, **1980**, 84, 3178 - 3183.
 - 28 Shih J.-S., Popov A.I., *Inorg. Chem.*, **1980**, 19, 1689 - 1692.
 - 29 Schmidt E., Popov A.I., *J. Am. Chem. Soc.*, **1983**, 105, 1873 - 1882.
 - 30 Soong L.-L., Leroi G.E., Popov A.I., *Inorg. Chem.*, **1990**, 29, 1366 - 1370.
 - 31 Pople J.A., Schneider W.G., Bernstein H.J., "High-resolution Nuclear Magnetic Resonance", **1959**, McGraw-Hill (New York).
 - 32 Shchori E., Jagur-Gordzinski J., Luz Z., Shporer H., *J. Am. Chem. Soc.*, **1971**, 93, 7133 - 7138.
 - 33 Popov A.I., *Pure Appl. Chem.*, **1979**, 51, 101 - 110.
 - 34 Lincoln S.F., *Prog. Reaction Kinetics*, **1977**, 9, 1 - 91.
 - 35 Harris R.K., "Nuclear Magnetic Resonance Spectroscopy", **1983**, Chapter 5, Pitman U.K. (London).
 - 36 Gutmann V., "Coordination Chemistry in Non-Aqueous Solvents", **1968**, Springer (New York).
 - 37 Erlich R.H., Roach E., Popov A.I., *J. Am. Chem. Soc.*, **1970**, 92, 4989 - 4990.
 - 38 DeWitte W.J., Popov A.I., *J. Solution. Chem.*, **1976**, 5, 231 - 240.
 - 39 Izatt R.M., Bradshaw J.S., Nielsen S.A., Lamb J.D., Christensen J.J., *Chem. Rev.*, **1985**, 85, 271 - 339.
 - 40 Lehn J.-M., Sauvage J.-P., *J. Am. Chem. Soc.*, **1975**, 97, 6700 - 6707.
 - 41 Shannon R.D., *Acta Cryst., Sect.A: Cryst. Phys. Diffr., Theor. Gen. Crystallog.*, **1976**, A32, 751 - 767.
 - 42 Lincoln S.F., Horn E., Snow M.R., Hambley T.W., Brereton I.M., Spotswood T.M., *J. Chem. Soc., Dalton Trans.*, **1986**, 1075 - 1080.
 - 43 Abou-Hamdan A., Lincoln S.F., Snow M.R., Tiekink E.R.T., *Aust. J. Chem.*, **1988**, 41, 1363 - 1367.
 - 44 This study, in collaboration,
Clarke P., Abou-Hamdan A., Hounslow A.M., Lincoln S.F., *Inorg. Chim. Acta*, **1988**, 154, 83 - 87.
 - 45 Cox B.G., Garcia-Rosas J., Schneider H., *J. Am. Chem. Soc.*, **1981**, 103, 1384 - 1389.

-
- 46 Lincoln S.F., Hounslow A.M., Boffa A.N., *Inorg. Chem.*, **1986**, 25, 1038 - 1042.
- 47 Lindoy L.F., "The Chemistry of Macrocyclic Ligand Complexes", **1989**, Cambridge University Press (Melbourne), Chapter 9, and references therein.
- 48 Lehn J.-M., *Pure Appl. Chem.*, **1979**, 51, 979 - 997.
- 49 Kirch M., Lehn J.-M., *Angew. Chem., Int. Ed. Engl.*, **1975**, 14, 555 - 556.
- 50 Chuang H.-J., Soong L.-L., Leroi G., Popov A.I., *J. Solution Chem.*, **1989**, 18, 759 - 770.
- 51 Dhillon R.S., Lincoln S.F., unpublished observations, **1991**.
- 52 Sesta B., D'Aprano A., *J. Solution Chem.*, **1989**, 18, 1163 - 1172.
- 53 Grell E., Funck T., Eggers F., in "Membranes", Eiseman G., Ed., **1975**, 3, Chapter 1, Marcel Dekker, (New York).

Chapter 4 : Pendant-Arm Ligand Complexes

4.1 : Introduction

The substitution of N-functionalised coordinating pendant arms on to polyaza macrocyclic ligands has attracted substantial interest in the search for sensors for metal ion selective molecules. Generally, the resulting complexes exhibit a considerable variation in their structure and lability. These characteristics depend upon the nature of the complexing metal ion, the nature of the pendant arms and the macrocyclic ring size.^{1-10,15,20} Metal complexation takes several hours to reach equilibrium for N-functionalised pendant arm ligands based on the 1,4,8,11-tetraazacyclotetradecane (cyclam) structure when the pendant arms lack donor groups, as in 1,4,8,11-tetramethyl-1,4,8,11-tetraazacyclotetradecane (tetramethylcyclam, TMC). However, where the pendant arms have donor groups, such as 1,4,8,11-tetrakis(2-hydroxyethyl)-1,4,8,11-tetraazacyclotetradecane (tetrahydroxyethylcyclam, THEC), equilibrium is reached in seconds.^{3,11} The observed increase in the rate of complexation, may be attributed to a fast initial coordination of the metal ion by the flexible hydroxyethyl arms, creating a large localised metal ion concentration in the region of the 1,4,8,11-tetraazacyclotetradecane (tetraaza) ring. This increased effective local concentration of the metal ion accounts for the greatly increased rate of coordination of the metal ion to the tetraaza ring.



Figure 4.1 Structural diagrams of the pendant arm cyclams 1,4,8,11-tetramethyl-1,4,8,11-tetraazacyclotetradecane (IUPAC) or TMC and 1,4,8,11-tetrakis(2-hydroxyethyl)-1,4,8,11-tetraazacyclotetradecane (IUPAC) or THEC.

The fact that the poorly coordinating 2-cyanoethyl pendant arms on cyclam fail to cause a significant increase in the rate of equilibration by comparison with TMC gives additional support to the proposition that a fast initial coordination of the metal ion to the better coordinating hydroxyethyl groups facilitates the complexation of the metal ion to the tetraaza ring.^{1,2,4} The coordination between the cyano- groups and the metal ions may occur beyond the range of influence of the tetraaza ring owing to the linear nature of the cyano- groups effectively holding the metal ions away from the ring. Furthermore, when the coordinating ability of the pendant arms is increased over that of the 2-hydroxyethyl arms, for example, by substitution with 2-aminoethyl,^{5,6} 3-aminopropyl,⁷ or 2-pyridylmethyl groups,⁸ the metal ion may be coordinated by two pendant arm donor groups and only two or three of the nitrogens of the tetraaza ring of the final complex. In these cases, the metal ion remains outside the macrocyclic ring and the potential discrimination of the metal ion by the ring size of the ligand is lost. However, where acetate is the pendant arm and Cu^{2+} is the complexing metal ion,^{9,10} the Cu^{2+} is coordinated in a square plane by the four nitrogens of the tetraaza ring, and axially by two acetate pendant arms. This is reasonable when it is considered that Cu^{2+} is in the favoured tetragonally distorted octahedral configuration.

An optimal type of donor pendant arm may be the 2-hydroxyethyl arm, as it has the potential to both accelerate metal ion complexation and retain the size selectivity of the macrocyclic ring for soft metal ions such as the divalent transition metal ions and heavy main group metal ions. For such metal ions, the four ring nitrogens should bind more strongly than the hydroxy groups. This is observed in the solid state for $[\text{Ni}(\text{THEC-H})]^+$, where THEC-H is the mono-deprotonated form of THEC.¹¹ No other solid state structure is available for a THEC complex, and the solution structures are not known with any certainty.

In this study, the complexation and dynamic properties of selected divalent metal ions with the ligand THEC are explored and discussed in detail.

4.2 : The Structures of Selected Divalent Metal Ion Complexes of 1,4,8,11-tetrakis(2-hydroxyethyl)-1,4,8,11-tetraazacyclotetradecane, THEC

4.2.1 : Assignment of Structures in Solution

The natural abundance 75.47 MHz ^{13}C NMR spectra in d_4 -methanol of THEC, $[\text{Cd}(\text{THEC})](\text{ClO}_4)_2$, $[\text{Pb}(\text{THEC})](\text{ClO}_4)_2$ and $[\text{Hg}(\text{THEC})](\text{ClO}_4)_2$, all exhibit five resonances in the intensity ratios of 2:2:2:2:1, at ambient temperature (Table 2.1).

Table 4.1 Comparison of Room Temperature (Fast Exchange) ^{13}C Chemical Shifts of THEC and of Selected THEC Complexes

	Temp.	Conc.	δ				
	K	mol dm $^{-3}$	ppm	ppm	ppm	ppm	ppm
THEC	293.0	0.050	58.63	56.61	51.19	49.24	23.99
$[\text{Cd}(\text{THEC})]^{2+}$	293.0	0.050	58.49	55.19	54.94	51.46	22.54
$[\text{Pb}(\text{THEC})]^{2+}$	296.0	0.019	57.6	56.54	56.01	52.02	22.97
$[\text{Hg}(\text{THEC})]^{2+}$	293.0	0.020	59.27	55.96	55.49	50.96	22.78
	Intensity Ratio		2:	2:	2:	2:	1

The THEC spectrum retains its five resonances as temperature is decreased, whereas the spectra of $[\text{M}(\text{THEC})]^{2+}$ where $\text{M}^{2+} = \text{Cd}^{2+}$, Hg^{2+} or Pb^{2+} , show that each resonance observed at ambient temperature broadens and then splits into two separate resonances at lower temperature (Table 2.2).

Table 4.2 Comparison of the (Slow Exchange) ^{13}C Chemical Shifts of $[\text{M}(\text{THEC})]^{2+}$ at *ca.* 200 K

	Temp.	Conc.	Chemical shift, δ				
	K	mol dm $^{-3}$	ppm	ppm	ppm	ppm	ppm
$[\text{Cd}(\text{THEC})]^{2+}$	195.1	0.050	60.55	56.23	55.71	55.41	54.56
			53.79	51.91	51.56	25.16	19.98
$[\text{Hg}(\text{THEC})]^{2+}$	200.4	0.020	60.15	57.71	56.03	55.65 ^a	55.65 ^a
			54.64	50.92	50.35	~24.9 ^b	~20.3 ^b
$[\text{Pb}(\text{THEC})]^{2+}$	200.4	0.019	58.01	56.59	56.34 ^a	56.34 ^a	55.98
			55.15	52.75	50.26	24.04	20.96

^a Two overlapping resonances; ^b Very broad peaks, of width $W_{1/2\text{obs}} \approx 100$ Hz.

The coalescence phenomena observed for the variable temperature ^{13}C NMR spectra of $[\text{M}(\text{THEC})]^{2+}$ is not observable for free THEC. This is consistent with each carbon exchanging between two inequivalent sites, with a simultaneous exchange of the metal ion between two sites.

The five observed ^{13}C resonances and the relative populations obtained in the fast exchange spectra of $[\text{M}(\text{THEC})]^{2+}$, arise from the five chemically different environments of the carbons in the ligand, THEC (Figure 4.2). For THEC, the ^{13}C resonances at 58.63 and 56.61 ppm are assigned to the hydroxyethyl arm carbons (sites **A** and **B** in Figure 4.2), as deduced by comparison with the ^{13}C -enriched spectrum of THEC, discussed later in this chapter. The resonance at 23.99 ppm is assigned to the medial carbon of the 1,3-diaminopropane moiety (site **E**, Figure 4.2) and the remaining two resonances (sites **C** and **D**, Figure 4.2) are assigned to the 1,2-diaminoethane moiety and the $-\text{NCH}_2-$ carbons of the 1,3-diaminopropane moiety. For the $[\text{Cd}(\text{THEC})]^{2+}$ spectrum, these correspond to the resonances at 55.19 and 54.94 ppm, 22.54 ppm, and 58.49 and 51.46 ppm respectively. For the $[\text{Pb}(\text{THEC})]^{2+}$ spectrum, these are the resonances at 57.37 and 56.54 ppm, 23.05 ppm, and 56.01 and 52.02 ppm respectively, and for the $[\text{Hg}(\text{THEC})]^{2+}$ spectrum, these are the resonances at 59.27 and 55.96 ppm, 22.78 ppm, and 55.49 and 50.96 ppm respectively.

Where :

A and **B** are pendant-arm carbons

C are the 1,2-diaminopropane carbons

D are the 1,3-diaminopropane carbons

and **E** are the medial carbons

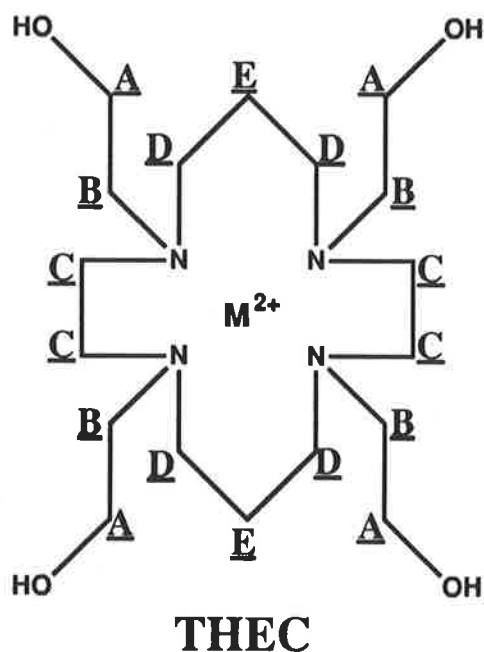


Figure 4.2 Structure and assignments of the ^{13}C resonances for THEC and the divalent metal ion complexes, $[\text{M}(\text{THEC})]^{2+}$.

The solution structures of $[M(\text{THEC})]^{2+}$ may be deduced from the slow-exchange ^{13}C NMR spectra (Table 4.2). In order to attain the five symmetrical pairs of resonances observed, the medial carbons of the two 1,3-diaminopropane moieties must be inequivalent, either within the same plane of symmetry, or on a C_2 axis. The spectra of $[\text{Hg}(\text{THEC})]^{2+}$ and $[\text{Pb}(\text{THEC})]^{2+}$ both show nine resonances and in each case there are two overlapping resonances. In addition, for $[\text{Cd}(\text{THEC})]^{2+}$ all ten resonances are clearly observed. Such structures require the metal ion to be coordinated by the four nitrogens of the tetraaza ring and the two hydroxyethyl arms at either end of the same 1,3-diaminopropane moiety. The five possible configurations of the tetraaza ring with four coplanar nitrogens coordinating to the metal ion are *trans*-I–V (Figure 4.3).

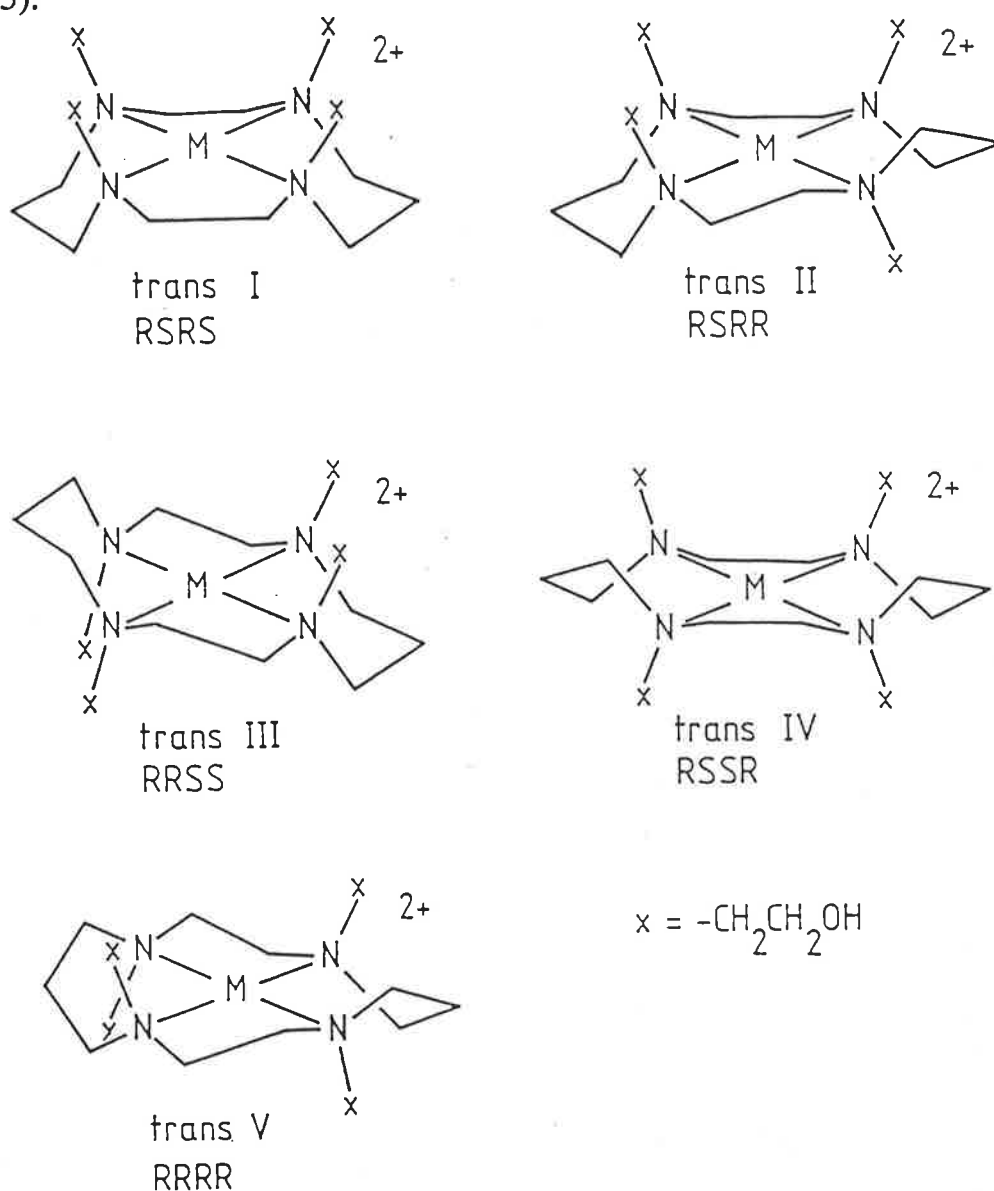


Figure 4.3 Possible configurational isomers of $[M(\text{THEC})]^{2+}$ in which the hydroxyethyl arms are shown uncoordinated.

The *trans*-II configuration, irrespective of the pair-wise coordination of the arms, would produce an asymmetric structure with 18 inequivalent carbon resonances in the ^{13}C spectra. Therefore this configuration for the structure of $[\text{M}(\text{THEC})]^{2+}$ may be eliminated.

Examination of the remaining four possible configurations for $[\text{M}(\text{THEC})]^{2+}$ show that each configuration could produce five pairs of ^{13}C resonances and retain the inequivalence of the medial carbon of the 1,3-diaminopropane moiety only if pair-wise coordination of the hydroxyethyl arms at either end of the 1,3-diaminopropane moiety occurs. Any other pair-wise coordination of the hydroxyethyl arms would result in the medial carbons being equivalent.

Given these constraints, *trans*- coordination of the hydroxyethyl arms to M^{2+} with one hydroxyethyl arm coordinating the metal ion from above the plane of the ring and one below, is required by the *trans*-IV and *trans*-V configurations for THEC in the complexed state. Both configurations incorporate the skew-boat conformation for the six membered chelate rings formed by the coordination of the 1,3-diaminopropane moiety to the metal ion. It is expected that the torsional bond strain of the skew-boat conformation for either the *trans*-IV or *trans*-V complex would make these configurations thermodynamically unstable. On these grounds the *trans*-IV or *trans*-V complex structures are considered unlikely for the $[\text{M}(\text{THEC})]^{2+}$ complex. The fact that no complexes involving ligands that incorporate the 1,4,8,11-tetraazacyclotetradecane ring have been observed in the *trans*-IV configuration supports the premise that $[\text{M}(\text{THEC})]^{2+}$ complexes are unlikely to be in this configuration.

There are complexes observed that incorporate the 1,4,8,11-tetraazacyclotetradecane ring in the *trans*-V configuration, but only after folding of the ring about a diagonal axis delineated by two nitrogens, so that these nitrogens occupy the *trans*- coordination sites of an octahedral metal ion, the other two occupy the metal ion *cis*-coordination sites. The remaining two coordination sites are occupied by other donor groups, as in *cis*- $[\text{Ni}(\text{cyclam})(\text{H}_2\text{O})_2]^{2+}$.¹⁸ If the folded *trans*-V configuration were adopted by the $[\text{M}(\text{THEC})]^{2+}$ complexes, the hydroxyethyl arms attached to the *trans*-coordinated nitrogens would then coordinate in the remaining two *cis*-coordination sites, but the hydroxyethyl arms attached to the *cis*-coordinating nitrogens could not coordinate. This structure possesses a C_2 axis passing through the metal ion and bisecting both the angle made by the pair of *cis*-coordinating nitrogens, and the angle made by the pair of *cis* coordinating hydroxyethyl arms. This

results in the medial carbon of the 1,3-diaminopropane moieties being equivalent. As a consequence, the folded *trans*-V configuration for the $[M(\text{THEC})]^{2+}$ complexes is ruled out, as it fails to produce the required inequivalence of the medial carbon of the 1,3-diaminopropane moieties.

In the *trans*-I configuration, the pair-wise coordination of the hydroxyethyl arms attached to the same 1,3-diaminopropane moiety should occur quite readily. However, this configuration would allow the coordination of hydroxyethyl arms attached to diagonally related nitrogens, or the hydroxyethyl arms pair-wise coordinated through the 1,2-diaminopropane moiety, to be as equally likely to occur. Therefore, such a *trans*-I structure would result in equivalence of the medial carbons of the 1,3-diaminopropane moieties, but no resonances attributable to either of these two structural possibilities are detectable in any of the slow-exchange ^{13}C NMR spectra for any of the three $[M(\text{THEC})]^{2+}$ complexes studied. Accordingly, the *trans*-I configuration is discounted as a possibility even though it is the binding configuration commonly adopted by ligands of this type with weak or non-coordinating pendant arms.^{12,13,15}

The 10-resonance ^{13}C spectra and the medial carbon inequivalence are best accounted for by a structure incorporating the *trans*-III configuration in which the metal ion lies above the tetraaza plane and is trigonal-prismatically coordinated by two hydroxyethyl arms and the four ring nitrogens. The two six membered chelate rings of this structure in the *trans*-III configuration are in the most thermodynamically stable boat-form. Trigonal prismatic coordination of Cd^{2+} has been reported in the solid state for $\text{K}[\text{Cd}(\text{acac})_3]$,¹⁴ and in a polyazamacrocyclic complex.¹⁵ Similarly for $[\text{Ni}(\text{THEC}-\text{H})]^+$, where THEC-H is mono-deprotonated THEC, the ligand conformation is *trans*-III.¹¹ Other cases where the *trans*-III structure exists for a polyaza macrocyclic complex are $[\text{CuL}]^{2+}$, where L is the fourteen membered ring macrocyclic ligand 1,4,8,11-tetrakis((hydroxyformyl)methyl)-1,4,8,11-tetraazacyclotetradecane,⁹ and also for the $[\text{NiL}'(\text{H}_2\text{O})]^{2+}$ and $[\text{CoL}'(\text{H}_2\text{O})]^{2+}$ complexes, where L' is the fourteen membered ring mono-pendant amino-group arm macrocyclic ligand 5-aminomethyl-2,5,10,12-tetramethyl-1,4,8,11-tetraazacyclotetradecane.¹⁷

4.2.2 : Assignment of Structures in the Solid State

Crystals suitable for X-ray diffraction for solid-state structure determinations were not obtained for any of the metal complexes. The solid-state CPMAS ^{13}C NMR spectra for both $[\text{Cd}(\text{THEC})](\text{ClO}_4)_2$ and $[\text{Hg}(\text{THEC})](\text{ClO}_4)_2$ (Figure 4.4) show two resonances at high field, 20.85 and 25.98 ppm and 21.14 and 26.57 ppm, respectively (Figure 4.4, referenced to external adamantane assigned a shift of 38.23 ppm). These two resonances in each spectra are attributed to inequivalent 1,3-diaminopropane medial carbons, (carbon E in Figure 4.2). In both solid state spectra, the multiple resonances bear a substantial similarity to the slow exchange solution spectra (see Figures 4.5 and 4.6), suggesting that the structures of $[\text{Cd}(\text{THEC})]^{2+}$ and $[\text{Hg}(\text{THEC})]^{2+}$ in the solid-state and in solution are similar.

In the case of $[\text{Pb}(\text{THEC})](\text{ClO}_4)_2$, in the solid state spectrum (Figure 4.4) only a single resonance is observed for the medial carbons of the 1,3-diaminopropane moiety at 21.90 ppm. This is in contrast to the slow exchange solution spectrum where two well resolved resonances are observed (Figure 4.7). This indicates either a fortuitous magnetic equivalence of the chemically inequivalent medial carbons, or that the solid state and solution structures are different. The *trans*-V configuration (Figure 4.3) of cyclam (1,4,8,11-tetraazacyclotetradecane) has been observed in the solid state for the *cis*- $[\text{Ni}(\text{cyclam})(\text{H}_2\text{O})_2]^{2+}$ ¹⁸ and $[\text{Pb}(\text{cyclam})(\text{H}_2\text{O})_2]^{2+}$.¹⁹ In both cases, the tetraaza ring is folded about a diagonal axis delineated by two nitrogens. If the folded *trans*-V configuration were adopted by $[\text{Pb}(\text{THEC})]^{2+}$ in the solid state, the four nitrogen atoms would occupy two *cis* and two *trans*- sites in the coordination octahedron, and the two remaining *cis* coordination sites would be occupied by the oxygens of the hydroxyethyl arms attached to the *trans*-coordinated nitrogens. The hydroxyethyl arms attached to the *cis*-coordinated nitrogens are not able to coordinate in this configuration. This structure possesses a C_2 axis, passing through the Pb^{2+} and bisecting the angle made by the pair of *cis*-coordinating nitrogens, and the angle made by the pair of *cis*-coordinating oxygens. Thus, it can be concluded that the medial carbons under these conditions are equivalent, and is consistent with the single resonance observed for the medial carbons in the solid state spectrum for $[\text{Pb}(\text{THEC})]^{2+}$. Eight further equivalent carbon pairs also exist for this structure, and a total of nine resonances should be observed.

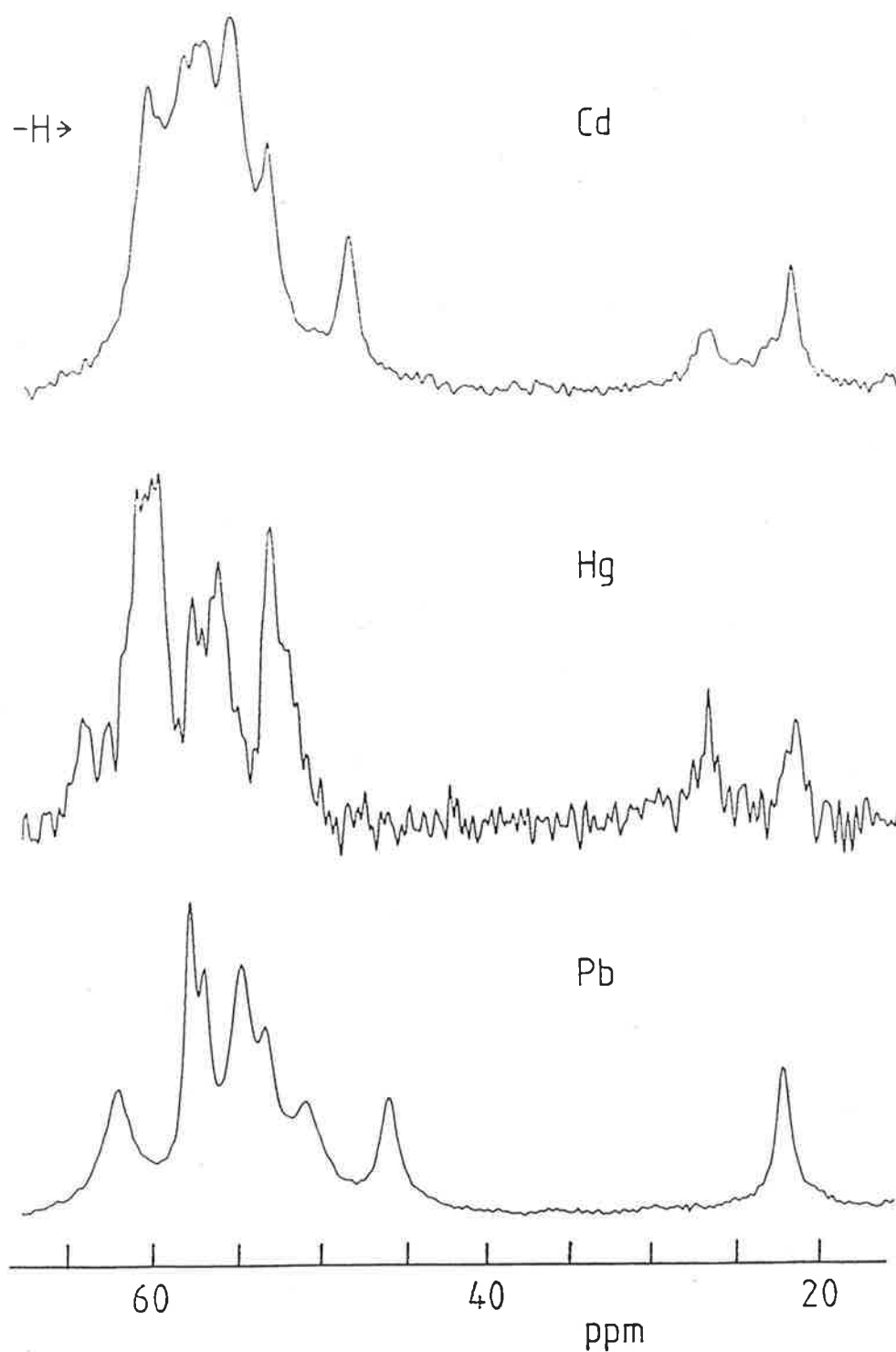


Figure 4.4 CPMAS ^{13}C 75.47 MHz NMR spectra of $[\text{M}(\text{THEC})]^{2+}$. The frequencies are referenced to external adamantane. The two resonances at high field are assigned to the inequivalent medial carbons of the 1,3-diaminopropane moieties where $\text{M}^{2+} = \text{Cd}^{2+}$ and Hg^{2+} . When $\text{M}^{2+} = \text{Pb}^{2+}$, the single high field resonance is assigned to two magnetically equivalent medial carbons of the 1,3-diaminopropane moieties.

Only eight resonances are clearly resolved in the solid state spectrum of $[\text{Pb}(\text{THEC})]^{2+}$ as shown in Figure 4.4, and it is possible that some resonance superimposition obscures a ninth resonance in the region 50–60 ppm. Therefore, a six-coordinate structure with THEC adopting a folded *trans*-V configuration may be a reasonable description for the structure of $[\text{Pb}(\text{THEC})]^{2+}$ in the solid state.

The cation Pb^{2+} has a tendency to form eight-coordinate structures in solid-state complexes, as observed for $[\text{Pb}(\text{cyclam})(\text{NO}_3)_2]$.²⁷ Both nitrates in this complex act as bidentate ligands resulting in a similar structure to that proposed for six-coordinated $[\text{Pb}(\text{THEC})]^{2+}$ in the solid-state, where the two monodentate hydroxyethyl arms are each replaced by a bidentate nitrate. If $[\text{Pb}(\text{THEC})]^{2+}$ had a structure similar to that observed for [(1,4,7,10-tetrakis(2-hydroxypropyl)-1,4,7,10-tetraazacyclododecane)lead]²⁺,²⁰ in which Pb^{2+} is coordinated by four nitrogens and four oxygens in a square-pseudoantiprismatic structure (with the ligand in the *trans*-I configuration) then this would result in only seven distinct ¹³C resonances for $[\text{Pb}(\text{THEC})]^{2+}$ in the solid state.

4.3 : Ligand Exchange Processes of $[M(\text{THEC})]^{2+}$ in d_4 -Methanol

4.3.1 : Intermolecular Ligand Exchange of [1,4,8,11-Tetrakis(2-hydroxyethyl)-1,4,8,11-tetraazacyclotetradecane]cadmium(II), $[\text{Cd}(\text{THEC})]^{2+}$, and its Mercury(II) and Lead(II) Analogues. A Natural Abundance ^{13}C NMR Study

In d_4 -methanol solution, the natural abundance ^{13}C NMR spectra at 297.8 K, of $[\text{Cd}(\text{THEC})]^{2+}$ and THEC (both 0.05 mol dm^{-3}), and of $[\text{Hg}(\text{THEC})]^{2+}$ and THEC (0.02 and 0.03 mol dm^{-3} respectively), separate ^{13}C resonances are observed for both species. The chemical shifts and linewidths of the resonances characterising each species in these solutions are equivalent to those observed for the individual spectra of THEC and $[M(\text{THEC})]^{2+}$. This indicates that the intermolecular exchange of THEC between free and complexed states is in the extreme slow exchange limit of the NMR timescale. However, an approximate upper limit for the rate constant of THEC exchange between free and complexed states, k_{THEC} , may be found:

$$\frac{3}{2} \pi W_{1/2\text{obs}} - \pi W_{1/2\text{obs}} = \frac{1}{\tau_{\text{THEC}}} = \frac{\chi_{\text{L}}}{\tau_{\text{L}} \chi_{\text{THEC}}} = k_{\text{THEC}} \quad 4.1$$

where:

$W_{1/2\text{obs}}$ is the observed width (Hz) of the $[M(\text{THEC})]^{2+}$ resonance at half amplitude;

$\frac{3}{2}W_{1/2\text{obs}}$ is the width that would be observed if the rate of intermolecular exchange were sufficient to increase the natural line width by 50%;

χ_{THEC} and χ_{L} are the mole fractions of $[M(\text{THEC})]^{2+}$ and THEC respectively; and

τ_{THEC} and τ_{L} are the corresponding mean lifetimes.

For $[\text{Cd}(\text{THEC})]^{2+}$, the values for $W_{1/2\text{obs}}$ range between 5.0 to 8.8 Hz and therefore, from Equation 4.1, the upper limit of k_{THEC} (298.2 K) is 8 - 14 s^{-1} . The medial carbon resonance of $[\text{Cd}(\text{THEC})]^{2+}$ exhibits broadening at ambient temperature, from the intramolecular exchange process discussed later, and was not used in the estimation of the intermolecular rate of exchange, k_{THEC} . The upper limit of intermolecular ligand exchange at 298.2 K for $[\text{Hg}(\text{THEC})]^{2+}$, is 8 - 15 s^{-1} , where $W_{1/2\text{obs}}$ varies between 5.0 to 9.0 Hz.

The ^{13}C resonances of free THEC and $[\text{Pb}(\text{THEC})]^{2+}$ in d_4 -methanol solution (0.03 and 0.02 mol dm $^{-3}$ respectively) are broadened as a consequence of intermolecular exchange. The ^{13}C resonances of $[\text{Pb}(\text{THEC})]^{2+}$ exhibit broadening at ambient temperature, from the intramolecular exchange process (as discussed later). Accordingly, only the broadening of the resonances of the THEC are used in the estimation of the intermolecular rate of exchange, k_{THEC} . The linewidths of the resonances of the spectra characterising THEC in such solutions are broader by approximately 5 - 8 Hz (with $W_{1/2}$ between 10 - 13 Hz) by comparison with those observed for the individual spectrum of THEC in solution (between 5 - 8 Hz). An approximate intermolecular exchange rate constant of between THEC and $[\text{Pb}(\text{THEC})]^{2+}$ that would lead to this amount of resonance broadening may be calculated as below:

$$\pi W_{1/2 \text{ obs}} - \pi W_{1/2 \text{ natural}} = \frac{1}{\tau_{\text{THEC}}} = \frac{\chi_{\text{L}}}{\tau_{\text{L}} \chi_{\text{THEC}}} = k_{\text{THEC}} \quad 4.2$$

The rate of intermolecular exchange between THEC and $[\text{Pb}(\text{THEC})]^{2+}$ in solution, k_{THEC} , is approximately 15 to 25 s $^{-1}$.

4.3.2 : Intermolecular Metal Ion Exchange of [1,4,8,11-Tetrakis(2-hydroxyethyl)-1,4,8,11-tetraazacyclotetradecane]cadmium(II), $[\text{Cd}(\text{THEC})]^{2+}$.

A ^{113}Cd NMR Study

A d_4 -methanol solution of solvated Cd^{2+} and $[\text{Cd}(\text{THEC})]^{2+}$ shows two distinct ^{113}Cd NMR resonances (Figure 4.5) indicating only a single resonance for $[\text{Cd}(\text{THEC})]^{2+}$ ($W_{1/2\text{C}} = 70$ Hz), and a narrower resonance for the solvated Cd^{2+} ($W_{1/2\text{S}} = 28$ Hz) at 300.6 K. The downfield shift of the $[\text{Cd}(\text{THEC})]^{2+}$ resonance with respect to that of solvated Cd^{2+} , is consistent with the ^{113}Cd deshielding usually observed as oxygen donor atoms are replaced by nitrogen donor atoms in the first coordination sphere.^{21,22} The larger $W_{1/2}$ of $[\text{Cd}(\text{THEC})]^{2+}$ is most likely due to a combination of unresolved coupling with the ^1H and ^{14}N of the THEC, and chemical shift anisotropy relaxation.^{23,24}

The resonances of the solvated Cd^{2+} and $[\text{Cd}(\text{THEC})]^{2+}$ narrow with increasing sample temperature (300 - 330 K). This is consistent with intermolecular metal ion exchange between the solvated Cd^{2+} and $[\text{Cd}(\text{THEC})]^{2+}$ being at the extreme slow exchange limit. Accordingly, an upper limit of the rate constant for the intermolecular metal ion exchange was estimated using an

equation analogous to Equation 4.1. For the $[\text{Cd}(\text{THEC})]^{2+}$ ^{113}Cd resonance, $W_{1/2\text{C}} = 70$ Hz at 300.6 K, thus the upper limit is $k_{\text{Cd}} = 110$ s $^{-1}$.

The upper limit values estimated for k_{THEC} and k_{Cd} (14 and 110 s $^{-1}$ respectively) are much less than the k (298.2 K) = $68\,000 \pm 18\,000$ s $^{-1}$ for the intramolecular medial carbon exchange process derived from the ^{13}C natural abundance spectra (discussed later in this chapter). Consequently, it may be concluded that the observed coalescence of the medial carbon resonances of the $[\text{Cd}(\text{THEC})]^{2+}$ in d_4 -methanol over the temperature range 230 K - 300 K is not due intermolecular exchange processes. The single resonance observed for $[\text{Cd}(\text{THEC})]^{2+}$ is consistent with the intramolecular exchange process of each carbon exchanging between two inequivalent sites occurring simultaneously with the exchange of the metal ion between two identical sites.

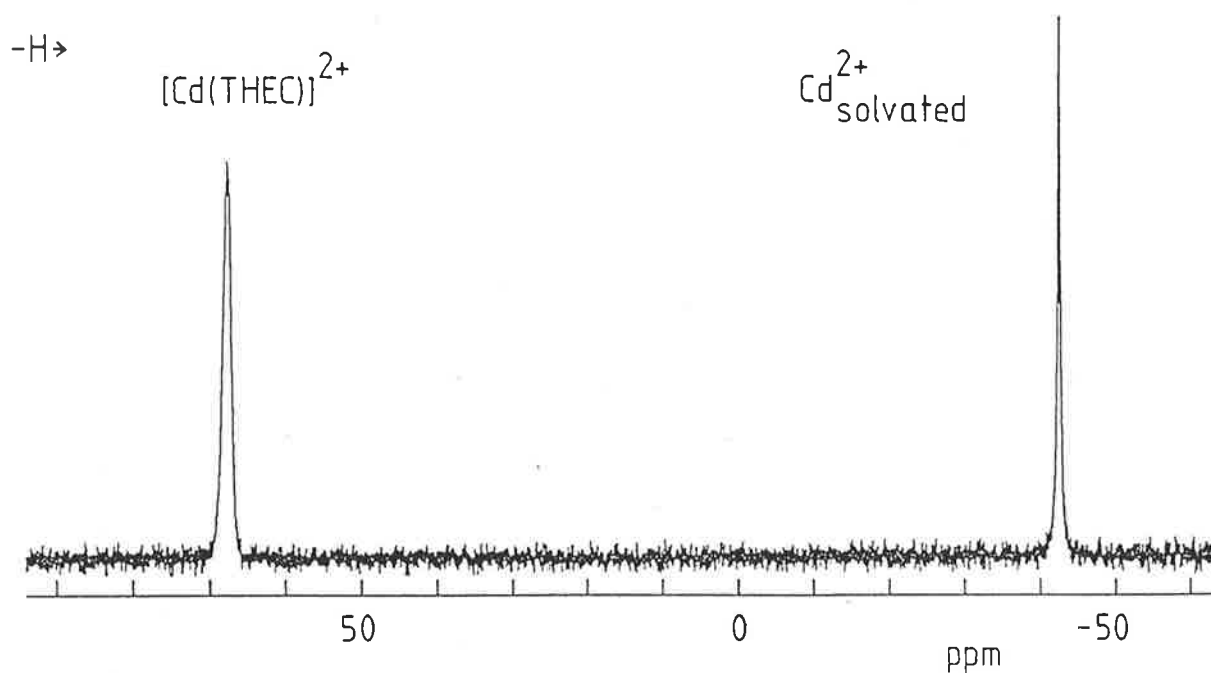


Figure 4.5 ^{113}Cd 66.55-Mhz NMR spectrum of $[\text{Cd}(\text{THEC})](\text{ClO}_4)_2$ (0.100 mol dm $^{-3}$) and $\text{Cd}(\text{ClO}_4)_2$ (0.067 mol dm $^{-3}$ in d_4 -methanol) at 300.6 K (4900 transients, recycle delay of 10 s). The frequencies are referenced to external 0.10 mol dm $^{-3}$ $\text{Cd}(\text{ClO}_4)_2$ in D_2O .

4.3.3 : Intramolecular Ligand Exchange of [1,4,8,11-Tetrakis(2-hydroxyethyl)-1,4,8,11-tetraazacyclotetradecane]cadmium(II), [Cd(THEC)]²⁺, and its Mercury(II) and Lead(II) Analogues. A Natural Abundance ¹³C NMR Study.

The natural abundance ¹³C NMR coalescence observed for [Cd(THEC)]²⁺, [Hg(THEC)]²⁺ and [Pb(THEC)]²⁺ in *d*₄-methanol solution are shown in Figures 4.7, 4.8 and 4.9, respectively. These coalescences are consistent with intramolecular ligand exchange.

The simplest mechanism for intramolecular exchange of the medial carbons and the intramolecular pair-wise exchange of the other carbons of [M(THEC)]²⁺ appears to be the transannular oscillation of the metal ion (Figure 4.6). The transition state, or reactive intermediate, may occur when the metal ion is in the plane of the tetraaza ring octahedrally coordinated to the four nitrogens and by two hydroxyethyl arms, one from each side of the macrocyclic plane. This structure is similar to that observed for the [Ni(THEC-H)]⁺ in the solid state,¹⁶ in which the tetraaza ring is in the *trans*-III configuration with the Ni²⁺ octahedrally coordinated by four nitrogens in the tetraaza plane and two hydroxyethyl arms, one each from either side of the macrocyclic plane and attached to diagonally related nitrogens in a manner similar to that shown in Figure 4.6. The difference between this Ni²⁺ structure and the structure proposed for the ground-state of [M(THEC)]²⁺ probably arises from the differences in the ionic radii²⁵ of the different metal ions. The radii of M²⁺ = Cd²⁺, Hg²⁺ and Pb²⁺ (0.95, 1.02 and 1.19 Å, respectively) are substantially greater than that of Ni²⁺ (0.69 Å), so that the latter metal ion may be more readily accommodated by the macrocyclic hole of THEC.

The mechanism shown in Figure 4.6 contrasts with that postulated for the intramolecular exchange of TMC (1,4,8,11-tetramethyl-1,4,8,11-tetraazacyclotetradecane) carbons, also studied by ¹³C NMR, in five coordinate [M(TMC)X]⁺, where M²⁺ = Zn²⁺, Cd²⁺, Hg²⁺ and X⁻ = monodentate anion. The intramolecular exchange of the TMC complexes proceeds through a Berry-type³⁷ mechanism involving rearrangements between equivalent trigonal-bipyramidal structures in which the TMC ligand is in a folded *trans*-I configuration and X⁻ occupies an axial site.^{26,27} The proposed mechanism also differs with the intramolecular exchange of cyclam (1,4,8,11-tetraazacyclotetradecane) carbons in the five coordinate [Pb(cyclam)X]⁺ (X⁻ =

monodentate anion), where cyclam interconverts between folded *trans-V* *R,R,R,R* and *S,S,S,S* configurations.¹⁹ These folded configurations for $[\text{Pb}(\text{cyclam})\text{X}]^+$ require the two 1,3-diaminopropane medial carbons to be equivalent, consistent with the single medial carbon resonance observed in the slow-exchange ^{13}C spectra of this complex, in contrast to the two inequivalent medial carbon resonances observed in the slow-exchange spectra of $[\text{M}(\text{THEC})]^{2+}$. This illustrates the effect of displacing the non-coordinating proton and methyl moieties of cyclam and TMC with the coordinating hydroxyethyl moieties of THEC on both complex structure and exchange mechanism.

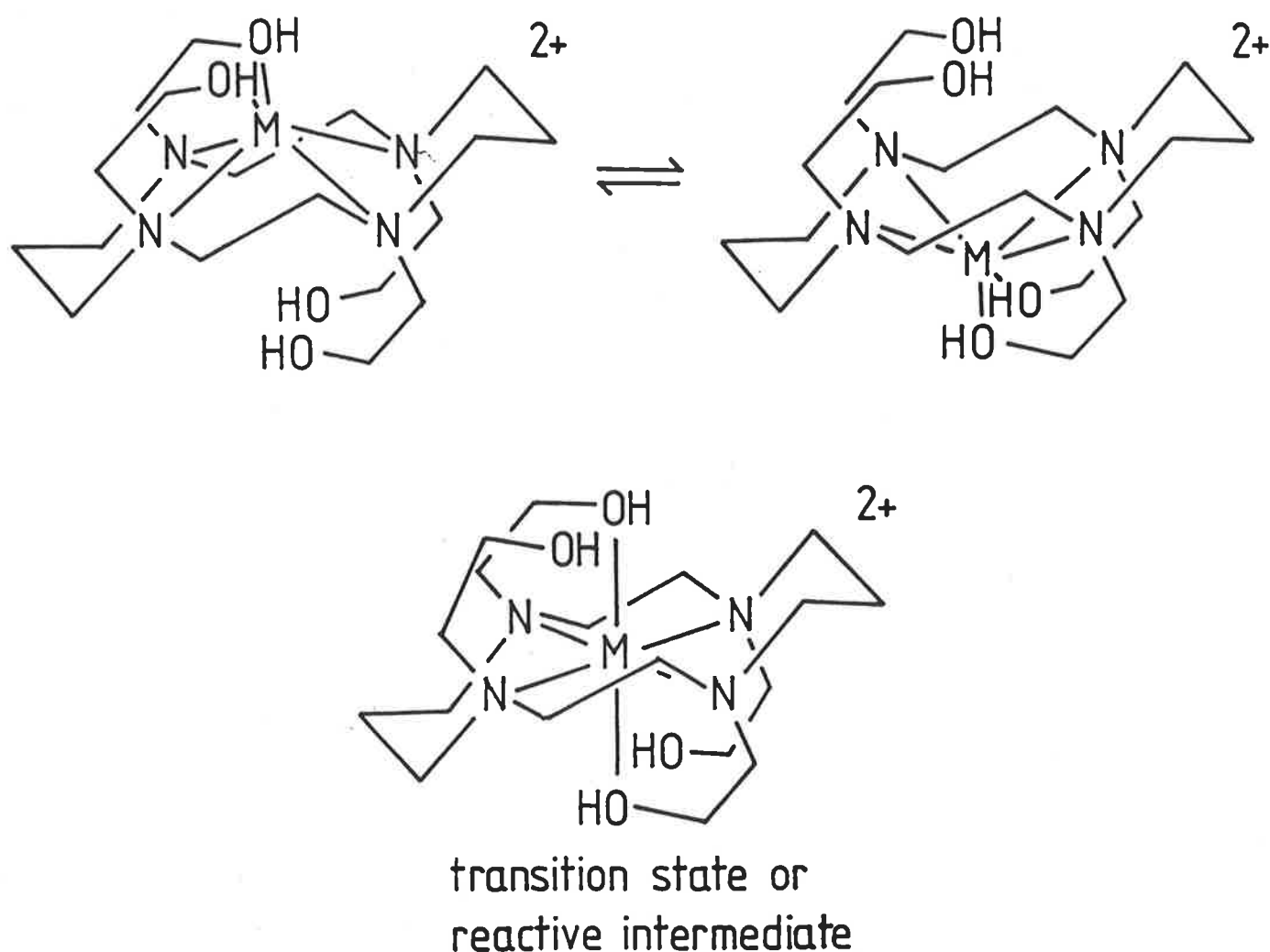


Figure 4.6 Proposed $[\text{M}(\text{THEC})]^{2+}$ structure showing the *trans-III* configuration of THEC and the transannular exchange mechanism.

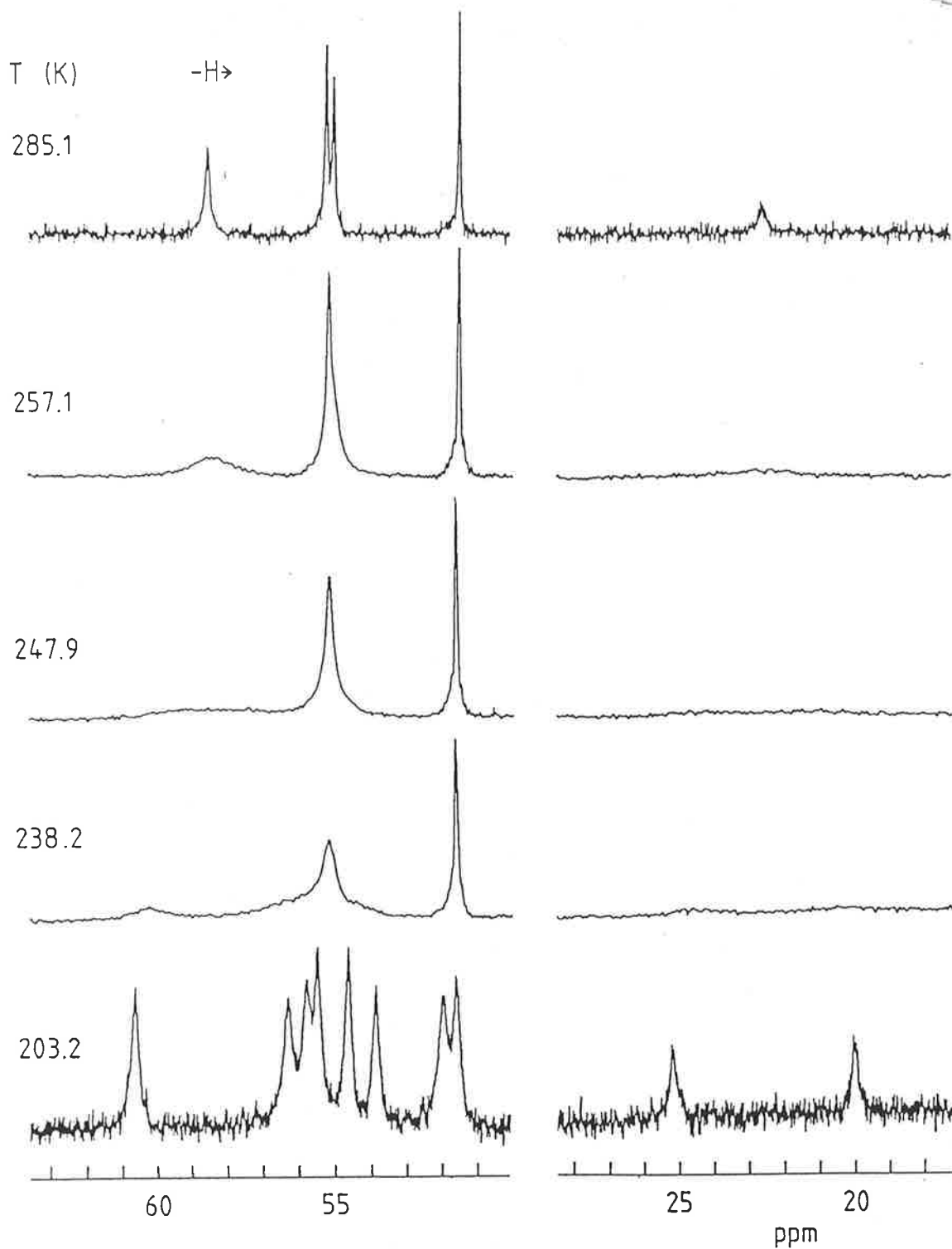


Figure 4.7 Temperature variation of ^{13}C 75.47 MHz broad-band proton decoupled NMR of $[\text{Cd}(\text{THEC})](\text{ClO}_4)_2$ ($0.050 \text{ mol dm}^{-3}$) in d_4 -methanol.

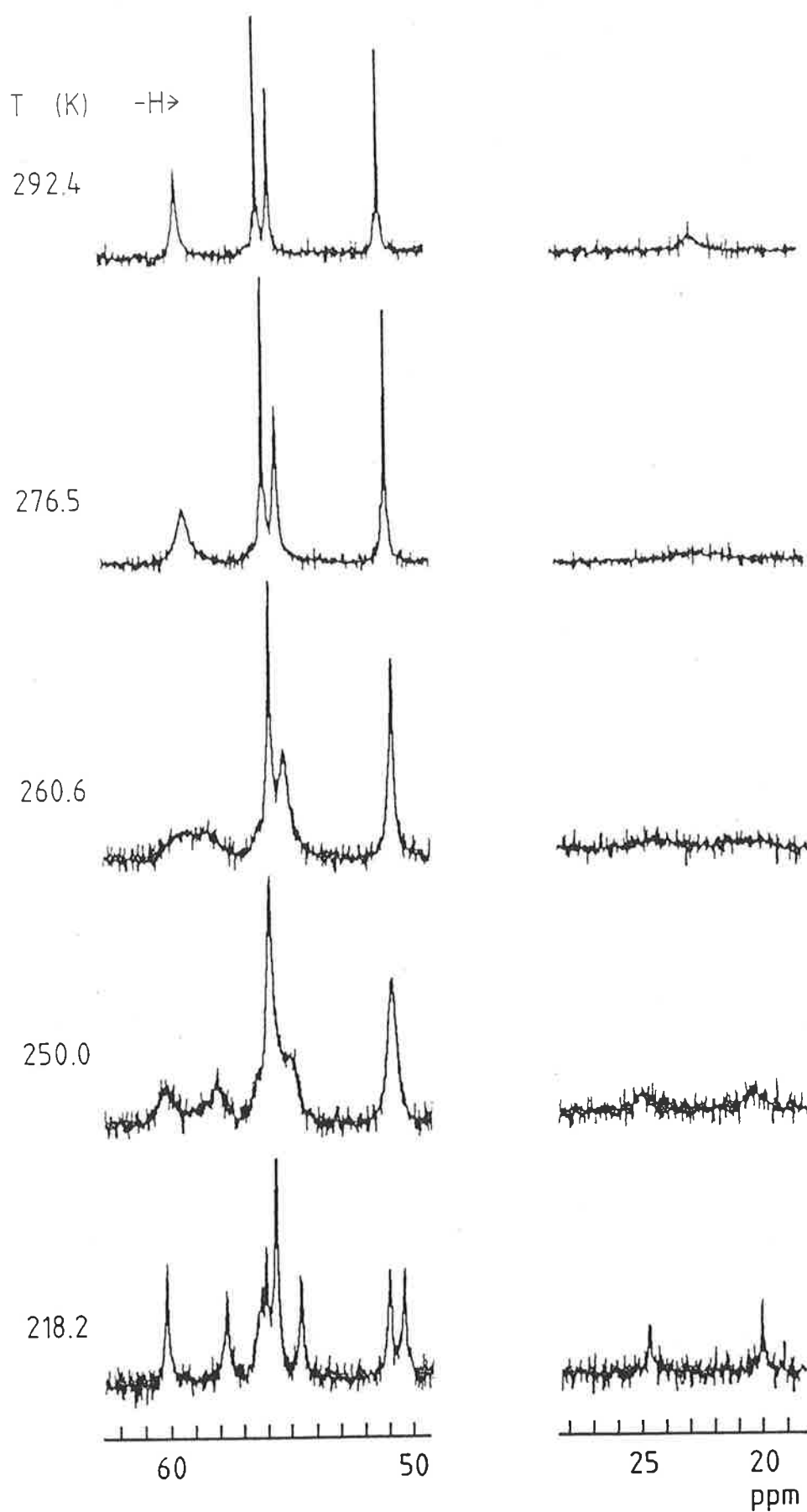


Figure 4.8 Temperature variation of ^{13}C 75.47 MHz broad-band proton decoupled NMR of $[\text{Hg}(\text{THEC})](\text{ClO}_4)_2$ ($0.020 \text{ mol dm}^{-3}$) in d_4 -methanol.

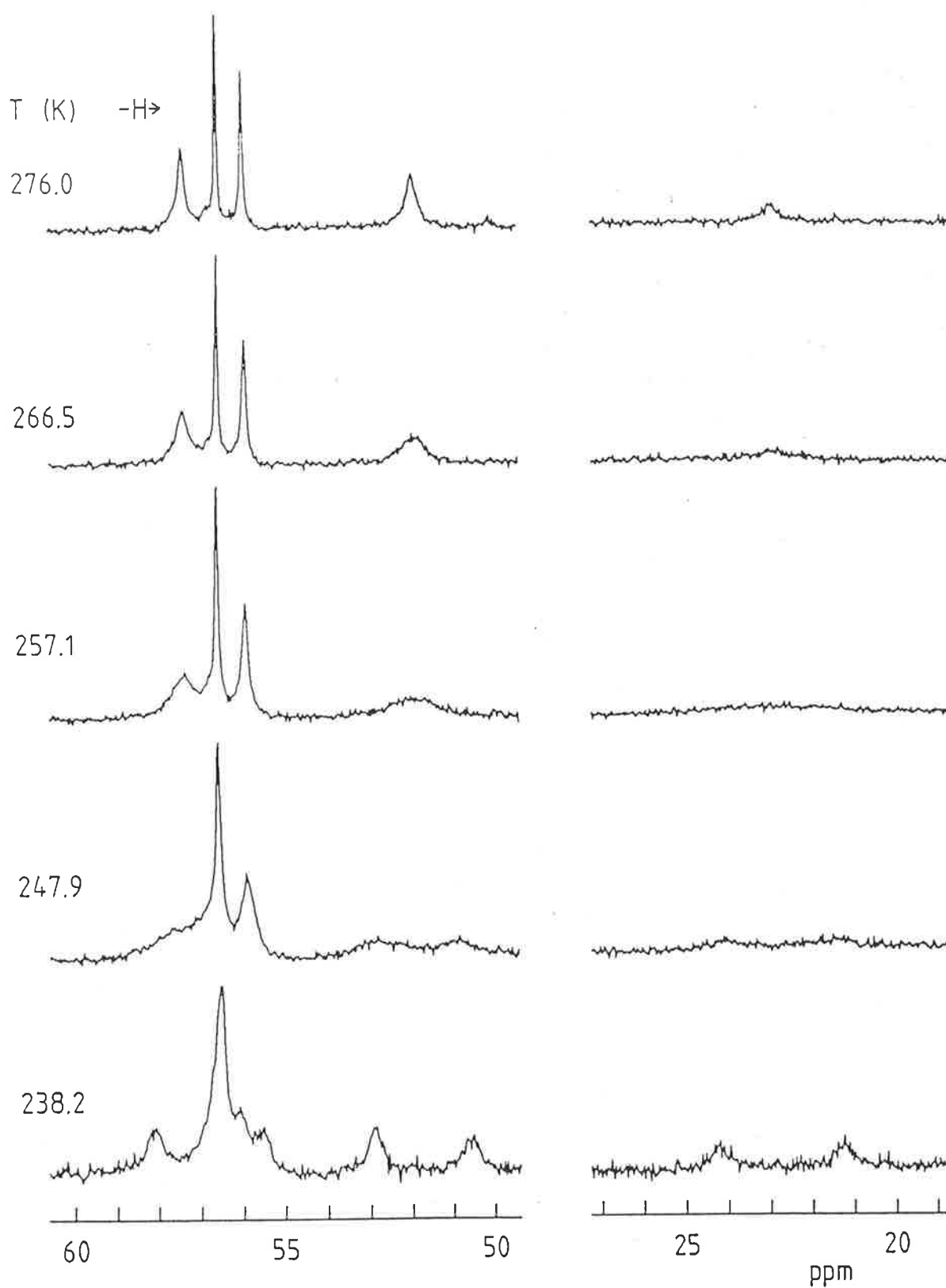


Figure 4.9 Temperature variation of ^{13}C 75.47 MHz broad-band proton decoupled NMR of $[\text{Pb}(\text{THEC})](\text{ClO}_4)_2$ ($0.019 \text{ mol dm}^{-3}$) in d_4 -methanol.

4.4 : ^{13}C -Enriched $[\text{M}(\text{THEC}^*)]^{2+}$ Spectra and Intramolecular Exchange Processes in d_4 -Methanol

In order to further understand the exchange processes, and also to better determine the kinetic parameters of the $[\text{M}(\text{THEC})]^{2+}$ intramolecular exchange processes, both methylene carbons of each of the four hydroxyethyl arms of THEC were enriched to 99 atom % in ^{13}C (the isotopic enrichment is denoted by an asterisk, that is, THEC*). As a consequence, under slow-exchange conditions, both the bidentate hydroxyethyl arms (where the oxygens of the arms and the corresponding ring nitrogens of the same arm are both coordinated to the metal ion) and monodentate hydroxyethyl arms (where the oxygens are not coordinated to the metal ion) are characterised by separate ^{13}C AB quartets. (Figure 4.10 and Table 4.3). The down-field quartets are assigned to the bidentate hydroxyethyl arm on the basis that the carbons in the doubly coordinated arms in $[\text{M}(\text{THEC}^*)]^{2+}$ will experience a greater decrease of electron density, when compared to the monodentate arms.

4.4.1 : Intramolecular Ligand Exchange of [1,4,8,11-Tetrakis(2-hydroxyethyl)-1,4,8,11-tetraazacyclotetradecane]cadmium(II), $[\text{Cd}(\text{THEC}^*)]^{2+}$, in d_4 -Methanol Solution. A ^{13}C -Enriched NMR Study

The bidentate and monodentate hydroxyethyl arms of $[\text{Cd}(\text{THEC}^*)]^{2+}$ in d_4 -methanol solution are each characterised by two ^{13}C AB quartets in slow exchange (Figure 4.10 and Table 4.3). However, under fast exchange conditions these two AB quartets coalesce to a single resonance (Figure 4.11). This is consistent with the relative chemical shifts of the N- $^{13}\text{CH}_2$ carbon and the HO- $^{13}\text{CH}_2$ carbon being reversed on coordination of the hydroxyethyl arm hydroxy-oxygen.

Complete lineshape analysis of the coalescence of the two AB quartets yielded the best-fit lineshapes (Figure 4.11). The spectra were subjected to complete lineshape analysis on a VAX 11780 computer with LINSHP, a FORTRAN-77 program using a density matrix algorithm (Appendix iii, and discussed in Chapter 6). The kinetic data derived from the lineshape analysis of the specifically enriched ^{13}C hydroxyethyl arms spectra are given in Table 4.4.

4.4.2 : Intramolecular Ligand Exchange of [1,4,8,11-Tetrakis(2-hydroxyethyl)-1,4,8,11-tetraazacyclotetradecane]mercury(II), [Hg(THEC*)]²⁺, and its Lead(II) Analogue in *d*₄-Methanol Solution. A ¹³C-Enriched NMR Study

The bidentate and monodentate hydroxyethyl arms of [Hg(THEC*)]²⁺ and [Pb(THEC*)]²⁺ are characterised by ¹³C AB quartets in the slow exchange regime in *d*₄-methanol solution (Figure 4.10, Table 4.3). The reversal of chemical shifts experienced for the [Cd(THEC*)]²⁺ does not occur for [Hg(THEC*)]²⁺ and [Pb(THEC*)]²⁺. The chemical shifts of their down-field quartets are substantially different, which is consistent with the expectation that the bidentate hydroxyethyl arm reflects the influence of variation in the nature of the complexed metal ion to a greater extent than it does for the monodentate arm. Consequently, for each system, the down-field quartet is assigned to the bidentate arms.

The variable temperature ¹³C spectra of [M(THEC*)]²⁺, where M²⁺ = Hg²⁺ and Pb²⁺, show two AB quartets coalescing to a single environmentally averaged quartet as the temperature is increased (Figures 4.12 and 4.13, respectively). Complete lineshape analysis of the coalescence of the two AB quartets yielded the best-fit lineshapes for the pair-wise exchange of the hydroxyethyl arms. The kinetic data derived from the lineshape analysis for the specifically ¹³C-enriched hydroxyethyl arms of [Hg(THEC*)]²⁺ and [Pb(THEC*)]²⁺ were determined by the same method as the [Cd(THEC*)]²⁺ system (Table 4.4) and are compared in Figure 4.14.

Table 4.3 The Chemical Shifts and Coupling Constants for each AB Quartet as Presented in Figure 4.10

	Temp. K	Conc. mol dm ⁻³	Chemical shift		
			ABI	ABII	<i>J</i> _{AB} (Hz)
[Pb(THEC*)] ²⁺	223.5	0.013	ABI	58.02	40.5
			ABII	56.39	40.2
[Hg(THEC*)] ²⁺	218.2	0.020	ABI	56.05	39.0
			ABII	55.63	39.2
[Cd(THEC*)] ²⁺	212.9	0.020	ABI	55.36	39.0
			ABII	54.54	39.3

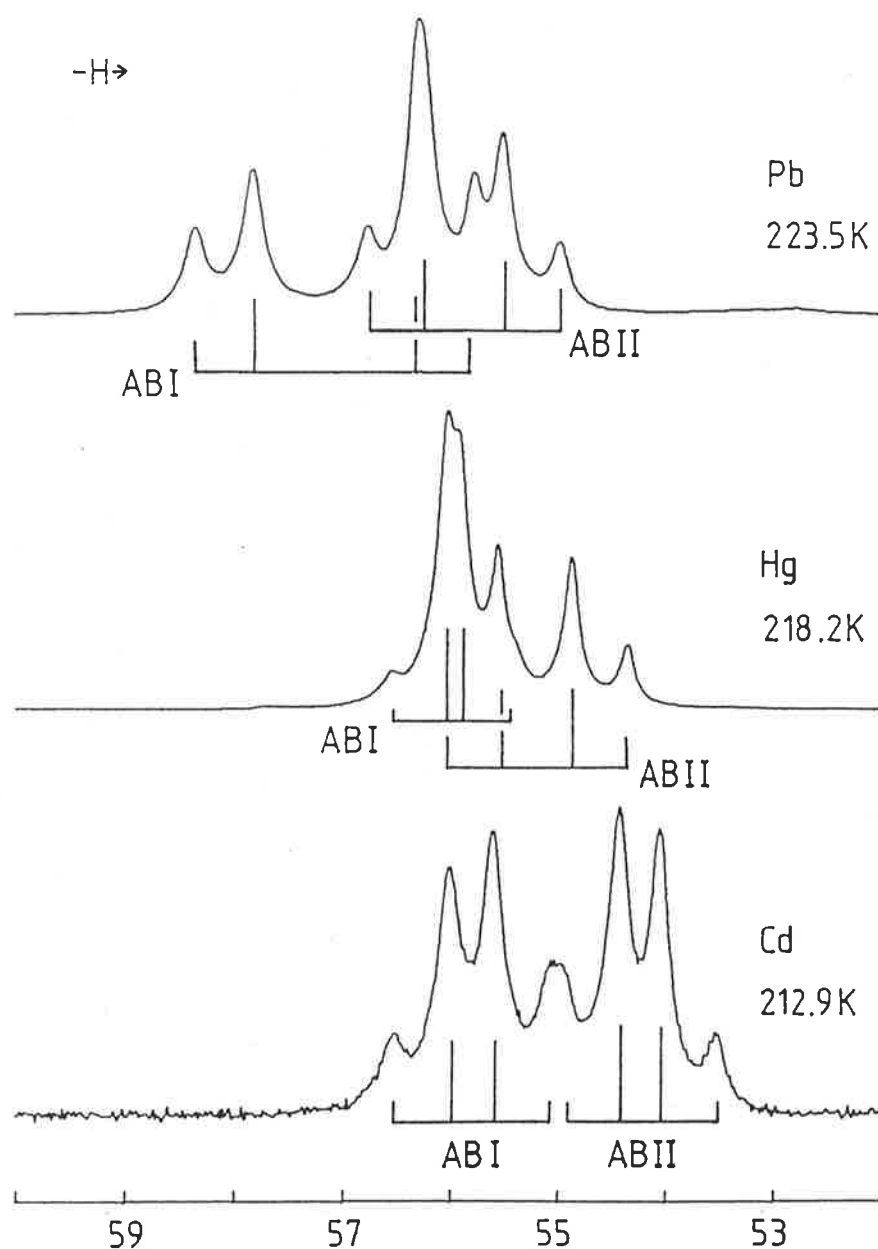


Figure 4.10 The ^{13}C 75.47 MHz NMR spectra of the 99 atom % ^{13}C -enriched hydroxyethyl arms of $[\text{M}(\text{THEC}^*)]^{2+}$ in d_4 -methanol. The individual AB quartets are shown as stick diagrams at the appropriate frequencies, and the height of the individual lines are proportional to the signal intensity.

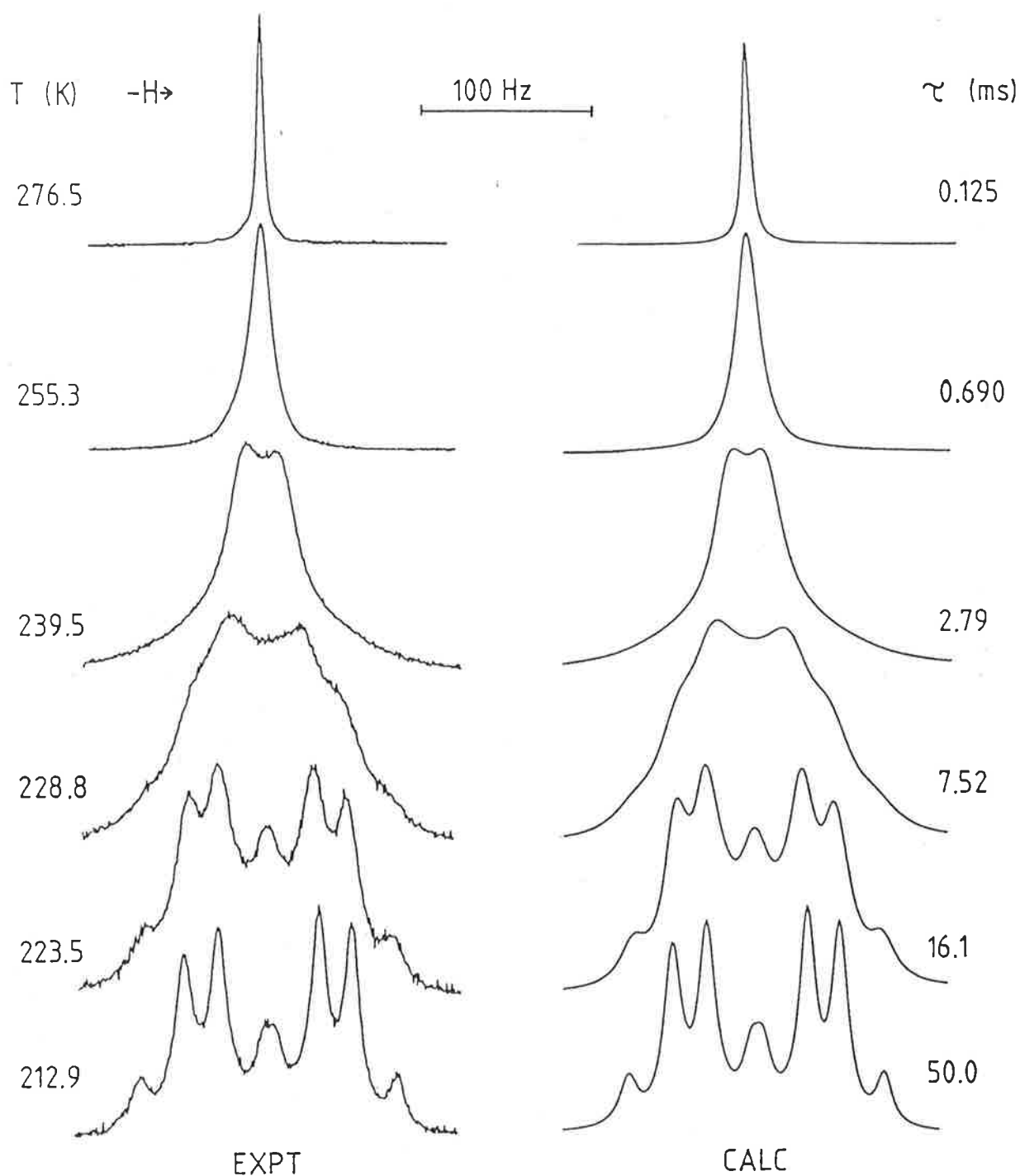


Figure 4.11 The ^{13}C 75.47 MHz NMR spectra of the 99 atom % ^{13}C -enriched hydroxyethyl arms of $[\text{Cd}(\text{THEC}^*)]^{2+}$ ($0.020 \text{ mol dm}^{-3}$) in d_4 -methanol. The experimental spectra and temperatures are on the left side, and the best fit calculated line shapes with the corresponding time-average site lifetimes are on the right.

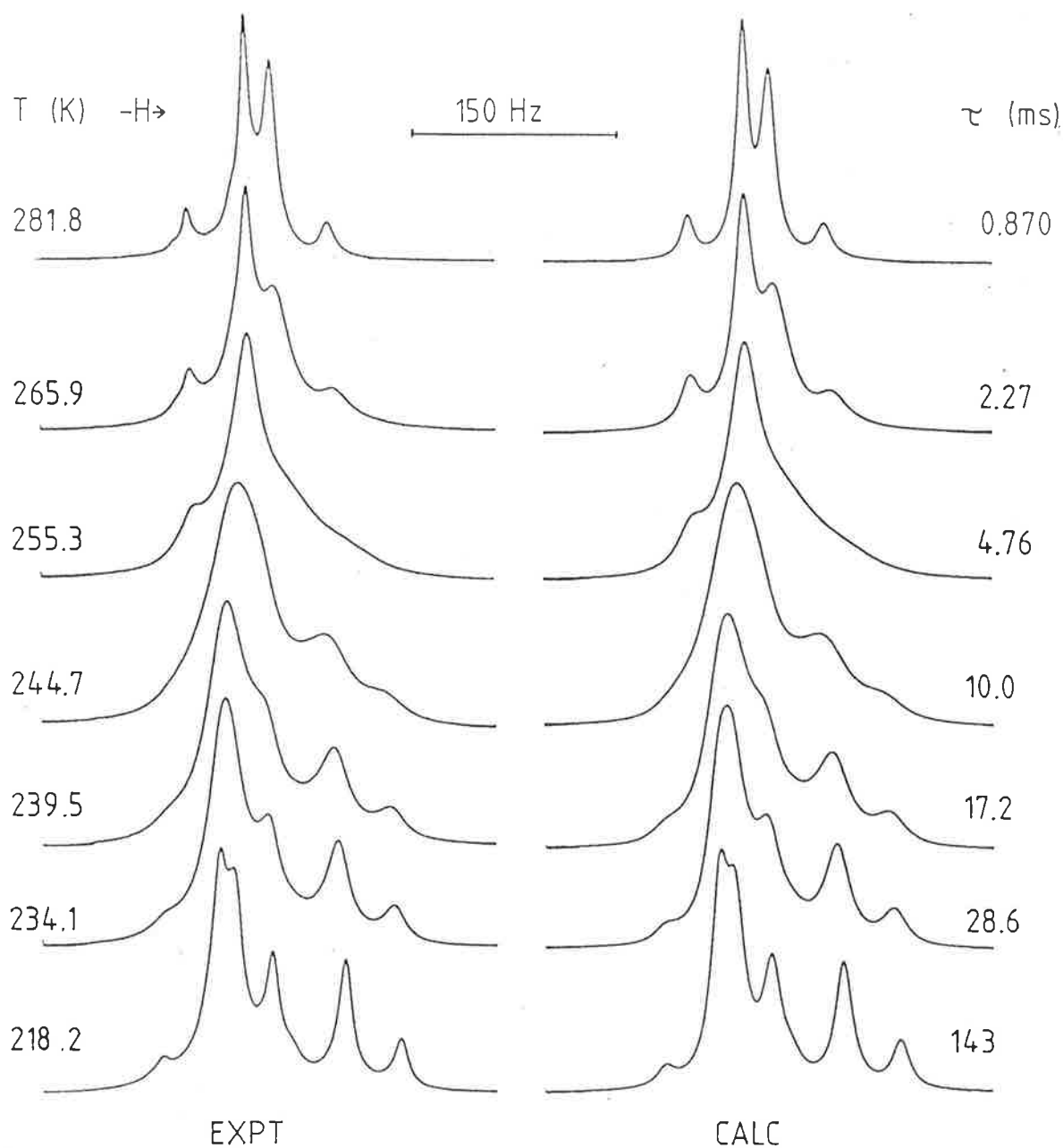


Figure 4.12 The ^{13}C 75.47 MHz NMR spectra of the 99 atom % ^{13}C -enriched hydroxyethyl arms of $[\text{Hg}(\text{THEC}^*)]^{2+}$ ($0.020 \text{ mol dm}^{-3}$) in d_4 -methanol. The experimental spectra and temperatures are shown on the left, and the best fit calculated line shapes and the corresponding time-average site lifetimes are given on the right.

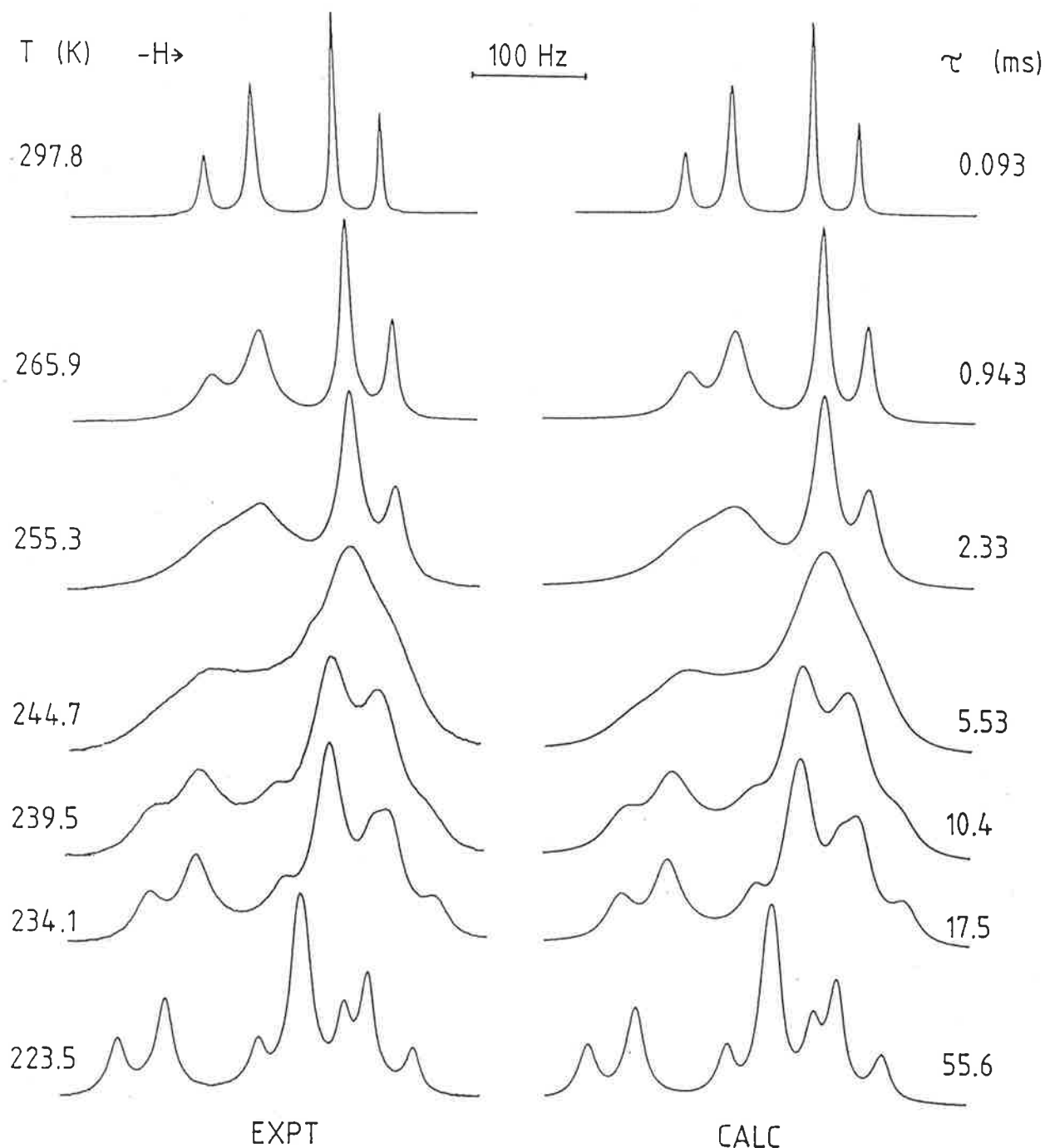


Figure 4.13 The ^{13}C 75.47 MHz NMR spectra of the 99 atom % ^{13}C -enriched hydroxyethyl arms of $[\text{Pb}(\text{THEC}^*)]^{2+}$ ($0.013 \text{ mol dm}^{-3}$) in d_4 -methanol. The experimental spectra and temperatures are on the left, and the best fit calculated line shapes with the corresponding time-average site lifetimes are on the right.

4.4.3 : [M(THEC)]²⁺, Intramolecular Exchange Processes

The kinetic parameters derived from the natural abundance ¹³C spectra (1.108 atom % ¹³C²⁸) of the coalescence of the medial carbon resonances, for each system, are given in Table 4.4. As a consequence of the poor signal to noise ratio, the errors in these parameters are large. However, these results are in sufficient agreement with the those derived from the lineshape analysis of the enriched ¹³C resonances to conclude that both coalescence phenomena arise from the same molecular process.

The intramolecular exchange mechanism proposed for [M(THEC*)]²⁺ and [M(THEC)]²⁺, where M²⁺ = Cd²⁺, Hg²⁺ and Pb²⁺ (Figure 4.6), is a highly concerted process in which no change in coordination number occurs. The low energy barrier for this process is consistent with the moderate ΔH^\ddagger values observed (Table 4.4) and are similar to those observed for the intramolecular processes of the related complexes, [Cd(TMC)]²⁺²⁷ and [Pb(TMC)]²⁺.¹⁹

Table 4.4 Kinetic Parameters for [M(THEC)]²⁺ Intramolecular Exchange Processes Derived from ¹³C NMR Studies in *d*₄-methanol

System	$k(250.0 \text{ K})$ ^{a,b} s ⁻¹	$k(298.2 \text{ K})$ ^a s ⁻¹	ΔH^\ddagger ^a kJ mol ⁻¹	ΔS^\ddagger ^a J K ⁻¹ mol ⁻¹
[Cd(THEC*)] ²⁺ ^c	940 ± 20	34 200 ± 1800	44.0 ± 0.6	-10.6 ± 2.2
[Cd(THEC)] ²⁺ ^d	760 ± 200	68 000 ± 18 000	46.6 ± 4.5	4 ± 15
[Hg(THEC*)] ²⁺ ^c	137 ± 2	3 130 ± 20	38.0 ± 0.6	-50.6 ± 2.1
[Hg(THEC)] ²⁺ ^d	353 ± 58	9 500 ± 3 000	40.0 ± 4.5	-34.3 ± 17.0
[Pb(THEC*)] ²⁺ ^c	275 ± 3	11 200 ± 220	45.4 ± 0.3	-15.2 ± 1.1
[Pb(THEC)] ²⁺ ^d	495 ± 90	25 000 ± 10 000	48.3 ± 4.4	1.4 ± 15

^a Errors represent one standard deviation for the fit of the τ data to the Eyring equation;

^b The $k(250.0 \text{ K})$ value is the most accurate as it is derived at the mid-point of the spectral coalescence temperature range; ^c Derived from specifically ¹³C-enriched hydroxyethyl [M(THEC)]²⁺; ^d Derived from natural abundance ¹³C medial carbon data.

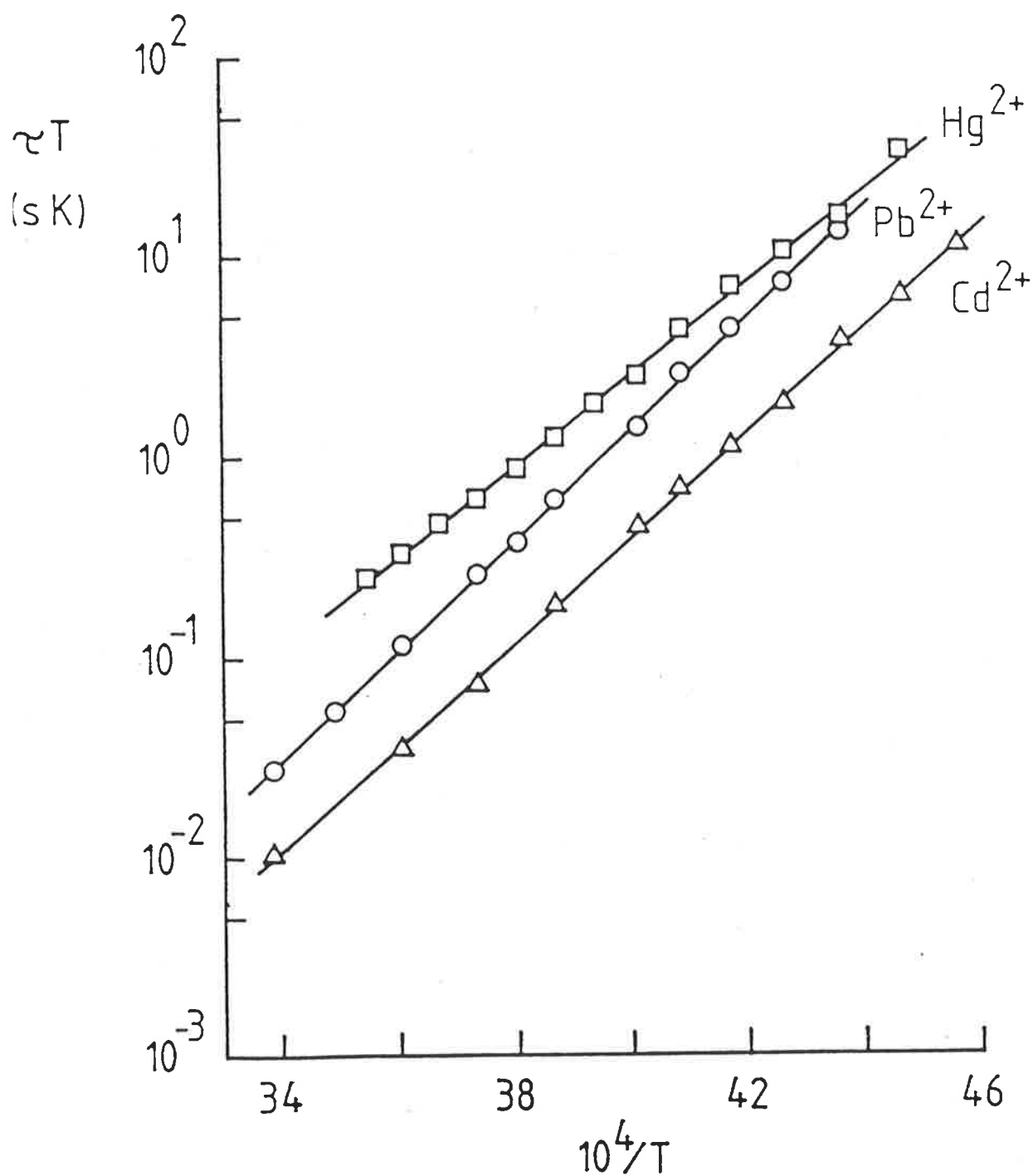


Figure 4.14 The temperature variations of τT of the intramolecular exchange of $[\text{Cd}(\text{THEC}^*)]^{2+}$, $[\text{Hg}(\text{THEC}^*)]^{2+}$ and $[\text{Pb}(\text{THEC}^*)]^{2+}$ derived from the complete lineshape analysis for each system (Figures 4.11 - 4.13) are represented by triangles, squares and circles, respectively. The solid curves represent the best fit of the data for each system.

The variation of the metal ion in the THEC complexes result in a decrease in the rate for intramolecular exchange as the radius increases from Cd^{2+} (0.95 Å²⁵) to Hg^{2+} (1.02 Å) as a result of a substantially more negative ΔS^\ddagger for $[\text{Hg}(\text{THEC})]^{2+}$. This is consistent with the larger Hg^{2+} being a tighter, optimal fit in the macrocyclic annulus of THEC compared to Cd^{2+} , therefore introducing a greater rigidity in the transition state envisaged (Figure 4.6). The macrocyclic hole radius is estimated to be about 1.35 Å on the basis of metal-nitrogen bond distances in similar systems.⁴⁰ However, the group 14 divalent cation, Pb^{2+} ($r = 1.19$ Å) does not appear to follow the trend of decreasing intramolecular rate with increasing cation size. The results for the kinetics of $[\text{Pb}(\text{THEC})]^{2+}$ are interposed between those of the group 12 divalent cations, Cd^{2+} and Hg^{2+} . This may be a consequence of the difference in electronic structure between the two groups partially negating the larger cation size of Pb^{2+} . The divalent cation, Pb^{2+} has two extra electrons in comparison with Hg^{2+} , and evidence has been presented that these electrons may occupy a coordination site as a “stereochemically active” lone pair in macrocyclic ligand complexes,²⁹ where the ligand has three or more nitrogen donor atoms. As a consequence, the coordination chemistry of Pb^{2+} resembles that of a smaller metal ion. It has been observed that the lower stability of $[\text{Pb}(\text{THEC})]^{2+}$ in water, as depicted by the variation of $\log(K_s / \text{dm}^3 \text{ mol}^{-1}) = 9.38, 17.94$ and 6.28 for $[\text{M}(\text{THEC})]^{2+}$ for $\text{M}^{2+} = \text{Cd}^{2+}, \text{Hg}^{2+}$ and Pb^{2+} respectively, may arise in part, from the destabilising effect of the Pb^{2+} lone pair.¹ The greater lability of $[\text{Pb}(\text{THEC})]^{2+}$ compared with $[\text{Hg}(\text{THEC})]^{2+}$, may be attributable to the Pb^{2+} lone pair destabilising $[\text{Pb}(\text{THEC})]^{2+}$. As a consequence of the limited range of kinetic data, it would be inappropriate to speculate without further investigation.

4.5 : Additional Studies on 1,4,8,11-Tetrakis(2-hydroxyethyl)-1,4,8,11-tetraazacyclotetradecane, THEC

4.5.1 : [1,4,8,11-Tetrakis(2-hydroxyethyl)-1,4,8,11-tetraazacyclotetradecane]zinc(II), [Zn(THEC)]²⁺, in *d*₄-Methanol. A Natural Abundance ¹³C NMR Study

The tetraaza macrocycle, [Zn(TMC)]²⁺,³⁰ behaves as a reversible CO₂ acceptor^{31,32} in alcoholic solution. This behaviour appears similar to that of the metalloenzyme carbonic anhydrase, where a Zn²⁺ cation, coordinated by three nitrogens, is in the active site,^{33,34} and is very efficient at fixing carbon dioxide and converting it to carbonic acid *in vivo* (kinetic rate constant³⁵ $k = 6 \times 10^5 \text{ s}^{-1}$ 298.2 K). An investigation of the variable temperature ¹³C NMR spectra of [Zn(THEC)]²⁺, aside from its intrinsic interest, may also be of value as a model for this enzyme.

The interpretation of the variable temperature spectra of [Zn(THEC)]²⁺, were not straight-forward, and examination of the spectrum at 301.3 K revealed at least three discernible species with a total of at least 12 resonances between 49 - 60 ppm, and at least 4 resonances between 19 - 23 ppm. At 253.5 K, there are at least 18 resonances between 49 - 60 ppm and 5 resonances between 19 - 23 ppm. The spectrum at 330.6 K seemed to coalesce into 5 broad peaks (ratio approximately 5:5:5:5:5) at 56.39, 55.15, 52.35, 51.62 and 20.15, and 10 sharp peaks (ratio approximately 2:2:2:2:2:2:2:2:1:1) at 56.91, 56.39 (overlapping the broad peak), 55.91, 55.53, 54.04, 52.07, 50.71, 48.38, 22.75 and 21.20. These results suggest that at higher temperature, there are at least two different structures in slow exchange with each other on the NMR timescale, which on lowering the temperature appear to further split into other conformations. This implies that in solution [Zn(THEC)]²⁺ exists in at least four different conformations, where the interchanges between the differing conformations have different rates of exchange.

4.5.2 : [1,4,8,11-Tetrakis(2-hydroxyethyl)-1,4,8,11-tetraazacyclotetradecane]nickel(II), [Ni(THEC)]²⁺, in *d*₄-Methanol. A Natural Abundance ¹³C NMR Investigation

The divalent metal ion complex, [Ni(THEC)]²⁺, was investigated using ¹³C NMR. It was hoped that a variable temperature ¹³C NMR investigation of [Ni(THEC)]²⁺ would yield results relevant to other studies with Ni²⁺ and THEC, where the protonation and decomplexation reactions of this system in aqueous solution were studied by stopped flow techniques.³⁶

Table 4.5 Comparison of ¹³C Chemical Shifts in *d*₄-Methanol of [Ni(THEC)](ClO₄)₂ at 290.0 K

	Temp. K	Conc. mol dm ⁻³	Chemical shift					
			ppm	ppm	ppm	ppm	ppm	ppm
[Ni(THEC)] ²⁺	290.0	0.050	56.79	53.55	50.22	35.53	35.31	21.33
Intensity Ratio			2:	2:	2:	1:	1	1

As Ni²⁺ ion is paramagnetic, the ¹³C spectra of [Ni(THEC)]²⁺ at 290.0 K were compared using a 10 000 Hz and 50 000 Hz sweep width. Subsequently, a number of other resonances could be ascertained, a broad resonance with a chemical shift of 58.5 ppm, ($W_{1/2} = \sim 150$ Hz), and three very broad peaks were found at approximately 130.5 ppm ($W_{1/2} = \sim 300$ Hz), -114 ppm ($W_{1/2} = \sim 300$ Hz) and -166 ppm ($W_{1/2} = \sim 600$ Hz). These drastically shifted and broadened resonances were probably due to the paramagnetic Ni²⁺ ion causing localised chemical shifts (over a 300 ppm range) and peak broadening due to enhanced relaxation on the ¹³C resonances influenced by the paramagnetic Ni²⁺ ion. As a result of these phenomena, the kinetic analysis by NMR was abandoned for the [Ni(THEC)]²⁺ system.

4.5.3 : Selectively ^{13}C -Enriched 1,4,8,11-Tetrakis(2-hydroxyethyl)-1,4,8,11-tetraazacyclotetradecane, THEC*, and $[\text{Ba}(\text{THEC}^*)]^{2+}$ in d_4 -Methanol. A Variable Temperature ^{13}C NMR Study

Variable temperature (200 - 300 K) ^{13}C NMR spectra of THEC* in the absence of any metal ion, and of $[\text{Ba}(\text{THEC}^*)]^{2+}$, have been studied (both in d_4 -methanol solution). Single AB quartet resonance patterns are observed in both systems at 296.0 K (Table 4.6), similar to $[\text{M}(\text{THEC}^*)]^{2+}$, where $\text{M}^{2+} = \text{Cd}^{2+}$, Hg^{2+} and Pb^{2+} (Figures 4.11 - 4.13).

Table 4.6 The Chemical Shifts and Coupling Constants for each AB Quartet for the ^{13}C Enriched Ligand, and $[\text{Ba}(\text{THEC}^*)]^{2+}$

	Temp.	Conc.	Chemical shift		Coupling constant
	K	mol dm ⁻³	δ_{A} (ppm)	δ_{B} (ppm)	J_{AB} (Hz)
$[\text{Ba}(\text{THEC}^*)]^{2+}$	296.0 K	0.010	58.33	54.84	40.2
"	221.7 K	"	58.26	53.64	39.6
THEC*	296.0 K	0.030	56.62	54.44	39.2
"	216.4 K	"	58.41	53.69	39.2

As the temperature decreases, both the THEC* and $[\text{Ba}(\text{THEC}^*)]^{2+}$ spectra retain a single AB quartet. By comparison, each of the $[\text{M}(\text{THEC}^*)]^{2+}$ AB quartet resonances split into two sets of AB quartets. The single AB quartet observed for the resonances of free THEC* and $[\text{Ba}(\text{THEC}^*)]^{2+}$, are seen throughout the temperature range examined, 185 - 300 K (the freezing point of d_4 -methanol is ~ 181 K). At lower temperatures the resonances for both systems become broader, consistent with an increase in solution viscosity. Thus, the intramolecular exchange process deduced for $[\text{M}(\text{THEC}^*)]^{2+}$, $\text{M}^{2+} = \text{Cd}^{2+}$, Hg^{2+} and Pb^{2+} could not be observed for THEC* or $[\text{Ba}(\text{THEC}^*)]^{2+}$ under similar conditions.

The absence of any observed exchange phenomena for THEC* is consistent with the intramolecular process observed for $[\text{M}(\text{THEC}^*)]^{2+}$, involving the transannular oscillation of the metal ion, as shown in Figure 4.6.

The lack of intramolecular exchange observed for $[\text{Ba}(\text{THEC}^*)]^{2+}$ may be due to an increased activation energy required for any transannular oscillation of the metal ion, through the THEC* annulus ($r = 1.35 \text{ \AA}$ as estimated from similar ligands¹⁶) as a consequence of the steric constraints of the larger Ba^{2+} cation ($r = 1.35 \text{ \AA}$,²⁵ compares with 0.95, 1.02, 1.19 \AA for Cd^{2+} , Hg^{2+} and Pb^{2+} , respectively). It is generally observed that for metal ions of increasing size, there is a corresponding increase in coordination number of the complexes formed. Thus, an increased coordination number for Ba^{2+} may result in a preference of a *trans*-I structure of $[\text{Ba}(\text{THEC})]^{2+}$, where Ba^{2+} is coordinated to all eight donor atoms of the ligand, THEC (the *trans*-III structure deduced for $[\text{M}(\text{THEC})]^{2+}$, $\text{M}^{2+} = \text{Cd}^{2+}$, Hg^{2+} and Pb^{2+} , results in a metal ion coordination number of six, Figures 4.3 and 4.6). In such a *trans*-I structure of $[\text{Ba}(\text{THEC})]^{2+}$, all four hydroxyethyl arms would be equivalent, which is consistent with the single AB coupled resonance observed at low temperature.

4.5.4 : Permutations of Coupling and Chemical Shift Differences of ^{13}C -Enriched Hydroxyethyl Arms of $[\text{M}(\text{THEC}^*)]^{2+}$

The variable temperature ^{13}C NMR spectra of ^{13}C -enriched $[\text{Cd}(\text{THEC}^*)]^{2+}$, $[\text{Hg}(\text{THEC}^*)]^{2+}$ and $[\text{Pb}(\text{THEC}^*)]^{2+}$ from 210 K to 300 K, have already been discussed in detail (see Figures 4.11 - 4.13). In all three complex systems, the spectra of the ^{13}C -enriched hydroxyethyl arms are characterised by two AB quartets under conditions of slow exchange (Figure 4.10 and Table 4.3). The two AB quartets of both $[\text{Hg}(\text{THEC}^*)]^{2+}$ and $[\text{Pb}(\text{THEC}^*)]^{2+}$ coalesce to form single environmentally averaged quartets as the temperature is increased.

In contrast, the two AB quartets characterising the slow exchange spectra of $[\text{Cd}(\text{THEC}^*)]^{2+}$, coalesce to a singlet under fast exchange conditions, and not to an averaged AB quartet (Figure 4.11). This is consistent with the relative chemical shifts of the methylene carbons of each pair of hydroxyethyl arms being reversed when they change between monodentate and bidentate coordination, such that the environmentally averaged chemical shifts in the fast exchange environment result in the single resonance observed.

An alternative possibility is that the single resonance observed under fast exchange conditions of the ^{13}C spectra of $[\text{Cd}(\text{THEC}^*)]^{2+}$ occurs as a result of a reversal in absolute magnitude of the coupling constant, J , between the monodentate and bidentate environments. This possibility is discounted by a comparison of theoretical lineshapes resulting from the ^{13}C - ^{13}C coupling constants and chemical shift differences, D , as measured from the experimental spectra of $[\text{Cd}(\text{THEC}^*)]^{2+}$ (Figure 4.15).

The theoretical spectra calculated for various site lifetimes of the exchange, $\text{AB}(\text{I}) \rightleftharpoons \text{AB}(\text{II})$ in Figure 4.15 are based on the following parameters:

- (i) The chemical shift difference, $D_{\text{AB}(\text{I})}$, and coupling constant, $J_{\text{AB}(\text{I})}$, for the AB(I) quartet, are of the same magnitude and sign as $D_{\text{AB}(\text{II})}$ and $J_{\text{AB}(\text{II})}$ for the AB(II) quartet. The relative parameters used to calculate the theoretical spectra for system (i) are:
 $W_{1/2}(\text{natural}) = 6 \text{ Hz}$ for all resonances;
 $D_{\text{AB}(\text{I})} = \delta_{\text{A}(\text{I})} - \delta_{\text{B}(\text{I})} = 36 \text{ Hz}$ and
 $D_{\text{AB}(\text{II})} = \delta_{\text{A}(\text{II})} - \delta_{\text{B}(\text{II})} = 41 \text{ Hz}$ corresponding to $[\text{Cd}(\text{THEC}^*)]^{2+}$
 at 297.8 K for the site lifetime $\tau = 0.0345 \text{ ms}$ (10^{-3} s);
 $D_{\text{AB}(\text{I})} = \delta_{\text{A}(\text{I})} - \delta_{\text{B}(\text{I})} = 57 \text{ Hz}$ and
 $D_{\text{AB}(\text{II})} = \delta_{\text{A}(\text{II})} - \delta_{\text{B}(\text{II})} = 55 \text{ Hz}$ corresponding to $[\text{Cd}(\text{THEC}^*)]^{2+}$
 at 212.9 K for the site lifetime $\tau = 50.0 \text{ ms}$;
 $\Delta\delta_{\text{AB}} = 0.5(\delta_{\text{A}(\text{I})} - \delta_{\text{A}(\text{II})}) + 0.5(\delta_{\text{B}(\text{I})} - \delta_{\text{B}(\text{II})}) = 119 \text{ Hz}$; and
 $J_{\text{AB}(\text{I})} = 39.0 \text{ Hz}$ and $J_{\text{AB}(\text{II})} = 39.3 \text{ Hz}$ at all temperatures.
- (ii) The relative parameters used to derive the theoretical spectra for system (ii) are the same as for system (i) except
 $J_{\text{AB}(\text{II})} = -39.3 \text{ Hz}$, that is, the sign of the coupling constant is reversed.
- (iii) The relative parameters used to derive the theoretical spectra for system (iii) are the same as for system (i) except:
 $D_{\text{AB}(\text{I})} = -36 \text{ Hz}$, for the site lifetime $\tau = 0.0345 \text{ ms}$ (297.8 K) to
 $D_{\text{AB}(\text{I})} = -57 \text{ Hz}$, for the site lifetime $\tau = 50.0 \text{ ms}$ (212.9 K), that is,
 the relative chemical shifts between sites A(I) and B(I) are reversed.

In all three systems, the chemical shift separations between AB(I) and AB(II), $\Delta\delta_{\text{AB}}$, is constant, with changing temperature, as is the magnitude of the coupling constants, J_{AB} . The chemical shift differences between sites, D_{AB} , decreases with temperature, as observed for the variable temperature spectra of $[\text{Cd}(\text{THEC}^*)]^{2+}$.

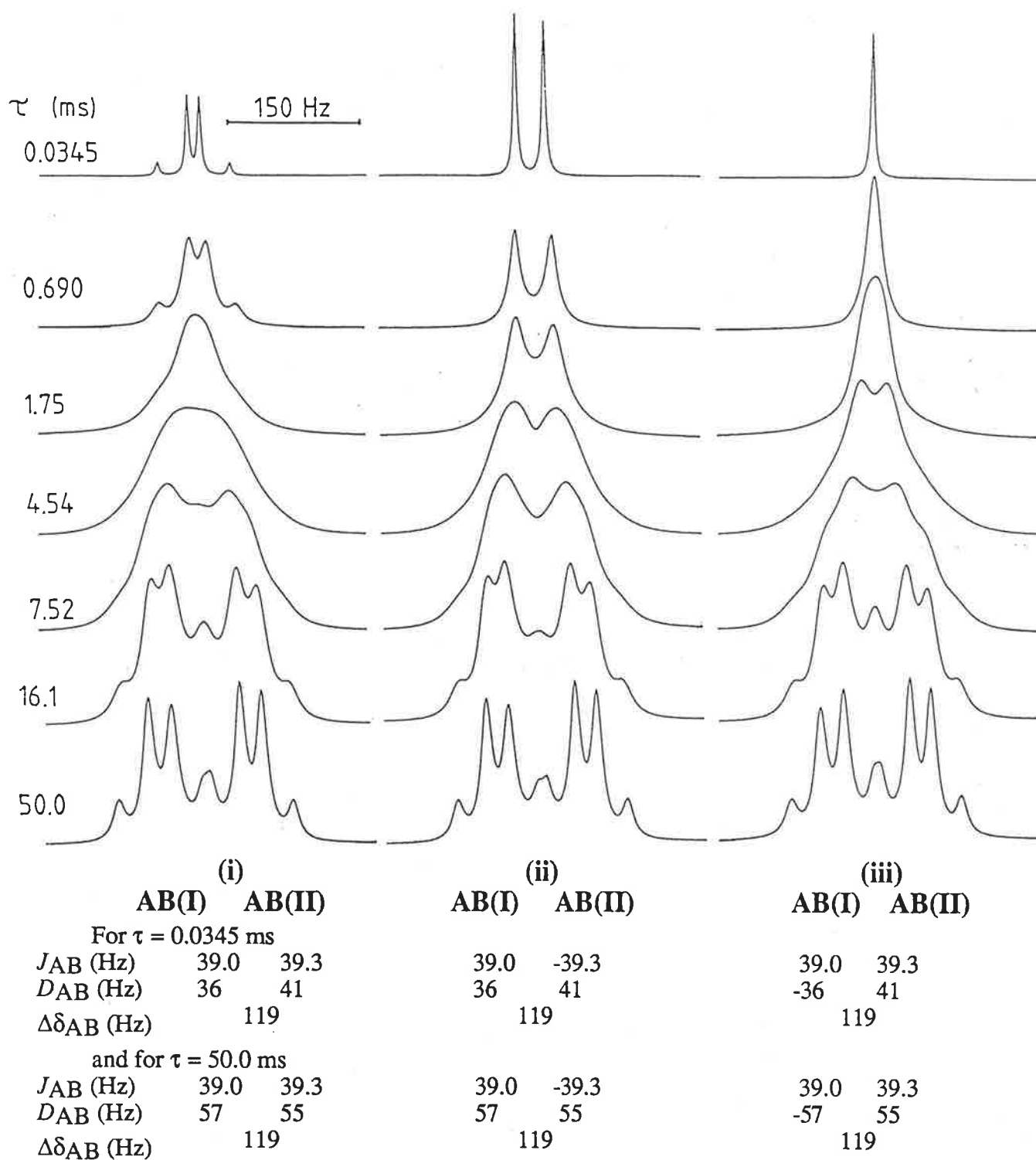


Figure 4.15 Variations in theoretical AB(I) \rightleftharpoons AB(II) exchange lineshapes where the chemical shifts and coupling constants of AB(I) and AB(II) are: (i) both positive (similar to [Hg(THEC*)]²⁺ and [Pb(THEC*)]²⁺); (ii) reversal of coupling constant; and (iii) reversal of chemical shift (similar to [Cd(THEC*)]²⁺).

4.6 : General Conclusions

In this study, the ^{13}C NMR spectra (typically 200 K and 295 K) of [1,4,8,11-tetrakis(2-hydroxyethyl)-1,4,8,11-tetraazacyclotetradecane]cadmium(II) perchlorate and its mercury(II) and lead(II) analogues, show that the most probable structure for these complexes in solution, is where the 1,4,8,11-tetraazacyclotetradecane (tetraaza) ring is in the *trans*-III configuration. In addition, the metal ion is positioned above the plane delineated by the four tetraaza ring nitrogens and coordinated by the four nitrogens and two hydroxyethyl pendant arms attached to the same 1,3-diaminopropane moiety. The ^{13}C solid state CPMAS NMR spectra of both $[\text{Cd}(\text{THEC})]^{2+}$ and $[\text{Hg}(\text{THEC})]^{2+}$ are consistent with the structure in solution. In comparison, the ^{13}C solid state CPMAS NMR spectrum of $[\text{Pb}(\text{THEC})]^{2+}$ shows only one resonance for the medial carbons of the 1,3-diaminopropane moieties, where the ligand may be in a *trans*-V configuration as a result of increased coordination number of Pb^{2+} in the solid state.

The variable temperature natural abundance ^{13}C NMR of each of these three species, show the spectral coalescence of five pairs of resonances from *ca.* 220 - 290 K. The lifetimes of these species were calculated by complete lineshape analysis of the medial carbons of each 1,3-diaminopropane moiety. In order to better determine the kinetic parameters of this exchange process, both methylene carbons of all four hydroxyethyl arms were enriched to 99 % atom ^{13}C . The slow exchange spectra of all three ^{13}C -enriched complexes are characterised by two ^{13}C AB quartets, which for $[\text{Hg}(\text{THEC})]^{2+}$ and $[\text{Pb}(\text{THEC})]^{2+}$ resolve to a single AB quartet in the fast exchange. However, the two AB quartets of $[\text{Cd}(\text{THEC})]^{2+}$ show a novel coalescence to a singlet under fast exchange conditions. The formation of this singlet is attributed to the relative chemical shifts of the methylene carbons of each hydroxyethyl arm being reversed when it changes from a monodentate coordination (the hydroxy oxygens are uncoordinated) to a bidentate coordination (both the ring nitrogen and the hydroxy oxygen are coordinated to the metal). In all three systems, these dynamic changes in the ligand occur simultaneously with the oscillation of the metal ion through the macrocyclic annulus. The complete lineshape analysis of the coalescence of the two AB resonances in each system yielded the most accurate measurement of the kinetic parameters, where there was sufficient agreement of these results with those of the natural abundance spectra to conclude they are due to the same molecular process.

- 1 Stetter H., Frank W., *Angew. Chem., Int. Ed. Engl.*, **1976**, 15, 686.
- 2 Häfliger H., Kaden T.A., *Helv. Chim. Acta*, **1979**, 62, 683 - 688, and references therein.
- 3 Madeyski C.M., Michael J.P., Hancock R.D., *Inorg. Chem.*, **1984**, 23, 1487-1489.
- 4 Wainwright K.P., *J. Chem. Soc., Dalton Trans.*, **1980**, 2117 - 2120.
- 5 Murase I., Mikuriya M., Sonoda H., Fukada Y., Kida S., *J. Chem. Soc., Dalton Trans.*, **1986**, 953 - 959.
Murase I., Ueda I., Marubayashi N., Kida S., Matsumoto N., Kudo M., Toyohara M., Hiata K., Mikuriya M., *Ibid*, **1990**, 2763 - 2769.
Murase I., Mikuriya M., Sonoda H., Kida S., *J. Chem. Soc., Chem. Commun.*, **1984**, 692 - 694.
- 6 Vučković G., Asato E., Matsumoto N., Kida S., *Inorg. Chim. Acta*, **1990**, 171, 45 - 52.
- 7 Wainwright K.P., Unpublished Observations.
- 8 Alcock N.W., Balakrishnan K.P., Moore P., *J. Chem. Soc., Dalton Trans.*, **1986**, 1743 - 1745.
Che C-M, Tang W-T., Mak T.C.W., *Ibid*, **1988**, 2879-2883.
Asato E., Toftlind H., Kida S., Mikurita M., Murray K.S., *Inorg. Chim. Acta*, **1989**, 165, 207 - 214.
Asato E., Kida S., Murase I., *Inorg. Chem.*, **1989**, 28, 800 - 802.
- 9 Reisen A., Zehnder M., Kaden T.A., *Acta Crystallogr., Sect. C: Cryst. Struct. Commun.*, **1988**, C44, 1740 - 1742.
- 10 Moi M.K., Yanuck M., Deshpande S.V., Hope H., DeNardo S.J., Meares C.F., *Inorg. Chem.*, **1987**, 26, 3458 - 3463.
- 11 Hay R.W., Pujari M.P., Moodie W.T., Craig S., Richens D.T., Perotti A., Ungaretti L., *J. Chem. Soc., Dalton Trans.*, **1987**, 2605 - 2613.
- 12 Kaden T.A., *Top. Curr. Chem.*, **1984**, 121, 157 - 179.
- 13 Buøen S., Dale J., Groth P., Krane J., *J. Chem. Soc., Chem. Commun.*, **1982**, 1172 - 1174.
- 14 Greaney T.M., Raston C.L., White A.H., Maslen E.N., *J. Chem. Soc., Dalton Trans.*, **1975**, 876 - 878.
- 15 Bencini A., Bianchi A., Castello M., Di Vaira M., Faus J., Garcia-Espana E., Micheloni M., Paoletti P., *Inorg. Chem.*, **1989**, 28, 347 - 351.

- 16 Hendrick K, Tasker P.A., Lindoy L.F., *Prog. Inorg. Chem.* **1985**, 33, 1 - 58.
- 17 Hay R.W., Pujari M., Korybut-Daszkiewicz B., Ferguson G., Ruhl B.L., *J. Chem. Soc., Dalton Trans.*, **1989**, 85 - 91.
- 18 Barefield E.K., Bianchi A., Billo E.J., Connolly P.J., Paoletti P., Summers J.S., Van Derveer D.G., *Inorg. Chem.*, **1986**, 25, 4197 - 4202.
- 19 Alcock N.W., Herron N., Moore P., *J. Chem. Soc., Dalton Trans.*, **1979**, 1486 - 1491.
- 20 Hancock R.D., Shaikjee M.S., Dobson S.M., Boeyens J.C.A., *Inorg. Chim. Acta*, **1988**, 154, 229 - 238.
- 21 Jensen C.F., Deshmukh S., Jakobsen H.J., Inners R.R., Ellis P.D., *J. Am. Chem. Soc.*, **1981**, 103, 3659 - 3666.
- 22 Summers M.F., Marzilli L.G., *Inorg. Chem.*, **1984**, 23, 521 - 523.
- 23 Summers M.F., *Coord. Chem. Rev.*, **1988**, 86, 43 - 134.
- 24 Jakobsen, H.J., Ellis P.D., Inners R.R., Jensen C.F., *J. Am. Chem. Soc.*, **1982**, 104, 7442 - 7452.
- 25 Shannon R.D., *Acta Crystallogr., Sect. A: Cryst. Phys., Diffr. Theor. Gen. Crystallogr.*, **1976**, A32, 751 - 767.
- 26 Alcock N.W., Herron N., Moore P., *J. Chem. Soc., Dalton Trans.*, **1978**, 1282 - 1288.
- 27 Alcock N.W., Curson E.H., Herron N., Moore P., *J. Chem. Soc., Dalton Trans.*, **1979**, 1987 - 1993.
- 28 Brüker Scientific Instruments, NMR Frequency Table, *Almanac* **1989**, 76 - 77.
- 29 Hancock R.D., Bhavan R., Wade P.W., Boeyens J.C.A., Dobson S.M., *Inorg. Chem.*, **1989**, 28, 187 - 194.
- 30 Kato M., Ito T., *Inorg. Chem.*, **1985**, 24, 504 - 508, *Ibid*, 509 - 514.
- 31 For a general background in carbon dioxide activation by metal ion complexes, see below, and references therein;
Szalda D.J., Fujita E., Creutz C., *Inorg. Chem.*, **1989**, 28, 1446 - 1450,
Fujita E., Szalda D.J., Creutz C., Sutin N., *J. Am. Chem. Soc.*, **1988**, 110, 4870 - 4871.
- 32 Kimura E., Shiota T., Koike T., Shiro M., Kodama M., *J. Am. Chem. Soc.*, **1990**, 112, 5805 - 5811.

-
- 33 Montgomery R, Dryer R.L., Conway T.W., Spector A.A.,
"Biochemistry", 1977, Ch.3, Second Ed., The C.V. Mosby Company.
 - 34 Williams R.J.P., *Endeavour New Series*, 1984, 8, 65 - 70.
 - 35 Chang R., "Physical Chemistry with Applications to Biological
Systems", 1983, (Chapter 17), Collier Macmillan Publishers.
 - 36 Dey B.K., University of Chittagong, Bangladesh, Masters thesis
(Adelaide),
Dey B.K., Lincoln S.F., 1991.
 - 37 Berry R.S., *J. Chem. Phys.*, 1960, 32, 933 - 938.

Chapter 5 : Experimental

5.1 : Cryptands and Cryptates

5.1.1 : Origin and Purification of Chemicals

LiClO_4 , NaClO_4 (Fluka), KClO_4 , CsClO_4 , TlClO_4 (BDH), and RbClO_4 , were vacuum dried at 353 - 363 K for 48 hours and then stored over P_2O_5 (Merck). AgClO_4 (Aldrich) was vacuum dried at ambient room temperature (298 K) for 48 hours. Linde 3Å and 4Å molecular sieves (BDH) were activated by heating in a furnace for 6 hours at 450 K.

Tetraethylammonium perchlorate (TEAP) was prepared by acidification of tetraethylammonium hydroxide (TEAOH, 40% in H_2O , Fluka) with a slight excess of perchloric acid. Upon cooling, the reaction solution formed a precipitate of TEAP. The TEAP was repeatedly recrystallised from hot H_2O , until free from acid ($\text{pH} > 6$). Alternatively, TEAP was prepared from concentrated aqueous tetraethylammonium bromide, TEABr (Aldrich), with perchloric acid and was recrystallised from water until free from acid with no trace of bromide ion (tested with aqueous AgNO_3 solution). The TEAP was then dried under vacuum in the presence of P_2O_5 at 335 K for 24 hours.

RbClO_4 was prepared by ion exchange of RbNO_3 on Amberlite IRA-400 resin (OH^- form) to give an aqueous solution of the hydroxide which was concentrated under vacuum and subsequently acidified with perchloric acid. The resulting RbClO_4 was repeatedly recrystallised from hot H_2O until acid free.

TlClO_4 was prepared¹ from an aqueous suspension of Tl_2CO_3 (Fluka) to which HClO_4 (70% in H_2O) was added until the suspension had completely dissolved. The solution was then filtered and the TlClO_4 precipitated out upon cooling. The resulting TlClO_4 was twice recrystallised from water.

4,7,13-trioxa-1,10-diazacyclopentadecane, C21 (Kryptofix 21, Merck), and 4,7,13,18-tetraoxa-1,10-diazabicyclo[8.5.5]eicosane C211, (Kryptofix 211, Merck) were distilled, dried and stored under dry nitrogen.

5.1.2 : Origin and Purification of Solvents

Acetonitrile (AR grade, Ajax), acetone (AR grade, Ajax), N,N-dimethylformamide (AR grade, BDH), N,N-diethylformamide (AR grade, BDH), N,N-dimethylacetamide (AR grade, BDH), dimethyl sulfoxide (AR grade, Ajax), pyridine (AR grade, BDH), propylene carbonate (Ultrapure grade, Arco) and methanol (AR grade, CSR) were purified and dried by methods consistent with those found in the literature.² Acetonitrile and methanol were then stored under nitrogen, over Linde 3 Å molecular sieves, whilst all other solvents were stored under nitrogen, over Linde 4 Å molecular sieves. The water content of these solvents was below the Karl-Fischer detection level of *ca.* 50 ppm. Deionised water was purified with a MilliQ-Reagent system to produce water with a specific resistance of > 15 MΩ cm.

5.1.3 : Synthesis and Purification of Cryptand

Lehn³ has discussed the cryptand C22C₅, but no details of its preparation could be found in the literature. Accordingly, C22C₅ was prepared (Figure 5.1) by a method analogous to that for C21C₅.^{4,5} A solution of 4,7,13,16-tetraoxa-1,10-diazacyclooctadecane (Kryptofix 22, Merck⁶) (2.0 g, 7.6 mmol) and triethylamine (Searle) (2.10 g, 19.1 mmol) in dry benzene (100 cm³), and a solution of glutaryldichloride (Fluka) (1.17 g, 6.9 mmol) in dry benzene (100 cm³) were added simultaneously to dry benzene (1200 cm³) over 8 hours at ambient room temperature, with vigorous stirring under an atmosphere of dry nitrogen using Perfusor motor driven syringes. The reaction solution was then filtered to remove the resultant solid triethylamine hydrochloride, and the benzene was removed under vacuum. The residue was then dissolved in CH₂Cl₂ and passed through a chromatography column⁷ with flash grade silica (Merck, 230-400 mesh, 4% v/v methanol in dichloromethane, R_f = 0.30). Subsequent removal of the methanol / CH₂Cl₂ solvent and drying under vacuum resulted in a white amorphous solid of the cryptand diamide (2.23 g, 90%). The diamide was then reduced to the product C22C₅ as follows.⁸ The diamide (2.23 g, 6.2 mmol) was dissolved in dry anhydrous tetrahydrofuran (THF) (30 cm³) at 325 K and boron trifluoride etherate (Fluka, 1.76 g, 12.4 mmol) was added drop-wise over 10 minutes under an atmosphere of nitrogen. The reaction mixture was heated to 335 K, and borane-dimethylsulphide complex (Fluka, 1.26 g, 16.5 mmol) was added drop-wise over 20 minutes. The mixture was refluxed for 3 hours, where diethylether and dimethylsulphide were distilled off as they formed. Subsequently, all the solvent THF was removed under vacuum and the pow-

dery white residue was refluxed in 10 mol dm⁻³ hydrochloric acid (Analar 10 N, 25 cm³) and H₂O (25 cm³) for 12 hours and then allowed to evaporate to dryness. The crude cryptand was obtained from the hydrochloride salt by anion exchange of an aqueous solution on Dowex 1-8x (OH⁻ form, 50-100 mesh). The basic eluent was then extracted with chloroform (4 × 50 cm³). The solvent, chloroform, was then removed from the combined extracts, leaving a clear oily residue. Distillation under vacuum in a Kugelrohr distillation apparatus (443 K, 0.005 Torr) yielded a colourless viscous oil 4,7,13,16-tetraoxa-1,10-diazabicyclo[8.8.5]tricosane (1.27 g, 3.9 mmol 62%).

¹H and ¹³C NMR spectral analysis of 4,7,13,16-tetraoxa-1,10-diazabicyclo[8.8.5]tricosane (C₂₂C₅): ¹H NMR (*d*₁-chloroform, TMS = 0.00 ppm); δ (in ppm) = 1.40 (4H, m, -CH₂- aliphatic); 1.71 (2H, m, -CH₂- aliphatic); 2.50 (4H, m, -NCH₂-); 2.61 (8H, m, -NCH₂-); 3.56 (12H, m, -OCH₂-); 3.79 (4H, m, -OCH₂-); ¹³C NMR (*d*₁-chloroform, *d*₁-chloroform = 77.00 ppm); δ = 25.76 (-CH₂- aliphatic); 29.08 (-CH₂- aliphatic); 55.46 (-NCH₂-); 56.30 (-NCH₂-); 68.96 (-OCH₂-); 70.34 (-OCH₂-).

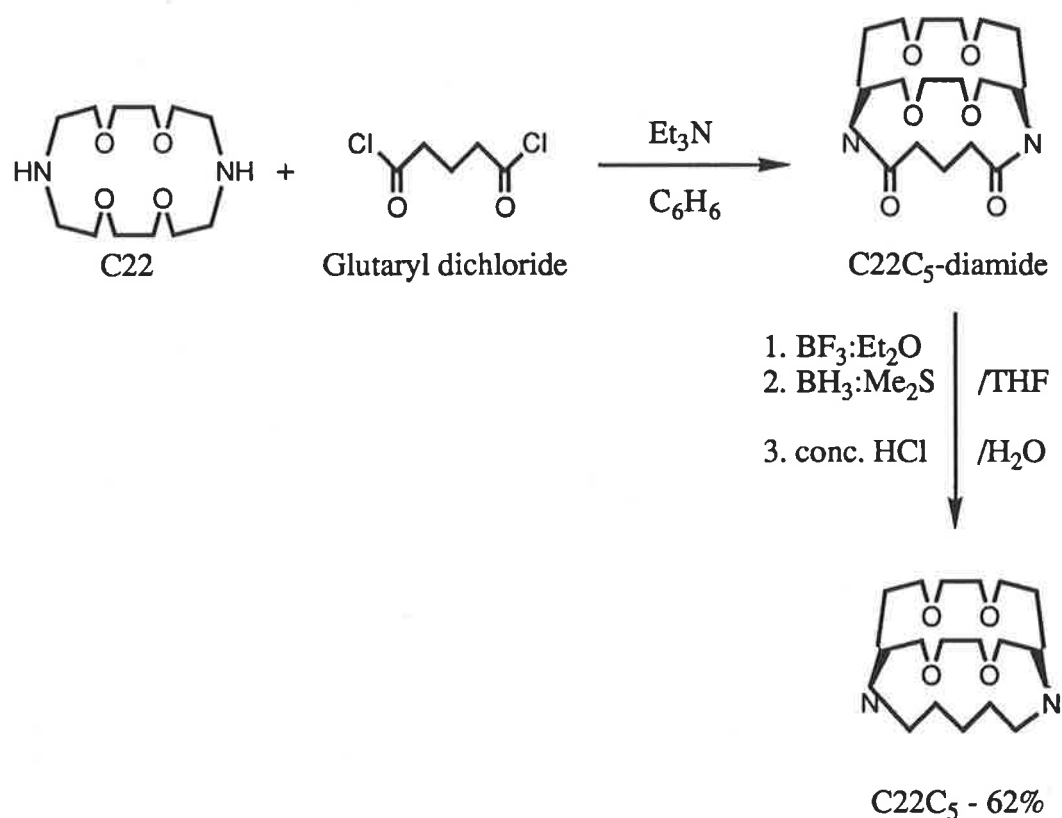


Figure 5.1 Synthesis of C₂₂C₅.

5.1.4 : Crystal Preparation

Crystals of $[\text{Na.C22C}_5]\text{ClO}_4$ were prepared by slow evaporation of an aqueous solution in which the mole ratio NaClO_4 to C22C_5 was 1:2. Crystals of $[\text{Cs.C22C}_5]\text{ClO}_4$ and $[\text{K.C22C}_5]\text{ClO}_4$ were prepared by placing saturated aqueous 1:1 mole ratio solutions of KClO_4 or CsClO_4 and C22C_5 in a refrigerator for 48 hours. Crystals of $[\text{H}_3\text{O.C22C}_5]\text{ClO}_4$ were obtained when a concentrated solution of C22C_5 in 1:1 volume ratio 0.05 mol dm^{-3} aqueous HClO_4 and acetonitrile was placed in a refrigerator for one week. Crystals of $[\text{Rb.C22C}_5]\text{ClO}_4$ suitable for X-ray diffraction studies proved to be unobtainable using similar methods to those described above.

5.1.5 : X-Ray Structure Determination

The structures of $[\text{Na.C22C}_5]\text{ClO}_4$, $[\text{K.C22C}_5]\text{ClO}_4$ and $[\text{H}_3\text{O.C22C}_5]\text{ClO}_4$ were determined by direct methods and that of $[\text{Cs.C22C}_5]\text{ClO}_4$ was solved from the interpretation of the Patterson map.¹⁰ Tables of bond angles, bond lengths and fractional atomic coordinates and ORTEP plots⁹ for all four structures are shown in Chapter 1. Space filling models showing the cationic interaction with the ligand (C22C_5) are also discussed in Chapter 1. The C(23) atom in the $\text{M}^+ = \text{H}_3\text{O}^+$ structure was found to be disordered over two positions. These were refined with fractional sites occupancies such that the sum = 1, and at the conclusion of the refinement, the site occupancy for the C(23) atom was 0.634(1). Similarly, two of the perchlorate O atoms, O(23) and O(24), were disordered and these were refined as for the C(23) atom such that the final site occupancy for the major component was 0.548(1). The location of three residual electron density peaks in the vicinity of the O(1) atom, consistent with the presence of three protons, confirmed the assignment of the cation as H_3O^+ . The positions of these protons (H atoms) were included in the final refinement, but were not refined. The crystallographic asymmetric unit for the $\text{M}^+ = \text{K}^+$ compound is comprised of two independent $[\text{K.C22C}_5](\text{ClO}_4)$ species, labelled molecule a and b, respectively. As for the $\text{M}^+ = \text{H}_3\text{O}^+$ complex, the perchlorate O atoms, O(23) and O(24) of molecule a, were found to be disordered, and these were refined as above such that the major component of the disorder had a fractional occupancy of 0.562(1). A weighting scheme of the form $w = k/[\sigma^2(F) + |g|F^2]$ was introduced and the refinements continued until convergence - final refinement details are listed in Table 5.1. The analysis of variance for each refinement showed no special feature, thus indicating that an appropriate weighting scheme had been employed. The analysis of

the $M^+ = H_3O^+$ complex was only of limited accuracy owing to the difficulty of obtaining suitable crystals - the results reported herein are the better of three data collections (including one measured at 200 K).

Table 5.1 Crystal Data for $[M.C22C_5](ClO_4)^{10}$

M^+	H_3O^+	Na^+	K^+	Cs^+
formula	$C_{17}H_{37}ClN_2O_9$	$C_{17}H_{34}ClN_2NaO_8$	$C_{17}H_{34}ClKN_2O_8$	$C_{17}H_{34}CsClN_2O_8$
fw	448.9	452.9	469.0	562.8
cryst. system	monoclinic	orthorhombic	triclinic	monoclinic
space group	$P2_1/n$, (C_{2h}^5 , No.14)	$Pbca$, (D_{2h}^{15} , No.61)	$P\bar{1}$, (C_i^1 , No.2)	$P2_1/n$, (C_{2h}^5 , No.14)
a , Å	14.166(2)	15.893(3)	13.596(2)	15.666(4)
b , Å	10.955(2)	15.782(2)	15.241(2)	9.535(2)
c , Å	15.007(1)	17.656(3)	11.765(1)	16.335(4)
α , deg	90	90	100.12(1)	90
β , deg	100.95(1)	90	98.52(1)	102.55(2)
γ , deg	90	90	100.66(1)	90
V , Å ³	2286.5	4428.5	2317.1	2381.7
Z	4	8	4	4
D_{calcd} , g cm ⁻³	1.304	1.359	1.344	1.570
$F(000)$	840	1928	996	1140
μ , mm ⁻¹	0.155	0.193	0.347	1.660
hkl range	$\pm h, +k, -l$	$+h, +k, +l$	$\pm h, \pm k, -l$	$\pm h, +k, -l$
No. of data collected	3338	4574	6491	3882
No. of unique data	2979	2894	6066	3116
R_{amal}^a	0.024	0.024	0.018	0.023
No. of unique data used with $I \geq 2.5\sigma(I)$	2006	1669	3087	2206
R	0.077	0.045	0.045	0.037
k	5.11	—	2.25	1
g	0.0005	0.0037	0.0006	0.0076
R_w	0.086	0.054	0.051	0.040
Residual e Å ⁻³	0.40	0.28	0.46	1.07

^a $R_{amal} = (\sum\{N\sum[w(F_{mean} - |F_o|^2)]\})/\sum[(N - 1)\sum(w|F_o|^2)]^{1/2}$ where the inner summation is over N equivalent reflections averaged to give F_{mean} , the outer summation is over all unique reflections and the weight, w , is taken as $[\sigma(F_o)]^{-2}$.

5.1.6 : Solution Studies, Potentiometric Titrations

All solutions were prepared under a stream of dry nitrogen, or under dry nitrogen in a glove box. Stability constants for the cryptate $[\text{Na.C22C5}]^+$ in a variety of solvents, were determined by duplicated potentiometric titrations of 20.0 cm^3 of *ca.* $10^{-3} \text{ mol dm}^{-3}$ NaClO_4 solutions with *ca.* 0.01 mol dm^{-3} C22C5 solutions. All solutions were $0.0500 \text{ mol dm}^{-3}$ in TEAP. The $[\text{Na.C22C5}]^+$ titrations were carried out under a stream of dry nitrogen in a thermostatted ($298.2 \pm 0.01 \text{ K}$) titration vessel using a Radiometer G502 Na^+ specific electrode and an Orion Research SA 720 digital voltmeter. Stability constants for $[\text{Ag.C22C5}]^+$ were determined by means of duplicated potentiometric titrations of 20.0 cm^3 of *ca.* $10^{-3} \text{ mol dm}^{-3}$ AgClO_4 solutions with *ca.* 0.01 mol dm^{-3} C22C5 solutions. Stability constants for $[\text{M.C22C5}]^+$, where $\text{M}^+ = \text{Li}^+, \text{Na}^+, \text{K}^+, \text{Rb}^+, \text{Cs}^+$ and Tl^+ , were determined using competitive methods by duplicated potentiometric titrations of 20.0 cm^3 of *ca.* $10^{-3} \text{ mol dm}^{-3}$ AgClO_4 solutions with *ca.* 0.01 mol dm^{-3} C22C5 and *ca.* 0.05 mol dm^{-3} MClO_4 solutions. The titrations were carried out using a silver wire electrode and an Orion Research SA 720 digital analyser. The reference electrode was a Ag wire in a solution of *ca.* 0.01 mol dm^{-3} AgClO_4 in the same solvent in which the titrations were carried out. For work with C21 and C211 in N,N-diethylformamide (DEF) and N,N-dimethylacetamide (DMF), the reference electrode was a Cu wire in a solution of *ca.* 0.01 mol dm^{-3} $\text{Cu}(\text{CH}_3\text{CO}_2)_2$ in the appropriate solvent.

The electrode response to metal ion concentration was calibrated by titration of a known concentration solution of either NaClO_4 (for the Na^+ ISE) or AgClO_4 solution (for the Ag^+ ISE) into a known volume of background electrolyte solution ($0.0500 \text{ mol dm}^{-3}$ TEAP) in the appropriate solvent. The electrode response to the change in concentration of the metal ion in solution may be described by the pseudo Nernstian relationship:

$$E = E_0 + C \ln[\text{M}^+] \quad 5.1$$

E_0 and C are determined by the plot of the potential (EMF in mV) of the given ion-selective electrode assembly (that is, the ion selective electrode used, and the reference electrode) versus the logarithm of the concentration of the metal ion species. The values for C and E_0 vary for different solvents, where the values for C range between 19.5 and 28.0 (with EMF in mV) and are consistent with values quoted in the literature.¹¹

The limit of detectability of the metal ion concentration by the ion selective electrode (ISE), varied from solvent to solvent, and could always be determined from the calibrations. For reliable and consistent results, the free metal ion concentrations in solution were required to be within the respective ranges of the two different ISE employed. Generally, for direct titrations using the Na^+ ISE, stability constants in the range $10^2 - 10^7$ could be measured, however, the actual minimum and maximum values depended on the solvent used. Similarly for an Ag^+ ISE, Ag^+ -complex stability constants in the range $10^2 - 10^{12}$ could be measured, and for Ag^+ / M^+ competitive titrations, differences of at least 10 between the stability constants of respective Ag^+ and M^+ complexes were required.

Under conditions where the metal ion concentration is near the lower limit of detectability in titrations, the effective buffering of the metal ion with the metal ion-complex results in solutions of much more stable and reliable EMF readings. These readings also have a much faster practical response time, when compared to the very low concentration (of metal ion) region of the calibration curve. This phenomena is analogous to the difficulty of measuring the pH of pure water (ideally $\text{pH} = 7$) when compared to measuring the pH of a buffered ($\text{pH} = 7$) solution.

5.1.7 : Solution Studies, pH-metric Titrations in Aqueous Solution

The pH-metric titrations were carried out under an inert atmosphere of water saturated nitrogen, in a water jacketed vessel maintained at 298.2 ± 0.01 K. The experimental data were obtained from 10.0 cm^3 aliquots of solutions containing $4 \times 10^{-3} \text{ mol dm}^{-3}$ HClO_4 , $0.100 \text{ mol dm}^{-3}$ TEAP, and $1.000 \times 10^{-3} \text{ mol dm}^{-3}$ cryptand C22C5, titrated with $0.1222 \text{ mol dm}^{-3}$ tetraethylammonium hydroxide (TEAOH).

A Metrohm E665 Dosimat autoburette equipped with a 5 cm^3 burette was used to deliver the titrant, and the potential was measured by an Orion Ross Sure-Flow 81-72BN combination electrode (containing $0.100 \text{ mol dm}^{-3}$ TEAP as the filling solution) connected to an Orion SA 720 pH meter. The autoburette and pH meter were interfaced to a Laser XT/3-8086 IBM compatible personal computer. The computer controlled the addition of titrant¹² so that successive additions of titrant caused an approximate decrease of 4 mV in the potential reading.

The electrode was regularly calibrated by titration of TEAOH with HClO₄ in the absence of ligand, and the resulting data was fitted to the Nernst equation:

$$E = E_0 + \frac{RT}{F} \ln[\text{H}^+] \quad 5.2$$

where E is the observed potential (Volts);
 E_0 is the standard potential for the electrode (Volts);
 R is the gas constant 8.314 (J K⁻¹ mol⁻¹);
 T is the temperature (Kelvin);
 F is Faraday's constant 9.6487×10^4 (Coulombs mol⁻¹); and
 $[\text{H}^+]$ is the hydrogen ion concentration.

Converting volts to millivolts and considering only the experimental temperature of 298.2 K, then Equation 5.2 becomes:

$$\text{pH} = \frac{E_0 - E}{59.15} \quad 5.3$$

where pH is defined as $-\log[\text{H}^+]$.

As the titrations were carried out under standard conditions and at constant ionic strength, no junction potential corrections were considered. Diffusion correction terms for 0.100 mol dm⁻³ TEAP in water were used in calculating the calibration parameters.¹³

The $\log K_1$, $\log K_2$ and stability constants were determined using the Fortran program MINQUAD.¹⁴ Stability constant data were gathered from solutions to which a 0.050 - 0.120 mol dm⁻³ metal ion perchlorate solution was added, so as to give a metal to ligand ratio in the range 0.5:1 to 20:1. At least three titrations, with different ratios, were performed for each metal ion. Deionised water was purified with a MilliQ-Reagent system to produce water with a specific resistance of $> 15 \text{ M}\Omega \text{ cm}$.

5.1.8 : Solution Studies, Multinuclear Variable Temperature Nuclear Magnetic Resonance Spectroscopy

For variable temperature ^{23}Na NMR spectroscopic studies, solutions were sealed under vacuum in 7 mm outer diameter (od) NMR tubes (513-PP, Wilmad Glass Co.) and coaxially mounted in 10 mm od NMR tubes (513-PP, Wilmad Glass Co.). These contained either D_2O (AAEC), d_6 -acetone, d_3 -acetonitrile or d_6 -dimethyl sulfoxide (Aldrich), in order to provide a lock signal. The ^{23}Na NMR spectra were run on a modified Brüker HX-90E spectrometer operating at 23.81 MHz, or alternatively, the ^{23}Na NMR spectra were run on a Brüker CXP-300 spectrometer operating at 79.39 MHz. For each solution, an average of 6000 transients were accumulated in a 2048 point data base.

For the variable temperature ^7Li NMR spectroscopic studies, all solutions were sealed under vacuum in 5 mm od NMR tubes (507-PP, Wilmad Glass Co.) and coaxially mounted in 10 mm od NMR tubes. These contained either D_2O , d_6 -acetone or d_3 -acetonitrile, in order to provide a lock signal. The ^7Li NMR spectra were run on a Brüker CXP-300 spectrometer operating at 116.64 MHz. For each solution, an average of 6000 transients were accumulated in a 2048 point data base. A Brüker B-VT-1000 variable temperature unit was used to control the sample temperature to within ± 0.3 K. For the range 200 - 300 K, the temperature was calibrated by the measurement of the variation of the chemical shift difference for the ^1H resonances of neat methanol, whilst for the range 300 - 370 K, the temperature was calibrated by using ^1H resonances of ethylene glycol.^{15,21,22}

5.2 : 1,4,8,11-Tetrakis(2-hydroxyethyl)-1,4,8,11-tetraazacyclotetradecane (THEC)

5.2.1 : Origin and Purification of Chemicals

1,4,8,11-Tetrakis(2-hydroxyethyl)-1,4,8,11-tetraazacyclotetradecane (THEC from the trivial name tetrahydroxyethylcyclam) was prepared and purified by the method reported in the literature.¹⁶ The site specific ¹³C enrichment of the hydroxyethyl arm methylene groups, -¹³CH₂-¹³CH₂-OH, of THEC was achieved using 99 atom% ¹³C₂ ethylene oxide (Cambridge Isotope Laboratories) in place of natural abundance ¹³C ethylene oxide. The [1,4,8,11-tetrakis(2-hydroxyethyl)-1,4,8,11-tetraazacyclotetradecane]M(II) perchlorate ([M(THEC)](ClO₄)₂) for M²⁺ = Zn²⁺, Ni²⁺, Pb²⁺ and Ba²⁺, were prepared by the same method as follows:¹⁷ For [Cd(THEC)](ClO₄)₂, a solution of hexaaquacadmium(II) perchlorate (0.64 g, 1.5 mmol) in 1-butanol (20 cm³) was added drop-wise to a stirred, refluxing solution of THEC (0.58 g, 1.5 mmol) in 1-butanol (20 cm³). The resulting suspension was stirred and refluxed for a further 20 minutes before cooling to room temperature. The mixture was chilled overnight at 278 K and then filtered under a positive pressure of argon. The resulting white microcrystalline precipitate was washed with diethylether (3 × 10 cm³) and then dried under vacuum to give the pure product (0.96 g, 93%). Microanalysis results calculated for C₁₈H₄₀CdCl₂N₄O₁₂: C, 31.4%; H, 5.9%; N, 8.2%. Found: C, 31.5%; H, 5.9%; N, 8.0%. IR(nujol) results: (br) 3425 cm⁻¹ (ν_{O-H}), and conductivity results : Λ_M 157 cm² Ω⁻¹ (methanol) (1:2).^{18,19}

The [Hg(THEC)](ClO₄)₂ is less stable than the other M²⁺ analogues and, as a result, was prepared by a different method. A solution of THEC (0.01 g, 0.26 mmol) in absolute ethanol (5 cm³), kept under dry argon, was cooled to 268 K. Mercury(II) perchlorate trihydrate²⁰ (0.12 g, 0.26 mmol) was added, and the resulting suspension was stirred for 30 minutes. The white microcrystalline product was collected by filtration, washed with cold (268 K) absolute ethanol (1 × 5 cm³) and then dried under vacuum (yield 0.16 g, 78%). The product [Hg(THEC)](ClO₄)₂, when stored under argon at 260 K in the absence of light, remains stable for several weeks.

5.2.2 : Nuclear Magnetic Resonance Spectroscopy

The ^{13}C (75.47 MHz) and ^{113}Cd (66.55 MHz) spectra were accumulated on a Brüker CXP-300 spectrometer, with a deuterium lock, using a Brüker 10 mm od VSP (300 MHz) probe. Solutions were prepared using d_4 -methanol (Aldrich) which was stored under nitrogen and over Linde 3Å molecular sieves. $\text{Zn}(\text{ClO}_4)_2(\text{H}_2\text{O})_6$ was dried over P_2O_5 at 350-360 K for 24 hours to produce anhydrous $\text{Zn}(\text{ClO}_4)_2$. The ^{13}C solution spectra were accumulated with broad-band proton decoupling. An average of 6000 transients, in a 8192 point data base, were collected at temperature intervals of *ca.* 5 K over the region of coalescence.

The Brüker B-VT-1000 variable temperature unit was used to control the sample temperature to within ± 0.3 K.

The ^{13}C chemical shift variation of a d_6 -acetone/ CCl_4 (50/50 v/v) mixture was measured in order to calibrate the temperature controller under conditions of ^1H broadband decoupling.²⁹ In order to simulate the possible effects of heating on the 0.02 - 0.05 mol dm^{-3} $[\text{M}(\text{THEC})](\text{ClO}_4)_2$ solutions, 0.05 mol dm^{-3} $\text{Zn}(\text{ClO}_4)_2$ was added. The resulting temperature calibrations, over the temperature range of 210 - 300 K, were 1.8 (± 0.3) K higher than both the coupled ^{13}C calibrations and the ^1H calibration of methanol in pure (10% d_4 -methanol) methanol over the same temperature range.^{21,22}

The Fourier transformed spectra were subjected to complete lineshape analysis on a VAX 11-780 computer. The FORTRAN-77 program LINSHP (Appendix iii) incorporates both a linear two-site algorithm for two-site lineshape analysis²³ and a density matrix algorithm for the lineshape analysis of strongly coupled sites²⁴⁻²⁶ (discussed in detail in Chapter 6). The temperature dependence of chemical shifts and line widths, in the absence of chemical exchange as required for lineshape analysis, were extrapolated from low temperature spectra where the rate of chemical exchange was slow on the NMR timescale, and also from the variable temperature spectra of THEC where there was no observable chemical exchange. The ^{13}C chemical shifts were referenced to internal d_4 -methanol, assigned the chemical shift of 47.05 ppm.²⁷

The CPMAS ^{13}C spectra of solid state $[\text{M}(\text{THEC})](\text{ClO}_4)_2$ where $\text{M}^{2+} = \text{Cd}^{2+}$, Pb^{2+} and Hg^{2+} , were obtained using standard procedures. Chemical shifts were referenced to the low-field resonance of external adamantane, which was assigned a chemical shift of 38.23 ppm.

The ^{113}Cd spectra were run without decoupling, and chemical shifts referenced to external $0.10 \text{ mol dm}^{-3} \text{ Cd}(\text{ClO}_4)_2$ in D_2O , which was assigned a chemical shift of 0.00 ppm.²⁸ It was found that the ^{113}Cd spectra were incompletely relaxed for recycle delays of less than 5 seconds. Consequently, the transients were accumulated with a delay of 10 seconds.

- 1 Cox B.G., Stroka J., Schneider I., Schneider H., *J. Chem. Soc., Faraday Trans. 1.*, **1989**, 85, 187 - 198.
- 2 Perrin D.D., Armarego W.L.F., "Purification of Laboratory Chemicals", Third Ed., Pergamon, (Oxford) **1980**.
- 3 Lehn, J.-M., *Pure Appl. Chem.*, **1979**, 51, 979 - 997.
- 4 Lincoln S.F., Horn E., Snow M.R., Hambley T.W., Brereton I.M., Spotswood T.M., *J. Chem. Soc., Dalton Trans.*, **1986**, 1075 - 1080.
- 5 Dietrich B., Lehn J.-M., Sauvage J.P., Blanzat J., *Tetrahedron*, **1973**, 29, 1629 - 1645.
- 6 Reagents MERCK, "Kryptofix: Polyoxadiazamacrocycles" Catalogue No. 22/II 16/1540/3/873 L, **1980**, 1 - 11.
- 7 Still W.C., Kahn M., Mitra A., *J. Org. Chem.*, **1978**, 43, 2973 - 2975.
- 8 Brown H.C., Narasimhan S., Choi Y.M., *Synthesis*, **1981**, 996 - 1003.
- 9 Johnson C.K., "ORTEP, Thermal Ellipsoid Plotting Program", Report ORNL-3794 Oak Ridge National Laboratory, Oak Ridge, Tennessee, **1971**.
Sheldrick G.M., "SHELX 86, Program for the Automatic Solution of Crystal Structure", University of Göttingen, Germany, **1986**.
- 10 Clarke P., Lincoln S.F., Tiekink E.R.T., *Inorg. Chem.*, **1991**, 30, 2747 - 2751. All crystal structure determinations were performed for each crystal structure by the following: for [Na.C22C₅](ClO₄) and [Cs.C22C₅](ClO₄) Tiekink E.R.T; for [K.C22C₅](ClO₄) and [H₃O.C22C₅](ClO₄) Tiekink E.R.T., Gulbis J.M.
- 11 Lehn J.-M., Sauvage J.-P., *J. Am. Chem. Soc.*, **1975**, 97, 6700 - 6707.
- 12 Duckworth P.A., University of Adelaide, private communication.
- 13 Kulstad S., Malmsten L.Å., *J. Inorg. Nucl. Lett.*, **1980**, 42, 573 - 578.
- 14 Sabatini A., Vacca A., Gans P., *Talanta*, **1974**, 21, 53 - 77.
- 15 Raiford D.S., Fisk C.L., Becker E.D., *Anal. Chem.*, **1979**, 51, 2050.
- 16 Madeyski C.M., Michael J.P., Hancock R.D., *Inorg. Chem.*, **1984**, 23, 1487 - 1489.
- 17 Clarke P., Hounslow A.M., Keough R.A., Lincoln S.F., Wainwright K.P., *Inorg. Chem.*, **1990**, 29, 1793 - 1797.
- 18 Geary W.J., *Coord. Chem. Rev.*, **1971**, 7, 81 - 122.

-
- 19 Elemental analyses were performed by the Australian Microanalytical Service. Infrared spectra were recorded on a Perkin-Elmer 297, conductivity of solutions at 293.2 K using a Phillips PW9504 conductivity bridge.
 - 20 As provided by Dr. K.P. Wainwright, Flinders University of South Australia, Adelaide, Australia.
 - 21 van Geet A.L., *Anal. Chem.*, **1970**, 42, 679 - 680.
 - 22 van Geet A.L., *Anal. Chem.*, **1968**, 40, 2227.
 - 23 Lincoln S.F., *Prog. React. Kinetics.*, **1977**, 9, 1 - 91.
 - 24 Johnson C.S., *J. Mag. Reson.*, **1969**, 1, 98 - 104.
 - 25 Creswell C.J., Harris R.K., *J. Mag. Reson.*, **1971**, 4, 99 - 108.
 - 26 Ba V., Song R.-f., Qiu Z.-w., *Mag. Reson. in Chem.*, **1989**, 27, 916 - 921.
 - 27 Breitmaier E., Haas G., Voelter W., "Atlas of Carbon-13 NMR Data", **1979**, Volume 1, Heyden (London)
 - 28 Maciel G.E., Borzo M., *J. Chem. Soc., Chem. Commun.*, **1973**, 394.
 - 29 Led J.J., Petersen S.B., *J. Mag. Reson.*, **1978**, 32, 1 - 17.

Chapter 6 : Analysis of the NMR Spectra for Chemical Systems Undergoing Site Exchange

6.1 : Two-Site Lineshape Analysis

Nuclear magnetic resonance spectroscopy is a very useful method for observing rapid chemical exchange processes in solution. In Chapter 3 of this study, the complete lineshape analysis of the spectral coalescence characterizing the chemical exchange of two sites, studied by ^7Li and ^{23}Na NMR spectroscopy, was described. In Chapter 4, a similar analysis was undertaken for systems studied by ^{13}C NMR spectroscopy. In order to explain how the lineshape analysis for these systems was undertaken, it is appropriate to describe the spectroscopic foundations and mathematical descriptions used in this study.

NMR spectroscopy may be employed to delineate the kinetic processes of reactions in dynamic equilibrium, that is, where no net chemical change occurs and ΔG is zero. The area of study of the resultant spectral changes is described as Dynamic NMR spectroscopy (DNMR), and there are many articles in the literature on the subject.¹⁻¹² These articles form the basis of the subsequent mathematical descriptions in the first section of this chapter.

Of particular concern in this study are the influences on the spectral lineshapes that are due to intermolecular, or intramolecular chemical site exchange processes that occur in solution. These processes are similar in that they involve time averaging, or partial time averaging of the nuclear environment.

A magnetic field, B_0 , is applied to a sample, providing a directional magnetic reference for the nuclear environment along the z-axis. Individual nuclear magnetic moments precess about the z-axis with a frequency ω_0 , the Larmor frequency. The lowest energy state occurs when the nuclear spins are aligned in the direction of the magnetic field. The population of nuclear spins occupying this state is favoured by a Boltzmann distribution, which leads to a net macroscopic magnetization, \vec{M} , and the z-component, M_z . The M_x and M_y contribution to \vec{M} is zero.

The application of an additional radio frequency field B_1 with a magnetic vector rotating in the xy -plane, of frequency ω , provides a magnetic field component along the x and y axes to give a total magnetic field:

$$\vec{B} = (B_1 \cos \omega t, -B_1 \sin \omega t, B_0) \quad 6.1$$

and \vec{M} is rotated away from the z -axis and into the xy -plane. The time required for M_z to regain its initial (equilibrium) value M_0 is defined by T_1 , the spin lattice or longitudinal relaxation time. The magnetization in the xy -plane takes a period characterised by T_2 (which is the spin-spin or transverse relaxation time) to fall to an equilibrium magnitude of zero after the initial perturbation by the field B_1 .

The time dependence of \vec{M} in the stationary frame was first described by Bloch¹³:

$$\frac{dM_x}{dt} = \gamma(M_y B_0 + M_z B_1 \sin \omega t) - \frac{M_x}{T_2} \quad 6.2$$

$$\frac{dM_y}{dt} = \gamma(-M_x B_0 + M_z B_1 \cos \omega t) - \frac{M_y}{T_2} \quad 6.3$$

$$\frac{dM_z}{dt} = -\gamma(M_x B_1 \sin \omega t + M_y B_1 \cos \omega t) - \frac{(M_z - M_0)}{T_1} \quad 6.4$$

where γ is the nuclear gyromagnetic ratio.

In the rotating frame of reference (about the z -axis), the frequency ω is assigned to the direction of B_1 along the x' -axis (the rotating frame x -axis) enabling the Equations 6.2 - 6.4 to be reformulated¹² into a more convenient form, Equations 6.5 and 6.6:

$$\frac{dM_{xy}}{dt} = -\alpha M_{xy} - i \gamma B_1 M_0 \quad 6.5$$

$$\frac{dM_z}{dt} = \gamma \nu B_1 + \frac{(M_0 - M_z)}{T_1} \quad 6.6$$

where :

M_{xy} is the transverse magnetization;

ν is the component of \vec{M} which is on the y' -axis
(90° out of phase with B_1); and

$$\alpha = \frac{1}{T_2} - i(\omega_0 - \omega).$$

The variation of M_z is dependent on ν , which corresponds to the observed absorption mode of the NMR signal at the frequency ω of field B_1 .

The absorption mode lineshape ν (derived from the total lineshape, for all frequencies ω) obtained from a pulsed Fourier transform experiment is, in general, equivalent to the lineshape obtained for the continuous wave, adiabatic slow passage experiment (see Appendix iv).¹⁴⁻¹⁸ As the continuous wave, adiabatic slow passage method is more easily visualized, the results under these conditions will be considered in detail.

Under continuous wave slow passage conditions, ω is swept slowly through ω_0 such that there is no change in \vec{M} with time, i.e. $\frac{dM_{xy}}{dt}$ and $\frac{dM_z}{dt} = 0$. If B_1 is smaller than B_0 , such that $M_z \approx M_0$, and M_{xy} is small, the absorption mode lineshape may be described as:

$$\nu = -M_z \text{ eq } \frac{\gamma B_1 T_2}{1 + T_2^2 (\omega_0 - \omega)^2 + \gamma^2 B_1^2 T_1 T_2} \quad 6.7$$

When B_1 is so small that the term $\gamma^2 B_1^2 T_1 T_2$ becomes negligible compared with the other denominator terms, the ν mode lineshape approximates a Lorentzian function:

$$\nu = -M_z \text{ eq } \frac{\gamma B_1 T_2}{1 + T_2^2 (\omega_0 - \omega)^2} \quad 6.8$$

Where the full width at half-maximum peak height, $W_{1/2}$, may be described in terms of T_2 (in frequency units, Hz):

$$W_{1/2} = \frac{1}{\pi T_2} \quad 6.9$$

The effects of site exchange can be incorporated into the Bloch equations by considering the effects of this exchange on the derivation of the absorption mode lineshape^{19,20} in Equation 6.7.

It is assumed that the time required for a nuclear spin to transfer from site **a** to site **b** is so small that no nuclear spin precession occurs in that time, and that the nucleus from site **a** arrives at site **b** with its phase memory intact, and vice versa. This transfer causes a dephasing of the nuclear spins at site **b** and results in an increase in M_{xyb} , the transverse magnetization at site **b** and a decrease in M_{xya} at the same rate. Similarly, the transfer of a nuclear spin from site **b** to site **a** causes dephasing at site **a**, increases M_{xya} , and decreases M_{xyb} at the same rate:

$$\frac{dM_{xya}}{dt} = \frac{M_{xyb}}{\tau_b} - \frac{M_{xya}}{\tau_a} \quad 6.10$$

$$\frac{dM_{xyb}}{dt} = \frac{M_{xya}}{\tau_a} - \frac{M_{xyb}}{\tau_b} \quad 6.11$$

where :

τ_a and τ_b are the mean site lifetimes of sites **a** and **b** respectively, and the rate of exchange of the two sites are related by their populations $\chi_a/\tau_a = \chi_b/\tau_b$.

Incorporation of this effect into Equation 6.5 for site **a** and site **b** results in:

$$\frac{dM_{xya}}{dt} = -\alpha_a M_{xya} - i \gamma B_1 M_{0a} + \frac{M_{xyb}}{\tau_b} - \frac{M_{xya}}{\tau_a} \quad 6.12$$

$$\frac{dM_{xyb}}{dt} = -\alpha_b M_{xyb} - i \gamma B_1 M_{0b} + \frac{M_{xya}}{\tau_a} - \frac{M_{xyb}}{\tau_b} \quad 6.13$$

where :

$$\alpha_a = \frac{1}{T_{2a}} - i(\omega_{0a} - \omega); \text{ and}$$

$$\alpha_b = \frac{1}{T_{2b}} - i(\omega_{0b} - \omega).$$

Under continuous wave, adiabatic slow passage conditions, the M_z components are essentially unchanged from M_0 . That is:

$$M_{za} = M_{0a} = \chi_a M_0 \quad \text{and} \quad M_{zb} = M_{0b} = \chi_b M_0 \quad 6.14$$

$$\frac{dM_{xya}}{dt} = \frac{dM_{xyb}}{dt} = 0 \quad 6.15$$

The effects of chemical exchange are incorporated into the total transverse component of the magnetization (i.e. $M_{xy} = M_{xya} + M_{xyb}$) and the total lineshape may be described in terms of τ_a and τ_b :^{1,12,21}

$$M_{xy} = \frac{-i \gamma B_1 M_z \text{ eq} [\tau_a + \tau_b + \tau_a \tau_b (\alpha_a \chi_b + \alpha_b \chi_a)]}{(1 + \alpha_a \tau_a) (1 + \alpha_b \tau_b) - 1} \quad 6.16$$

The absorption intensity at frequency ω (rad s⁻¹) is proportional to the imaginary portion of the complex magnetization M_{xy} :^{4,12}

$$\nu = \frac{-\gamma B_1 M_z \text{ eq} \left\{ Y \left[1 + \tau \left(\frac{\chi_b}{T_{2a}} + \frac{\chi_a}{T_{2b}} \right) \right] + QR \right\}}{Y^2 + R^2} \quad 6.17$$

where :

$$\tau = \chi_b \tau_a = \chi_a \tau_b;$$

$$\Delta\omega = \omega_{0a} - \omega_{0b};$$

$$\delta\omega = \frac{1}{2} (|\omega_{0a} - \omega_{0b}|) - \omega;$$

$$Y = \tau \left(\frac{1}{T_{2a} T_{2b}} - \delta\omega^2 + \frac{\Delta\omega^2}{4} \right) + \frac{\chi_a}{T_{2a}} + \frac{\chi_b}{T_{2b}};$$

$$Q = \tau \left(\delta\omega - \frac{\Delta\omega}{2} (\chi_a - \chi_b) \right); \text{ and}$$

$$R = \delta\omega \left[1 + \tau \left(\frac{1}{T_{2a}} + \frac{1}{T_{2b}} \right) \right] + \frac{\Delta\omega}{2} \tau \left(\frac{1}{T_{2b}} - \frac{1}{T_{2a}} \right) + \frac{\Delta\omega}{2} (\chi_a - \chi_b).$$

Using Equation 6.17 above, the complete lineshape for exchanging chemical systems may be solved by calculating the absorption mode intensity, ν , for a discrete set of frequencies. A discussion on the application of these calculations is contained in section 6.3.

6.1.1 : Simplified Kinetic Analysis for Systems in Slow Exchange

A simplified kinetic analysis may be applied in the slow exchange regime for systems where the rate of chemical exchange is too slow to be studied by complete lineshape analysis. In the slow exchange regime, if the lifetimes of sites **a** and **b**, τ_a and τ_b , are sufficiently large (that is, the rates of exchange are sufficiently small), in comparison to the inverse of the separation of the frequency differences of these sites, $(\omega_a - \omega_b)^{-1}$, the spectrum will consist of two distinct resonances in the vicinity of the frequencies ω_a and ω_b . For example, for the continuous wave, adiabatic slow passage experiment,²² if the radio frequency ω is close to ω_a , and thus far away from ω_b , M_{xyb} is effectively zero:

$$M_{xy} \approx M_{xya} \approx -i \gamma B_1 M_z \text{ eq } \frac{\chi_a \tau_a}{1 + \alpha_a \tau_a} \quad 6.18$$

The imaginary part then is:

$$v = -\gamma B_1 M_z \text{ eq } \frac{\chi_a T'_{2a}}{1 + (T'_{2a})^2 (\omega_a - \omega)^2} \quad 6.19$$

where T'_{2a} is the apparent, or observed transverse relaxation time of site **a**.

Equation 6.19 describes a broadened signal centred at ω_a with an observed width, $W'_{1/2a}$ at half maximum amplitude. There will be a corresponding signal centred on ω_b , characterised by an equation similar to Equation 6.19.

The additional dephasing effect of the exchange process on the transverse magnetization leads to relaxation times shorter than T_{2a} and T_{2b} , and consequently, to additional broadening of the individual resonances. If T_{2a} is known, then $W_{1/2a}$ in the absence of exchange is also known (Equation 6.9). The difference between $W_{1/2a}$ in the absence of exchange and $W'_{1/2a}$, the width at half of the broadened resonance found experimentally may be used to estimate the site lifetime, τ_a .

$$\pi W'_{1/2a} - \pi W_{1/2a} = \frac{1}{T'_{2a}} - \frac{1}{T_{2a}} = \frac{1}{\tau_a} \quad 6.20$$

For resonances at the slow exchange limit, one method to obtain a minimum lifetime (hence maximum rate of exchange) is to calculate the lifetime of the exchanging species that would cause a broadening of each resonance by 50%. This means that $W_{1/2a}$, the width at half maximum amplitude (in frequency units, Hz) of the resonance at site **a**, becomes:

$$W_{1/2a}^* = \frac{3}{2} W_{1/2a} - W_{1/2a} = \frac{1}{2} W_{1/2a} = \frac{1}{\pi\tau_a} \quad 6.21$$

Where $W_{1/2a}^*$ may be considered the width at half maximum amplitude for site **a** in excess of the natural $W_{1/2a}$ (in this case by the assumed 50% of the natural width at half maximum amplitude, $W_{1/2a}$) so that the minimum lifetime, τ_a , may be estimated:

$$\tau_a = \frac{2}{\pi W_{1/2a}} \quad 6.22$$

and the lifetime for site **b**, τ_b , may be related to τ_a by the fractional populations of both sites, χ_a and χ_b :

$$\tau_b = \frac{\tau_a \chi_b}{\chi_a} \quad 6.23$$

6.1.2 : Simplified Kinetic Analysis for Systems at Intermediate Rates of Exchange

The region of intermediate rates of exchange is defined as that region where the rate of exchange is faster than in the slow exchange limit, and slower than the fast exchange limit, where there is a composite, intermediate effect on the NMR spectral lineshape. In the slow exchange region (faster than the slow exchange limit), the two separate resonances of sites **a** and **b** have achieved a sufficient rate of chemical exchange such that they become broadened from their natural linewidths, and that their inherent chemical shifts begin to approach each other as the rate of exchange increases. As the rates of exchange further increase, the two separate resonances coalesce to form one broadened resonance which narrows upon further increases of the rate of exchange. This single resonance continues to narrow as the rate of exchange increases, until the fast exchange limit is attained and a single Lorentzian resonance is formed. The single Lorentzian resonance has a chemical shift and width which is the average of these properties of the two separate sites.

The change from a spectrum of the two separate resonances to the single broadened resonance (coalescence) occurs when the lifetimes τ_a and τ_b are in the order of $(\omega_a - \omega_b)^{-1}$. If the simplifying constraints $\chi_a = \chi_b = \frac{1}{2}$, and $\tau_a = \tau_b$ are applied, and if the width of the resonances in the absence of exchange is small compared with their separation, then :

$$\frac{1}{T_{2a}} = \frac{1}{T_{2b}} = 0 \quad \text{and} \quad M_{za} = M_{zb} = \frac{1}{2}M_z \quad 6.24$$

and the result for the absorption mode is:

$$\nu = \frac{1}{2}\gamma B_1 M_z \frac{\tau_a(\omega_a - \omega_b)^2}{(\omega_a + \omega_b - 2\omega)^2 + \tau_a^2(\omega_a - \omega)^2 (\omega_b - \omega)^2} \quad 6.25$$

Expressing this formula in terms of frequencies ν (in Hz, $= \omega / 2\pi$), then:

$$f(\nu) = C \frac{2\tau_a(\nu_a - \nu_b)^2}{[\nu - \frac{1}{2}(\nu_a + \nu_b)]^2 + \pi^2\tau_a^2(\nu_a - \nu)^2 (\nu_b - \nu)^2} \quad 6.26$$

where C is a normalizing constant.

Harris²¹ rearranged an equation equivalent to Equation 6.26 and recast it into a form involving a dimensionless abscissa; $x = \Delta\nu / \nabla$, and a parameter, $\psi = \pi\tau_a\nabla$, where $\Delta\nu = \nu - \frac{1}{2}(\nu_a + \nu_b)$ and $\nabla = \frac{1}{2}(\nu_a - \nu_b)$, to give :

$$f(x) = \frac{2\tau_a}{[x^2 + \psi^2(x^2-1)^2]} \quad 6.27$$

The shape of the NMR spectra described by this function depends solely upon the product ψ . Under slow exchange conditions ($\psi \gg 1$) this gives rise to two Lorentzian lines, centred at approximately ν_a and ν_b . At intermediate rates of exchange, as τ_a (and τ_b) decreases from infinity, the two individual resonances broaden, and their maxima draw closer together. This occurs until $\psi = (\sqrt{2})^{-1}$, where the resonances coalesce into a single broad signal, with a maximum at the mean position of the two resonances, $\frac{1}{2}(\nu_a + \nu_b)$. The single broad resonance narrows further under faster exchange conditions ($\psi \ll 1$) until the fast exchange limit is reached. At this point, the function gives rise to a single Lorentzian line of double intensity at the mean position, $\frac{1}{2}(\nu_a + \nu_b)$.

In systems undergoing chemical exchange, a reasonable approximation of the site lifetimes of the exchanging species, τ , may be estimated where the resonances in the spectra are seen to coalesce into a single broad resonance. That is, when $\psi = (\sqrt{2})^{-1}$

$$\tau = \tau_a = \tau_b = \frac{\sqrt{2}}{\pi (\nu_a - \nu_b)} \quad 6.28$$

If the chemical shifts of the two sites in the absence of chemical exchange, ν_a and ν_b , may be reliably estimated, an approximate lifetime for the exchanging species, τ , may be calculated by means of Equation 6.28 above.

6.1.3 : Simplified Kinetic Analysis for Systems in Fast Exchange

In an approach analogous to that for calculating the minimum lifetime in the slow exchange, the maximum lifetime (and hence minimum rate of exchange) may be calculated for exchanging systems in the fast exchange of the NMR timescale.

As the rates of chemical exchange approach the fast-exchange regime, τ_a and τ_b become small. Under these conditions, derivation of Equation 6.17 yields a single Lorentzian resonance centred at the population weighted average of the individual resonances ω_a and ω_b , (i.e. $\omega_{\text{MEAN}} = \chi_a \omega_a + \chi_b \omega_b$) with a width at half maximum amplitude (in frequency units, Hz) of:

$$W_{1/2} = \frac{1}{\pi T_{2\text{obs}}} = \frac{\chi_a}{\pi T_{2a}} + \frac{\chi_b}{\pi T_{2b}} \quad 6.29$$

The absorption lineshape may be described by substituting ω_{MEAN} into Equation 6.19:

$$\nu = -\gamma B_1 M_z \text{ eq } \frac{T_2'}{1 + (T_2')^2 (\chi_a \omega_a + \chi_b \omega_b - \omega)^2} \quad 6.30$$

If the exchange is not at the fast exchange limit, the single averaged resonance at ω_{MEAN} will appear to have a width at half maximum amplitude larger than that arrived at by Equation 6.30. If ω_{MEAN} is substituted for ω in Equation 6.16, then the effective transverse relaxation time T_2' becomes:²²

$$\frac{1}{T_2'} = \frac{\chi_a}{T_{2a}} + \frac{\chi_b}{T_{2b}} + \chi_a^2 \chi_b^2 (\omega_a - \omega_b)^2 (\tau_a + \tau_b) \quad 6.31$$

If a population weighted average ω_{MEAN} , is considered, then by analogy to the slow exchange regime approximation, the composite (population weighted average) functions τ_{MEAN} and $T_{2\text{MEAN}}$ are related as follows:

$$\frac{1}{T_2} = \frac{1}{T_{2\text{MEAN}}} + \frac{1}{\tau_{\text{MEAN}}} \quad 6.32$$

where $T_{2\text{MEAN}}$ is the composite T_2 value at the fast exchange limit (analogous to T_{2a} in the absence of exchange for the slow exchange approximation, in Equation 6.20).

If the relative chemical shift difference, $(\nu_a - \nu_b)$, $W_{1/2a}$, and $W_{1/2b}$ (in the absence of exchange) can be reliably estimated and given, χ_a and χ_b then, τ_{MEAN} may be derived (in frequency units, Hz):

$$\tau_{\text{MEAN}} = \frac{\Delta W_{1/2}}{4 \pi \chi_a^2 \chi_b^2 (\nu_a - \nu_b)^2} \quad 6.33$$

where $\Delta W_{1/2}$ is the observed linewidth in excess of the population weighted average $W_{1/2\text{MEAN}}$ for the sites **a** and **b** in the absence of exchange.

6.2 : Lineshape Analysis for Two-Site Exchange Between Coupled Sites

The approach to the complete lineshape analysis for chemically exchanging sites in the previous section is inadequate to describe the spin magnetization transfer between coupled spin systems that are also undergoing chemical exchange. Generalized treatments to describe spin magnetization transfer between exchanging, coupled spin systems have been derived from the quantum mechanical description of nuclear spin states (and transitions) in terms of the spin Hamiltonian.²²⁻²⁵ A number of further treatments expanded and applied to special cases such as intramolecular²⁶ and intermolecular²⁷ chemical exchange can be found in the literature.^{12,26-32}

The lineshape analysis treatment used in this study is based upon that derived by Johnson³²⁻³⁶ using the Kubo-Sack probability matrices. This treatment accounts for the spin magnetization transfer that occurs for strongly coupled, chemically exchanging sites, as occurs for the intramolecular exchange of the ¹³C - ¹³C coupled spectra of the divalent metal ion complexes of ¹³C enriched hydroxyethyl arm carbons of 1,4,8,11-tetrakis(2-hydroxyethyl)-1,4,8,11-tetraazacyclotetradecane (THEC*) discussed in Chapter 4 of this study.

To calculate the lineshapes of intramolecular AB(I) \rightleftharpoons AB(II) exchanging systems, it is first necessary to describe the complex magnetizations, M_{xy} , for the four uncoupled sites, A(I), B(I), A(II) and B(II). The complex magnetizations are incorporated into the exchange-modified Bloch equations, analogous to Equations 6.12 and 6.13 discussed previously.

$$\frac{dM_{xyAI}}{dt} = -\alpha_{AI} M_{xyAI} + \frac{M_{xyAII}}{\tau_{AII}} - \frac{M_{xyAI}}{\tau_{AI}} - i\gamma B_1 M_{0AI} \chi_{AI} \quad 6.36$$

$$\frac{dM_{xyBI}}{dt} = -\alpha_{BI} M_{xyBI} + \frac{M_{xyBII}}{\tau_{BII}} - \frac{M_{xyBI}}{\tau_{BI}} - i\gamma B_1 M_{0BI} \chi_{BI} \quad 6.37$$

$$\frac{dM_{xyAII}}{dt} = -\alpha_{AII} M_{xyAII} + \frac{M_{xyAI}}{\tau_{AI}} - \frac{M_{xyAII}}{\tau_{AII}} - i\gamma B_1 M_{0AII} \chi_{AII} \quad 6.38$$

$$\frac{dM_{xyBII}}{dt} = -\alpha_{BII} M_{xyBII} + \frac{M_{xyBI}}{\tau_{BI}} - \frac{M_{xyBII}}{\tau_{BII}} - i\gamma B_1 M_{0BII} \chi_{BII} \quad 6.39$$

where:

$$\alpha_{AI} = \frac{1}{T_{2AI}} - i(\omega_{0AI} - \omega);$$

$$\alpha_{BI} = \frac{1}{T_{2BI}} - i(\omega_{0BI} - \omega);$$

$$\alpha_{AII} = \frac{1}{T_{2AII}} - i(\omega_{0AII} - \omega);$$

$$\alpha_{BII} = \frac{1}{T_{2BII}} - i(\omega_{0BII} - \omega);$$

χ_{AI} , χ_{BI} , χ_{AII} and χ_{BII} are the fractional populations at each site; and $i = \sqrt{-1}$.

The absorption spectrum is then given by:

$$f(\nu) = \text{Im} (M_{xyAI} + M_{xyBI} + M_{xyAII} + M_{xyBII}) \quad 6.40$$

where $\text{Im}()$ is the imaginary component of a complex number (i.e. $\text{Re} + i\text{Im}$).

Equations 6.36 - 6.39 may now be solved under the steady state conditions, as in Equation 6.16 (that is, $d M_{xyAI} / dt = d M_{xyAII} / dt = 0$ and similarly for exchanging sites B(I) and B(II)). The population contribution of each site is individually accounted for, and then expressed in matrix form, as described by Johnson^{34,35}:

$$-i \gamma B_1 M_z \text{eq} \begin{bmatrix} \chi_{AI} \\ \chi_{BI} \\ \chi_{AII} \\ \chi_{BII} \end{bmatrix} = \quad 6.41$$

$$\begin{bmatrix} (\alpha_{AI} - 1/\tau_{AI}) & 0 & 1/\tau_{AII} & 0 \\ 0 & (\alpha_{BI} - 1/\tau_{BI}) & 0 & 1/\tau_{BII} \\ 1/\tau_{AI} & 0 & (\alpha_{AII} - 1/\tau_{AII}) & 0 \\ 0 & 1/\tau_{BI} & 0 & (\alpha_{BII} - 1/\tau_{BII}) \end{bmatrix} \begin{bmatrix} M_{xyAI} \\ M_{xyBI} \\ M_{xyAII} \\ M_{xyBII} \end{bmatrix}$$

The transpose of both sides yields Equation 6.42:

$$-i \gamma B_1 M_z \text{ eq } [\chi_{AI}, \chi_{BI}, \chi_{AII}, \chi_{BII}] = [M_{xyAI}, M_{xyBI}, M_{xyAII}, M_{xyBII}] \quad 6.42$$

$$\times \begin{bmatrix} (\alpha_{AI} - 1/\tau_{AI}) & 0 & 1/\tau_{AI} & 0 \\ 0 & (\alpha_{BI} - 1/\tau_{BI}) & 0 & 1/\tau_{BI} \\ 1/\tau_{AII} & 0 & (\alpha_{AII} - 1/\tau_{AII}) & 0 \\ 0 & 1/\tau_{BII} & 0 & (\alpha_{BII} - 1/\tau_{BII}) \end{bmatrix}$$

or in matrix notation:

$$-i \gamma B_1 M_z \text{ eq } P = M.A \quad 6.43.$$

and since (in matrix notation) $f(\nu) = \text{Im}(M.1)$, multiplying Equation 6.43 from the right by A^{-1} and then by 1 results in:

$$f(\nu) = -i \gamma B_1 M_z \text{ eq } \text{Im}(P.A^{-1}.1) \quad 6.44$$

$$= C \text{Re}(P.A^{-1}.1) \quad 6.44a$$

where:

$\text{Im}()$ is the imaginary component;

$\text{Re}()$ is the real component of a complex number (i.e. $\text{Re} + i\text{Im}$);

$f(\nu)$ is the function describing the absorption spectrum lineshape, and is equivalent to ν in Equations 6.7, 6.8 and 6.17;

C is a normalizing constant;

P is a row vector the elements of which are the N fractional populations of the nuclear sites ($\chi_{AI}, \chi_{BI}, \chi_{AII}, \chi_{BII}$);

1 is a column unity vector (where each element = 1); and

A is a 4×4 complex matrix.

The above derivation at this point is entirely consistent with the derivation for the simple two-site exchange phenomena described in the previous section, in Equations 6.16 and 6.17, when extended to describe two sets of simultaneously exchanging pairs of sites. Equation 6.42 describes the simultaneous two site exchange between two pairs of sites, A(I) exchanging with A(II), and B(I) exchanging with B(II). The effects of coupling between sites A(I) and B(I) and sites A(II) and B(II) must be taken into account.

It has been demonstrated³⁴ that coupling between two sets of AB spin coupled pairs may be directly included into the exchange-modified Bloch equations. This is possible when the Hamiltonians for the two sites differ only

in the interchange of the chemical shifts of the spins, as is the case for AB(I) exchanging with AB(II).

This is achieved by considering the four spin states for each AB pair - $\alpha_i\alpha_i$, $\alpha_i\beta_i$, $\beta_i\alpha_i$ and $\beta_i\beta_i$ (that is, $\alpha_i\alpha_i$ denotes the $+1/2,+1/2$ spin pair site, $\alpha_i\beta_i$ the $+1/2,-1/2$ site etc...). When the selection rule $\Delta M_s = \pm 1$ is applied, only the (1,2), (1,3), (2,4) and (3,4) transitions and the corresponding elements of the density matrix need be considered. Consequently, the complex magnetization of each site (M_{xyAI} , M_{xyBI} , M_{xyAII} and M_{xyBII}) becomes two sets of simultaneous equations, being the complex magnetizations for each of the four transitions, and A becomes an 8×8 matrix.

A simplification of the complete matrix of exchange is possible as the AB(I) \rightleftharpoons AB(II) system exchange occurs with a continuity of coupling between the AB nuclei. This causes transverse magnetization mixing solely between A(I) \rightleftharpoons A(II) and B(I) \rightleftharpoons B(II) sites, with no mixing between A(I) and B(I), B(II) or A(II) and B(I), B(II) sites. Therefore, coupling need only be considered for the A(I), B(I) and A(II), B(II) cross elements respectively. An additional simplification is that as the sites are all of equal population, the rates of exchange between A(I) \rightleftharpoons A(II) and B(I) \rightleftharpoons B(II) sites are equivalent. Consequently, only one rate constant, or lifetime need be considered, that is, $1/k = \tau = \tau_{AI} = \tau_{AII} = \tau_{BI} = \tau_{BII}$. The coupled Bloch equations become two independent sets of four simultaneous equations where, following the derivation for the absorption spectrum $f(\nu)$, the matrix A becomes:

$$A = \begin{vmatrix} \alpha_{AI} - i\frac{J_I}{2} - \frac{1}{\tau} & i\frac{J_I}{2} & \frac{1}{\tau} & 0 \\ i\frac{J_I}{2} & \alpha_{BI} - i\frac{J_I}{2} - \frac{1}{\tau} & 0 & \frac{1}{\tau} \\ \frac{1}{\tau} & 0 & \alpha_{AII} - i\frac{J_{II}}{2} - \frac{1}{\tau} & i\frac{J_{II}}{2} \\ 0 & \frac{1}{\tau} & i\frac{J_{II}}{2} & \alpha_{BII} - i\frac{J_{II}}{2} - \frac{1}{\tau} \end{vmatrix}$$

Where: τ is the lifetime for all sites;

J_I and J_{II} are the magnitude of coupling for sites I and II, respectively;

$$\alpha_{AI} = \frac{1}{T_{2AI}} - i(\omega_{0AI} - \omega),$$

$$\alpha_{BI} = \frac{1}{T_{2BI}} - i(\omega_{0BI} - \omega),$$

$$\alpha_{AII} = \frac{1}{T_{2AII}} - i(\omega_{0AII} - \omega),$$

$$\alpha_{BII} = \frac{1}{T_{2BII}} - i(\omega_{0BII} - \omega),$$

Matrix A , in Equation 6.45 describes only the first set of transitions. The remaining spectrum caused by the second set of transitions may be found by changing the sign of the coupling, J , in the matrix A above. The lineshape of the complete theoretical spectrum may then be described by the sum of these contributions, as shown in Chapter 4, Figures 4.11 - 4.14.

As the resonant frequency for each site in the absence of exchange is split into two resonances separated by the frequency of the coupling constant, J , it is important to accurately model the intensity of each transition. For the four transitions of a coupled AB system, Harris²¹ has shown that the transition frequencies and intensities are dependant upon the ratio of the coupling constant J to the difference in the A and B resonance frequencies, D ($= \delta_A - \delta_B$), that is, the ratio J/D . The spectra vary from, in one limit, an AX spectra ($J/D \rightarrow 0$) of four equal intensity resonances, to an A₂ spectra ($J/D \rightarrow \infty$) of a single resonance. The relationship of the four resonances, as described by Harris, may be found in Table 6.1, below.

Table 6.1 NMR Spectrum of the AB system

Transition	Frequency	Intensity
$\beta\beta \leftarrow \beta\alpha$ $4 \leftarrow 2$	$\frac{1}{2}(\nu_A + \nu_B) + \frac{1}{2}J + \frac{1}{2}D$	$1 - \sin 2\theta$
$\beta\beta \leftarrow \alpha\beta$ $4 \leftarrow 3$	$\frac{1}{2}(\nu_A + \nu_B) + \frac{1}{2}J - \frac{1}{2}D$	$1 + \sin 2\theta$
$\beta\alpha \leftarrow \alpha\alpha$ $3 \leftarrow 1$	$\frac{1}{2}(\nu_A + \nu_B) - \frac{1}{2}J + \frac{1}{2}D$	$1 + \sin 2\theta$
$\alpha\beta \leftarrow \alpha\alpha$ $2 \leftarrow 1$	$\frac{1}{2}(\nu_A + \nu_B) - \frac{1}{2}J - \frac{1}{2}D$	$1 - \sin 2\theta$

where the relationship $D^2 = [(\nu_B - \nu_A)^2 + J^2]$ holds and all units are in Hz.

6.3 : Calculation of Kinetic Parameters

6.3.1 : NMR Data Handling

For two-site lineshape analysis on the systems involving ^{23}Na variable temperature NMR spectroscopy on the the complexation of Na^+ with C211 and C21 in solvents DEF and DMA, the spectra were either accumulated on a Brüker HX-90E NMR spectrometer or were transferred from a Brüker CXP-300 NMR spectrometer via the Brüker data transfer program SPECNET. The subsequent lineshape analysis was carried out on the microcomputer of the HX-90E, a NICOLET BNC-12, using an interactive program LINSHP.^{12,37} With the use of a cathode ray oscilloscope, the program displayed a variable scale output of the experimental lineshape simultaneously against a theoretical spectrum which had been generated from the input parameters.

For all other lineshape analyses, spectra were accumulated and transformed on a CXP-300 NMR spectrometer, and then transferred by serial cable to a Macintosh SE microcomputer using the standard data transfer program KERMIT.³⁸ The Aspect 24-bit 3-byte binary files were converted into floating point decimal files using NMR-Spec³⁹ on the Macintosh, and transferred using standard methods to a VAX 11-780 mainframe computer where the non-interactive program LINSHP (Appendix iii) was used.

The input parameters required to generate theoretical spectra for lineshape analysis of uncoupled systems, $\text{a} \rightleftharpoons \text{b}$, are: ν_{a} and ν_{b} , the frequency (in Hz) of each resonance of a coalescing pair of peaks in the absence of exchange; $W_{1/2\text{a}}$ and $W_{1/2\text{b}}$, the width at half maximum amplitude (in Hz) of each resonance in the absence of exchange; χ_{a} and χ_{b} , the relative populations of each site; and R , (where $R = 1/\tau_{\text{a}}\chi_{\text{b}} = 1/\tau_{\text{b}}\chi_{\text{a}}$). For the coupled exchange of two pairs of exchanging sites, $\text{AB(II)} \rightleftharpoons \text{AB(II)}$, the input parameters required to generate theoretical spectra are: ν_{AI} , ν_{BI} , ν_{AII} and ν_{BII} , the frequency (in Hz) of each resonance of the two coalescing pair of peaks, in the absence of exchange and coupling; $W_{1/2\text{AI}}$, $W_{1/2\text{BI}}$, $W_{1/2\text{AII}}$ and $W_{1/2\text{BII}}$, the width at half maximum amplitude (in Hz) of each resonance in the absence of exchange; J_{ABI} and J_{ABII} , the $^{13}\text{C} - ^{13}\text{C}$ coupling constants (in Hz); and R .

In order to minimise the introduction of systematic errors, the variations of the above parameters were obtained from the region of very slow exchange,

and from the population weighted average parameters obtained in the very fast exchange region. For all the systems lineshaped in this study, no variations were observed in the relative populations of the exchanging species. However, there were monotonic variations observed for other parameters, and in each case these were extrapolated into the region of coalescence.

For the systems in this study subjected to simplified kinetic analysis in fast or intermediate exchange, it was not possible to determine the chemical shifts or linewidths in the absence of exchange by extrapolation of these parameters from the region of very slow exchange. Consequently, these parameters were determined from solutions containing the complexed metal ion and the solvated metal ion alone, at the same temperature and total mean concentration as that of the exchanging solution.

6.3.2 : Calculation of Kinetic Data from the Results of Lineshape Analysis

For the variable temperature NMR analysis, the intra- or intermolecular rate constants, k , were determined at each temperature by complete lineshape analysis of the corresponding experimental spectrum. The experimental spectra were visually compared with the theoretical NMR lineshape, as generated by the LINSHP program on the Nicolet BNC-12 or the FORTRAN-77 program in Appendix iii, for the given set of input parameters to give the best fit lineshape. Examples of theoretical versus experimental spectra are shown in Figures 3.1, 3.2, 3.4 and 3.6 in Chapter 3 and Figures 4.12 - 4.14 in Chapter 4 of this study.

The variation of the rate constants, k ($1/\tau$), with temperature were related to the enthalpy and entropy of activation, according to the Eyring equation of the transition state theory for a one term rate law:⁴⁰

$$\ln (T\tau) = \left[\frac{-\Delta S^\ddagger}{R} + \ln \left(\frac{h}{k_B} \right) \right] + \frac{\Delta H^\ddagger}{RT} \quad 6.46$$

where :

k_B = Boltzmann's constant (1.38062×10^{-23} J K⁻¹);

h = Planck's constant (6.62620×10^{-34} J s);

R = Universal gas constant (8.31434 J mol⁻¹ K⁻¹);

ΔH^\ddagger = enthalpy of activation (J mol⁻¹);

ΔS^\ddagger = entropy of activation (J mol⁻¹ K⁻¹); and

T = temperature (K).

A plot of $\ln(T\tau)$ against $1/T$, yields a straight line with a slope of $\frac{\Delta H^\ddagger}{R}$ and an intercept $\left[\frac{-\Delta S^\ddagger}{R} + \ln\left(\frac{h}{k_B}\right)\right]$. Examples of these plots are shown in Figures 3.3, 3.5 and 3.7 in Chapter 3 and Figures 4.10 and 4.15 in Chapter 4.

For the final calculation of ΔH^\ddagger , ΔS^\ddagger and k , a non-linear, weighted least squares method of fit was used, employing the computer program DATAFIT^{41,42} on a VAX 11-780. This program was used to model the experimental variations of $T\tau$ with $1/T$, the non-logarithmic form of Equation 6.46 above.

DATAFIT minimises the residual differences in an n-dimensional sum of squares space set, between a calculated and experimental hyper-surface using the method of Pitha and Jones.⁴³ The errors quoted are the standard deviations for each parameter in the sum of squares space. It should be noted that these error values take into account only the errors between the input parameters, and not any errors associated with the individual input parameters.

- 1 Gutowsky H.S., "Time Dependant Magnetic Perturbations"- in "Dynamic Nuclear Resonance Spectroscopy" - Jackman L.M., Cotton F.A. (Ed.), Academic Press (New York), **1975**, 1 - 21, and references therein.
- 2 Gutowsky H.S., Holm C.H., *J. Chem. Phys.*, **1956**, 25, 1228 - 1234.
- 3 Piper T.S., Wilkinson G., *J. Inorg. Nucl. Chem.*, **1956**, 3, 104 - 124.
- 4 Sutherland I.O., *Ann. Reports NMR Spectros.*, **1971**, 4, 71 - 235.
- 5 Steigel A., in "NMR Basic principles and Progress", Diehl P., Fluck E., Kosfeld R., (Eds.), **1978**, 15, 1 - 53.
- 6 Kaplan J.I., Fraenkel G., "NMR of Chemically Exchanging Systems" Academic Press (New York), **1980**.
- 7 Sandström J., "Dynamic NMR Spectroscopy", Academic Press, **1982**, (London).
- 8 Oki M., "Applications of Dynamic NMR Spectroscopy to Organic Chemistry", VCH, **1985**, (Deerfield Beach, Fl, USA).
- 9 Gamliel D., Luz Z., Vega S., *J. Chem. Phys.*, **1988**, 88, 25 - 42.
- 10 Orrell K., Šik V., Stephenson D., *Prog. NMR Spec.*, **1990**, 22, 141 - 208.
- 11 Perrin C.L., Dwyer T.J., *Chem. Rev.*, **1990**, 90, 935 - 967.
- 12 Lincoln S.F., *Prog. React. Kinetics*, **1977**, 9, 1 - 91.
- 13 Bloch F., *Phys. Rev.*, **1946**, 70, 460 - 474.
- 14 Kaplan J.I., *J. Chem. Phys.*, **1972**, 57, 5615 - 5616.
- 15 Ernst R.R., *J. Chem. Phys.*, **1973**, 59, 989.
- 16 Kaplan J.I., *J. Chem. Phys.*, **1973**, 59, 990.
- 17 Farrar T.C., Becker E.D., "Pulse and Fourier Transform NMR", **1971**, Academic Press (New York).
- 18 Gupta R.K., Pitner T.P., Wasyrishen R., *J. Mag. Reson.*, **1974**, 13, 383 - 385.
- 19 Hahn E.L., Maxwell D.E., *Phys. Rev.*, **1952**, 88, 1070 - 1084.
- 20 McConnell H.M., *J. Chem. Phys.*, **1958**, 28, 430 - 431.
- 21 Harris R.K., "Nuclear Magnetic Resonance Spectroscopy", **1983**, Pitman (London U.K.).
- 22 Pople J.A., Schneider W.G., Bernstein H.J., "High-resolution Nuclear Magnetic Resonance", **1959**, McGraw-Hill (New York).
- 23 Kaplan J.I., *J. Chem. Phys.*, **1958**, 28, 278 - 282.
- 24 Kaplan J.I., *J. Chem. Phys.*, **1958**, 29, 462.

-
- 25 Gutowsky H.S., McCall D.W., Slichter C.P., *J. Chem. Phys.*, **1953**, 21, 279 - 292.
- 26 Alexander S., *J. Chem. Phys.*, **1962**, 37, 967 - 974.
- 27 Alexander S., *J. Chem. Phys.*, **1962**, 37, 974 - 980.
- 28 Ba Y., Song R.-f., Qiu Z.-w., *Mag. Reson. Chem.*, **1989**, 27, 916 - 921.
- 29 Li F., Song R.-f., *Mag. Reson. Chem.*, **1991**, 29, 735 - 739.
- 30 Cremonini M.A., Lunazzi L., Placucci G., Okazaki R., Yamamoto G., *J. Am. Chem. Soc.*, **1990**, 112, 2915 - 2921.
- Although no mention of the method of analysis is directly stated.
- 31 Johnson C.S., *J. Chem. Phys.*, **1964**, 41, 3277 - 3278.
- 32 Lynden-Bell R.M., *Prog. NMR Spectros.*, **1967**, 2, 163 - 204.
- 33 Johnson C.S., *Adv. Mag. Reson.*, **1965**, 1, 33 - 102.
- 34 Johnson C.S., *Amer. J. Phys.*, **1967**, 35, 929 - 933.
- 35 Johnson C.S., *J. Mag. Reson.*, **1969**, 1, 98 - 104.
- 36 Johnson C.S., Moreland C.G., *J. Chem. Ed.*, **1973**, 50, 477 - 483.
- 37 Williams E.H. PhD Thesis, University of Adelaide **1980**, and references therein.
- 38 Brüker, CXP-300 version available as Pacsal code, Catchings W., da Cruz F., Schilit W., Aebi M., Placeway P., Mac-kermit v 0.98(69), **1989**, Columbia University, Info-Kermit@cunixc.cc.columbia.edu.
- 39 Christie J.R., NMR-Spec v 1.2, **1988**.
- 40 Gladstone S., Laidler K.J., Eyring., "Theory of Rate Processes", **1941**, McGraw-Hill (New York).
- 41 Kurucsev T., Unpublished Material, **1990**, University of Adelaide.
- 42 Kurucsev T., *J. Chem. Educ.*, **1978**, 55, 128 - 129.
- 43 Pitha J., Jones R.N., *Can. J. Chem.*, **1966**, 44, 3031 - 3050.

Publications :

Cryptands and Cryptates, Chapters 1-3 of this study.

“Kinetic and Equilibrium Studies of the Sodium(I) Cryptates [Na.C211]⁺ and [Na.C21C₅]⁺, and the Sodium(I) Diaza Crown Ether Complex [Na.C21]⁺ in Non-aqueous Solution ”

Clarke P., Abou-Hamdan A., Hounslow A. M., Lincoln S. F.,
Inorg. Chim. Acta, **1988**, 154, 83 - 87.

“Structural, Equilibrium, and Kinetic Study of the Complexation of Sodium(I) by the Cryptand 4,7,13,16-Tetraoxa-1,10-diazabicyclo[8.8.5]tricosane, C₂₂C₅”

Clarke P., Lincoln S. F., Tiekink E. R. T., *Inorg. Chem.*, **1991**, 30,
2747 - 2751.

“Complexation of Alkali Metal Ions by the Cryptand 4,7,13,16-Tetraoxa-1,10-diazabicyclo[8.8.5]tricosane, C₂₂C₅. A Structural and Equilibrium Study.”

Clarke P., Gulbis J. M., Lincoln S. F., Tiekink E. R. T.,
Submitted for Publication.

Divalent Metal Ion Complexes of THEC, Chapter 4 of this study

“Carbon-13 and Cadmium-113 Nuclear Magnetic Resonance Evidence for a Novel Transannular Oscillation of Cadmium(II) in the Pendant Arm Macrocyclic Complex [1,4,8,11-Tetrakis(2-hydroxyethyl)-1,4,8,11-tetraazacyclotetradecane]cadmium(II)”

Clarke P., Hounslow A.M., Keough R., Lincoln S.F., Wainwright K.P.,
Inorg. Chem., **1990**, 29, 1793 - 1797.

“Transannular Oscillation of Metal Centers in the Pendant Arm Macrocyclic Complex [1,4,8,11-Tetrakis(2-hydroxyethyl)-1,4,8,11-tetraazacyclotetradecane]mercury(II) and Its Lead(II) Analogue. NMR Study of the ¹³C Natural Abundance and Specifically Enriched Complexes”

Clarke P., Lincoln S.F., Wainwright K.P.,
Inorg. Chem., **1991**, 30, 134 - 139.

Appendix i : STAB a FORTRAN-77 Program for the VAX 11-780 Computer

```

PROGRAM STAB
REAL*8 AgTOT(200),AgFREE(200),CFREE(200),XAgFREE(200)
REAL*8 XTOT(200),XFREE(200)
REAL*8 CTOT(200),MV(200),TITVOL(200),OMADBA(200)
REAL*8 STABCON(200),MINFXN(200),LNAg(200),LNSTAB(200)
REAL*8 LCFREE(200),LOMADBA(200),COMPEZ,COMPEY(200),COMPEX(200)
REAL*8 RESVOL,SLOPE,INTER,CINIT,AgINIT,XINIT
CHARACTER*80 TITLE

C      LINE 1: TITLE UP TO 80 CHARACTERS
C      LINE 2: SLOPE, INTERCEPT OF THE CALIBRATION EQUATION...
C      MV = INTERCEPT + SLOPE * ln [Ag+]free
C      LINE 3: KKK1=1 DRAW.PLT OF [C]f vs (1-a)/a
C      KKK2=0:lnK,minfxn      =1: fullinfo      =2: 1+[c]free,(1-a)/a
C      KKK3=1 TIT.PLT of Vol. vs mV
C      KKK4=1 ln([C]f vs ln((1-a)/a)
C      KKK5=0 Na+ DIR.TIT.      =1 Ag+ DIR.TIT. =2 Ag+ COMP.TIT.
C      LINE 4: INITIAL LIGAND, MEAS.METAL ION,
C      (FOR KNTL5=2 ONLY:: COMPET.METAL ION CONCENTRATIONS (MOLAR))
C      LINE 5: INITIAL VOLUME OF 0.001M[Ag+] OR 0.001M[Na+] (usua.
C      20.0ml (mls)) AND No. OF DATA POINTS
C      LINE 6 + : TITRATION VOLUME (mls) MILLIVOLTS

READ(1,1000)TITLE
READ(1,*)SLOPE,INTER
READ(1,*)KKK1,KKK2,KKK3,KKK4,KKK5
IF(KKK5.EQ.0)READ(1,*)CINIT,AgINIT
IF(KKK5.EQ.1)READ(1,*)CINIT,AgINIT
IF(KKK5.EQ.2)READ(1,*)CINIT,AgINIT,XINIT
READ(1,*)RESVOL,NNN
DO 10 I=1,NNN
  READ(1,*)TITVOL(I),MV(I)
10 CONTINUE
DO 20 I=1,NNN
  LNAg(I) = (MV(I) - INTER) / SLOPE
  AgFREE(I) = EXP(LNAg(I))
  IF(KKK5.EQ.0)THEN
    IF(AgFREE(I).LT.1E-7)WRITE(2,1005)I
  ELSE
    IF(AgFREE(I).LT.1E-10)WRITE(2,1010)I
  ENDIF
  AgTOT(I) = (AgINIT * RESVOL) / (RESVOL + TITVOL(I))
  CTOT(I) = (CINIT * TITVOL(I)) / (RESVOL + TITVOL(I))

C
C      IF
C      COMPETATIVE      K (X/Ag) =  $\frac{[AgC+] * [X+(free)]}{[Ag+(free)] * [XC+]}$ 
C
C      IF
C      DIRECT      K (Ag) =  $\frac{[AgC+]}{[Ag+(free)] * [C(free)]}$ 
C
C      IF(KKK5.EQ.2)THEN
  XTOT(I) = (XINIT * TITVOL(I)) / (RESVOL + TITVOL(I))
  STABCON(I) = (XTOT(I) - CTOT(I) + AgTOT(I) - AgFREE(I)) * (AgTOT(I) -
+ AgFREE(I)) / (AgFREE(I) * (CTOT(I) - AgTOT(I) + AgFREE(I)))
  ELSE
  STABCON(I) = (AgTOT(I) - AgFREE(I)) / (AgFREE(I) *
+ (CTOT(I) - AgTOT(I) + AgFREE(I)))
  ENDIF

C
C      FOLLOWING CONDITIONAL WILL FAIL ON STABCON(I)=0.00000
C
C      IF(STABCON(I).GT.0.0000)THEN
  LNSTAB(I) = LOG10(STABCON(I))
  ELSE

```



```

LNSTAB(I) = LOG10(-STABCON(I))
ENDIF
MINFXN(I) = ABS(AgTOT(I) - 2 * AgFREE(I)) +
+ ABS(CTOT(I) - AgTOT(I)) +
+ ABS(CTOT(I) + 2 * AgFREE(I) - 2 * AgTOT(I))
IF(KKK5.EQ.2) THEN
C
C Removing large & relatively unchanging XTOT(I) equiv. to - 3*XTOT(I)
C
MINFXN(I) = MINFXN(I) + ABS(CTOT(I)) + ABS(AgTOT(I) - CTOT(I))
+ ABS(2*AgTOT(I) - 2*CTOT(I) - 2*AgFREE(I))
ENDIF
XAgFREE(I) = AgFREE(I) / AgTOT(I)
OMADBA(I) = (1 - XAgFREE(I)) / XAgFREE(I)
CFREE(I) = CTOT(I) + AgFREE(I) - AgTOT(I)
XFREE(I) = XTOT(I) - CTOT(I) + AgTOT(I) - AgFREE(I)
20 CONTINUE
K = 0
DO 25 I=1,NNN
J = I - K
IF(OMADBA(I).GT.0.0000) THEN
LOMADBA(J) = LOG10(OMADBA(I))
if(cfree(i).gt.0) then
LCFREE(J) = LOG10(CFREE(I))
else
lcfree(j) = 0.0
endif
ELSE
K = K + 1
ENDIF
NN = J
25 CONTINUE
WRITE(2,1000) TITLE
IF(KKK2.EQ.0) THEN
WRITE(2,1015)
DO 30 I=1,NNN
WRITE(2,1020) LNSTAB(I), STABCON(I), MINFXN(I)
30 CONTINUE
ENDIF
IF(KKK2.GE.1) THEN
IF(KKK5.EQ.2) THEN
WRITE(2,1026)
DO 35 I=1,NNN
WRITE(2,1031) TITVOL(I), LNSTAB(I), AgFREE(I), CFREE(I)
+ , XFREE(I), MINFXN(I)
35 CONTINUE
ELSE
IF(KKK5.EQ.0) WRITE(2,1024)
IF(KKK5.EQ.1) WRITE(2,1025)
DO 40 I=1,NNN
WRITE(2,1030) TITVOL(I), LNSTAB(I), AgFREE(I), CFREE(I)
+ , MINFXN(I)
40 CONTINUE
ENDIF
ENDIF
IF(KKK2.GE.2) THEN
IF(KKK5.EQ.2) THEN
WRITE(2,1036)
DO 45 I=1,NNN
COMPEZ=OMADBA(I)*XFREE(I)
WRITE(2,*) CFREE(I), COMPEZ
IF(CFREE(I).LT.0.0) JJJ=1
45 CONTINUE
ELSE
WRITE(2,1035)
DO 50 I=1,NNN
WRITE(2,*) CFREE(I), OMADBA(I)
IF(CFREE(I).LT.0.0) JJJ=1
IF(CFREE(I).LT.0.0) CFREE(I)=0.0
50 CONTINUE
ENDIF
IF(JJJ.EQ.1) WRITE(2,1040)

```

```

ENDIF
DO 55 I=1, NNN
  IF (KKK5.EQ.2) THEN
    COMPEY (I) =OMADBA (I) *XFREE (I)
    IF (XFREE (I) .LE.0.0) XFREE (I) =1E-5
    COMPEX (I) =LOMADBA (I) + LOG10 (XFREE (I))
  ELSE
    COMPEY (I) =OMADBA (I)
    COMPEX (I) =LOMADBA (I)
  ENDIF
55 CONTINUE
  IF (KKK1.EQ.1) CALL FOO (TITLE, NNN, CFREE, COMPEY, KKK5)
  IF (KKK3.EQ.1) CALL FOOTOO (TITLE, NNN, TITVOL, MV)
  IF (KKK4.EQ.1) CALL FOOMOO (TITLE, NNN, NN, LCFREE, COMPEX, KKK5)
1000 FORMAT (1X, A80)
1005 FORMAT (2X, '***[Na+]f IS BELOW (1E-7 M) LIMIT AT Pt ', I3)
1010 FORMAT (2X, '***[Ag+]f MAY BE BELOW (1E-12 M) LIMIT AT Pt ', I3)
1015 FORMAT (2X, ' lnK ', 2X, ' K ', 2X, ' Min. ')
1020 FORMAT (2X, F7.4, 2X, F16.0, 2X, F12.7)
1024 FORMAT (2X, ' mls.', 4X, 'lnK', 5X, '[Na+]free', 9X, '[C]free', 8X,
+ 'Min.Fxn')
1025 FORMAT (2X, ' mls.', 4X, 'lnK', 5X, '[Ag+]free', 9X, '[C]free', 8X,
+ 'Min.Fxn')
1026 FORMAT (2X, ' mls.', 4X, 'lnK', 5X, '[Ag+]free', 9X, '[XC+] ', 7X,
+ '[X+]free', 6X, 'Min.Fxn')
1030 FORMAT (2X, F6.3, 2X, F7.4, 2X, F14.12, 2X, F14.12, 2X, F10.7)
1031 FORMAT (2X, F6.3, 2X, F7.4, 2X, F14.12, 2X, F14.12, 2X, F11.9, 2X, F10.7)
1035 FORMAT (//, 2X, 'LIST OF PLOTTING VALUES FOR', //, 2X, '[C]FREE '10X,
+ '(1-ALPHA) / ALPHA ')
1036 FORMAT (//, 2X, 'LIST OF VALUES FOR', //, 6X, '[XC+] '5X,
+ '[X+]free * (1-ALPHA) / ALPHA ')
1040 FORMAT (2X, 'NOTE:: [Cry] or [XCry+] < 0.0M !!')
STOP
END

SUBROUTINE FOO (HEADER, NNN, XVAL, YVAL, K5)
REAL*8 YVAL (200), XVAL (200)
REAL*8 XVALXX (200), YVALXX (200)
CHARACTER HEADER*80
YMAX=-1.0E+25
YMIN=1.0E+25
XMAX=-1.0E+25
XMIN=1.0E+25
DO 10 I=1, NNN
  IF (YVAL (I) .GT.YMAX) YMAX=YVAL (I)
  IF (YVAL (I) .LT.YMIN) YMIN=YVAL (I)
  IF (XVAL (I) .GT.XMAX) XMAX=XVAL (I)
  IF (XVAL (I) .LT.XMIN) XMIN=XVAL (I)
10 CONTINUE
YINT=(YMAX-YMIN)/10.0
XINT=(XMAX-XMIN)/10.0
OPEN (UNIT=7, STATUS='NEW', FILE='DRAW.PLT')
WRITE (UNIT=7, FMT=100) HEADER
WRITE (UNIT=7, FMT=200) NNN
WRITE (UNIT=7, FMT=300)
WRITE (UNIT=7, FMT=400) XMIN, XMAX, XINT
IF (K5.EQ.2) THEN
  WRITE (UNIT=7, FMT=501)
ELSE
  WRITE (UNIT=7, FMT=500)
ENDIF
WRITE (UNIT=7, FMT=600) YMIN, YMAX, YINT
IF (K5.EQ.2) THEN
  WRITE (UNIT=7, FMT=701)
ELSE
  WRITE (UNIT=7, FMT=700)
ENDIF
WRITE (UNIT=7, FMT=750)
WRITE (UNIT=7, FMT=800)
WRITE (UNIT=7, FMT=900) NNN
WRITE (UNIT=7, FMT=1200) (XVAL (I), YVAL (I), I=1, NNN)
RETURN

```

```

100 FORMAT(2X,A80)
200 FORMAT(2X,'No.Pts= ',I5)
300 FORMAT(2X,' ')
400 FORMAT(2X,3(F10.8,2X),'1 1 18 NOARROW')
500 FORMAT(2X,'[LIGAND]free')
501 FORMAT(2X,'[XC+]')
600 FORMAT(2X,3(F15.5,2X),'1 1 12 NOARROW')
700 FORMAT(2X,'(1-a)/a')
701 FORMAT(2X,'[X+]free * (1-a)/a')
750 FORMAT(2X,'R 1.0')
800 FORMAT(2X,'P 1')
900 FORMAT(2X,I5)
1200 FORMAT(2X,F10.8,2X,F15.5)
      END

      SUBROUTINE FOOTOO(HEADER,NNN,XVAL,YVAL)
      REAL*8 YVAL(200),XVAL(200)
      REAL*8 XVALXX(100),YVALXX(100)
      CHARACTER HEADER*80
      YMAX=-1.0E+25
      YMIN=1.0E+25
      XMAX=-1.0E+25
      XMIN=1.0E+25
      DO 10 I=1,NNN
         IF (YVAL(I).GT.YMAX) YMAX=YVAL(I)
         IF (YVAL(I).LT.YMIN) YMIN=YVAL(I)
         IF (XVAL(I).GT.XMAX) XMAX=XVAL(I)
         IF (XVAL(I).LT.XMIN) XMIN=XVAL(I)
10 CONTINUE
      YINT=(YMAX-YMIN)/10.0
      XINT=(XMAX-XMIN)/10.0
      OPEN(UNIT=7,STATUS='NEW',FILE='TIT.PLT')
      WRITE(UNIT=7,FMT=100)HEADER
      WRITE(UNIT=7,FMT=200)NNN,XMAX
      WRITE(UNIT=7,FMT=300)
      WRITE(UNIT=7,FMT=400)XMIN,XMAX,XINT
      WRITE(UNIT=7,FMT=500)
      WRITE(UNIT=7,FMT=600)YMIN,YMAX,YINT
      WRITE(UNIT=7,FMT=700)
      WRITE(UNIT=7,FMT=750)
      WRITE(UNIT=7,FMT=800)
      WRITE(UNIT=7,FMT=900)NNN
      WRITE(UNIT=7,FMT=1000)(XVAL(I),YVAL(I),I=1,NNN)
      RETURN
100 FORMAT(2X,A80)
200 FORMAT(2X,'No.Pts= ',I5,' Max Vol. added',F10.5)
300 FORMAT(2X,' ')
400 FORMAT(2X,3(F6.3,2X),'1 1 18 NOARROW')
500 FORMAT(2X,'Vol. Added')
600 FORMAT(2X,3(F7.1,2X),'1 1 12 NOARROW')
700 FORMAT(2X,'mVolts')
750 FORMAT(2X,'R 1.0')
800 FORMAT(2X,'P 1')
900 FORMAT(2X,I5)
1000 FORMAT(2X,F6.3,2X,F7.1)
      END

      SUBROUTINE FOOMOO(HEADER,NNN,NN,XVAL,YVAL,K5)
      REAL*8 YVAL(200),XVAL(200)
      REAL*8 XVALXX(200),YVALXX(200)
      CHARACTER HEADER*80
      YMAX=-1.0E+25
      YMIN=1.0E+25
      XMAX=-1.0E+25
      XMIN=1.0E+25
      DO 10 I=1,NN
         IF (YVAL(I).GT.YMAX) YMAX=YVAL(I)
         IF (YVAL(I).LT.YMIN) YMIN=YVAL(I)
         IF (XVAL(I).GT.XMAX) XMAX=XVAL(I)
         IF (XVAL(I).LT.XMIN) XMIN=XVAL(I)
10 CONTINUE
      YINT=(YMAX-YMIN)/10.0

```

```

XINT=(XMAX-XMIN)/10.0
OPEN(UNIT=7,STATUS='NEW',FILE='LOG.PLT')
WRITE(UNIT=7,FMT=100)HEADER
WRITE(UNIT=7,FMT=200)NN
WRITE(UNIT=7,FMT=300)(NNN-NN)
WRITE(UNIT=7,FMT=400)XMIN,XMAX,XINT
IF(K5.EQ.2)THEN
  WRITE(UNIT=7,FMT=501)
ELSE
  WRITE(UNIT=7,FMT=500)
ENDIF
WRITE(UNIT=7,FMT=600)YMIN,YMAX,YINT
IF(K5.EQ.2)THEN
  WRITE(UNIT=7,FMT=701)
ELSE
  WRITE(UNIT=7,FMT=700)
ENDIF
WRITE(UNIT=7,FMT=750)
WRITE(UNIT=7,FMT=800)
WRITE(UNIT=7,FMT=900)NN
WRITE(UNIT=7,FMT=1200)(XVAL(I),YVAL(I),I=1,NN)
C  WRITE(UNIT=7,FMT=1100)
C  WRITE(UNIT=7,FMT=900)NN
C  50 WRITE(UNIT=7,FMT=1200)(XVAL(I),YVAL(I),I=1,NN)
  RETURN
100 FORMAT(2X,A80)
200 FORMAT(2X,'No.Pts used = ',I5)
300 FORMAT(2X,I5,' pts rejected  ')
400 FORMAT(2X,3(F6.3,2X),'1 1 18 NOARROW')
500 FORMAT(2X,'ln [LIGAND]free')
501 FORMAT(2X,'ln [XC+]')
600 FORMAT(2X,3(F6.3,2X),'1 1 12 NOARROW')
700 FORMAT(2X,'ln((1-a)/a)')
701 FORMAT(2X,'ln((1-a)/a) + ln[X+]free')
750 FORMAT(2X,'R 1.0')
800 FORMAT(2X,'P 1')
900 FORMAT(2X,I5)
1200 FORMAT(2X,F6.3,2X,F6.3)
C 1100 FORMAT(2X,'L 1')
  END

```

VAX- VMS 4.1 Macro for Executing the Program LINSHP

```

$ start:
$ directory
$ write sys$output " "
$ inquire P1 "data file name? "
$ write sys$output " "
$ copy 'P1' for001.dat
$ run d2:[pclarke.titration]stab.exe
$ write sys$output " "
$ write sys$output " To save the output from this program      "
$ write sys$output " you will have to rename them              "
$ write sys$output " "
$ inquire P2 " Rename system to: (don't include suffix)?"
$ write sys$output " "
$ write sys$output " **** .out, .plt, .log and .tit suffixes"
$ write sys$output " "
$ directory *.plt,*.dat
$ write sys$output " "
$ rename draw.plt 'P2'.plt
$ rename for002.dat 'P2'.out
$ rename tit.plt 'P2'.min
$ delete/confirm for00*.dat;*,draw.plt;*,log.plt;*,tit.plt;*
$ inquire P7 "Any more data? y/n "
$ if P7 then goto start
$ write sys$output "                               Good bye! "

```

Example Input Data File

```
Cs+ c22c5 in methanol compet.Ag+ titr.  
28.61,124.7  
1,2,1,0,2  
0.002052,0.0001003,0.0021  
20.0,14  
0.0      -139.4  
0.0      -140.6  
0.1      -151.8  
0.2      -166.0  
0.3      -242.0  
0.4      -318.8  
0.5      -424.0  
0.6      -467.8  
0.7      -495.8  
0.8      -517.0  
0.9      -532.6  
1.0      -530.0  
1.2      -539.5  
1.4      -550.2
```

The Program STAB, Acknowledgements

The PLXY subroutine generates a text file in the format required by the graphics drawing program DRAW for the VAXen and Unix networks at the University of Adelaide and was kindly provided by D. Beard, University of Adelaide.

This program was originally written by P. Clarke in FORTRAN-77 to execute on a VAX 11-780 mainframe computer, 1988. The algorithm used is for systems for which the number of complexation steps = 1, as discussed in "Determination of Stability Constants" by F. Rossotti and H. Rossotti, Chapter 5, 1961, McGraw-Hill (New York).

Appendix ii : VISP a FORTRAN-77 Program for the VAX 11-780 Computer

```

PROGRAM VISP
  REAL*8 T(200),C(200),X(200),K(249),F(200),LOGK(249),RESVOL
  REAL*8 MV(200),MV CALC(200),DELTA(200),ADDDVOL(200),TITVOL(200)
  REAL*8 SURD,KM1,QA,QB,QC,RESID(200),STEPLOG,FEXPT(200)
  REAL*8 AGINIT,CINIT,XINIT
  REAL*8 SIGMA(249),SIGMASQ(249),SLOPE,INTER,DENSITY,FLAG
  INTEGER IBAD(249),JBAD(200),MULTI(200),JARRAY(4),KKO(200)
  CHARACTER*80 TITLE
  CHARACTER POINT*1
  COMMON/A/POINT
C   LINE 1: "eg.vis example title (up to 80 chars)"      ....
C   TITLE UP TO 80 CHARACTERS
C   LINE 2: slope,intercept
C   SLOPE, INTERCEPT OF THE CALIBRATION EQUATION..
C   mV = INTERCEPT + SLOPE * ln [Ag+]free
C   LINE 3: titration_type,method_of_comparison
C   expt_type =0  Na+ DIRECT TITRATION
C   SAME EXCEPT RESERVOIR VOLUME READ IN ON LINE 9
C   expt_type =1  Ag+ DIRECT TITRATION
C   expt_type =2  Ag+ COMPETATIVE TITRATION
C   ****(1) expt_type =3  Xn+ COMPETATIVE TITRATION
C   expt_type =4  THEORETICAL DIRECT TITRATION
C   expt_type =5  THEORETICAL COMPETATIVE TITRATION
C   comparison =0 COMPARISON BY mV(expt.) vs. mV(calc.)
C   =1  " + ****.MIN file of titvol vs. sigma(mV)
C   ( if -VE then min.plt has axes etc.)
C   =2 COMPARISON BY [Ag+]free(expt) vs. (calc)
C   =3  " + MIN.PLT titvol vs. sigma(Ag+free)
C   LINE 4: expt_draw_type,calc_draw_type,diff_draw_type
C   expt_draw =0  NO EXPT. PLOT      calc_draw =0 NO CALC. PLOT
C   expt_draw =1  PLOT EXPT. "X"          =1 PLOT CALC. "X"
C   ****(2) expt_draw =2  PLOT EXPT. "."          etc.
C   expt_draw =3  PLOT EXPT. AS A TRIANGLE
C   expt_draw =4  PLOT EXPT. AS A SQUARE  diff_draw =0 NO DIFF
C   . PLOT
C   expt_draw =5  PLOT EXPT. SOLID LINE          =1 PLOT
C   (EXPT-CALC) "X"
C   expt_draw =6  PLOT EXPT. 1xDASHED LINE
C   expt_draw =7  PLOT EXPT. 2xDASHED LINE
C   expt_draw =8  PLOT EXPT. 3xDASHED LINE
C   ****(2) expt_draw =9  PLOT EXPT. any character you like, must be
C   specified on LINE 8: *****
C   LINE 5: No._of_LOGK's,Method_of_input_LOGK
C   No. =1  NORMAL EXPERIMENT
C   No. =2  MULTIPLE STABILITY CONSTANTS CALC.
C   method =0 ==> LINE 6 READS:: LOGK(1),LOGK(2),...,LOGK(No.)
C   =1      " , " multiple up to =100
C   =2 ==> LINE 6 READS:: MINLOGK,STEPsize
C   =3      " , " ,MULTstepsizesize
C   LINE 6: LOGK etc. see LINE 5:
C   LINE 7: [Ag+]or[Na+]init_conc,ligand_init (FOR COMPET.ONLY):[X+]init
C   INITIAL [Ag+] Conc. in resevoir,INITIAL [LIGAND] in burette
C   (if COMPETATIVE TIT.)... " ,INITIAL [LIG.X+], INITIAL [X+
C   total] in burette
C   LINE 8: (OPTIONAL) (if_draw_type=9)draw_char) A SINGLE CHARACTER for
C   example "*"
C   LINE 9: (OPTIONAL) (if_reservoir_Vol._not=20mls)reservoir_volume(mls)
C   only if expt_type .ge. 6
C   ****(1) COMPET.EXPT EXCEPT FLAG= -1 ( for -ve value under SQRT!)
C

```

```

READ (3,1000) TITLE
READ (3,*) SLOPE, INTER
READ (3,*) K1, K8
READ (3,*) K4, K5, K6
READ (3,*) K3, K7
IF (K7.EQ.0) READ (3,*) (LOGK(I), I=1, K3)
IF (K7.EQ.1) MULT=K3
IF (K7.EQ.2) READ (3,*) LOGK(1), STEPLOG
IF (K7.EQ.3) READ (3,*) LOGK(1), STEPLOG, MULT
IF (MULT.GE.2) THEN
DO 2 I=2, K3, MULT
MULTI (I-1)=1
2 CONTINUE
ENDIF
IF (K7.GE.2) THEN
DO 5 I=2, K3
LOGK(I)=LOGK(1)+(I-1)*STEPLOG
5 CONTINUE
ENDIF
IF (K1.LT.2.OR.K1.EQ.4) READ (3,*) CINIT, AGINIT
IF (K1.GE.2.AND.K1.NE.4) READ (3,*) CINIT, AGINIT, XINIT
IF (K4.EQ.9.OR.K5.EQ.9.OR.K6.EQ.9) READ (3,1005) POINT
IF (K1.GE.6) THEN
READ (3,*) RESVOL
K1=K1-6
ELSE
RESVOL=20.0
ENDIF
NNN=0
DO 20 I=1, 200
READ (UNIT=3, FMT=*, END=25) TITVOL(I), MV(I)
NNN=NNN+1
20 CONTINUE
25 WRITE (4,1000) TITLE
IF (K8.LT.0) KK8=K8
IF (K8.LT.0) K8=-K8
IF (K1.EQ.0.OR.K1.EQ.6) WRITE (4,*) ' mV = ', INTER, ' + ', SLOPE,
+ ' * ln[Na+]free'
IF (K1.NE.0.AND.K1.NE.6) WRITE (4,*) ' mV = ', INTER, ' + ', SLOPE,
+ ' * ln[Na+]free'
IF (K1.LT.2) WRITE (4,1010)
IF (K1.LT.2) TYPE 1010
FLAG=1.0
IF (K1.GE.2) WRITE (4,1011)
IF (K1.GE.2) TYPE 1011
IF (KK8.NE.0) WRITE (4,*) ' Multiple Log K in .PLT files! '
IF (K8.LE.1) WRITE (4,*) ' mV vs. Burette Volume'
IF (K8.GE.2) WRITE (4,*) ' [M+]free vs. Burette Vol.'
IF (K6.NE.0) WRITE (4,*) ' a .DIF plot file produced'
IF (K8.EQ.1.OR.K8.EQ.3) WRITE (4,*) ' a .MIN plot file produced'
WRITE (4,1013) LOGK(1), LOGK(K3), K3
IF (K1.EQ.0) WRITE (4,1015) AGINIT, CINIT
IF (K1.EQ.1.OR.K1.EQ.4) WRITE (4,1017) AGINIT, CINIT
IF (K1.EQ.2.OR.K1.EQ.3) WRITE (4,1019) AGINIT, CINIT, XINIT
IF (K3.GT.100.AND.XINIT.LT.(4*CINIT)) WRITE (4,*) ' WARNING X<4C'
28 DO 200 J=1, K3
30 DO 100 I=1, NNN
ADDVOL(I)=RESVOL+TITVOL(I)
T(I)=AGINIT*RESVOL/ADDVOL(I)
C(I)=CINIT*TITVOL(I)/ADDVOL(I)
K(J)=(DBLE(10.0))**(LOGK(J))
IF (K1.GE.2) THEN
X(I)=XINIT*TITVOL(I)/ADDVOL(I)
KM1=K(J)-1.0
QA=KM1
QB=KM1*C(I)+X(I)+T(I)-KM1*T(I)
QC=T(I)*(C(I)-X(I)-T(I))
ELSE
QA=K(J)
QB=1.0-K(J)*T(I)+K(J)*C(I)
QC=-1*T(I)
ENDIF

```

```

SURD=QB*QB-4*QA*QC
IF (SURD.LT.0.0) WRITE (4,1020) I
IF (SURD.LT.0.0) TYPE 1020, I
IF (SURD.LT.0.0) SURD=-1*SURD
IF (K1.EQ.3) FLAG=-1.0
F(I)=(-1*QB+FLAG*DSQRT(SURD))/(2*QA)
IF (K8.LE.1) THEN
  IF (F(I).LT.1E-12) THEN
    F(I)=1E-12
    IBAD(J)=IBAD(J)+1
    JBAD(IBAD(J))=I
  ENDIF
  MVCALC(I)=SLOPE*DLOG(F(I)) + INTER
ENDIF
FEXPT(I)=DEXP((MV(I)-INTER)/SLOPE)
IF (K8.GE.2) THEN
  DELTA(I)=FEXPT(I) - F(I)
ELSE
  DELTA(I)=MV(I) - MVCALC(I)
ENDIF
SIGMA(J) = SIGMA(J) + ABS(DELTA(I))
SIGMASQ(J) = SIGMASQ(J) + (DELTA(I))**2
KKO(I)=0
100 CONTINUE
DO 101 I=1, NNN
  IF (ABS(DELTA(I)).GT.(0.1*SIGMA(J))) KKO(I)=1
101 CONTINUE
IF (MULTI(J).EQ.1) WRITE (4,2040) LOGK(J)
IF (K8.LE.1) THEN
  IF (MULTI(J).EQ.1) CALL APPEND(NNN, TITVOL, MVCALC, K5)
ELSE
  IF (MULTI(J).EQ.1) CALL APPEND(NNN, TITVOL, F, K5)
ENDIF
IF (IBAD(J).GT.0.AND.LAST.EQ.1) THEN
  WRITE (4,1030)
  WRITE (4,1031) LOGK(J)
  WRITE (4,*) (JBAD(II), II=1, IBAD(J))
  TYPE 1030
  TYPE 1031, LOGK(J)
ENDIF
IF (LAST.EQ.1) GOTO 400
200 CONTINUE
IF (K3.GE.2) THEN
  JBEST=1
  DO 250 JJ=1, K3
    IF (JJ.EQ.1) WRITE (4,1090)
    WRITE (4,1091) LOGK(JJ), SIGMA(JJ), SIGMASQ(JJ)
    IF (SIGMA(JJ).LT.SIGMA(JBEST)) JBEST=JJ
250 CONTINUE
  LAST=1
  J=JBEST
ELSE
  J=1
ENDIF
WRITE (4,1070) NNN, LOGK(J)
DO 300 I=1, NNN
  RESID(I)=NNN*DELTA(I)/SIGMA(J)
300 CONTINUE
IF (LAST.EQ.1) SIGMA(J)=0.0
IF (LAST.EQ.1) SIGMASQ(J)=0.0
IF (LAST.EQ.1) GOTO 30
400 IF (K3.GT.100.AND.K8.LE.1) THEN
C I.E. RESOLUTION =100 OR MORE AND USING MV COMPARISON
KOUNT=0
DO 500 J=1, K3
  IF (KOUNT.EQ.1) GOTO 450
  IF (KOUNT.EQ.2) GOTO 500
  IF (SIGMA(J).LT.(1.1*SIGMA(JBEST))) JMIN=J
  IF (SIGMA(J).LT.(1.1*SIGMA(JBEST))) KOUNT=1
450 IF (JBEST.GT.J) GOTO 500
  IF (SIGMA(J).GT.(1.1*SIGMA(JBEST))) JMAX=J
  IF (SIGMA(J).GT.(1.1*SIGMA(JBEST))) KOUNT=2

```



```

500    CONTINUE
      ENDIF
C    ERROR REPORT
      TYPE *, ' Values for:'
      WRITE(4,*) ' Values for:'
      TYPE *, ' Best          Lower Limit Upper Limit'
      WRITE(4,*) ' Best          Lower Limit Upper Limit'
      TYPE *, ' LOG K ='
      WRITE(4,*) ' LOG K ='
      TYPE 2010, LOGK(JBEST), LOGK(JMIN), LOGK(JMAX)
      WRITE(4,2010) LOGK(JBEST), LOGK(JMIN), LOGK(JMAX)
      TYPE *, ' SIGMA ='
      WRITE(4,*) ' SIGMA ='
      TYPE 2020, SIGMA(JBEST), SIGMA(JMIN), SIGMA(JMAX)
      WRITE(4,2020) SIGMA(JBEST), SIGMA(JMIN), SIGMA(JMAX)
      TYPE *, ' SI**2 ='
      WRITE(4,*) ' SI**2 ='
      TYPE 2030, SIGMASQ(JBEST), SIGMASQ(JMIN), SIGMASQ(JMAX)
      WRITE(4,2030) SIGMASQ(JBEST), SIGMASQ(JMIN), SIGMASQ(JMAX)
      J=JBEST
      JARRAY(1)=JBEST
      JARRAY(2)=JMIN
      JARRAY(3)=JMAX
      JARRAY(4)=KK8
      IF(K8.GE.2) THEN
C BEGIN [Ag+] free PLOTS
      IF(K1.EQ.0) THEN
        WRITE(4,1040)
        WRITE(4,1042) LOGK(J), SIGMA(J), SIGMASQ(J)
        WRITE(4,1051)
        DO 700 I=1, NNN
          WRITE(4,1061) TITVOL(I), FEXPT(I), F(I), RESID(I)
          IF(KK0(I).EQ.1.AND.K3.GE.101) WRITE(4,*) ' ****DELTA>10%'
700    CONTINUE
        ELSE
          WRITE(4,1040)
          WRITE(4,1042) LOGK(J), SIGMA(J), SIGMASQ(J)
          WRITE(4,1052)
          DO 710 I=1, NNN
            WRITE(4,1062) TITVOL(I), FEXPT(I), F(I), RESID(I)
            IF(KK0(I).EQ.1.AND.K3.GE.101) WRITE(4,*) ' ****DELTA>10%'
710    CONTINUE
        ENDIF
      IF(K1.LE.1) THEN
      IF(K4.NE.0) CALL FOO(TITLE, NNN, TITVOL, FEXPT, F, 7, K4, K5)
      IF(K6.NE.0) CALL FOO(TITLE, NNN, TITVOL, DELTA, RESID, 5, K6, 0)
      IF(K8.EQ.3) CALL JJJ(K3, LOGK, SIGMA, SIGMASQ, JARRAY)
      ELSE
      IF(K1.GE.4) THEN
      IF(K4.NE.0) CALL FOO(TITLE, NNN, TITVOL, F, MV, 6, K4, 0)
      ELSE
      IF(K4.NE.0) CALL FOO(TITLE, NNN, TITVOL, FEXPT, F, 8, K4, K5)
      IF(K6.NE.0) CALL FOO(TITLE, NNN, TITVOL, DELTA, RESID, 5, K6, 0)
      IF(K8.EQ.3) CALL JJJ(K3, LOGK, SIGMA, SIGMASQ, JARRAY)
      ENDIF
      ENDIF
C BEGIN mV. PLOTS
      ELSE
      WRITE(4,1040)
      WRITE(4,1042) LOGK(J), SIGMA(J), SIGMASQ(J)
      WRITE(4,1050)
      DO 720 I=1, NNN
        WRITE(4,1060) TITVOL(I), MV(I), MVCALC(I), RESID(I)
        IF(KK0(I).EQ.1.AND.K3.GE.101) WRITE(4,*) ' ****DELTA>10%'
720    CONTINUE
      IF(K1.LE.1) THEN
      IF(K4.NE.0) CALL FOO(TITLE, NNN, TITVOL, MV, MVCALC, 2, K4, K5)
      IF(K6.NE.0) CALL FOO(TITLE, NNN, TITVOL, DELTA, RESID, 0, K6, 0)
      IF(K8.EQ.1) CALL JJJ(K3, LOGK, SIGMA, SIGMASQ, JARRAY)
      ELSE
      IF(K1.GE.4) THEN
      IF(K4.NE.0) CALL FOO(TITLE, NNN, TITVOL, MVCALC, MV, 1, K4, 0)

```

```

ELSE
  IF (K4.NE.0) CALL FOO (TITLE, NNN, TITVOL, MV, MVCALC, 3, K4, K5)
  IF (K6.NE.0) CALL FOO (TITLE, NNN, TITVOL, DELTA, RESID, 0, K6, 0)
  IF (K8.EQ.1) CALL JJJ (K3, LOGK, SIGMA, SIGMASQ, JARRAY)
ENDIF
ENDIF
  ENDIF
C END [Ag+]free OR mV PLOTS
1000  FORMAT(2X,A80)
1005  FORMAT(2X,A1)
1010  FORMAT(2X,' DIRECT TITRATION',/)
1011  FORMAT(2X,' COMPETATIVE TITRATION',/)
1013  FORMAT(2X,' LOG K RANGE= ',F6.3,' - ',F6.3,I4,' STEPS. ')
1015  FORMAT(2X,' [Na+]=',F9.7,' [C]=',F8.6)
1017  FORMAT(2X,' [Ag+]=',F9.7,' [C]=',F8.6)
1019  FORMAT(2X,' [Ag+]=',F9.7,' [XC+]=',F8.6,' [X+]=',F8.6)
1020  FORMAT(/,2X,' SQRT OF -VE FUNC. AT Pt.',I3,/,2X,' FXN=-1*FXN')
1030  FORMAT(2X,' IF [Ag+]free is <1E-12M set = to 1E-12M',/,2X,
+  /,'if <0.0M implies K(I), or [LIG]init. to large?! ',/)
1031  FORMAT(2X,F6.3,' [Ag+]free is too small at Pt(s).')
1040  FORMAT(/,2X,' LOG K',3X,' SIGMA ',13X,' SIGMA**2 ',/)
1042  FORMAT(2X,F6.3,2X,G14.8,2X,G14.8,/, ' For the best LOG K',/)
1050  FORMAT(/,2X,' TIT.VOL.',3X,' mV',7X,' mV(Calc.)',5X,' Residual.',/)
1051  FORMAT(/,2X,' TIT.VOL.',3X,' [Na+]free',4X,' Calc',2X,' Resid.',/)
1052  FORMAT(/,2X,' TIT.VOL.',3X,' [Ag+]free',8X,' Calc.',14X,' Resid.',/)
1060  FORMAT(2X,F6.3,3X,F8.2,3X,F8.2,6X,F12.4)
1061  FORMAT(2X,F6.3,3X,F13.9,3X,F13.9,10X,F12.4)
1062  FORMAT(2X,F6.3,3X,F16.12,3X,F16.12,19X,F12.4)
1070  FORMAT(/,2X,I3,' points, best LOG K = ',F6.3,/)
1090  FORMAT(/,2X,' FOR LOG K = ',6X,' SIGMA = ',13X,' S**2 = ')
1091  FORMAT(3X,F6.3,8X,G13.7,7X,G13.7)
C 1092  FORMAT(/,2X,' FOR +- 10 PTS AROUND MIN. SIGMA...',/)
1200  FORMAT(A1)
C 2000  FORMAT(/,2X,' FOR THE SMALLEST SIGMA VALUE ...')
2010  FORMAT(2X,3(F6.3,6X))
2020  FORMAT(3(2X,F10.2))
2030  FORMAT(3(1X,F11.0),/)
2040  FORMAT(/,2X,' MULTIPLE PLOT FOR LOG K = ',F6.3,/)
END

```

```

SUBROUTINE FOO(HEADER, NUMB, XVAL, YVAL, YCALC, KA, KB, KC)
REAL*8 YVAL(200), XVAL(200), YCALC(200), YMIN, YMAX, XMIN, XMAX
REAL*8 XVALXX(200), YVALXX(200), XINT, YINT
INTEGER IARRAY(4)
CHARACTER HEADER*80, POINT*1, PRPOINT*3
COMMON/A/POINT

```

```

C          -MV          -FREE[Ag+]
CKA=    0 : DIFF.PLT    5 : DIFF.PLT    KB ... PLOT TYPES FOR EXPT. PTS
C       1 : THEOR.     6 : etc.        KC ... PLOT TYPES FOR CALC. PTS
C       2 : DIRECT     7 :           3 : COMPET.    8 :

```

```

IF (KA.GE.2) IPASS=2
IF (KA.EQ.5.OR.KA.EQ.6) IPASS=1
IF (KA.LT.2) IPASS=1
YMAX=-1.0E+25
YMIN=1.0E+25
XMAX=-1.0E+25
XMIN=1.0E+25
DO 10 I=1, NUMB
  IF (YVAL(I).GT.YMAX) YMAX=YVAL(I)
  IF (YVAL(I).LT.YMIN) YMIN=YVAL(I)
  IF (KA.GE.2.AND.KA.NE.6.AND.KA.NE.5) THEN
    IF (YCALC(I).GT.YMAX) YMAX=YCALC(I)
    IF (YCALC(I).LT.YMIN) YMIN=YCALC(I)
  ENDIF
  IF (XVAL(I).GT.XMAX) XMAX=XVAL(I)
  IF (XVAL(I).LT.XMIN) XMIN=XVAL(I)
10 CONTINUE
  IF (KA.LE.4) THEN
    YINT=(YMAX-YMIN)/100
    YINT=10.0*INT(YINT+1)
  ELSE
    YINT=0.05

```

```

        IF (KA.EQ.5) YINT=0.002
    ENDIF
XDELTA=(XMAX-XMIN)
IF (XDELTA.LT.3.0) THEN
    XINT=(XMAX-XMIN)/10.0
ELSE
    XINT=1.0
ENDIF
IF (KA.GE.1.AND.KA.NE.5) OPEN (UNIT=7, STATUS='NEW', FILE='VVIS.PLT')
IF (KA.EQ.0.OR.KA.EQ.5) OPEN (UNIT=7, STATUS='NEW', FILE='VVIS.DIF')
WRITE (UNIT=7, FMT=100) HEADER
WRITE (UNIT=7, FMT=200) NUMB
WRITE (UNIT=7, FMT=300)
    IF (YINT.LE.0.05) THEN
        DO 15 I=1, NUMB
            YVAL(I)=1000.*YVAL(I)
            YCALC(I)=1000.*YCALC(I)
15        CONTINUE
            YMIN=1000.*YMIN
            YMAX=1000.*YMAX
            YMIN=YMIN - 0.05
            IF (KA.EQ.5) YMIN=YMIN+0.048
        ELSE
            YMIN=YMIN-20.0
            YMAX=YMAX+10.0
C above: holds for mV only
    ENDIF
WRITE (UNIT=7, FMT=400) XMIN, XMAX, XINT
    IF (XINT.LT.0.1) THEN
        WRITE (UNIT=7, FMT=502)
    ELSE
        WRITE (UNIT=7, FMT=500)
    ENDIF
IF (KA.NE.5) WRITE (UNIT=7, FMT=600) YMIN, YMAX, YINT
IF (KA.EQ.5) WRITE (UNIT=7, FMT=601) YMIN, YMAX, YINT
IF (KA.GE.1.AND.KA.LE.4) WRITE (UNIT=7, FMT=700)
IF (KA.GT.5) WRITE (UNIT=7, FMT=701)
IF (KA.EQ.0.OR.KA.EQ.5) WRITE (UNIT=7, FMT=702)
WRITE (UNIT=7, FMT=750)
20    IF (KB.LE.4) WRITE (UNIT=7, FMT=800) KB
        IF (KB.GT.4.AND.KB.LT.9) WRITE (UNIT=7, FMT=801) (KB-4)
        IF (KB.EQ.9) WRITE (UNIT=7, FMT=802)
        WRITE (UNIT=7, FMT=900) NUMB
        IF (KB.NE.9) THEN
            WRITE (UNIT=7, FMT=1200) (XVAL(I), YVAL(I), I=1, NUMB)
        ELSE
            WRITE (UNIT=7, FMT=1210) (XVAL(I), YVAL(I), POINT, I=1, NUMB)
        ENDIF
        IF (KD.EQ.-1) WRITE (UNIT=7, FMT=1200) XVAL(NUMB), YVAL(1)
        IPASS=IPASS-1
        KB=KC
C activate line below for vert line at end of plots
    DO 30 I=1, NUMB
        YVAL(I)=YCALC(I)
30    CONTINUE
        IF (IPASS.EQ.1) GOTO 20
        RETURN
100 FORMAT (2X, A80)
200 FORMAT (2X, 'No.Pts= ', I5)
300 FORMAT (2X, ' ')
400 FORMAT (2X, 3 (F8.3, 2X), '0 1 12 NOARROW')
500 FORMAT (2X, 'Vol.Added ml')
502 FORMAT (2X, '1000*[Ctot]')
600 FORMAT (2X, 3 (F11.5, 2X), '0 2 9 NOARROW')
601 FORMAT (2X, 3 (F11.5, 2X), '0 5 9 2 NOARROW')
700 FORMAT (2X, ' mV')
701 FORMAT (2X, '[Ag+]free *1000 ')
702 FORMAT (2X, 'EXPTL. - CALC.')
750 FORMAT (2X, 'R 20.0')
800 FORMAT (2X, 'P ', I1)
801 FORMAT (2X, 'L ', I1)
802 FORMAT (2X, 'T Times-Roman 0.5')

```

```

900 FORMAT (2X, I3)
1200 FORMAT (2X, F10.6, 2X, G12.6)
1210 FORMAT (2X, F10.6, 2X, G12.6, 2X, '  ' , A1, '  ' )
      END

      SUBROUTINE JJJ (NUMB, XVAL, YVAL, YSQ, IARRAY)
      REAL*8 YVAL (249), XVAL (249), YSQ (249)
      REAL*8 XMAX, XMIN, XINT, YMAX, YMIN, YINT
      INTEGER IARRAY (4), IXXX (3), IYYY (3)
      YMAX=-1.0E+25
      YMIN=1.0E+25
      XMAX=-1.0E+25
      XMIN=1.0E+25
      DO 10 I=1, NUMB
          IF (YVAL (I) .GT. YMAX) YMAX=YVAL (I)
          IF (YVAL (I) .LT. YMIN) YMIN=YVAL (I)
          IF (XVAL (I) .GT. XMAX) XMAX=XVAL (I)
          IF (XVAL (I) .LT. XMIN) XMIN=XVAL (I)
10 CONTINUE
      YINT= (YMAX-YMIN)
      YMIN=YMIN-3*YINT
      YINT=YINT/10.0
      XINT=1.0
      IF (IARRAY (4) .LT. 0) THEN
          XMIN=XVAL (1)
          XMAX=XVAL (NUMB)
          IF ( (XMAX-XMIN) .LE. 0.1) XINT=0.1
      ENDIF
      OPEN (UNIT=8, STATUS='NEW', FILE='VVIS.MIN')
      WRITE (UNIT=8, FMT=100)
      WRITE (UNIT=8, FMT=200) NUMB
      WRITE (UNIT=8, FMT=300)
      WRITE (UNIT=8, FMT=400) XMIN, XMAX, XINT
      WRITE (UNIT=8, FMT=500) XVAL (IARRAY (1))
      WRITE (UNIT=8, FMT=600) YMIN, YMAX, YINT
      WRITE (UNIT=8, FMT=700)
      WRITE (UNIT=8, FMT=750)
      WRITE (UNIT=8, FMT=800)
      WRITE (UNIT=8, FMT=900) NUMB
      WRITE (UNIT=8, FMT=1200) (XVAL (I), YVAL (I), I=1, NUMB)
      WRITE (UNIT=8, FMT=800)
      WRITE (UNIT=8, FMT=901)
      WRITE (UNIT=8, FMT=1200) XVAL (NNNN), (YMIN+30*YINT)
      WRITE (UNIT=8, FMT=1200) XVAL (NNNN), YMAX
      DO 80 I=2, 3
          IXXX (I) =IARRAY (I)
          IYYY (I) =IARRAY (I)
80 CONTINUE
      IF (IARRAY (2) .EQ. 0 .AND. IARRAY (3) .EQ. 0) THEN
          GOTO 90
      ELSE
          IF (IARRAY (2) .EQ. 0) IXXX (2) =1
          IF (IARRAY (2) .EQ. 0) IYYY (2) =NUMB
          IF (IARRAY (2) .EQ. 0) IXXX (3) =NUMB
          IF (IARRAY (2) .EQ. 0) IYYY (2) =1
          WRITE (UNIT=8, FMT=800)
          WRITE (UNIT=8, FMT=901)
          WRITE (UNIT=8, FMT=1200) (XVAL (IXXX (I)), YVAL (IYYY (I)), I=2, 3)
90 ENDIF
      RETURN
100 FORMAT (2X, ' SIGMAPLT')
200 FORMAT (2X, 'No.Pts= ', I5)
300 FORMAT (2X, ' ')
400 FORMAT (2X, 3 (F8.5, 1X), '0 1 18 NOAXIS')
500 FORMAT (2X, 'LOG K (MIN) = ', F6.3)
600 FORMAT (2X, 3 (G14.8, 1X), '0 2 16 NOAXIS')
700 FORMAT (2X, ' SIGMA FXN')
750 FORMAT (2X, 'R 20.0')
800 FORMAT (2X, 'L 1')
900 FORMAT (2X, I3)
901 FORMAT (2X, '2')
1200 FORMAT (2X, F10.6, 2X, G14.8)

```

```
END

SUBROUTINE APPEND (NUMB, XVAL, YCALC, KB)
REAL*8 XVAL (200), YCALC (200)
OPEN (UNIT=9, STATUS='UNKNOWN', FILE='APPEND.PLT')
WRITE (UNIT=9, FMT=801) KB-4
WRITE (UNIT=9, FMT=900) NUMB
WRITE (UNIT=9, FMT=1200) (XVAL (I), YCALC (I), I=1, NUMB)
RETURN
801 FORMAT (2X, 'L ', I1)
900 FORMAT (2X, I3)
1200 FORMAT (2X, F10.6, 2X, G12.6)
END
```

VAX- VMS 4.1 Macro for Executing the Program VISP

```
$ start:
$ directory
$ write sys$output " "
$ inquire P1 "data file name? "
$ on error then exit
$ if P1 .eqs. "" then exit          ! exit if no file given
$ write sys$output " "
$ copy 'P1' for003.dat
$ $run d2:[pclarke.titration]visp.exe
$ write sys$output " "
$ write sys$output " Output files will be renamed to "
$ write sys$output " **** .out, .plt, .dif and .min suffixes"
$ write sys$output " "
$ inquire P2 "Rename system to: (don't include suffix)?"
$ write sys$output " "
$ rename vvis.*; 'P2'.*;
$ rename for004.dat 'P2'.out
$ write sys$output " "
$ inquire P9 " more data?"
$ if P9 then goto start
$ delete/noconfirm/nolog for00*.dat;*
$ write sys$output " "
$ exit
```

Example Input Data File

```
Cs+ c22c5 in methanol compet.Ag+ titr.  
28.61,124.7  
2,0  
1,5,0  
1,2  
6.3,0.01  
0.003052,0.0001003,0.0031  
0.0      -139.4  
0.0      -140.6  
0.1      -151.8  
0.2      -166.0  
0.3      -242.0  
0.4      -318.8  
0.5      -424.0  
0.6      -467.8  
0.7      -495.8  
0.8      -517.0  
0.9      -532.6  
1.0      -530.0  
1.2      -539.5  
1.4      -550.2
```

The Program VISP, Acknowledgements

The FOO, and JJJ subroutines generate a text file in the format required by the graphics drawing program DRAW for the VAXen and Unix networks at the University of Adelaide and was kindly provided by D. Beard, University of Adelaide.

This program was originally written by P. Clarke with additional assistance from U. Nachstedt (Universität Bielefeld, Germany) in FORTRAN-77 to execute on a VAX 11-780 mainframe computer, 1989.

Appendix iii : LINSHP a FORTRAN-77 Program for the VAX 11-780 Computer

PROGRAM LINSHP

```

C -----
C PROGRAM TO MATCH EXPERIMENTAL AND THEORETICAL SPECTRA FOR
C SEVERAL COALESCING DOUBLETS (UP TO 10).
C BY DENSITY MATRIX METHOD (JOHNSON,1969).
C THE TOTAL NUMBER OF POINTS IN THE THEORETICAL SPECTRUM MUST
C BE LESS THAN OR EQUAL TO 1,000.
C T.M.SPOTSWOOD AUGUST 1973
C THIS VERSION CONVERTED TO FORTRAN 5 AND MODIFIED A.WHITE
C MAY 1983 MORE CONVERSIONS P.CLARKE APR. 1988.
C CONVERTED TO DENSITY MATRIX JUN. 1988
C -----
C To LINK the IMSL Subroutines library to your program use
C the following DCL command.
C $ LINK yourprogram,SYS PACK:IMSLIBx/LIB
C x = s for SINGLE precision
C d for DOUBLE precision
C TERM IS ZERO IF THIS IS THE LAST DECK ,NOT ZERO IF THERE ARE
C MORE DECKS TO COME.
C LPX IS THE POINT NUMBER TO START FIT.
C KNTL1 ETC ARE CONTROL PARAMETERS.
C IF KNTL1 = 1 THE QUICKPLOT OF ERROR VS SHIFT IS SUPPRESSED
C EXCEPT FOR THE BEST VALUE OF R.
C IF KNTL1 = 2 THE QUICKPLOT OF ERROR VS SHIFT IS SUPPRESSED
C COMPLETELY.
C IF KNTL2 IS > OR = TO 1 THEORETICAL QUICKPLOTS WILL BE PRODUCED,
C IF KNTL2 = 1 THEORETICAL ONLY IS ASSUMED
C THE CORRESPONDING VALUE OF R IS RECORDED BELOW EACH PLOT,
C IF KNTL3 = 1, A ZETA PLOT WILL BE PRODUCED,EXPTL AND THEOR.
C IF KNTL3 = 2, [BEARD] DRAW FILE PRODUCED
C IF KNTL4 = 0, TABLE OF FREQ,Y(EXPT),Y(EXPT)NORM,Y(CALC) IS PRINTED
C IF KNTL4 = 2, TABLE OF FREQ,Y(EXPT)NORM,Y(CALC) IS PRINTED
C IF KNTL5 = 0, THE PROGRAM ASSUMES FOUR SITE J-COUPLED EXCHANGE
C IF KNTL5 = 2, THE PROGRAM ASSUMES TWO SITE EXCHANGE
C CALCULATED BY THE NAKAGAWA METHOD
C R IS THE LOWER LIMIT OF VISUALLY ESTIMATED RANGE OF RATE CONSTANTS
C STEP IS THE RATE CONSTANT STEP SIZE.
C NO IS THE NUMBER OF STEPS.
C LPT IS THE NUMBER OF EXPERIMENTAL POINTS
C NSH IS THE MAXIMUM NUMBER OF POINTS TO BE SHIFTED FOR MAXIMUM
C OVERLAP
C BETWEEN THEORETICAL AND EXPERIMENTAL SPECTRA (IN UNITS OF SINC)
C START AND END ARE THE THEORETICAL START AND END FREQUENCIES.
C FRF AND FRE ARE THE EXPERIMENTAL START AND END FREQUENCIES.
C THEORETICAL SPECTRA ARE QUICKPLOTED FOR R=R TO R=R+STEP*(NO-1)
C THEN R IS SET EQUAL TO THE FIRST EXPERIMENTAL POINT (YT(IL)) AND
C QUICKPLOTS ARE PRODUCED FOR R=YT(IL) TO R=YT(IL)+STEP*(NO-1)
C AND SO ON FOR ALL THE EXPERIMENTAL POINTS.
C NPOP = -1 FOR DIAGNOSTIC INFORMATION TO BE PRINTED.
C NPEK IS THE NUMBER OF DOUBLETS.
C XJ(I) = THE COUPLING CONSTANT IN HERTZ
C WA(I) AND WB(I) ARE THE WIDTHS AT HALF HEIGHT OF PEAKS A AND B
C OF DOUBLET I.
C FRA(I) AND FRB(I) ARE THE FREQUENCIES OF A AND B OF DOUBLET I.
C PA(I) AND PB(I) ARE THE POPULATIONS OF ENVIRONMENTS A AND B OF
C DOUBLET I.
C FSCAL(I) IS THE INTERDOUBLET SCALING FACTOR.
C -----

```

```

DIMENSION RA(10),RB(10),PA(10),PB(10),FRA(10),FRB(10)
DIMENSION YT(2100),NN(2100,2),F(2100),B(4200),XJ(10),FSCAL(10)
DIMENSION XDIF(200),AXMIN(200),AR(200),SHIFF(200),STDY(2100)
C !STDY=standardized y
DIMENSION WA(10),WB(10),TAU1(10),TAU2(10),DIFRAY(2100)
COMMON/A/YT,NN,F,B,XDIF,SHIFF
COMMON/B/NPT,LPT,IL,LL,JTOT,NSH,LPX
COMMON/C/STV(200),SDV(200)
COMMON/D/RA,RB,FRA,FRB,R,PA,PB,SUMX,FN,WA,WB,XJ
COMMON/E/KNTL2,FSCAL
CHARACTER HEAD*80
REAL NN,L,K,INTENS
PI=3.14159
ISW=1
IRCNT=0
1 READ (3,1010,END=10000)HEAD !INPUT DATA
READ (3,*,END=10000)TERM,LPX,KNTL1,KNTL2,KNTL3,KNTL4,KNTL5
READ (3,*,END=10000)R,STEP,NO
READ (3,*,END=10000)LPT,NSH,START,END,FRF,FRE
READ (3,*,END=10000)NPOP,NPEK,XJ(1),XJ(2)
10000 DO 10 I=1,NPEK
READ (3,*,END=10)WA(I),WB(I),FRA(I),FRB(I),PA(I),PB(I),FSCAL(I)
IF(KNTL5.EQ.0) THEN
RA(I) = 1./(PI*WA(I))
RB(I) = 1./(PI*WB(I))
ELSE
IF(KNTL5.EQ.2) THEN
DELTA = ABS(2.0 * (FRA(I) - FRB(I) ))
RA(I) = WA(I) / DELTA
RB(I) = WB(I) / DELTA
ENDIF
ENDIF
10 CONTINUE
C CALCULATE NO OF POINTS IN PLOT
IF(KNTL2.EQ.1) THEN
LPTT=LPT
LPT=500
ENDIF
IF(END.EQ.0.)END=100.
FR=(FRE-FRF) !delta freq. Df
SINC=FR/FLOAT(LPT) !delta freq./n Df/N
NPT= NINT((END-START)/SINC) !NPT=Df(calc)/Df(expt)*n(expt)
C
C CLEAR Y AND PLACE EXPTL POINTS IN CORRECT POSITION
DO 15 I=1,1000
YT(I)=0.
IL=NINT((FRF-START)/SINC)
IF(IL.LE.0)IL=1
LL=IL+LPT-1
IF(NPOP.EQ.-1) WRITE(4,2000) IL,LL
IF(KNTL2.NE.1)THEN
READ(3,1060,END=10001)(YT(I),I=IL,LL)
10001 CONTINUE
ENDIF
IF(NPOP.EQ.-1) WRITE(4,2005) (YT(I),I=IL,LL)
20 CONTINUE
AMN=R
WRITE(4,2010) HEAD
IF(NPOP.EQ.-1) THEN
WRITE(4,2020) (I,RA(I),RB(I),PA(I),PB(I),FRA(I),FRB(I),FSCAL(I),
+XJ(I),I=1,NPEK)
WRITE(4,2025) (I,WA(I),WB(I),I=1,NPEK)
WRITE(4,2030) LPT,NPT,NSH
WRITE(4,2040) START,END,FRF,FRE
WRITE(4,2080) R,STEP,NO
WRITE(4,2090) KNTL1,KNTL2,KNTL3,KNTL4,KNTL5
ENDIF
30 CONTINUE
IF(ISW.EQ.0)NO=1
DO 100 IJK=1,NO
R=AMN+(IJK-1)*STEP
DO 35 IM=1,1000

```



```

NN(IM,1)=0.
35 NN(IM,2)=0.
   DO 40 J=1,NPT
   F(J)=START+J*SINC
40 CONTINUE
   IF(KNTL5.EQ.0) THEN
   CALL DENSE(F,NN(1,1),XJ(1),XJ(2))
   ELSE
   IF(KNTL5.EQ.2) THEN
   DO 500 I=1,NPEK
   DAB=ABS(FRB(I)-FRA(I))
   RRA=RA(I)
   RRB=RB(I)
   PPA=PA(I)
   PPB=PB(I)
   AA=2.0*PI*DAB/R
   DO 700 J=1,NPT
   FL=(F(J)-FRA(I))/DAB
   K=(RRA*PPA+RRB*PPB)+AA*(RRA*RRB-FL*(FL-1.0))
   L=FL*(1.0+AA*RRA+AA*RRB)-(AA*RRA+PPB)
   INTENS=((1.0+AA*RRA*PPB+AA*RRB*PPA)*K
+ AA*(FL+PPB-1.0)*L)/(K*K+L*L)
   INTENS=FSCAL(I)*ABS(INTENS)
   NN(J,1)=NN(J,1)+INTENS
700 CONTINUE
500 CONTINUE
   ELSE
   WRITE(4,2200)
   ENDIF
   ENDIF
C
C NAKAGAWA METHOD FOR TWO SITE LINESHAPE ANALYSIS
C WHERE A = 2 Pi|Va-Vb| / R
C AND FL= (V-Vb) / (Vb-Va)
C AND RRA = Wa / ( 2*|Va-Vb| ) ditto for RRB
C AND INTENS = THE SIGNAL INTENSITY AT FREQ. V
C THIS PROGRAM IS CURRENTLY SET FOR EQUAL POPULATION DOUBLETS
C (E.G. PA(1)+PB(1) = PA(2)+PB(2))
C
   IF(KNTL2.GE.1) THEN
   WRITE(4,2097) R
   IF(KNTL2.EQ.1) THEN
   DO 42 I=1,NPT
   B(I)=NN(I,1)
42 CONTINUE
   CALL QIKPLT(0,LPT,B,B,F)
C QIKPLT A THEORETICAL ONLY HERE
   ENDIF
   ENDIF
   IF(KNTL2.EQ.1) GO TO 100
C NORM SCALES EXPTL SPECTRUM TO THEOR ON AREAS AND STORES IN
C NNN(1:NPT,2).
C COMP IS FOR A NON-SHIFTED COMPARISON.
   CALL NORM
   CALL COMP(1)
   CALL SHIFT
   IF(KNTL1.EQ.2) GOTO 49
   IF(KNTL1.EQ.1.AND.NO.GT.1)GO TO 49
   DO 45 I=1,NPT
   DIFRAY(I)=STDY(I)-NN(I,1)
45 CONTINUE
C CALL QIKPLT(0,NPT,DIFRAY,DIFRAY,F)
C QIKPLT A DIFFERENCE SPEC. HERE
49 CONTINUE
   AMIN=XDIF(1)
   IM=1
   DO 50 I=2,JTOT
   IF(XDIF(I).LT.AMIN) THEN
   AMIN=XDIF(I)
   IM=I
   II=2*(I-1)+LPX
C

```

```

C      DETERMINE ACTUAL INCREMENT FROM INDEX I
      ENDIF
50     CONTINUE
C
C      STORE THE MINIMUM VALUE FOR COMPARISON
      AXMIN(IJK)=AMIN
      AR(IJK)=R
      SDV(IJK)=STV(IM)
C
C      SHIFT THEORETICAL SPECTRUM AND ADJUST POSITION B LOCATION
      DO 60 I=1,1000
60     B(I)=0.
      MX=II-IL
      DO 70 KK=1,NPT
      IF(KK+MX.GT.NPT.OR.KK+MX.LE.0) THEN
        B(KK)=0.
      ELSE
        B(KK)=NN(KK+MX,1)
      ENDIF
70     CONTINUE
100    CONTINUE
      IF(KNTL2.EQ.1) THEN
        IF(IRCNT.GE.LPTT) GOTO 150
        R = YT(IRCNT + IL)
        IRCNT = IRCNT + 1
        GOTO 20
      ENDIF
C
C      RETURN TO 20 IF KNTL2 = 1 TO PRINT QIKPLTS FOR ALL R VALUES.
      IF(NO.EQ.1) WRITE(4,2060)
      WRITE(4,2100) (I,AR(I),AXMIN(I),SDV(I),I=1,NO)
      XMN=AXMIN(1)
      IFL=1
      IF(NO.EQ.1)GO TO 115
      DO 110 I=1,NO
      IF(AXMIN(I).LT.XMN) THEN
        XMN=AXMIN(I)
        IFL=I
      ENDIF
110    CONTINUE
C
C      QIKPLT S THE RMS ERROR VALUES
      CALL QIKPLT(0,NO,AXMIN,AXMIN,AR)
C
C      NOW RECALCULATE THE THEORETICAL SPECTRUM AND ADJUST WITH THIS R
      ISW=0
      AMN=AR(IFL)
      GO TO 30
115    CONTINUE
      DO 116 K=1,NPT
      STDY(K)=NN(K,2)
116    CONTINUE
      WRITE(4,2110)
      CALL QIKPLT(1,NPT,STDY,B,F)
C      !Y(TH) vs Y(EX)
      DO 119 I=1,NPT
      DIFRAY(I)=B(I)-STDY(I)
C      !DIFFERENCE SPEC.
119    CONTINUE
      CALL QIKPLT(0,NPT,DIFRAY,DIFRAY,F)
      IF(KNTL4.EQ.0)THEN
        WRITE(4,2130)
        WRITE(4,2140) (F(I),YT(I),NN(I,2),B(I),I=1,NPT)
      ENDIF
      IF(KNTL4.EQ.2)THEN
        WRITE(4,2135)
        WRITE(4,2145) (F(I),NN(I,2),B(I),I=1,NPT)
      ENDIF
120    CONTINUE
      WRITE(4,2160) HEAD
      DO 145 LF=1,NPEK
      TAU1(LF)=1./(AR(1)*PA(LF))

```

```

145  TAU2(LF)=1./(AR(1)*PB(LF))
      WRITE(4,2170) AR(1),AXMIN(1),SDV(1)
      WRITE(4,2180)
      WRITE(4,2190) (I,PA(I),WA(I),TAU1(I),PB(I),WB(I),TAU2(I),I=1,NPEK)
      IF(KNTL3.EQ.2)CALL FOO(HEAD,NPT,STDY,B,F)
      IF(TERM.NE.0.) THEN
          ISW=1
          GO TO 1
      ENDIF
C
C      RETURN TO READ STATEMENTS IF THERE ARE MORE DECKS OF DATA
C      (I.E. IF TERM IS NOT ZERO) .
150  CONTINUE
1010 FORMAT(BZ,A80)
1020 FORMAT(A80)
1060 FORMAT(BZ,10F9.2)
2000 FORMAT('0////////// DIAGNOSTIC INFORMATION ////////// STORAGE OF
      + THE EXPTL DATA IS IN ELEMENTS ',I3,' TO ',I3)
2010 FORMAT(1H1,10X,A80)
2020 FORMAT(1H ,5X,'DOUBLET',I5,5X,'RA = ',F10.5,2X,'RB= ',F10.5,2X,
      + 'PA=',F10.5,2X,'PB= ',F10.5,40X,'FRA=',F10.5,2X,'FRB=',F10.5,
      + 2X,'FSCAL= ',F2.0,' XJ= ',F6.3/)
2025 FORMAT('0 THE ABOVE RA/RB VALUES WERE CALCULATED FROM THE FOLLOWIN
      1G WIDTHS AT HALF HEIGHT.'/3X,
      + ' PEAK NO.',11X,'WA (HZ)',13X,'WB (HZ)'/
      + ( I9,11X,F10.3,10X,F10.3))
2030 FORMAT(1H0,' EXPTL POINTS',I5,' THEOR POINTS',I5,' SHIFT RANGE',
      + I5)
2040 FORMAT(1H0,'START',F10.5,10X,'END',F10.5,10X,'START(EXPT)',F10.5,
      + 10X,'END(EXPT)',F10.5/)
2060 FORMAT(1H , 'THE BEST VALUES OF R AND ERRORS ARE')
2080 FORMAT(1H ,20X,'VALUE OF R = ',F10.3,10X,'STEP =',F10.5,10X,'NO ='
      + ,I5/)
2090 FORMAT(1H ,20X,'VALUES OF CONTROL PARAMETERS ARE',5X,5(5X,I5))
2095 FORMAT('////////0 THIS IS A 'I1
      + ' SITE PROBLEM.'/,T23,'THE KS PROBABILITY MATRIX USED IS...'/
      + ,(T24,8F10.4))
2097 FORMAT(1H ,10X,'THEORETICAL PLOT FOR R =',F10.2/)
2100 FORMAT(1H , 'RUN NO',I5,5X,'VALUE OF R',F10.2,5X,'RMS
      + ERROR',F10.5,15X,'STANDARD DEVIATION',F10.8)
2110 FORMAT(1H ,40X,'EXPERIMENTAL SPECTRUM')
2120 FORMAT(1H ,40X,'SHIFTED THEORETICAL SPECTRUM')
2130 FORMAT(1H1,2(5X,'FREQUENCY',7X,'Y(EXPT)',7X,'Y(EXPT)NORM',4X,'
      + Y(CALC)'))
2135 FORMAT(1H ,3(2X,'FREQUENCY',5X,'Y(EXPT)NORM',5X,'Y(CALC)'))
2140 FORMAT(1H ,8(5X,F10.5))
2145 FORMAT(1H ,3(2X,F10.2,2(2X,F10.5)))
2160 FORMAT('1',40X,'SUMMARY FOR ',A80)
2170 FORMAT('/' BEST R VALUE IS ',F8.2,' . ITS RMS ERROR IS ',F10.5
      + ', AND STANDARD DEVIATION,',F10.5)
2180 FORMAT(' BASED ON THIS R VALUE, THE BOUND LIFETIME IS AS BELOW'
      + '/' (N.B. TAU(B)=1/(R*POPN(F) ) AS POPN(F) IS EITHER PA OR PB, TAU
      2 IS CALCULATED FOR BOTH.))
2190 FORMAT('0DOUBLET NO.',2X,'I',3X,'POPN. A',11X,'WIDTH',13X,'TAU',12
      + X,'I',2X,'POPN. B',11X,'WIDTH',13X,'TAU'/(1X,I10,3X,'I',3X,F1
      + 0.6,8X,F10.3,8X,E14.7,' I',2X,F10.6,8X,F10.3,8X,E14.7 ))
2200 FORMAT(1X,'NON-VALID SITE EXCHANGE VALUE')
2005 FORMAT('0////////// DIAGNOSTIC INFORMATION ////////// THE EXPTL
      +DATA READ IN IS.../(8E15.7))
      END

```

```

SUBROUTINE DENSE(FR, FN, XJ1, XJ2)
C   T1, T2, T3, T4 ARE THE RECIPROCAL TRANSVERSE RELAXATION TIMES FOR
C   SITES 1, 2, 3, 4 IN THE ABSENCE OF EXCHANGE - MEASURED FROM
C   LINEWIDTHS. R IS THE RECIPROCAL LIFETIME OF A PROTON IN SITE 1.
C   N.B. TAU(1)/P(1)=TAU(2)/P(2)=TAU(3)/P(3)=TAU(4)/P(4) ETC.
C   THIS RATIO IS INCORPORATED IN THE PROBABILITY MATRICES ADENSE
C   AND BDENSE TO OBTAIN TAU(2), TAU(3), TAU(4) IN TERMS OF TAU(1).
C   DEL2-DEL4 ARE THE RESPECTIVE PROPORTIONALITY CONSTANTS.
C   A TERMS ARE ELEMENTS OF THE KUBO SACK MATRIX
C   THE IMSL LIBRARY ROUTINE LEQT1C IS USED TO INVERT A.MATRIX ZZ
C   IS THE INVERSE OF A. INITIALLY ZZ IS THE COMPLEX UNITY MATRIX.
DIMENSION RA(10), RB(10), PA(10), PB(10), FRA(10), FRB(10)
DIMENSION FR(2100), FN(2100)
DIMENSION ADENSE(4, 4), BDENSE(4, 4), B(4), CC(8)
DIMENSION T(4), F(4)
DIMENSION WORKA(4), WORKB(4), ZI(4, 4), ZII(4, 4)
COMMON/B/NPT, LPT, IL, LL, JTOT, NSH, LPX
COMMON/D/RA, RB, FRA, FRB, R, PA, PB, SUMX
COMPLEX WORKA, WORKB, ZI, ZII, ADENSE, BDENSE
COMPLEX CC, B, SUMX
PI=3.14159

C
C   UNIVERSAL DEFINITIONS FIRST.
T(1)=1./RA(1)
T(2)=1./RB(1)
T(3)=1./RA(2)
T(4)=1./RB(2)
F(1)=FRA(1)
F(2)=FRB(1)
F(3)=FRA(2)
F(4)=FRB(2)
DEL2=PA(1)/PB(1)
DEL3=PA(1)/PA(2)
DEL4=PA(1)/PB(2)

C
C   THE MAJOR LOOP.           R=1/(TAU(a)*POP(b)) (TWO SITS)
DO 100 JN=1, NPT
X= 0.50
ADENSE(1, 1) = CMPLX(-T(2)-R, -2*PI*(F(2)-FR(JN)+X*XJ1))
ADENSE(1, 2) = CMPLX(0.0, 2*PI*X*XJ1)
ADENSE(1, 3) = CMPLX(0.0, 0.0)
ADENSE(1, 4) = CMPLX(DEL2*R, 0.0)
ADENSE(2, 1) = CMPLX(0.0, 2*PI*X*XJ1)
ADENSE(2, 2) = CMPLX(-T(1)-DEL2*R, -2*PI*(F(1)-FR(JN)+X*XJ1))
ADENSE(2, 3) = CMPLX(R, 0.0)
ADENSE(2, 4) = CMPLX(0.0, 0.0)
ADENSE(3, 1) = CMPLX(0.0, 0.0)
ADENSE(3, 2) = CMPLX(DEL4*R, 0.0)
ADENSE(3, 3) = CMPLX(-T(4)-DEL3*R, -2*PI*(F(4)-FR(JN)+X*XJ2))
ADENSE(3, 4) = CMPLX(0.0, 2*PI*X*XJ2)
ADENSE(4, 1) = CMPLX(DEL3*R, 0.0)
ADENSE(4, 2) = CMPLX(0.0, 0.0)
ADENSE(4, 3) = CMPLX(0.0, 2*PI*X*XJ2)
ADENSE(4, 4) = CMPLX(-T(3)-DEL4*R, -2*PI*(F(3)-FR(JN)+X*XJ2))
X= -0.50
BDENSE(1, 1) = CMPLX(-T(2)-R, -2*PI*(F(2)-FR(JN)+X*XJ1))
BDENSE(1, 2) = CMPLX(0.0, 2*PI*X*XJ1)
BDENSE(1, 3) = CMPLX(0.0, 0.0)
BDENSE(1, 4) = CMPLX(DEL2*R, 0.0)
BDENSE(2, 1) = CMPLX(0.0, 2*PI*X*XJ1)
BDENSE(2, 2) = CMPLX(-T(1)-DEL2*R, -2*PI*(F(1)-FR(JN)+X*XJ1))
BDENSE(2, 3) = CMPLX(R, 0.0)
BDENSE(2, 4) = CMPLX(0.0, 0.0)
BDENSE(3, 1) = CMPLX(0.0, 0.0)
BDENSE(3, 2) = CMPLX(DEL4*R, 0.0)
BDENSE(3, 3) = CMPLX(-T(4)-DEL3*R, -2*PI*(F(4)-FR(JN)+X*XJ2))
BDENSE(3, 4) = CMPLX(0.0, 2*PI*X*XJ2)
BDENSE(4, 1) = CMPLX(DEL3*R, 0.0)
BDENSE(4, 2) = CMPLX(0.0, 0.0)
BDENSE(4, 3) = CMPLX(0.0, 2*PI*X*XJ2)
BDENSE(4, 4) = CMPLX(-T(3)-DEL4*R, -2*PI*(F(3)-FR(JN)+X*XJ2))
DO 42 I=1, 4

```

```

DO 41 J=1,4
IF (I.EQ.J) THEN
  ZI(I,I)=(1.0,0.0)
  ZII(I,I)=(1.0,0.0)
ELSE
  ZI(I,J)=(0.0,0.0)
  ZII(I,J)=(0.0,0.0)
ENDIF
41 CONTINUE
42 CONTINUE
B(1)=PA(1)
B(2)=PB(1)
B(3)=PA(2)
B(4)=PB(2)
CALL LEQT1C (ADENSE,4,4,ZI,4,4,0,WORKA,IER)
CALL LEQT1C (BDENSE,4,4,ZII,4,4,0,WORKB,IER)
CC(1)=B(1)*ZI(1,1)+B(2)*ZI(2,1)+B(3)*ZI(3,1)+B(4)*ZI(4,1)
CC(2)=B(1)*ZI(1,2)+B(2)*ZI(2,2)+B(3)*ZI(3,2)+B(4)*ZI(4,2)
CC(3)=B(1)*ZI(1,3)+B(2)*ZI(2,3)+B(3)*ZI(3,3)+B(4)*ZI(4,3)
CC(4)=B(1)*ZI(1,4)+B(2)*ZI(2,4)+B(3)*ZI(3,4)+B(4)*ZI(4,4)
CC(5)=B(1)*ZII(1,1)+B(2)*ZII(2,1)+B(3)*ZII(3,1)+B(4)*ZII(4,1)
CC(6)=B(1)*ZII(1,2)+B(2)*ZII(2,2)+B(3)*ZII(3,2)+B(4)*ZII(4,2)
CC(7)=B(1)*ZII(1,3)+B(2)*ZII(2,3)+B(3)*ZII(3,3)+B(4)*ZII(4,3)
CC(8)=B(1)*ZII(1,4)+B(2)*ZII(2,4)+B(3)*ZII(3,4)+B(4)*ZII(4,4)
SUMX=(0.,0.)
SUMX=CC(1)+CC(2)+CC(3)+CC(4)+CC(5)+CC(6)+CC(7)+CC(8)
FN(JN)=REAL(SUMX)
FN(JN)=ABS(FN(JN))
100 CONTINUE
RETURN
END

SUBROUTINE NORM
C SCALES EXPTL SPECTRUM TO THEORETICAL ON AREAS AND STORES IN NN(1:NPT,2).
DIMENSION YT(2100),NN(2100,2),F(2100),B(4200)
DIMENSION XDIF(200),SHIFF(200)
COMMON/A/YT,NN,F,B,XDIF,SHIFF
COMMON/B/NPT,LPT,IL,LL,JTOT,NSH,LPX
COMMON/C/STV(200),SDV(200)
REAL NN
SUM1=0.
SUM2=0.
SUM=0.
DO 1 I=1,10
IA=IL+I-1
IB=LL-I+1
1 SUM=SUM+YT(IA)+YT(IB)
SUM=SUM/20.
YMAX=YT(1)
DO 5 IJ=1,NPT
IF (YT(IJ).GT.YMAX) YMAX=YT(IJ)
5 CONTINUE
YS=(YMAX-SUM)/30.
DO 10 I=1,NPT
C AN ARBITRARY CUT OFF FOR NORMALIZING DISCARDING LOW INTENSITY
IF ((YT(I)-SUM).LE.YS) GO TO 10
SUM1=SUM1+NN(I,1)
SUM2=SUM2+YT(I)-SUM
10 CONTINUE
IF (SUM2.EQ.0.) THEN
RE = 1.
ELSE
RE = SUM1/SUM2
ENDIF
DO 20 J=1,NPT
NN(J,2)=(YT(J)-SUM)*RE
IF (NN(J,2).LT.0.) NN(J,2)=0.
IF (J.LT.IL.OR.J.GT.LL) NN(J,2)=0.
20 CONTINUE
RETURN
END

```

```

SUBROUTINE COMP (LQ)
C   COMP IS FOR A NON SHIFTED COMPARISON
   DIMENSION YT (2100), NN (2100, 2), F (2100), B (4200)
   DIMENSION XDIF (200), SHIFF (200)
   COMMON/A/YT, NN, F, B, XDIF, SHIFF
   COMMON/B/NPT, LPT, IL, LL, JTOT, NSH, LPX
   COMMON/C/STV (200), SDV (200)
   REAL NN
   S2=0.
   DO 10 I=1, NPT
     S=NN (I, 1) - NN (I, 2)
10  S2=S*S+S2
   XDIF (LQ) = SQRT (S2 / FLOAT (NPT))
   RETURN
   END

SUBROUTINE SHIFT
   DIMENSION YT (2100), NN (2100, 2), F (2100), B (4200)
   DIMENSION XDIF (200), AXMIN (200), AR (200), SHIFF (200)
   COMMON/A/YT, NN, F, B, XDIF, SHIFF
   COMMON/B/NPT, LPT, IL, LL, JTOT, NSH, LPX
   COMMON/C/STV (200), SDV (200)
   REAL NN
   KI=0
   DO 5 I=1, 200
     SHIFF (I) = 0.
5  CONTINUE
   IF (LPX.EQ.0) LPX=2
   JSH=LPX+NSH
   DO 20 J=LPX, JSH, 2
     IF (LPT+J.GT.NPT) GO TO 20
     KI=KI+1
     DIF1=0.
     DIF2=0.
     DO 10 IP=IL, LL
       JP=IP-IL+J
       DIF=NN (JP, 1) - NN (IP, 2)
       DIF1=DIF1+DIF
       DIF2=DIF*DIF+DIF2
10  CONTINUE
     XDIF (KI) = SQRT (DIF2 / FLOAT (LPT))
     SHIFF (KI) = J
     STV (KI) = SQRT ((DIF2 - DIF1 * DIF1 / FLOAT (LPT)) / (FLOAT (LPT) - 1.))
20  CONTINUE
   JTOT=KI
   RETURN
   END

SUBROUTINE QIKPLT (IEXP, N, YE, YC, X) ! IEXP=0 RESID. PLOT
   IMPLICIT REAL*8 (A-H, O-Z) ! IEXP=1 Y(EX) vs Y(TH) PLOT
   DIMENSION YE (2100), YC (4200), X (2100), XX (101)
   DIMENSION YY (101), EE (101)
   ISHTAR=N
   IF (N.GT.100) THEN
     SCALEF=ISHTAR/100
     NUNGA=INT (SCALEF) + 1
     J=1
     DO 100 I=1, ISHTAR, NUNGA
       YY (J) = YC (I) ! CALC
       XX (J) = X (I)
       EE (J) = YE (I) ! EXPT
       J=J+1
100  CONTINUE
     ISHTAR=J
   ELSE
     DO 200 I=1, ISHTAR
       YY (I) = YC (I)
       XX (I) = X (I)
200  EE (I) = YE (I)
   ENDIF
   CALL PLXY (IEXP, ISHTAR, EE, YY, XX)
   RETURN
   END

```

```

SUBROUTINE PLXY (IEXP, N, E, Y, X)
C T.KURUCSEV'S QUICKPLOTING ROUTINE
  IMPLICIT REAL*8 (A-H, O-Z)
  DIMENSION Y (200), X (200), E (200), IY (201), IX (201), IE (201), IP (101),
+XVAL (10)
  CHARACTER IB*1, IC*1, IV*1, IEQ*1, IPP (101)
  DATA IB, IC, IV, IEQ/' ', 'O', 'X', '='/
  IF (IEXP.NE.0) GOTO1010
  DO 1000 I=1, N
1000 E (I)=Y (I)
1010 XMAX=-1.0D+25
  YMAX=-1.0D+25
  XMIN=+1.0D+25
  YMIN=+1.0D+25
  DO 1020 I=1, N
  IF (X (I).GT.XMAX) XMAX=X (I)
  IF (X (I).LT.XMIN) XMIN=X (I)
  IF (Y (I).GT.YMAX) YMAX=Y (I)
  IF (E (I).GT.YMAX) YMAX=E (I)
  IF (Y (I).LT.YMIN) YMIN=Y (I)
  IF (E (I).LT.YMIN) YMIN=E (I)
1020 CONTINUE
  XINC=(XMAX-XMIN)/100.0D0
  YINC=(YMAX-YMIN)/50.0D0
  YVAL=YMAX
  WRITE (4, 310)
  WRITE (4, 320)
  DO 1030 I=1, N
  IY (I)=0
  IX (I)=0
1030 IE (I)=0
  DO 1040 I=1, N
  IK=INT (0.5D0+(Y (I)-YMIN)/YINC)
  II=51-IK
  IY (I)=II
  IK=INT (0.5D0+(X (I)-XMIN)/XINC)
  II=IK+1
  IX (I)=II
  IK=INT (0.5D0+(E (I)-YMIN)/YINC)
  II=51-IK
1040 IE (I)=II
  L=0
  I=0
1100 I=I+1
  L=L+1
  IF (I.GE.52) GOTO2000
  DO 1110 K=1, 101
1110 IP (K)=0
  DO 1120 J=1, N
  IF (IE (J).NE.I) GOTO1120
  JJ=IX (J)
  IP (JJ)=1
1120 CONTINUE
  DO 1130 J=1, N
  IF (IY (J).NE.I) GOTO1130
  JJ=IX (J)
  IF (IP (JJ).GE.2) GOTO1130
  IP (JJ)=IP (JJ)+2
1130 CONTINUE
  DO 1180 J=1, 101
  IF (IP (J).NE.0) GOTO1140
  IPP (J)=IB
  GOTO 1180
1140 IF (IP (J)-2) 1150, 1160, 1170
1150 IPP (J)=IV
  GOTO 1180
1160 IPP (J)=IC
  GOTO 1180
1170 IPP (J)=IEQ
1180 CONTINUE
  IF (I.EQ.1) GOTO1195

```



```
300 FORMAT(2X,'R= ? .....')
400 FORMAT(2X,3(F7.2,2X),'1 1 18 NOARROW')
500 FORMAT(2X,'FREQ')
600 FORMAT(2X,3(F8.3,2X),'1 1 12 NOARROW')
700 FORMAT(2X,'I*10')
750 FORMAT(2X,'R 1.0')
800 FORMAT(2X,'L 1')
900 FORMAT(2X,I5)
1000 FORMAT(4(2X,F8.1,2X,F8.3))
1100 FORMAT(2X,'L 2')
      END
```

VAX- VMS 4.1 Macro for Executing the Program LINSHP

```
$ start:
$ directory
$ write sys$output " "
$ inquire P1 "Data file name?"
$ write sys$output " "
$ copy 'P1' for001.dat
$ inquire P2 "What size is your data? ( 05k 1k 2k or 4k)"
$ run d2:[pclarke.density.natural]test'P2'
! Converts data from two columns, floating point, to ten columns
! of standard fortran format (10F(8.2))
$ inquire P3 "Header file name?"
$ write sys$output " "
$ append 'P3',for002.dat for003.dat
$ write sys$output " Ignore the preceeding error! "
$ write sys$output " "
$ run d2:[pclarke.density.natural]twosit
$ write sys$output " To save the output from this program      "
$ write sys$output " you will have to rename them              "
$ write sys$output " "
$ inquire P4 "What do you wish to rename for004.dat to?"
$ rename for004.dat 'P4'
$ write sys$output " "
$ inquire P5 "What do you wish to rename draw.plt to?"
$ rename draw.plt 'P5'
$ inquire P6 "Any more data? y/n "
$ if P6 then goto start
$ exit
```

Example Input Data for Header File

```
HGTHECNA.11 275K 2097 PTS 5154Hz SW FULL SPEC -20HZ
0.0 1 2 0 2 1 2
1920.0 20.0 1
2097 50 1.0 5155.0 1.0 5155.0
0 8 .0 .0 .0 .0 .0 .0 .0 .0 .0 .0 .0 .0 .0 .0
6.5 6.5 358.0 524.0 0.5 0.5 2.0
4.0 4.0 643.0 653.0 0.5 0.5 0.5
6.5 6.5 642.0 722.0 0.5 0.5 2.0
6.5 6.5 653.0 789.0 0.5 0.5 2.0
6.5 6.5 1015.0 1095.0 0.5 0.5 2.0
20.0 20.0 1255.0 1455.0 0.5 0.5 9.0
6.7 6.7 2922.0 3288.0 0.5 0.5 1.0
4.0 4.0 3585.0 3595.0 0.5 0.5 5.5
```

Data is then read in from a file in the format :

FORMAT(10F8.2)

i.e. ten columns of data in standard FORTRAN F8.2 format.

The Program LINSHP, Acknowledgements

The QIKPLT subroutine was kindly provide by T. Kurucsev, University of Adelaide.

The PLXY subroutine generates a text file in the format required by the graphics drawing program DRAW for the VAXen and Unix networks at the University of Adelaide and was kindly provided by D. Beard, University of Adelaide.

The program LINSHP was originally written by T.M.Spotswood in 1973.

Converted to Nicolet BNC-12 machine code to execute on a Brüker HX-90E NMR spectrometer by E. Williams 1980.

Converted to FORTRAN-5 to execute on a Cyber-173 mainframe computer by A. White 1983.

Converted to FORTRAN-77 to execute on a VAX 11-780 mainframe computer by P. Clarke 1987, using D. Beard's DRAW 1988, and incorporation of the Density Matrix algorithm 1988.

Appendix iv : The Equivalence of Continuous Wave and Fourier Transform NMR for Chemical Exchange Phenomena

The transient and steady state solutions of the modified Bloch equations describe the response, in the simple case of an uncoupled spin system undergoing chemical exchange, between two non-equivalent sites and form a Fourier Transform pair.^{1,2}

Under pulsed NMR conditions, in the rotating frame (x' , y' , z) about the z -axis with angular velocity $\omega = \omega_0 = \gamma B_0$, a short (10^{-4} - 10^{-6} s) r.f. pulse of high energy, B_1 , is directed along the x' -axis, applying a torque to \vec{M} (initially aligned with the z -axis) causing it to tilt towards the y' -axis, generating a transverse component of \vec{M} . Immediately after the pulse, \vec{M} begins to relax back to its equilibrium position aligned with the z -axis. Transverse relaxation causes the M_{xy} component of magnetization to undergo free induction decay (FID) and subsequently, the M_{xy} component falls to zero intensity. Solving the modified differential Bloch equations, Chapter 6, Equations 6.11 and 6.12, with $B_1 = 0$ gives the equation describing the FID:

$$M_{xy} = C_1 e^{-\phi + t} + C_2 e^{-\phi - t} \quad \text{iv.1}$$

where C_1 and C_2 are constants of integration and

$$2\phi_{\pm} = \left(\alpha_a + \frac{1}{\tau_a} + \alpha_b + \frac{1}{\tau_b} \right) \pm \left[\left(\alpha_a + \frac{1}{\tau_a} - \alpha_b - \frac{1}{\tau_b} \right)^2 + \frac{4}{\tau_a \tau_b} \right]^{1/2} \quad \text{iv.2}$$

The Fourier transform of the FID is given by:

$$S = \int_0^{\infty} M_{z \text{ eq}} e^{-i(\omega - \omega_1)t} dt \quad \text{iv.3}$$

$$= \frac{i M_{z \text{ eq}} [\tau_a + \tau_b + \tau_a \tau_b (\alpha_a \chi_b + \alpha_b \chi_a)]}{(1 + \alpha_a \tau_a)(1 + \alpha_b \tau_b) - 1} \quad \text{iv.4}$$

where $\alpha_a = \frac{1}{T_{2a}} + i(\omega_{0a} - \omega)$; and $\alpha_b = \frac{1}{T_{2b}} + i(\omega_{0b} - \omega)$;

ω = the variable frequency; and ω_1 = the fixed pulse carrier frequency.

The absorption mode lineshape is derived from the imaginary part of Equation iv.4 and is the same as that obtained in the continuous wave case. In general, the lineshape obtained for an uncoupled spin system undergoing chemical exchange from a pulsed Fourier transform experiment is equivalent to that derived from a continuous wave experiment. More complex systems do not lend themselves to this simple treatment, however a more sophisticated method which involves density matrix equations has been described in the literature.³⁻⁶ Early computational studies by Kaplan *et al*³⁻⁵ show that differences in amplitude of equivalent resonance peaks of about 5% were obtained for a coupled exchanging system with a lifetime of 10^{-3} s.

-
- 1 Gupta R.K., Pitner T.P., Wasyrishen R., *J. Mag. Reson.* **1974**, 13, 383 - 385.
 - 2 White A., PhD Thesis , University of Adelaide **1987**.
 - 3 Kaplan J.I., *J. Chem. Phys.* **1972**, 57, 5615 - 5616.
 - 4 Ernst R.R., *J. Chem. Phys.* **1973**, 59, 989.
 - 5 Kaplan J.I., *J. Chem. Phys.* **1973**, 59, 990.
 - 6 Farrar T.C., Becker E.D., "Pulse and Fourier Transform NMR", **1971**, Academic Press (New York).

Appendix v : The Gutmann Donor Number D_N as a Measure of Solvent Strength

The majority of solvents have the ability to donate partial electron density (which may be described as electron pair donor power) to an electron density acceptor, for example to metal ions. Ligands coordinated to an acceptor cation in solution have to compete for coordination of the cation with the solvent, thus a measure of the competitive ability of a solvent is an important aspect of metal ion - ligand complexation studies. An empirical electron pair donor power measurement that has been used with some success to correlate kinetic as well as equilibrium studies of cations in various oxygen and nitrogen donor solvents,¹ is the Gutmann donor number, D_N .^{2,3} The enthalpy of complex formation, $-\Delta H$, (kJ mol^{-1}) of the 1:1 adduct between that solvent and antimony(V) chloride, SbCl_5 , (as the reference acceptor) in the non-coordinating solvent 1,2-dichloroethane:



is defined to be D_N , such that the electron donor power increases as D_N increases. The Table A.1 shows the D_N numbers for solvents used in this study.

Table A.1 The Gutmann Donor Number D_N for Selected Solvents

Solvent	D_N^a	D_N^b
1,2-dichloroethane	0.0	
acetonitrile	14.1	
propylene carbonate	15.1	
acetone	17.0	
methanol	19.0	23.5
N,N-dimethylformamide (DMF)	26.6	
N,N-dimethylacetamide (DMA)	27.8	
dimethyl sulphoxide	29.8	
N,N-diethylformamide (DEF)	30.9	
water	18.0	33.0
pyridine	33.1	

^a References 2,3; ^b References 4,5.

It has been suggested that for the solvents water and methanol, $D_N = 33$ and 23.5, respectively, are more appropriate^{4,5} than $D_N = 18.0$ and 19.0, respectively, obtained for water and methanol in 1,2-dichloroethane solution where the intermolecular hydrogen bonding structure of protic solvents is disrupted.

-
- 1 Cox B.G., Garcia-Rosas J., Schneider H., *J. Am. Chem. Soc.*, **1981**, 103, 1054 - 1059.
 - 2 Mayer U., Gutmann V., *Top. Curr. Chem.*, **1972**, 27 113 - 140.
 - 3 Gutmann V. "Coordination Chemistry in Non-Aqueous Solvents", **1968**, Springer, New York.
 - 4 Erlich R.H., Roach E., Popov A.I., *J. Am. Chem. Soc.*, **1970**, 92, 4989 - 4990.
 - 5 DeWitte W.J., Popov A.I., *J. Soln. Chem.*, **1976**, 5, 231 - 240.